

Responsiveness of plasma membrane and microdomain to cold acclimation in association with freezing tolerance

Daisuke TAKAHASHI



Division of Thermo-Biosystem Relations
Specialty of Cryobiosystems Science
United Graduate School of Agricultural Sciences
Iwate University

2015. 3

Table of Contents

Chapter 1

General introduction.....	1
Plants and abiotic stress.....	1
Plasma membrane and cold acclimation	2
Plasma membrane microdomain in plants.....	3
Glycosylphosphatidylinositol-anchored proteins in plants	4
Aims and outline of the thesis	4

Chapter 2

Detergent-resistant plasma membrane proteome in oat and rye: similarities and dissimilarities between two monocotyledonous plants.....	6
Summary	6
Introduction	7
Experimental procedures.....	9
Results and discussion.....	12
Tables and figures	21

Chapter 3

Changes of detergent-resistant plasma membrane proteins in oat and rye during cold acclimation association with difference in freezing tolerance	29
Summary	29
Introduction	30
Experimental procedures.....	32
Results and discussion.....	35
Tables and figures	47

Chapter 4

Lipid profiles of detergent resistant fractions of the plasma membrane in oat and rye suggest their relationship with cold acclimation and freezing tolerance	57
Summary	57
Introduction	58
Experimental procedures.....	59
Results	62
Discussion	67

Tables and figures	74
--------------------------	----

Chapter 5

Extensive proteomic approaches to identifying glycosylphosphatidylinositol-anchored proteins in <i>Arabidopsis</i> reveal diverse responses during cold acclimation	85
Summary	85
Introduction	86
Experimental procedures	87
Results	93
Discussion	98
Tables and figures	105

Chapter 6

A GPI-anchored glycosyl hydrolase 17 family protein is involved in the enhancement of freezing tolerance during cold acclimation	115
Summary	115
Introduction	116
Experimental procedures	117
Results	121
Discussion	125
Tables and figures	129

Chapter 7

General discussion	142
Cold acclimation and plasma membrane microdomain	142
Role of glycosylphosphatidylinositol-anchored protein in CA	145

Chapter 8

Concluding remarks and perspectives	148
--	------------

Acknowledgements	150
-------------------------------	------------

References	153
-------------------------	------------

Chapter 1

General introduction

Plants and abiotic stress

Plants are immovable organisms and spend all life within a small area where once plants set roots deep. Therefore, monitoring environmental conditions and response to their changes properly are always necessary for plant survival. Without environmental stress perception and response, plants cannot survive in external environment, often severe and harsh. However, plants are one of the most diversified organisms and living from under water to alpine area.

Environmental stress can be grouped into biotic and abiotic stress. Biotic stress affects plants locally and species-specifically but abiotic stress is a stress affecting plants homogenously, extensively and species-nonspecifically in most cases. Abiotic stress contains many kinds of environmental factors such as drought, salt, flooding, light, nutrition, physical pressure, and extreme temperatures. Among them, cold temperature is a most influential factor on plant growth and survival because cold stress is sometimes accompanied by a state change from water to ice (Levitt, 1980; Steponkus, 1984). Extracellular freezing induces reduction of enzyme activity, mechanical and dehydration stresses, ice crystal formation and transferring intracellular water to extracellular ice (Steponkus, 1984). In addition, extracellular as well as intracellular solutes are concentrated in the unfrozen portions of water and then cell surface both inside and outside is exposed to osmotic stress (Steponkus, 1984). On the other hand, intracellular freezing is a lethal event for plants (Steponkus, 1984). Thus, cold temperature has many aspects and influence on plant cells in various ways. In freezing injury mechanism, the plasma membrane (PM) has been the most focused part of the plant cell for survival, because the PM is thought to be a primary site of freezing injury in plant cells and needs to withstand extracellular ice formation, stop penetration of ice crystal into unfrozen intracellular space, and maintain functions under low temperature and extracellular freeze-induced mechanical/dehydration/hyperosmotic stress conditions (Gordon-Kamm and Steponkus, 1984a; Steponkus, 1984; Gordon-Kamm and

Steponkus, 1984b; Lynch and Steponkus, 1987; Steponkus et al., 1988; Uemura and Steponkus, 1989; Webb and Steponkus, 1993; Uemura and Steponkus, 1994; Webb et al., 1994).

Plasma membrane and cold acclimation

Freezing tolerance varies by plant species as tropical plant cannot tolerant to cold and freezing temperature, and alpine plants have higher freezing tolerance. Among plant species, many temperate plants have an adaptation mechanism to increase their freezing tolerance by sensing the decrease of air temperature and the shortening of day length (Levitt, 1980), which is referred to cold acclimation (CA). In CA process, accumulation of solutes including sugars, amino acids and specific proteins (e.g. dehydrin) occur for prevention of membranes from freeze-induced denaturing and disruption (Koster and Lynch, 1992; Welin et al., 1994; Danyluk et al., 1998; Wanner and Junttila, 1999; Kosová et al., 2008). These processes are carried out by the increase of specific gene expression as represented by C-repeat binding factors (CBFs) under non-freezing low temperature condition (Thomashow, 1998; Thomashow, 1999).

In freezing stress, the PM is the primary site of freezing injury as described above. During freezing, many ultrastructural changes are observed in the PM such as fracture-jump lesion and lamellar-to-hexagonal II (H_{II}) phase transitions, which is inter bilayer interactions between the PM and other closely-positioned endomembranes and induced by freeze-induced dehydration (Gordon-Kamm and Steponkus, 1984a; Gordon-Kamm and Steponkus, 1984b; Steponkus et al., 1988; Uemura and Steponkus, 1989; Webb et al., 1993; Webb and Steponkus, 1993; Webb et al., 1994; Webb et al., 1995). During CA, plants are known to change their own PM composition to adapt freezing temperature. About 30 years ago, many studies dealing with PM lipid changes in plant during CA were reported (Steponkus, 1984; Uemura and Yoshida, 1984; Yoshida and Uemura, 1984; Ishikawa and Yoshida, 1985; Palta et al., 1993; Uemura and Steponkus, 1994; Uemura et al., 1995). Two principal changes in plant PM lipid compositions during CA are (a) to increase unsaturation degree of phospholipids to maintain membrane fluidity under low temperature and (b) to decrease hydrophobicity to prevent membrane-membrane fusion under freeze-induced dehydration condition. On the other hand, another major component of the PM, PM protein, has also been studied for many years. First, Yoshida and Uemura (1984), and Uemura and Yoshida (1984) reported compositional changes of PM proteins during CA. Subsequently, mass spectrometric approaches were applied for the identifications of CA-responsive PM proteins in plant (Kawamura and Uemura, 2003; Li et al., 2012). Physiological and

biochemical assays also demonstrated functional changes of plant PM during CA. For example, increase of P-type ATPase activity, disassembly of microtubules and accumulation of several dehydrin family proteins occur on the PM for maintenance of cellular homeostasis and stabilize the PM under low temperature (Ishikawa and Yoshida, 1985; Danyluk et al., 1998; Abdrakhamanova et al., 2003; Kosová et al., 2008). Therefore, compositional and functional changes of the PM are considered necessary for acquisition of freezing tolerance during CA.

Plasma membrane microdomain in plants

At present, structure of the PM is represented as fluid mosaic model (Singer and Nicolson, 1972). In this model, lipids and proteins are freely diffusible in the lipid bilayer of the PM and form mosaic-like structure. In 1997, Simons and Ikonen proposed a new model, microdomain model, for understanding and describing membrane functions along with fluid mosaic model (Simons and Ikonen, 1997). Microdomain model is basically the same thing as fluid mosaic but specific PM lipids and proteins are considered to be laterally localized in small area and form cluster-like structure in the PM. Sphingolipids, a microdomain lipid, have carbohydrate heads and predominantly saturated carbohydrate chain, and weakly interact with one another. Since sphingolipid head group occupies large space in the PM and makes void volume in intrabilayer, sterols fill the spaces between associating sphingolipids. The tightly-packed sphingolipid/sterol structure in animal cells can also interact with many specific proteins as represented by glycosylphosphatidylinositol-anchored proteins (GPI-APs; Sargiacomo et al., 1993; Danielsen and van Deurs, 1995). The cluster-like mobile structure in membrane has an advantage in modulation of enzyme activity and formation of cellular polarity.

Since tightly-packed microdomain has high lipid content, these microdomains are insoluble in the detergent Triton X-100 at 4°C and can be isolated as detergent resistant membrane (DRM) fractions (Ahmed et al., 1997; Schroeder et al., 1998). In plant, Peskan et al. (2000) first isolated DRM fractions from tobacco leaves. Later, many studies demonstrated that specific lipids and proteins are contained in DRM, suggesting that plant microdomain also has specific functions in the PM (Mongrand et al., 2004; Shahollari et al., 2004; Borner et al., 2005; Morel et al., 2006; Lefebvre et al., 2007; Fujiwara et al., 2009; Kierszniowska et al., 2009; Raffaele et al., 2009; Furt et al., 2010). For CA, only Minami et al. (2009) reported the compositional changes of lipids and proteins in both PM and DRM. In this study, each lipid class was exercised for quantification process. DRM protein identifications were carried out with 2-dimensional

electrophoresis (2-DE) based proteomic approach. Thus, lipid and protein changes were roughly characterized but this study did not deal with lipid molecular species and low expressed DRM proteins. In addition, DRM fractions are prepared from *Arabidopsis* leaves in this study and no studies used monocotyledonous plants for experimental plants (Webb et al., 1994). Therefore, it is still unknown what lipids and proteins are partitioned into microdomain in detail and correlate with the difference between dicotyledonous and monocotyledonous plants, or low and high freezing tolerance in plants.

Glycosylphosphatidylinositol-anchored proteins in plants

As described above, GPI-AP is a principal microdomain component in animal cells. GPI anchor is one of the post-translational lipid modifications in specific protein and attached to extracellular leaflet of the PM (Sherrier et al., 1999; Borner et al., 2002). As an interesting property, GPI-AP can be released from PM surface by endogenous phosphatidylinositol-specific phospholipase C (PI-PLC) and transferred to apoplastic space (Bütikofer and Brodbeck, 1993). For identification of GPI-APs, many GPI-AP prediction algorithms were developed: Borner et al. (2003), big-PI Plant Predictor (Eisenhaber et al., 2003), PredGPI (Pierleoni et al., 2008), GPI-SOM (Fankhauser and Maser, 2005) and fragAnchor (Poisson et al., 2007). As an example, Borner et al. (2003) estimated that 248 GPI-APs are encoded in *Arabidopsis* genome. Some studies deduced the functions of GPI-APs as lipid transport (DeBono et al., 2009; Edstam et al., 2014), organizing cellular expansion (Schindelman, 2001; Roudier et al., 2002; Li et al., 2003; Roudier et al., 2005), cell adhesion (Johnson et al., 2003; Shi et al., 2003; MacMillan et al., 2010) and callose deposition (Simpson et al., 2009). Furthermore, Borner et al. (2003), Elortza et al. (2003) and Elortza et al. (2006) focused on GPI-APs from the perspective of proteomic study, but only 30, 44 and 35 GPI-APs are identified, respectively. Thus, there are no comprehensive proteomics studies focusing on GPI-APs even though GPI-APs are deduced to be one of the important components of microdomain and may play crucial roles in cellular process. It is also important that previous studies have never mentioned the relationship between GPI-APs and freezing tolerance or CA mechanisms.

Aims and outline of the thesis

Based on the background as described above, the aims of this thesis was to clarify the changes of microdomain components in relation to CA and freezing tolerance. As experimental plants, I selected oat and rye that are monocotyledonous plants and

have vastly different freezing tolerance (Webb et al., 1994). These plants are useful for discussion about the difference of microdomain components between dicotyledonous and monocotyledonous plants and the relationship between microdomain components and freezing tolerance during CA. First, newly developed label-free shotgun proteomics technologies were applied to identification of microdomain proteins in DRM fractions. This study revealed that shotgun proteomics was an effective method for identification of membrane proteins comprehensively. In this study, I could detect similarity with some dissimilarity in DRM protein compositions between oat and rye (Chapter 2). Using the same workflow, I conducted analysis of proteins and lipid changes during CA in DRM (Chapters 3 and 4). These studies showed that specific DRM proteins and lipids changed during CA but CA-induced changes of DRM proteins and lipids were partly different from those in the PM. When CA responses of DRM components compared with high freezing-tolerant rye and low freezing-tolerant oat, specific DRM proteins and lipids differently changed during CA. These analyses showed putative correlations between CA-dependent changing patterns in DRM and plant freezing tolerance.

Subsequently, I focused on GPI-APs, which are largely unknown proteins in relation to microdomain functions and CA mechanisms in plant. I successfully isolated GPI-AP enriched fractions from *Arabidopsis* PM and identified 163 GPI-APs from these fractions in addition to the PM, DRM and apoplast fractions (Chapter 5). In this study, I revealed that many GPI-APs were CA responsive proteins and they showed diversified responses to CA treatment in the PM, DRM and apoplast fractions, meaning that GPI-APs have a variety of functions during CA and some GPI-AP changes during CA are possible to be involved in acquisition of freezing tolerance. Based on the data obtained in Chapter 5, a putative CA-associated GPI-AP, At3g04010, was selected and characterized to understand its functions during CA in association with freezing tolerance (Chapter 6). Temporal and histological analysis of *At3g04010* gene expression in response to CA indicated that At3g04010 is up-regulated during CA and associated with phloem tissue. *At3g04010* knock-down mutant (*at3g04010*) demonstrated that At3g04010 affects plant freezing tolerance and recovering process, and plays a role for callose turnover in CA process. The current results show that At3g04010 influence on regulation of plasmodesmal opening for proper phloem transport during CA. Finally, up-regulation of At3g04010 on the PM surface during CA may be necessary for freezing tolerance and post-thaw recovering process.

Chapter 2

Detergent-resistant plasma membrane proteome in oat and rye: similarities and dissimilarities between two monocotyledonous plants

Summary

The plasma membrane (PM) is involved in important cellular processes that determine the growth, development, differentiation and environmental signal responses of plant cells. Some of these dynamic reactions occur in specific domains in the PM. In this study, I performed comparable nano-LC-MS/MS-based large-scale proteomic analysis of detergent-resistant membrane (DRM) fractions prepared from the PM of oat and rye. A number of proteins showed differential accumulation between the PM and DRM, and some proteins were only found in the DRM. Numerous proteins were identified as DRM proteins in oat (219 proteins) and rye (213 proteins), of which about half were identified only in the DRM. The DRM proteins were largely common to those found in dicotyledonous plants (*Arabidopsis* and tobacco), which suggests common functions associated with the DRM in plants. Combination of semiquantitative proteomic analysis and prediction of post-translational protein modification sites revealed differences in several proteins associated with the DRM in oat and rye. It is concluded that protein distribution in the DRM is unique from that in the PM, partly because of the physicochemical properties of the proteins and the unique distribution of these proteins may define the functions of the specific domains in the PM in various physiological processes in plant cells.

Introduction

The plant plasma membrane (PM) has a number of important physiological functions that are critical to maintain survival of cells and whole plants. The PM is a highly organized structure composed of proteins and lipids, and locates at the communication points with cell walls, neighboring cells and the external environment. Functions of the PM include uptake and transport of water, nutrient elements and metabolites, gas exchange, perception of hormonal and exogenous environmental signals, and recognition of biotic organisms. For these diverse processes, the function of proteins associated with partner proteins in close vicinity in an appropriate lipid environment is tightly controlled by a variety of regulatory mechanisms.

Increasingly, it is accepted that biological membranes, including the PM, consist of various microdomains each with specific protein and lipid compositions and differentiated in function. The membrane microdomain concept assumes that movement of membrane lipids and proteins is regulated and, hence, localization of these molecules is non-homogeneous in the membrane (Kusumi et al., 2005; Lillemeier et al., 2006). In animals and microorganisms, domains in the PM are often called membrane microdomains or membrane rafts and their existence, chemical composition and biological functions are well characterized (Simons and Ikonen, 1997; Bagnat et al., 2000; Schley et al., 2007; Veatch et al., 2008; Pike, 2009). The microdomains in the plant PM, however, are to be investigated to elucidate their functions.

In plants, specific fractions, called detergent-resistant membrane (DRM) fractions, have been prepared by exposure of the purified PM preparations to ice-cold, detergent solutions and subjected to compositional analyses (Peskan et al., 2000). In many cases, the DRM was analyzed to obtain information on membrane microdomains. DRM fractions are enriched in sterols, sphingolipids and specific proteins associated with signal transduction, solute/water transport, cell wall–PM interactions, intracellular membrane trafficking, and pathogen infection (Mongrand et al., 2004; Borner et al., 2005; Morel et al., 2006). Some of the functions assigned to the plant DRM are similar to those for microdomains of animal and microorganism cells. Furthermore, using fluorescence and electron microscopy, several PM components have been localized to distinct regions of the PM (Lefebvre et al., 2007; Raffaele et al., 2009; Furt et al., 2010). The putative roles of the PM microdomains in plant–microbe interactions have been reported (Fujiwara et al., 2009; Stanislas et al., 2009; Keinath et al., 2010). Nevertheless, it is still necessary to characterize microdomain function and composition to understand how microdomains in the PM are involved in various physiological processes in plants.

Recently, Kawamura and Uemura (2003) and Minami et al. (2009) successfully elucidated dynamics of the PM and DRM proteins during cold acclimation of *Arabidopsis thaliana*, a model dicotyledonous plant. Using matrix-assisted laser desorption-ionization time-of-flight mass spectrometry (MALDI-TOF-MS), they identified a number of PM proteins altered quantitatively in the PM in response to cold acclimation including those associated with the fusion-associated membrane repair process and protection of the membrane against osmotic stress (Kawamura and Uemura, 2003). Using two-dimensional difference gel electrophoresis (2D-DIGE) combined with MALDI-TOF-MS and LC-MS/MS techniques, they further revealed abundance of P-type H⁺-ATPases, aquaporins and endocytosis-related proteins increased and, conversely, that of tubulins, actins and V-type H⁺-ATPase subunits decreased in the DRM during cold acclimation (Minami et al., 2009). In addition, functional categorization of cold-responsive proteins in the DRM indicates plant PM microdomains function as platforms of membrane transport, membrane trafficking and cytoskeleton interaction, and there is a close association of DRM with plant cold acclimation. Thus, it is reasonable to consider that DRM is somehow involved in the plant cold acclimation process to increase survival under cold conditions.

Nevertheless, it is still necessary to demonstrate the DRM proteome profiles in different plant species in order to consider the importance of the DRM in physiological processes during the plant life cycle. In the present study, I performed a comparative proteomic analysis to determine the distribution of proteins between the DRM and non-DRM regions in the PM of two monocotyledonous crop plant species, oat (*Avena sativa* L.) and rye (*Secale cereale* L.). Although very limited genomic information for these two species is available at this moment, they are widely cultivated and have been used in a variety of physiological studies, including investigations of photoreception and environmental stress adaptation (Boylan and Quail, 1989; Hon et al., 1994; Hurry et al., 1995; Livingston, 1998). I am particularly interested in oat and rye because freezing tolerance and lipid composition of the PM are vastly different between the two species (Webb et al., 1994). Examination of the composition of DRM proteins in the two plant species is the first step to understand the involvement of the DRM in different physiological processes. In the present study, using nano-LC-MS/MS-based proteomic techniques, I revealed a number of proteins are unique to and common in the DRM of oat and rye, and some of the proteins unique to the DRM are common to both monocotyledonous and dicotyledonous plants. In addition, semiquantitative proteomic analysis combined with predictions of post-translational protein modifications indicated some differences in the protein compositions of the DRM exist between oat and rye,

which is suggestive of functional differentiation of the DRM in plant species. To the best of our knowledge, this is the first report of a large-scale proteomic analysis of the DRM fraction prepared from monocotyledonous plants.

Experimental procedures

Plant Materials

Seeds of oat (*Avena sativa* cv. New Almighty) and rye (*Secale cereale* cv. Maskateer) were germinated and grown in vermiculite supplemented with Hoagland solution at 18°C with a 16 h photoperiod (90 $\mu\text{mol}/\text{m}^2/\text{s}$). After 12 to 14 days, leaves were harvested for experimental analysis.

Isolation of Plasma Membrane and Detergent-Resistant Membrane Fractions

Harvested leaves were used immediately for preparation of plasma membrane (PM) fractions using a polyethylene glycol-dextran aqueous two-phase partition system as described previously (Uemura and Yoshida, 1983). All procedures were conducted at 0–4°C. Leaves (about 70 g fresh weight) were collected, cut into small pieces with razor blades, and homogenized in 300 ml homogenizing medium (0.5 M sorbitol, 50 mM Mops/KOH (pH 7.6), 5 mM EGTA, 5 mM EDTA, 5% (w/v) polyvinylpyrrolidone (MW: 40,000), 5% (w/v) BSA, 2.5 mM phenylmethanesulfonyl fluoride, 4 mM salicylhydroxamic acid and 2.5 mM dithiothreitol) using a Polytron (Kinematica PT10-35, Brinkmann Instruments, Westbury, NY, USA). Homogenates were filtered through four layers of gauze and then centrifuged at $10,000 \times g$ for 15 min. Supernatants were collected and centrifuged at $231,000 \times g$ for 50 min. Pellets were collected and suspended in microsome suspension (MS) medium (0.25 M sucrose and 10 mM $\text{KH}_2\text{PO}_4/\text{K}_2\text{HPO}_4$ [pH 7.8]) and centrifuged again as described above. The resultant pellets were resuspended in 5 ml MS medium and applied to 16.6 ml of a two-phase partition system, the final composition of which was 5.8% (w/w) polyethylene glycol (MW: 3,350; Sigma-Aldrich, St Louis, MO, USA), 5.8% (w/w) dextran (Sigma-Aldrich), 0.25 M sucrose, 30 mM NaCl, and 10 mM $\text{KH}_2\text{PO}_4/\text{K}_2\text{HPO}_4$ (pH 7.8). After mixing well, the mixtures were centrifuged at $650 \times g$ for 5 min, and the resultant upper phase was collected and loaded onto a newly prepared lower phase of the two-phase partition. The two-phase partitioning was carried out three times to increase the purity of the PM, and the final upper phase was collected and centrifuged as described above. The PM pellets were suspended in PM suspension medium (0.25 M sucrose, 10 mM Mops/KOH (pH 7.3) and 2 mM EGTA).

Detergent-resistant plasma membrane (DRM) fractions were prepared using the method of Peskan et al. (2000). A PM pellet (equivalent to 2 mg protein) was resuspended in 2.7 ml of TED buffer consisting of 50 mM Tris-HCl (pH 7.4), 3 mM EDTA, and 1 mM dithiothreitol and added to 300 μ l of 10% (w/v) Triton X-100. Final ratio of detergent to protein (w/w) was 15:1, which is the same to the ratio that has been widely used in biochemical studies of DRM fractions from a various plant species (e.g., *Arabidopsis*, tobacco and rice; Fujiwara et al., 2009; Minami et al., 2009; Raffaele et al., 2009). After incubation for 30 min on ice, the sample was immediately added to 12 ml of 65% (w/v) sucrose in TED buffer and mixed well. This solution was overlaid with 48, 35, 30, and 5% (w/v) sucrose-TED solutions and then centrifuged at $141,000 \times g$ for 20 h at 4°C using a swing-type rotor P28S (Hitachi, Japan). The DRM fractions were observed at the interface of the 30/35% (w/v) sucrose layers as a white band. The band was collected, centrifuged at $231,000 \times g$ for 50 min, and finally diluted with PM suspension medium. Protein content was measured using the Bradford assay (Bio-Rad, Munich, Germany).

One-dimensional SDS-PAGE

The PM and DRM samples were suspended in SDS sample buffer (2% [w/v] SDS, 50 mM Tris-HCl [pH 6.8], 6% [v/v] β -mercaptoethanol, 10% [w/v] glycerol and bromophenol blue). Samples were heated at 95°C for 20 min in the SDS sample buffer to dissolve membrane proteins, separated on a 10% polyacrylamide gel with 4.5% stacking gel, and visualized by silver staining (Kawamura and Uemura, 2003). Electrophoresis was carried out at 100 V for 4–5 h at room temperature. Protein bands were subjected to silver staining.

Sample Preparation for Nano-LC-MS/MS Analysis

All of the sample preparation steps for nano-LC-MS/MS analysis were performed carefully on a clean bench to avoid contamination from keratin, dust and other materials. First, membrane samples (approximately 50 μ g protein) were precipitated by ultracentrifugation. Membrane proteins were dissolved in a detergent mixture (MPEX PTS Reagents for MS, GL Science, Tokyo, Japan) and the protein content was determined with the Pierce BCA Protein Assay Kit (Pierce, Rockford, IL, USA). As reported elsewhere, the MPEX detergent mixture was suitable for membrane proteins including highly hydrophobic proteins such as those with multiple transmembrane domains (Masuda et al., 2008). Subsequent processes were performed in

accordance with the instruction manual for the MPEX kit. The peptide samples were desalted with SPE C-TIP (AMR, Tokyo, Japan) and the volume was adjusted to 15 μ l.

Nano-LC-MS/MS Analysis of PM and DRM Proteins

Proteins were digested with trypsin in accordance with the instruction manual for the MPEX kit. Digested peptide solutions were subjected to nano-LC-MS/MS analysis. Peptide solutions were trapped and concentrated in a trap column (L-column Micro 0.3 x 5 mm; CERI, Japan) using an ADVANCE UHPLC system (MICHROM Bioresources, Auburn, CA, USA). After elution from the trap column with 0.1% (v/v) formic acid in acetonitrile, concentrated peptides were separated with a Magic C18 AQ nano column (0.1 x 150 mm; MICHROM Bioresources) using a linear gradient of acetonitrile (from 5% [v/v] to 45% [v/v]) at a flow rate of 500 nL/min. Ionization of peptides was performed at a spray voltage of 1.8 kV using an ADVANCE spray source (MICHROM Bioresources). Mass analysis was performed using an LTQ Orbitrap XL mass spectrometer (Thermo Fisher Scientific, Waltham, MA, USA) equipped with Xcalibur software (version 2.0.7, Thermo Fisher Scientific). Under the data-dependent scanning mode, full scan mass spectra were obtained in the range of 400 to 1800 m/z with a resolution of 30,000. Collision-induced fragmentation was applied to the five most intense ions at a threshold above 500. These experiments were repeated four times with samples collected from biologically independent plants.

Analysis of Nano-LC-MS/MS Data

Raw files of MS/MS spectra were obtained from nano-LC-MS/MS and converted to the mgf format using Proteome Discoverer (ver. 1.1.0.263, Thermo Fisher Scientific). The parameters for the conversion from raw files to mgf files were as follows: precursor mass range, m/z 350–5000; highest and lowest charge state, 0; lower and upper RT limit, 0; the minimum total intensity of a spectrum, 0; and the minimum number of peaks in a spectrum, 1. Using mgf files, peptide data were searched and proteins were identified using the MASCOT search engine (version 2.3.02, Matrix Science, London, UK) searching against the NCBI nr Green Plants database (version 20110131 comprising 12,852,469 sequences). One missed cleavage was allowed. Fixed and variable modifications were set as carbamidomethylation of cysteines and oxidation of methionine, respectively. Peptide mass tolerance was 5 ppm. The MS/MS tolerance was 0.6 Da. Peptide charges were set to +2, +3 and +4. As a result, the false discovery rate (FDR) of peptide identifications, which was based on a search of the Mascot decoy database, was less than 5%. To generate a representative list

of proteins with increased reliability, the proteins were defined as ‘identified’ if the protein matched at least one unique top-ranking peptide with an expect value ≤ 0.05 . In addition, proteins identified two or more times in four repeated experiments were recruited into the protein lists. If a peptide was assigned to multiple proteins, the highest-scoring protein was selected in the list. For semiquantitative analysis of PM and DRM proteins, Progenesis LC-MS software (version 2.5, Nonlinear Dynamics, New Castle, UK) was applied to experimental raw data files. Acquired profile data were processed according to the software’s instructions. In this process, peptides that were compared between PM and DRM proteins were filtered with ANOVA ($p < 0.05$) and max fold change (> 2). The resultant peptides were reanalyzed and identified with the Mascot search engine as described above.

Topology and Post-translational Modification Prediction

Exported sequences of PM and DRM proteins derived from the Mascot and Progenesis analyses were used for prediction of transmembrane domains, signal peptides, cellular locations, and sites of glycosylphosphatidylinositol (GPI) modification and myristoylation. The numbers of transmembrane domains and cellular locations (C, chloroplast; M, mitochondrion; and S, signal peptide) were predicted by the SOSUI engine version 1.10 (<http://bp.nuap.nagoya-u.ac.jp/sosui/>) and TargetP 1.1 server (<http://www.cbs.dtu.dk/services/TargetP/>), respectively. Predictions of signal peptides (S) and membrane anchor peptides (A) were performed with the SignalP 3.0 server (<http://www.cbs.dtu.dk/services/SignalP/>) and by Hidden Markov models. GPI modification and N-terminal myristoylation sites were analyzed by the Big-PI Plant Predictor (http://mendel.imp.ac.at/gpi/plant_server.html) and Plant-Specific Myristoylation Predictor (<http://plantsp.genomics.purdue.edu/plantsp/html/myrist.html>), respectively.

Results and discussion

Isolation of PM and DRM Fractions and Nano-LC-MS/MS-Based Proteomic Analysis

The PM of oat and rye leaves was prepared using a polyethylene glycol–dextran aqueous two-phase partition system. The purity of the PM samples of rye leaves obtained with the same method was estimated to be high (approximately 90%) based on a number of evaluation methods (*e.g.*, marker enzyme distribution, PM-specific phosphotungstic acid–chromic acid staining, *N*-1-naphthylphthalamic acid binding capacity, and resistance to low pH and zinc ion; Uemura and Yoshida, 1983). In oat, the

same two-phase partition method was applied successfully for PM isolation (Uemura and Steponkus, 1994).

Although recovery of PM fractions after the two-phase partition was similar in both rye and oat (2.5 mg protein from 70 g leaves), recovery of DRM fractions from the purified PM fractions was somewhat greater in oat (10–20% proteins of the PM fraction) than in rye (8–12%) based on protein content measured using the Bradford assay. First, I determined the PM and DRM protein compositions using one-dimensional SDS-PAGE and silver-staining methods (Fig. 2-1). Considerable differences in protein patterns were indicated between the two species and between the PM and DRM membrane fractions. However, the differences between the membrane fractions were more apparent than those between the two species (see arrows in Fig. 2-1). Some proteins were present in lower amounts in the DRM than in the PM fraction or vice versa, and some proteins were only detectable in one of the two membrane fractions. In addition, there were proteins stained strongly in the DRM of both rye and oat. Similar results were observed in the PM and DRM fractions of tobacco BY-2 cells and *Arabidopsis* (Mongrand et al., 2004; Borner et al., 2005; Morel et al., 2006), which indicates a distinct protein composition in the DRM with enrichment of specific proteins is conserved in monocotyledonous and dicotyledonous plants. In addition, there are differences in the DRM protein composition in oat and rye. Thus, it is reasonable to deduce that DRM protein compositions are somewhat different among plant species.

Some studies indicate DRM fractions are useful to determine the composition, function and property of microdomains in the PM (Schuck et al., 2003; Shogomori and Brown, 2003). Biochemical analyses reveal plant DRM fractions are enriched in sphingolipids, sterol lipids and specific proteins associated with membrane trafficking, PM–cell wall interactions and membrane transport (Mongrand et al., 2004; Borner et al., 2005; Morel et al., 2006). Proteins that show these cellular functions, except for those in the PM–cell wall interactions category, are reported frequently in animal cells and are closely related to well-established characteristics of PM microdomains (or rafts; Lingwood and Simons, 2010). Furthermore, there is evidence that the plant PM contains specific domains with specific protein and lipid compositions, such that microscopic analysis using plant PM vesicles clearly demonstrates DRM-localized proteins are organized as a patch-like structure. For example, the distribution of remorin, which is enriched in DRM fractions, is non-homogenous in PM vesicles and changes to a homogenous pattern after treatment with the sterol-chelating agent methyl- β -cyclodextrin (Raffaele et al., 2009). There are some concerns DRM fractions might not be completely consistent with functional microdomains in the PM and that

analysis of the DRM does not fully allow elucidation of microdomain functions (Tanner et al., 2011). However, it is certainly possible that I could deduce certain functions and properties of distinct PM domains from analysis of plant DRM fractions. In fact, Minami et al. reported previously that DRM lipids and proteins prepared from *Arabidopsis* leaves changed in response to cold acclimation (Minami et al., 2009). Therefore, I continued to determine DRM proteomes of oat and rye as the first step to understand DRM functions in plant cellular processes.

I identified PM and DRM proteins, including proteins that showed a low expression level, by a shotgun proteomic approach with nano-LC-MS/MS and deduced the DRM domain function. I identified 643 proteins in total in the PM and DRM fractions of oat and rye (Supplemental Table 2-1). Before further analysis described below, I considered a few issues that may affect the quality of the analysis of DRM protein populations in oat and rye. First, under our experimental conditions (*i.e.*, identification of proteins searching against the NCBI nr Green Plants database), there may be differences in the peptide matching efficiency between oat and rye. However, I think that it is not problematic because I first compared protein lists between PM and DRM within the same species (oat or rye) and obtained the ratio of protein abundance in DRM and PM so that the peptide matching efficiency difference, if any, will not be significant. Subsequently, based in the protein ratio in DRM and PM, I discussed similarities and dissimilarities in DRM protein localization between oat and rye. Second, I excluded RubisCO, the most abundant protein on earth, from our analysis because RubisCO, the most abundant protein, is reported to be problematic for analysis of proteins that show low expression levels (Neilson et al., 2011). In addition, there were proteins in the list that are predictably targeted to chloroplast or mitochondria according to the Target P program. However, it is a good possibility that these proteins are localized in different membranes in cell because of various endogenous and/or exogenous reasons (Marmagne et al., 2007). Thus, I included these proteins in our subsequent analysis.

According to the accession numbers of the identified proteins, I generated Venn diagrams to show proteins unique to the PM or DRM and those shared between the PM and DRM of oat and rye (Fig. 2-2). Our results showed that 96 and 113 proteins that were shared between the PM and DRM in oat and rye, respectively, and 123 and 100 proteins were categorized as unique to the oat and rye DRM, respectively. Because DRM proteins are a part of the PM proteins, the unique proteins are regarded as highly enriched proteins in the DRM. The number of DRM proteins was similar in oat (219)

and rye (213), and the proportion of unique proteins was statistically similar in oat (56%) and rye (47%).

I found numerous DRM proteins that were identified previously as DRM proteins in dicotyledonous plants such as tobacco and *Arabidopsis* (Mongrand et al., 2004; Borner et al., 2005; Morel et al., 2006; Minami et al., 2009). These include H⁺-ATPase, aquaporin, clathrin, tubulin and hypersensitive-induced reaction protein. Therefore, plant DRM fractions (microdomains) are likely to have common functions in plants. Plant microdomains are regarded to be an infection point on the PM during fungal penetration. Syntaxin proteins, which were identified in the DRM of both oat and rye in the present study, are reported to be putative microdomain-enriched proteins associated with fungal infection (Bhat et al., 2005; Hardham et al., 2007). In addition, other DRM proteins, such as dynamins and 14-3-3 proteins, are also inferred to function in elicitor signaling in tobacco (Stanislas et al., 2009).

I further categorized the identified proteins based on their functional category as described by Bevan et al. (1998). Proteins were classified into 13 categories (Fig. 2-3). Functional categorization of the PM fractions of oat and rye was similar, with only a small difference found in the number of metabolism-related proteins (18 proteins [7%] in oat vs. 31 proteins [11%] in rye). In addition, protein synthesis-related proteins were also somewhat different (22 proteins [10%] in oat vs 30 proteins [14%] in rye). Comparison of the PM and DRM in oat showed transporters were more enriched in the DRM, whereas metabolism, energy, and protein synthesis-related proteins were less enriched in the DRM. Most of the proteins in these latter categories, however, were classified as ribosomal, chloroplast and mitochondrial proteins. As described above, however, there is a good possibility that these proteins can be associated with different membranes including PM but removed from the DRM samples by detergent treatment during the DRM preparation process. In addition, although ribosomal proteins are primarily associated with ER, there is evidence that ER is known to be involved in PM recycling and be associated with plasmodesmata due to PM anchor domains in ER (Staehelin, 1997).

The rye PM and DRM proteins were similar to those of the oat samples with one notable difference: signal transduction proteins, including a variety of kinases such as calcium-dependent kinases, occurred more frequently in the PM than in the DRM in oat. Nevertheless, I confirmed a number of signaling proteins were located in the DRM, which is consistent with previous reports (Mongrand et al., 2004; Shahollari et al., 2004; Borner et al., 2005; Morel et al., 2006; Minami et al., 2009). Some 20–25% of the proteins could not be assigned to defined functional categories in each fraction.

Semiquantitative Analysis to Reveal Different Accumulation Patterns in PM and DRM

Next, I carried out a semiquantitative analysis to determine enrichment of proteins in the DRM or PM fractions by analyzing the peptide signal intensity data with the Progenesis software. From the data obtained, I formulated a list of proteins that were statistically significantly more abundant (>2 -fold) or less abundant (<0.5 -fold) in the DRM with an ANOVA score of $p < 0.05$. I found 289 proteins in oat and 269 proteins in rye that showed different accumulation patterns between the DRM and PM (Supplemental Table 2-2), and subsequently extracted proteins detected in both oat and rye for comparison (Table 2-1). Surprisingly, of the 60 proteins extracted, 59 proteins were enriched in either the DRM or non-DRM in both plant species. The single exception was early salt stress and cold acclimation-induced protein 2-1 (gi|62861393), which was enriched in the DRM of oat but not in the DRM of rye. Thus, the protein enrichment patterns in the DRM were highly similar in the two plant species. It should be mentioned that some proteins, mainly peripheral, hydrophilic proteins, are removed by detergent treatment during preparation of the DRM from PM samples and, hence, these results must be confirmed by further experiments. Nevertheless, many DRM-enriched proteins reported previously (Mongrand et al., 2004; Borner et al., 2005; Morel et al., 2006; Lefebvre et al., 2007; Minami et al., 2009), such as aquaporins, tubulins, H^+ -ATPases and clathrins, were enriched in oat and rye DRM, which indicated DRM protein composition is conserved in a wide range of plant species.

Cellulose synthases (gi|33186651, gi|67003917 and gi|261599417 in oat and gi|39726035 and gi|166863531 in rye) and 1,3- β -glucan synthases (gi|33391246, gi|55295882 and gi|18461174 in oat and gi|20197794, gi|55295882 and gi|18461174 in rye), which are classified as cell wall-related proteins, were identified as DRM fraction-enriched proteins in both oat and rye (Supplemental Table 2-2). In particular, 1,3- β -glucan synthases were highly enriched in the DRM (five to nine times greater than in the PM). Cellulose synthase and 1,3- β -glucan synthase were segregated in the DRM fractions in tobacco BY-2 cells, oomycetes and hybrid aspen (Morel et al., 2006; Bessueille et al., 2009; Briolay et al., 2009). In embryonic and post-embryonic tissues of *Arabidopsis* sterol-deficient mutants, levels of cellulose were reduced, whereas callose deposition was normal in the mutants (Schrack et al., 2004). Thus, it is possible that cell wall formation is affected by sterol composition and directly and/or indirectly regulated in sterol-enriched microdomains.

Proteins enriched in the DRM or non-DRM PM fractions (summarized in Supplemental Table 2-2) were further classified based on deduced protein functions (Fig. 2-4). Transporters, such as ATPases (e.g., gi|5080816 and gi|50400847) and

aquaporins (e.g., gi|68533200 and gi|7381267), were indicated to be more abundant among the DRM-enriched proteins than the non-DRM PM proteins, which was consistent with the prediction of microdomain functions in plants, animals and yeast cells (Bagnat et al., 2001; Zheng and Bollinger Bollag, 2003; Mongrand et al., 2004; Morel et al., 2006). In contrast, proteins classified into categories of metabolism, energy, and protein synthesis-related proteins (such as synthases, phosphoglycerate kinases, and ribosomal proteins) were less abundant among DRM-enriched proteins. Although signal transduction proteins were not apparently enriched in the DRM, a receptor-like protein (e.g., gi|15128407) was enriched in the DRM of both oat and rye. These results indicate not all signaling proteins are necessarily enriched in PM microdomains, despite a general prediction derived from results with animal PM microdomains.

In rye, a dynamin-like protein (gi|4803836), which is classified as an intracellular traffic protein, was identified as a DRM-enriched protein as was a putative clathrin heavy chain protein (gi|77548264). Also, in oat, further analyses revealed that a hypothetical protein (gi|147805382, 5.7 times enriched in DRM) and an unknown protein (gi|224031193, 9.7 times enriched in DRM) showed sequence similarities to predicted dynamin-related protein 5A (gi|359489735) and dynamin-related protein 1C (gi|226494351), respectively. In addition, cell structure-related proteins, such as actins and tubulins, were enriched in the DRM fractions. Actin is known to interact with dynamins on caveolae, a type of microdomain in the PM of animal cells (Pelkmans et al., 2002). Because dynamins interact with clathrins to mediate membrane dynamics (Konopka et al., 2008), it is possible that detergent-resistant microdomains in oat and rye might permit efficient interactions between the actin cytoskeleton, dynamins and clathrins as a membrane dynamic scaffold.

The results further revealed interesting findings in the enrichment patterns of proteins in DRM among plant species. In *Arabidopsis*, the DRM is enriched in fasciclin proteins and the enrichment is thought to be due to the association of the proteins with sterol lipids (Kierszniowska et al., 2009). Although I confirmed the proportion of sterol lipids was greater in the DRM than in the PM for both oat (1.73-fold; 42.6 mol% in DRM vs 73.6 mol% in PM) and rye (1.63-fold; 39.2 mol% in DRM vs 63.8 mol% in PM; Takahashi et al., 2011), no fasciclin-like proteins were enriched in the DRM of oat and rye (Table 2-1 and Supplemental Table 2-2). These results suggest that DRM is not simple as to be designated as sterol-enriched regions in the PM but more complicated and rich in diversity both compositionally and functionally. In addition to fasciclin-like proteins, 14-3-3 proteins were identified as DRM proteins in *Arabidopsis* (Mongrand et al., 2004) and accumulated in the DRM in response to cryptogenic treatment in tobacco

(Stanislas et al., 2009). 14-3-3 proteins are associated with a plant H⁺-ATPase, which is also a DRM-enriched protein (Baunsgaard et al., 1998). However, these proteins were not enriched in the DRM of oat and rye (Table 2-1 and Supplemental Table 2-2). Similarly, the DRM/PM ratio of syntaxin (gi|110555559 in oat and gi|33465457 in rye) was less than 0.5 in both species, although syntaxin is indicated to reside in the lipid raft in animal cells (Xia et al., 2004; Kinoshita et al., 2008) and accumulates in some PM domains during pathogen penetration in barley and *Arabidopsis* (Bhat et al., 2005). Thus, the protein composition of the DRM (and microdomains) might be somewhat different between plants and animals.

In previous reports on plant DRM protein composition, remorin proteins were used widely as a plant sterol-dependent raft marker (Mongrand et al., 2004; Borner et al., 2005; Lefebvre et al., 2007; Raffaele et al., 2009). In the present study, a remorin-related protein (gi|102140033) was detected as a DRM-enriched protein in oat (Supplemental Table 2-2). An additional BLAST homology search for proteins assigned with the rice gene number only revealed that Os07g0569100 (gi|115472875) in oat and Os03g0111200 (gi|115450243) in rye show similarities to remorin-like proteins (gi|102140033 for oat and gi|115450243 for rye). Thus, the finding that remorins are enriched in the DRM might be a common feature in higher plants.

Predictions of Topology and Modifications of Proteins Reveal Differences in Oat and Rye DRM

To examine the topology of DRM-enriched and non-DRM-enriched proteins, transmembrane domains were predicted with the SOSUI engine. Integral proteins with transmembrane domains were much more abundant in DRM-enriched proteins than in non-DRM-enriched proteins (Fig. 2-5). This finding is consistent with the result described above that the DRM is enriched with transporters such as ATPases and aquaporins. However, it is necessary to consider the possibility that peripheral membrane proteins and soluble proteins loosely associated with the PM are removed from DRM fractions by detergent treatment during the DRM preparation process.

I predicted glycosylphosphatidylinositol (GPI) modification sites with the Big-PI Plant Predictor. In the PM, four and eight proteins were identified as GPI-anchored proteins (GPI-APs) in oat and rye, respectively. One and three GPI-APs were present in the DRMs of oat and rye, respectively (Table 2-2). From the semiquantification results, most of the GPI-APs were enriched in the non-DRM fraction, but not in the DRM fraction (Table 2-3). GPI anchoring is one of the principal post-translational modifications of the PM proteins. GPI bound to specific proteins is

embedded in the exoplasmic leaflet of the PM (Kinoshita et al., 2008). In mammalian cells, some GPI-APs are presumed to be associated with lipid microdomains (Paulick and Bertozzi, 2008; Lingwood and Simons, 2010). In fact, microscopic observations using the depolarization fluorescence resonance energy transfer method revealed that GPI-APs were localized in cholesterol-dependent microdomain-like structures, the diameter of which was smaller than 70 nm, in live Caco-2 cells (Varma and Mayor, 1998). However, not all GPI-APs are enriched in microdomains in animal cells (Sharma et al., 2004). The results of the present study indicated that all of the identified GPI-APs, with the exception of early salt stress and cold acclimation-induced protein 2-1 in oat and putative 1,3- β -glucan synthase in rye, were not enriched in the DRM. In *Arabidopsis* and tobacco BY-2 DRM fractions, only eight GPI-APs have been identified, whereas 248 proteins were predicted to be GPI-APs from the *Arabidopsis* genome sequence (Borner et al., 2005; Morel et al., 2006). Based on these results, plant DRM might contain specific GPI-APs only as described in animal cells.

It should be noted here that there are differences in GPI-APs identified in rye and oat: the numbers of GPI-APs in rye PM and DRM are greater than those in oat PM and DRM (Table 2-2). Although there is a possibility that these differences are due to the difference in peptide matching efficiency under our analytical conditions, these data suggest that GPI-AP compositions are characteristically different between oat and rye while the two species PM and DRM contains many proteins in common. As I showed previously, rye is more tolerant to a variety of abiotic stresses than oat (Webb et al., 1994). Eventually, a few GPI-APs (fasciclin-like proteins) are shown to be related to salt tolerance through cell wall structuring in *Arabidopsis* and response to cold acclimation in wheat (Shi et al., 2003; Faik et al., 2006). Collectively, the localization and amount of GPI-APs in plant PM and/or DRM might be species dependent and affect plant's own stress responsiveness.

I predicted N-terminal myristoylation sites using the Plant-Specific Myristoylation Predictor. With myristoylation, a 14-carbon saturated fatty acid is added to the protein and the acyl chain is inserted into the cytoplasmic leaflet of the PM (Towler et al., 1988). It has been suggested myristoylation is important for partition of proteins into lipid microdomains in animal cells (Zacharias et al., 2002). In the present study, I identified many putative myristoylated proteins, and the number of myristoylated proteins in oat and rye was similar in both the PM and DRM (Supplemental Table 2-3). The proteins identified were similar in oat and rye, including a calcium-dependent protein kinase, ADP-ribosylation factor and callose synthase. According to the DRM/PM ratio predicted by the Progenesis analysis, the number of

DRM-enriched or non-DRM-enriched proteins with possible N-terminal myristoylation was also similar. In the plant PM, the distribution of myristoylated proteins might be strictly controlled on the membrane surface to maintain the proper cellular function of these proteins.

Supporting information

Supplemental Table 2-1. Identified PM and DRM proteins in oat and rye.

Supplemental Table 2-2. Identified proteins that are differentially accumulated in PM and DRM fractions in oat and rye as determined using Progenesis software.

Supplemental Table 2-3. Putative myristoylated proteins in oat and rye.

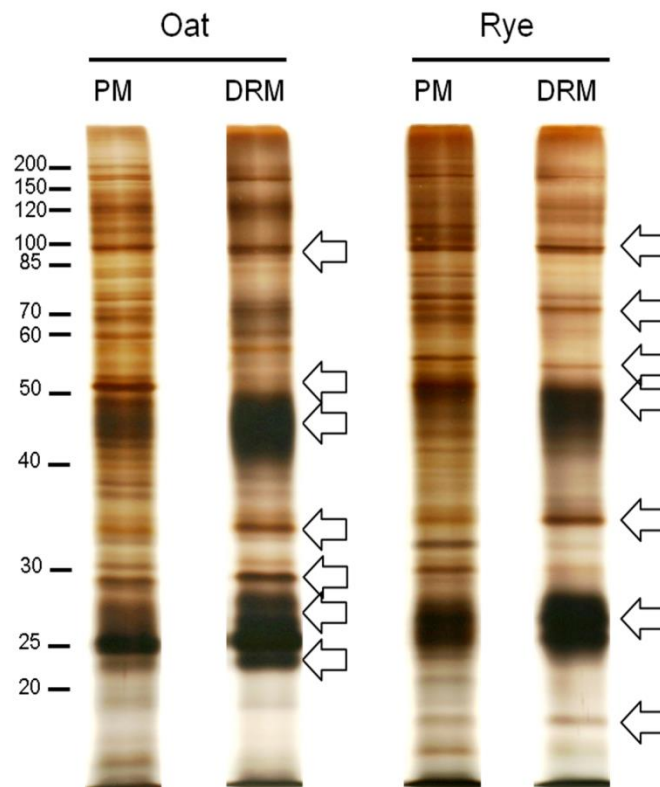


Fig. 2-1. SDS-PAGE profiles of PM and DRM proteins in oat and rye. Isolated PM and DRM fractions were separated by one-dimensional SDS-PAGE and subsequently visualized by silver staining. Arrows indicate proteins that show different accumulation patterns between the PM and DRM in oat or rye.

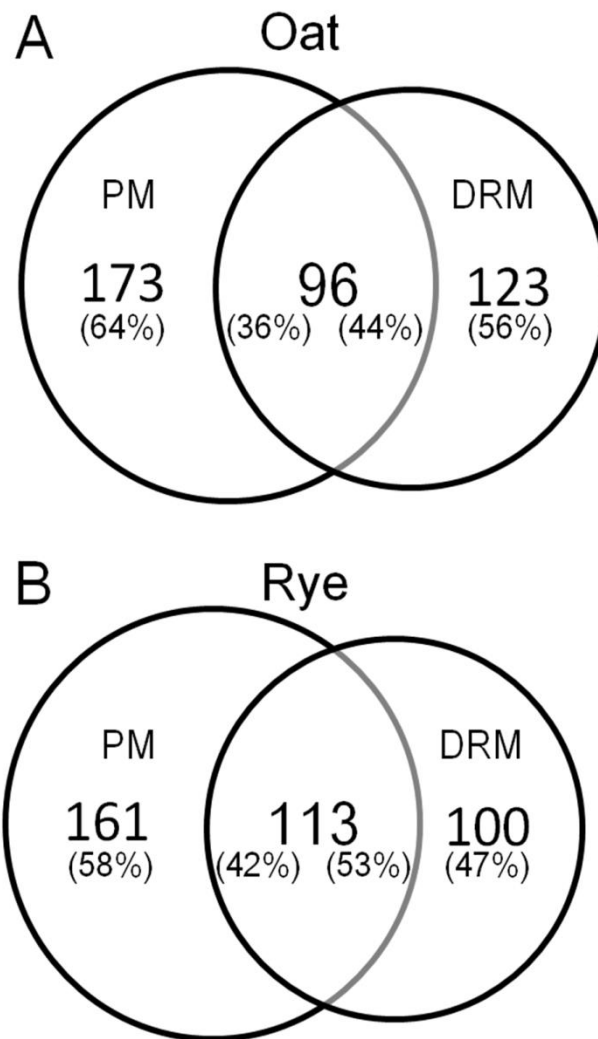


Fig. 2-2. Venn diagrams of PM and DRM proteins identified in oat and rye. (A) In oat, 268 PM proteins and 219 DRM proteins were identified by nano-LC-MS/MS based proteomic analysis. (B) In rye, 274 PM proteins and 213 DRM proteins were identified. The results indicated 96 and 113 proteins (shown in the overlapped areas in the diagram) are detected in both the PM and DRM fractions in oat and rye, respectively, based on GI accession number.

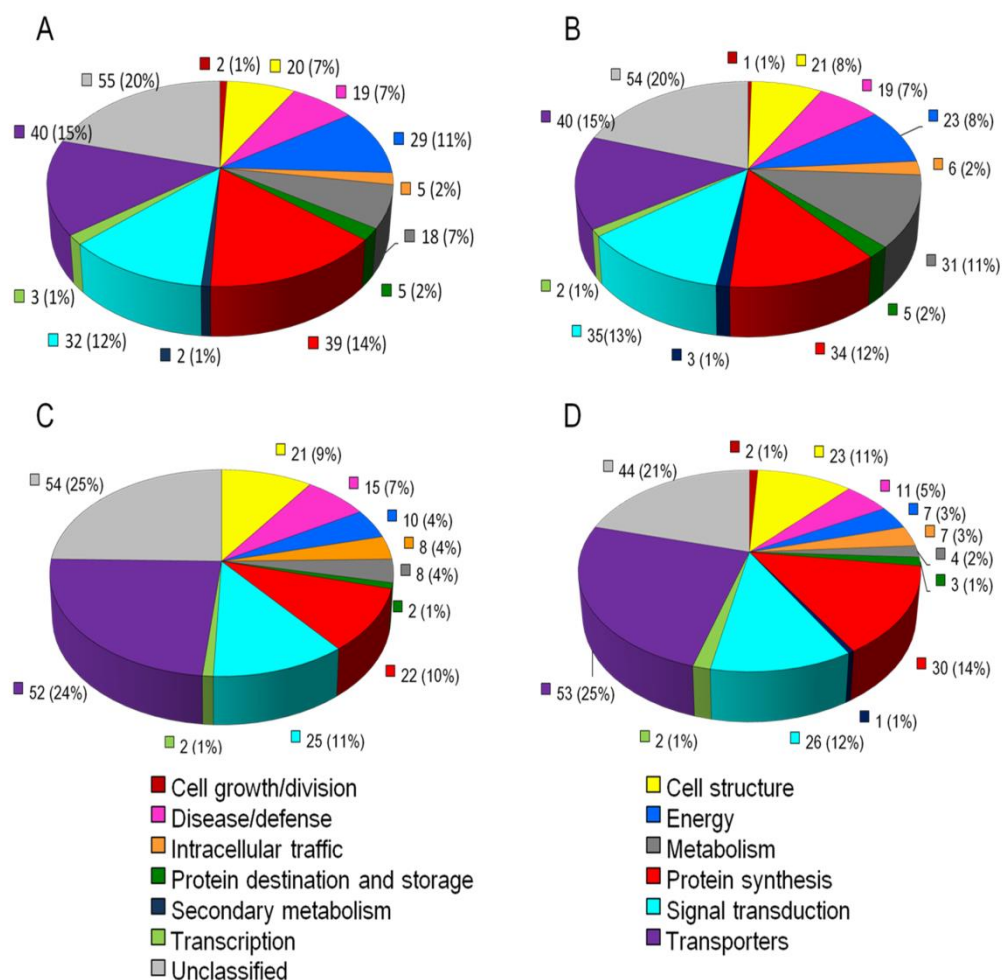


Fig. 2-3. Functional classification of identified PM and DRM proteins in oat and rye. Proteins identified were classified based on 13 categories previously described by Bevan et al. (1998). The number and proportion of proteins classified into each functional category are shown. (A) Oat PM, (B) rye PM, (C) oat DRM, and (D) rye PM.

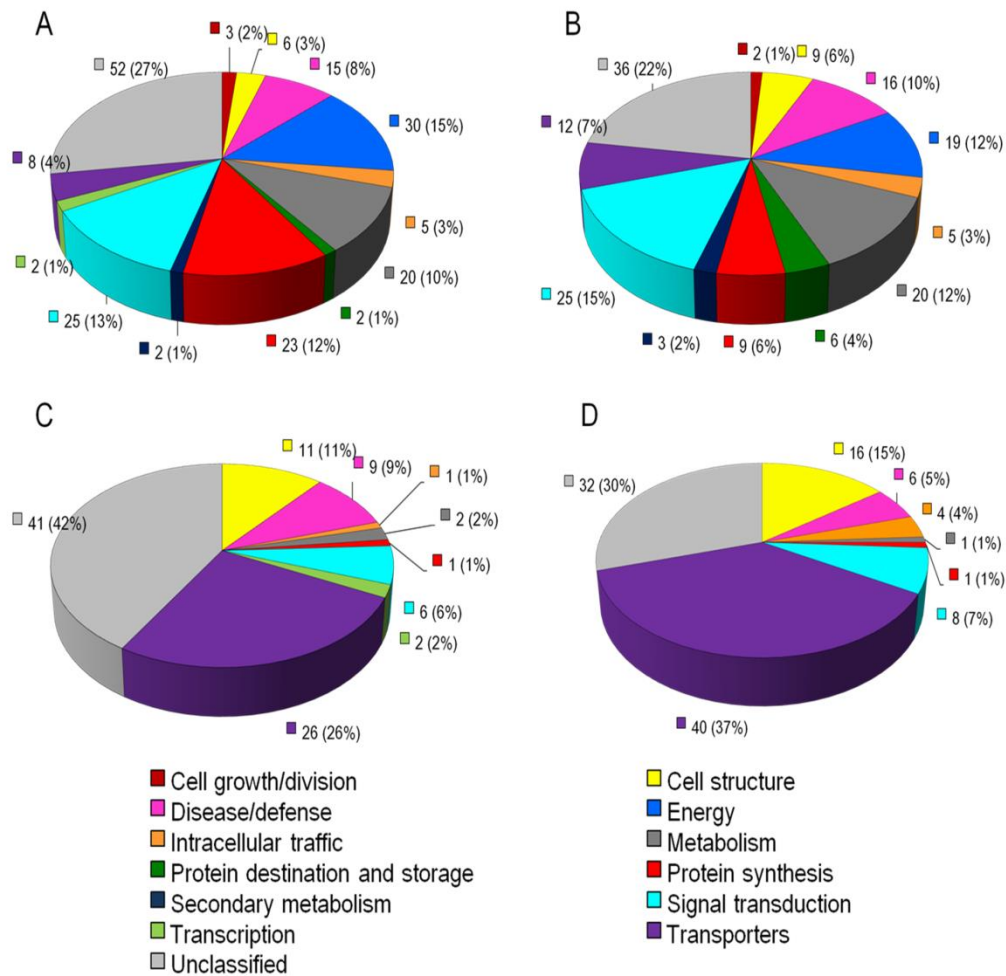


Fig. 2-4. Functional classification of identified proteins that show differential accumulation levels between PM and DRM in both oat and rye. Peptides with significantly different abundances between the PM and DRM were analyzed with Progenesis software with the following criteria: ANOVA $p < 0.05$; DRM/PM ratio, >2.0 or <0.5 ; expect value cut off, >0.05 . Subsequently, proteins were identified using the Mascot server and classified into 13 categories similar to the methods described in Fig. 2-3. Proteins with DRM/PM ratio <0.5 are shown for oat (A) and rye (B). Proteins with DRM/PM ratio >2.0 are shown for oat (C) and rye (D).

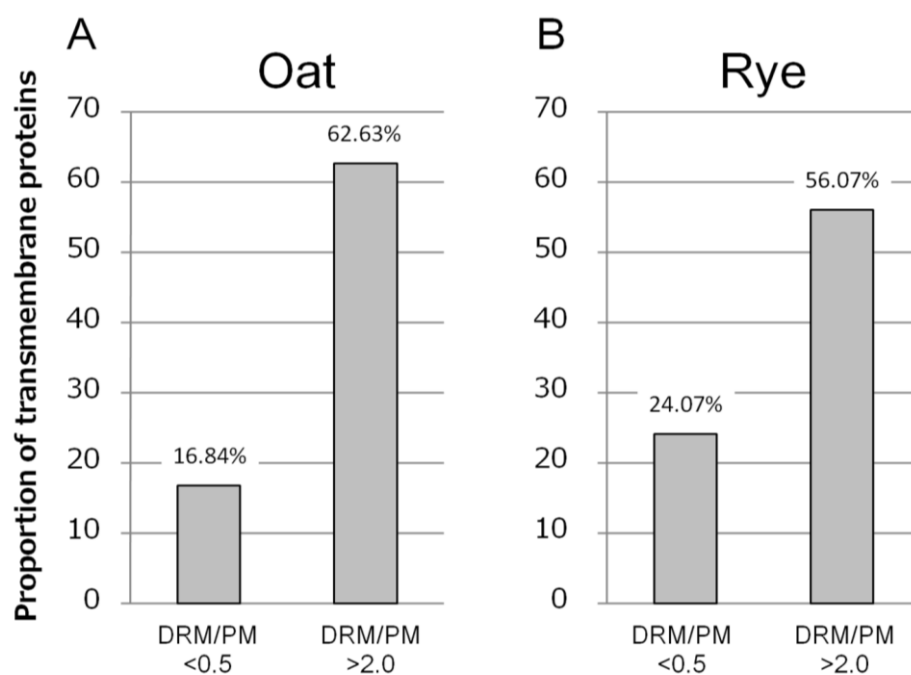


Fig. 2-5. Percentage of DRM-enriched and non-DRM-enriched membrane integral proteins. After Progenesis software analysis, sequences of proteins with different abundances between the PM and DRM were exported from the Mascot server. Using these sequences, transmembrane helices were predicted by the SOSUI engine.

Table 2-1. Proteins with differential distribution patterns common to the DRM and PM of oat and rye determined using Progenesis software. Accession no., NCBI GI number; Oat or rye confidence score, numbers generated from Progenesis software based on each peptide; Description, protein name identified using NCBI non-redundant protein database with Viridiplantae (green plant) taxonomy; Oat or rye DRM/PM, DRM/PM ratio of normalized abundance in oat and rye, respectively.

Accession no.	Oat confidence score	Rye confidence score	Description	Oat DRM/PM	Rye DRM/PM
gi 62861393	55.76	107.09	early salt stress and cold acclimation-induced protein 2-1	233.1650	0.2110
gi 15128407	142.15	77.16	putative receptor-like protein kinase	10.1739	3.6022
gi 18461174	102.87	59.01	1,3-beta-glucan synthase component-like	7.0112	9.3689
gi 55295882	162.01	211.6	putative beta 1,3 glucan synthase	5.8356	7.7014
gi 5080816	92.86	88.73	Putative ATPase	5.6228	9.7766
gi 205830697	72.12	65.4	Unknown protein 18	5.2707	9.8136
gi 23345042	799.05	507.19	hypersensitive-induced reaction protein 1	4.5199	3.2360
gi 224085778	117.7	119.17	predicted protein	4.2179	5.5787
gi 255644900	440.44	200.24	unknown	3.9797	3.2015
gi 115465815	45.75	30.35	Os05g0594500	3.8429	4.1762
gi 218191976	165.42	163.17	hypothetical protein OsI_09759	3.8166	4.8883
gi 108925894	78.48	186.52	vacuolar proton-ATPase D subunit	3.8055	3.6548
gi 242041551	65.55	185.95	hypothetical protein SORBIDRAFT_01g040970	3.2060	5.2347
gi 242041797	107.95	72.44	hypothetical protein SORBIDRAFT_01g043120	3.1558	3.2117
gi 68533200	173.61	560.79	PIP aquaporin isoform	3.1278	4.1047
gi 219885379	87.77	193.85	unknown	2.9883	3.0615
gi 7381267	99.5	248.23	plasma membrane intrinsic protein 1	2.9405	4.2838
gi 50400847	3196.21	1692.2	Plasma membrane ATPase; AltName: Full=Proton pump	2.8740	2.4096
gi 2655098	147.28	60.05	peptide transporter	2.7179	2.4255
gi 300119934	37.59	43.01	aquaporin	2.6548	6.9238
gi 77548264	584.88	199.57	Clathrin heavy chain, putative, expressed	2.4521	2.2652
gi 90289608	243.91	550.54	alpha tubulin-4D	2.2335	2.6986
gi 115474531	155.24	49.32	Os08g0117400	0.4659	0.4490
gi 312618322	55.17	198.16	phosphoinositide-specific phospholipase C1	0.4197	0.2659
gi 1703374	198.8	197.44	ADP-ribosylation factor 1	0.3904	0.4395
gi 16380	65.56	30.41	laminin receptor homologue	0.3332	0.3701
gi 8134568	112.54	131.49	5-methyltetrahydropteroyltriglutamate--homocysteine methyltransferase	0.3230	0.3808
gi 41052998	28.12	37.09	hypothetical protein	0.3099	0.1893
gi 53829387	35.03	34.31	SNARE 12	0.2723	0.2534
gi 15236014	45.74	56.16	lipid-associated family protein	0.2715	0.1928
gi 12585326	54.73	67.02	Phosphoglucosyltransferase, cytoplasmic	0.2425	0.3751
gi 354318	95.13	123.07	calmodulin	0.2271	0.1802
gi 642121	95.89	46.44	small GTP-binding protein	0.2270	0.4329
gi 303732	88.3	205.78	GTP-binding protein	0.2117	0.4145
gi 683502	39.72	55.15	protein phosphatase 2A 65 kDa regulatory subunit	0.1903	0.3844
gi 129916	30.28	38.2	Phosphoglycerate kinase, cytosolic	0.1870	0.1371
gi 303844	157.58	99.97	eukaryotic initiation factor 4A	0.1775	0.3954
gi 115458768	419.8	173.23	Os04g0459500	0.1772	0.2622
gi 12229949	47.03	39.79	40S ribosomal protein S12	0.1726	0.3990
gi 728594	55.12	42.3	glycine rich protein, RNA binding protein	0.1600	0.1334
gi 55773942	88.51	83.97	putative acyl-CoA synthetase	0.1410	0.1692
gi 55296571	119.06	138.61	putative nitrate-induced NOI protein	0.1381	0.0751
gi 115349904	47.61	41.27	fasciclin-like protein FLA10	0.1266	0.3703
gi 6136111	106.58	88.85	UTP--glucose-1-phosphate uridylyltransferase	0.1229	0.0270
gi 115441357	288.62	287.25	Os01g0874700	0.1221	0.0611
gi 115479005	42	63.73	Os09g0394900	0.1005	0.4708
gi 22607	307.41	663.92	14-3-3 protein homologue	0.0936	0.1804
gi 115435222	41.3	111.49	Os01g0210600	0.0775	0.1771
gi 162462820	83.88	38.33	LOC542588	0.0597	0.3282
gi 115451911	185.16	241.4	Os03g0248600	0.0385	0.0350
gi 400404	55.89	83.76	Nucleoside diphosphate kinase 1	0.0336	0.0107
gi 226897529	34.99	61.75	superoxide dismutase	0.0314	0.2359
gi 587546	53.64	44.7	P23 protein	0.0301	0.1268
gi 9798603	142.12	142.25	TaWIN1	0.0301	0.0866
gi 439586	90.84	98.91	calreticulin	0.0277	0.0582
gi 115442509	98.25	26.35	Os01g0971500	0.0272	0.1765
gi 544242	58.56	52.42	Endoplasmic reticulum chaperone	0.0176	0.0368
gi 223018643	504.78	183.7	chloroplast fructose-bisphosphate aldolase	0.0052	0.0085
gi 18650668	113.56	140.15	temperature stress-induced lipocalin	0.0023	0.0227
gi 1885312	51.56	74.15	PM2	0.0016	0.1623

Table 2-2. Putative GPI-anchored proteins in oat and rye. Accession no., NCBI GI number; Description, protein name identified using NCBI non-redundant protein database with Viridiplantae (green plant) taxonomy; Max. score, Max. match and Max. coverage, maximum of each experimental value in four experiments; Number of identified, the times that the protein was identified in four independent experiments; Function, functional category of identified proteins based on Bevan et al. (1998).

Accession no.	Description	Max. score	Max. match	Max. coverage	Number of identified	Function
Oat PM						
gij115349890	fasciclin-like protein FLA3	61	1	2.6	4	Cell structure
gij115455021	Os03g0722500	58	1	2.5	2	Cell structure
gij115349904	fasciclin-like protein FLA10	58	2	10.2	2	Cell structure
gij108706373	Protease inhibitor/seed storage/LTP family protein, expressed	50	2	9.6	4	Protein destination and storage
Rye PM						
gij115349916	fasciclin-like protein FLA16	203	6	29.7	4	Cell structure
gij115349890	fasciclin-like protein FLA3	109	2	7.2	4	Cell structure
gij115349914	fasciclin-like protein FLA15	94	3	9.7	3	Cell structure
gij115349920	fasciclin-like protein FLA18	70	4	13.3	4	Cell structure
gij38636838	putative blue copper binding protein	55	1	8.4	2	Energy
gij82780752	lipid transfer protein	52	3	14.6	4	Transporters
gij4104058	blue copper-binding protein homolog	48	1	5.7	4	Energy
gij62861393	early salt stress and cold acclimation-induced protein 2-1	47	2	9.2	4	Disease/defense
Oat DRM						
gij115435214	Os01g0209800	50	1	2.3	2	Transporters
Rye DRM						
gij115435214	Os01g0209800	104	3	2.3	3	Transporters
gij115349890	fasciclin-like protein FLA3	102	2	7.2	2	Cell structure
gij82780752	lipid transfer protein	56	3	11.4	4	Transporters

Table 2-3. Putative GPI-anchored proteins in oat and rye together with the ratio of DRM/PM from Progenesis analyses. Accession no., NCBI GI number; Description, protein name identified using NCBI non-redundant protein database with Viridiplantae (green plant) taxonomy; Confidence score, numbers generated from Progenesis analysis based on each peptide; ANOVA (*p*), ANOVA *p*-value from all matched peptides in four replicates; DRM/PM, the ratio of protein abundance in DRM to PM calculated with Progenesis software; Function, functional category of identified proteins based on Bevan et al. (1998).

Accession no.	Description	Matched peptides	Confidence score	ANOVA (<i>p</i>)*	DRM/PM	Function
Oat DRM/PM						
gi 62861393	early salt stress and cold acclimation-induced protein 2-1	1	55.76	0.0019	233.1650	Disease/defense
gi 41469392	putative protease inhibitor	1	38.78	3.65E-05	0.1290	Protein destination and storage
gi 115349904	fasciclin-like protein FLA10	1	47.61	0.0028	0.1266	Cell structure
gi 115349890	fasciclin-like protein FLA3	1	61.44	0.0018	0.1095	Cell structure
Rye DRM/PM						
gi 20197794	putative 1,3-beta-D-glucan synthase	2	99.48	0.0015	4.5811	Cell structure
gi 115349904	fasciclin-like protein FLA10	1	41.27	0.0212	0.3703	Cell structure
gi 82780752	lipid transfer protein	3	113.77	0.0072	0.3143	Transporters
gi 115476754	Os08g0459300	1	36.77	0.0023	0.3130	Unclassified
gi 115349914	fasciclin-like protein FLA15	2	97.81	0.0362	0.2569	Cell structure
gi 115349920	fasciclin-like protein FLA18	3	126.95	0.0050	0.2542	Cell structure
gi 4104058	blue copper-binding protein homolog	1	48.19	0.0006	0.2359	Energy
gi 62861393	early salt stress and cold acclimation-induced protein 2-1	2	107.09	0.0129	0.2110	Disease/defense
gi 115349916	fasciclin-like protein FLA16	5	325.43	0.0053	0.1483	Cell structure
gi 115349912	fasciclin-like protein FLA14	1	35.15	0.0001	0.1197	Cell structure
gi 38636838	putative blue copper binding protein	1	55.13	0.0343	0.0281	Energy

Chapter 3

Changes of detergent-resistant plasma membrane proteins in oat and rye during cold acclimation: association with difference in freezing tolerance

Summary

Cold acclimation (CA) results in an increase in freezing tolerance of plants, which is closely associated with functional changes of the plasma membrane (PM). Although proteomic studies have revealed compositional changes of the PM during CA, there has been no large-scale study of how the microdomain in the PM, which contains specific lipids and proteins, changes during CA. Therefore, I conducted semiquantitative shotgun proteomics using microdomain-enriched detergent-resistant membrane (DRM) fractions extracted from low freezing-tolerant oat and highly freezing-tolerant rye. I identified 740 and 809 DRM proteins in oat and rye, respectively. Among the proteins identified, the abundances of a variety of proteins, such as P-type ATPase and aquaporins, were affected by CA in both oat and rye. Some CA-responsive proteins in the DRM fractions, such as heat shock protein 70, changed differently in oat and rye. In addition, changes in lipocalins and sugar transporters in the DRM fractions were different from those found in total PM fraction during CA. This is the first report to describe compositional changes in the DRM during CA at a large scale. The proteomic profiles obtained in the present study hint at many possible microdomain functions associated with CA and freezing tolerance.

Introduction

Freezing tolerance of temperate plants increases significantly, when the plants are exposed to non-freezing, low temperatures. This is termed cold acclimation (CA), which is one of the abiotic stress adaptation mechanisms of plants. During this process, many intracellular changes occur that enhance plant freezing tolerance in a complex manner. These changes include expressional changes of transcription factors and their target genes (Thomashow, 1999). As a result, cold-induced proteins, such as LEA (late embryogenesis abundant) and COR (cold regulated) proteins (Welin et al., 1994; Thomashow, 1998) accumulate, and compatible solutes (Koster and Lynch, 1992) are synthesized. In addition, compositional and functional changes of the plasma membrane (PM) occur, which together contribute to the increase in freezing tolerance (Steponkus, 1984; Thomashow, 1999). Under cold conditions, the PM plays important roles in temperature sensing and signal transduction (Murata and Los, 1997; Plieth, 1999; Örvar et al., 2000). In addition, the PM behaves as the final barrier against dehydration and invasion of ice crystals from the outside of cells during extracellular freezing, a typical way of freezing in temperate herbaceous plants, and tolerates an extreme change of surface area during a freeze-thaw cycle (Steponkus, 1984; Khan et al., 2009). Thus, damage to PM function and structure would be lethal to cells, and plants must have mechanisms to protect the PM against stresses imposed by a freeze-thaw cycle. In fact, manifestation of freezing injury associated with the PM has been frequently reported as ultrastructural changes, such as fracture-jump lesions and hexagonal II phase transitions occurring at freezing temperature (Gordon-Kamm and Steponkus, 1984b; Webb and Steponkus, 1993). Thus, it is reasonable to assume that compositional changes in the PM influence directly on the development of freezing tolerance during CA. As expected, several studies have shown that the lipid (such as lipid class and unsaturation degree of acyl chains in glycerolipids) and protein (both qualitative and quantitative) compositions of the PM change dynamically during CA (Uemura and Yoshida, 1983; Yoshida and Uemura, 1984; Lynch and Steponkus, 1987; Uemura and Steponkus, 1994; Kawamura and Uemura, 2003).

Distribution of lipid and protein components in the PM was thought to be homogenous, and to move dynamically in the membrane as proposed in the fluid-mosaic model (Singer and Nicolson, 1972). However, the concept of a microdomain that is enriched in specific lipids and proteins with restricted movement has been proposed recently (Simons and Ikonen, 1997). Microdomains contain sphingolipids and sterols, both of which tend to gather together because of their hydrophobic characteristics (Brown and London, 1998; Brown and London, 2000;

London and Brown, 2000), and specific functional proteins. In animal cells, microdomains act as scaffolds in association with membrane trafficking, signal transduction and the endocytosis and exocytosis pathways. Microdomains can be biochemically extracted as detergent-resistant membranes (DRMs), which is a fraction resistant to non-ionic detergent treatment on ice (Schroeder et al., 1994; Simons and Ikonen, 1997; Brown and London, 1998). In plants, DRMs have been used widely for microdomain research in several species, such as tobacco, *Arabidopsis thaliana*, leek, *Medicago truncatula*, potato, rice, oat and rye (Peskan et al., 2000; Mongrand et al., 2004; Borner et al., 2005; Laloi et al., 2006; Morel et al., 2006; Lefebvre et al., 2007; Krügel et al., 2008; Fujiwara et al., 2009; Minami et al., 2009; Takahashi et al., 2012). Plant microdomains are also suggested to be involved in pollen tube tip growth and intercellular movement of viruses (Liu et al., 2009; Raffaele et al., 2009).

The relationship between CA and PM microdomains has been studied recently in *Arabidopsis* cells using isolated DRM fractions (Minami et al., 2009; Minami et al., 2010). During CA, the lipid composition of *Arabidopsis* DRM fractions changed considerably, but differently, from those of the total PM fraction. Furthermore, DRM-enriched proteins such as H⁺-ATPases, aquaporins, clathrins and dynamin-related proteins showed significant changes during CA. These results suggest that microdomains have specific roles in the CA mechanism. I previously characterized DRM fractions prepared from oat (*Avena sativa*) and rye (*Secale cereale*) grown under non-acclimated (NA) conditions. The protein compositions of DRM fractions in these two monocotyledonous plants were similar, and some proteins were conserved in oat, rye and *Arabidopsis* (Takahashi et al., 2012; Chapter 2 in this thesis). I selected these two monocotyledonous plants because these are closely related phylogenically, but have vastly different freezing tolerances after CA (Webb et al., 1994). Therefore, it is reasonable to hypothesize that the protein compositions of oat and rye change differently during CA, permitting us to discuss the roles of DRM proteins in the mechanisms of CA and freezing tolerance in plants.

In the present study, I performed shotgun proteomic analyses of DRMs isolated from the PMs of leaves of oat and rye before and after CA. In addition, label-free semi-quantification of DRM proteins was carried out to further profile how DRM proteins change during CA. To the best of our knowledge, this is the first large-scale analysis of DRM proteins associated with an abiotic environmental stress response in a plant system using label-free shotgun proteomics. Based on these results, I will discuss possible functional contributions of the DRM fraction to CA in plants.

Experimental procedures

Plant Materials

Seeds of oat (*Avena sativa* cv. New Almighty) and rye (*Secale cereale* cv. Maskateer) were sown in vermiculite supplemented with Hoagland solution at 18°C with a 16 h photoperiod (90 $\mu\text{mol}/\text{m}^2/\text{s}$). After 12 to 14 days, leaves were harvested for experiments as NA plants. To obtain CA plants, NA oat and rye plants were further grown at 2°C with a 12 h photoperiod (100 $\mu\text{mol}/\text{m}^2/\text{s}$) for 4 weeks.

Evaluation of Freezing Tolerance

The electrolyte leakage method has been used widely for evaluation of plant freezing tolerance (Murray et al., 1989; Maier et al., 1994) and was employed in the present study. Harvested leaves were washed with precooled water and dried with Kimtowel. The leaves were cut into 1 cm pieces, put into glass tubes with aliquots of water (100 μl) and cooled in an alcohol bath (NCB-3400, EYELA, Tokyo, Japan) at -2°C for 15 min. After ice nucleation by addition of ice droplets (50 μl in volume) and equilibration of the temperature at -2°C for 2 h, samples were cooled further at a rate of -2°C/h. At specified temperatures, samples were transferred at 4°C. After incubation overnight for thawing, 4 ml of water were added and samples were shaken for 150 min. Then, a conductance meter (Twin Cond, HORIBA, Kyoto, Japan) was used to measure electrolytes that had leaked from cells during freeze-thawing. Subsequently, samples were boiled for 20 min and shaken for 150 min. Then, electrolytes fully leaked from cells were measured again. Using the two measured values, the ratio of electrolyte leakage caused by freeze-thawing was calculated (leakage at the first measurement/leakage at the second measurement).

Isolation of Plasma Membrane and Detergent-resistant Membrane Fractions

A PM preparation was performed using a polyethylene glycol-dextran aqueous two-phase partition system, as described previously (Uemura and Steponkus, 1994; Takahashi et al., 2012). All procedures were conducted on ice. Leaves were chopped and homogenized in a medium composed of 0.5 M sorbitol, 50 mM Mops/KOH (pH 7.6), 5 mM EGTA, 5 mM EDTA, 5% (w/v) polyvinylpyrrolidone (MW: 40,000), 5% (w/v) BSA, 2.5 mM phenylmethanesulfonyl fluoride, 4 mM salicylhydroxamic acid and 2.5 mM dithiothreitol using a Polytron (Kinematica PT10-35, Brinkmann Instruments, Westbury, NY, USA). After filtering with gauze, homogenates were centrifuged at $10,000 \times g$ for 15 min and subsequently at $231,000 \times g$ for 50 min. The pellets obtained were suspended in a microsome suspension medium (0.25 M sucrose and 10 mM

KH₂PO₄/K₂HPO₄ [pH 7.8]) and centrifuged again as above. The resultant pellets were resuspended in a two-phase partition solution consisting of 5.8% (w/w) polyethylene glycol (MW: 3,350; Sigma-Aldrich, St Louis, MO, USA), 5.8% (w/w) dextran (Sigma-Aldrich), 0.25 M sucrose, 30 mM NaCl, and 10 mM KH₂PO₄/K₂HPO₄ (pH 7.8). The two-phase system was mixed well and centrifuged at 650 × *g* for 5 min. The resultant upper phase was collected and added into a newly-prepared lower phase, mixed and then centrifuged as above. These processes were repeated three times to increase the purity of the PM. The final upper phase was collected, diluted with a PM suspension medium (0.25 M sucrose, 10 mM Mops/KOH (pH 7.3) and 2 mM EGTA) and precipitated by ultracentrifugation as described above. This process was repeated twice to remove the polymers completely.

Preparation of DRM fractions was carried out according to the method of Peskan et al. (2000). Purified PM pellets were resuspended in 2.7 ml of TED buffer consisting of 50 mM Tris-HCl (pH 7.4), 3 mM EDTA, and 1 mM dithiothreitol. An aliquot of 10% (w/v) Triton X-100 in TED buffer (300 µl) was then added into PM suspension and the PM-TX-100 mixture was incubated for 30 min on ice. To the PM-TX-100 mixture, 12 ml of 65% (w/w) sucrose in TED buffer were immediately added and mixed well. Then, 48, 35, 30, and 5% (w/w) sucrose-TED solutions were subsequently overlaid on the PM-TX-100 mixture and centrifuged at 141,000 × *g* for 20 h at 4°C using a swing-type rotor P28S (Hitachi Koki, Tokyo, Japan) to obtain DRM fractions. After centrifugation, a white band at the interface of the 30% and 35% (w/w) sucrose layers (Fig. 3-1.) was collected, diluted with PM suspension medium and centrifuged at 231,000 × *g* for 50 min. This fraction was designated DRM. Protein content of PM and DRM suspensions were measured using the Bradford assay (Bio-Rad, Munich, Germany) with BSA as a standard.

One-dimensional SDS-PAGE

PM and DRM samples (equivalent to 1 µg protein) were suspended in an equal volume of sodium dodecyl sulfate (SDS) sample buffer (2% [w/v] SDS, 50 mM Tris-HCl [pH 6.8], 6% [v/v] β-mercaptoethanol, 10% [w/v] glycerol and bromophenol blue) and denatured by heating at 95°C for 20 min. Proteins were separated on a 10% (w/v) polyacrylamide gel with a 4.5% (w/v) stacking gel, and visualized by silver staining (Kawamura and Uemura, 2003).

Sample Preparation and Data Acquisition for Nano-LC-MS/MS Analysis

Protein samples (50 µg protein) were subjected to in-solution tryptic digestion for nano-LC-MS/MS analysis according to the protocol of Takahashi et al. (2012; Chapter 2 in this thesis). Membrane fractions were precipitated by centrifugation and dissolved in a detergent mixture (MPEX PTS Reagents for MS, GL Science, Tokyo, Japan). Proteins (5 µg) determined with the Pierce BCA Protein Assay Kit (Pierce, Rockford, IL, USA) were digested by trypsin according to instruction manual of MPEX PTS Reagents provided by the manufacturer. The peptide samples were desalted with SPE C-TIP (AMR, Tokyo, Japan) and the volume was adjusted to 15 µl with 0.1% [v/v] trifluoroacetic acid. Peptide solutions were subjected to nano-LC-MS/MS analysis (Takahashi et al., 2012a). The data acquisition steps using ADVANCE UHPLC system (MICHROM Bioresources, Auburn, CA, USA) and LTQ Orbitrap XL mass spectrometer (Thermo Fisher Scientific, Waltham, MA, USA) are described in Takahashi et al. (2012). These experiments were repeated four times with samples collected from biologically independent plants.

Analysis of Nano-LC-MS/MS Data

Raw files of MS/MS spectra were converted to the mgf format using Proteome Discoverer (ver. 1.1.0.263, Thermo Fisher Scientific) under the following parameters: precursor mass range, m/z 350–5000; highest and lowest charge state, 0; lower and upper RT limit, 0; the minimum total intensity of a spectrum, 0; and the minimum number of peaks in a spectrum, 1. Peptide data obtained were searched and proteins were identified using the MASCOT search engine (version 2.3.02, Matrix Science, London, UK) searching against the NCBI nr Green Plants database (version 20121002, comprising 1,095,445 sequences) for quantification of DRM fraction proteins according to the following parameters: number of missed cleavage, 1; fixed modifications, carbamidomethylation (C); variable modifications, oxidation (M); peptide mass tolerance, 5 ppm; MS/MS tolerance, 0.6 Da; and Peptide charges, +1, +2 and +3. The false discovery rate (FDR), which is based on a search of the Mascot decoy database, was less than 5%. Definitions of identified proteins were based on the following filters: including at least one unique top-ranking peptide; ion score cut off ≤ 0.05 ; and identified two or more times in four repeated experiments. If a peptide was assigned to multiple proteins, the highest-scoring protein was selected in the list. In semi-quantitative analysis, raw files were subjected to Progenesis LC-MS software (version 4.0, Nonlinear Dynamics, New Castle, UK). Peptides were assigned to proteins by

MASCOT searching as described above. Finally, significant proteins were filtered with ANOVA ($p < 0.05$) and fold change (> 2.0) according to normalized peptide intensity.

Topology and Post-translational Modification Prediction

Acquired proteins were used for prediction of transmembrane domains, signal peptides, cellular locations, sites of glycosylphosphatidylinositol (GPI) modification and myristoylation using the following online tools: transmembrane domains, SOSUI engine version 1.10 (<http://bp.nuap.nagoya-u.ac.jp/sosui/>); cellular locations, TargetP 1.1 server (<http://www.cbs.dtu.dk/services/TargetP/>); signal peptides and membrane anchor peptides, SignalP 3.0 server (<http://www.cbs.dtu.dk/services/SignalP/>); GPI modification, Big-PI Plant Predictor (http://mendel.imp.ac.at/gpi/plant_server.html); and N-terminal myristoylation, Plant-Specific Myristoylation Predictor (<http://plantsp.genomics.purdue.edu/plantsp/html/myrist.html>).

Results and discussion

Freezing Tolerance in Oat and Rye

Freezing tolerance of oat and rye leaves was measured during CA by the electrolyte leakage method (Fig. 3-2). Various evaluation methods have been reported for determining plant freezing tolerance, such as electrolyte leakage measurement, the re-growth method and photosynthesis activity measurement (Oquist et al., 1993; Ehlert and Hinch, 2008). The electrolyte leakage method, which measures conductivity derived from electrolytes in medium leaked from the cytoplasm by a freeze-thawing, determines the extent of freezing injury directly occurring on the PM, which is the primary site of the freezing injury (Steponkus, 1984; Murray et al., 1989). Thus, I believe that the electrolyte leakage measurement is suitable for characterizing PM proteome changes during CA.

In NA plants, the temperature at which 50% of electrolyte leakage occurs (LT_{50}) was -5°C in oat and -8°C in rye. CA decreased the LT_{50} in both oat and rye. In oat, CA treatment for 1 week increased freezing tolerance to the LT_{50} of -8°C , but the LT_{50} did not change further after CA for 2 weeks or longer. On the other hand, the LT_{50} in rye decreased to -16 to -18°C after CA for 1 week and was further lowered with prolonged CA; after CA for 4 weeks, the LT_{50} was -20°C . These results showed that freezing tolerances of oat and rye are different in NA plants, and the difference was further enhanced after CA. Our observations are consistent with results of a previous study (Webb et al., 1994). Additional increases in freezing tolerance were not observed after

CA for 5 weeks in both oat and rye (Webb et al., 1994); therefore, I used oat and rye leaves before and after 4 weeks of CA for PM and DRM proteomic studies.

Isolation and Characterization of PM and DRM Fractions

The overall workflow of the present study is described in Fig. 3-3. PM fractions were prepared from leaves of oat and rye before and after CA with four biological independent plant samples, and a half of each fraction was used for extraction of the DRM fraction. All these fractions were subsequently subjected to nano-LC-MS/MS analysis and identification of compositional differences among the samples under the same conditions.

When purified PM samples were incubated with Triton X-100 on ice and subsequently subjected to sucrose density gradient centrifugation, a white band that is considered to contain DRM was visible at the interface of the 30 and 35% sucrose layers for both oat and rye (Fig. 3-1.). In our previous study, the recovery of DRM from PM fractions (based on protein amount) in NA samples was 10-20% and 8-12% for oat and rye, respectively (Takahashi et al., 2012; Chapter 2 in this thesis). This tendency was the same and the recovery was less in the CA samples than in the NA samples: the recovery of DRM fraction from the PM was 6-12% in oat and 5-8% in rye (data not shown). The decrease in the recovery of DRM fractions after CA was also reported for PMs of *Arabidopsis* (Minami et al., 2009). This might reflect differences in lipid and protein compositions in DRMs in leaves before and after CA (Minami et al., 2009; Minami et al., 2010), which may change the resistance to detergent treatment.

One-dimensional SDS-PAGE revealed considerable differences in protein compositions between the DRM and PM in both NA and CA samples, as well as between NA and CA in both PM and DRM fractions (Fig. 3-4). Some proteins were highly enriched in the DRM and some of the DRM fraction proteins changed during CA. Several proteins were enriched in DRM in both species before and after CA (i.e. No. 4 in oat and No. 2 in rye in Fig. 3-4). These results are consistent with previous studies in *Arabidopsis* and tobacco (Mongrand et al., 2004; Borner et al., 2005; Morel et al., 2006), in which the authors reported vast differences in protein compositions between the DRM and PM.

Furthermore, in both oat and rye, some proteins increased or decreased in DRM and PM fractions during CA (Fig. 3-4). Although some proteins changed during CA in both PM and DRM fractions (e.g., No. 2 in CA oat PM and DRM, and No. 3 and No. 4 in CA rye PM and DRM), there were proteins that changed only in the DRM fraction but not in the PM fraction (e.g., No. 5 in CA oat DRM and No. 6 in CA rye DRM).

CA-induced changes in DRM protein composition have been reported in *Arabidopsis* (Minami et al., 2009). When CA-induced changes in the DRM were compared between oat and rye, some proteins were found to change in both species (e.g., No. 2 in CA oat DRM and No. 3 in CA rye DRM). However, changes of some proteins were species-dependent (e.g., No. 5 in CA oat DRM and No. 9 in rye DRM). Collectively, these results suggest that the microdomain has specific functions in the PM and has different effects on the CA mechanism depending on plant freezing tolerance.

Identification and Functional Categorization of DRM proteins

PM and DRM proteins were subjected to LTQ Orbitrap XL mass spectrometry analysis after digestion with trypsin. I identified 304 PM proteins and 227 DRM fraction proteins in oat, and 329 PM proteins and 255 DRM fraction proteins in rye under NA conditions (Supplemental Tables 3-1 and 3-2). Furthermore, 283 PM proteins and 199 DRM fraction proteins in oat and 314 PM proteins and 256 DRM fraction proteins in rye were identified under CA conditions. Identified proteins were classified into 13 functional categories, according to Bevan et al. (1998). In particular, cell structure-related proteins, signal transduction-related proteins and transporters were frequently identified in both the PM and DRM in oat and rye. For example, 21% of identified DRM fraction proteins in NA rye were transporters.

Signal intensities, which are related to the extent of accumulation of each peptide, were then calculated and normalized using Progenesis LC-MS software. In this software, quantification steps were based on not fragment ion mass, but on peptide mass signals (Matros et al., 2011). Protein identification processes then were conducted using multiplex mass data sets derived from PM and DRM analysis under NA and CA conditions in each of four replicates to minimize data loss and increase proteome coverage. From these analyses, I identified 740 and 809 DRM fraction proteins in oat and rye, respectively. Among them, 136 and 220 DRM proteins responded to CA treatment in oat and rye (fold change >2.0, ANOVA $p < 0.05$), and were analyzed further to elucidate the function of DRM in CA (Supplemental Table 3-3).

The accumulation of each protein in the PM and DRM fractions was first compared to reveal the enrichment in the DRM before and after CA. In the quantification process, the DRM/PM ratio of proteins was calculated using the normalized abundance of each protein. Subsequently, DRM-enriched (DRM/PM > 2.0, ANOVA $p < 0.05$), DRM-non-enriched proteins (DRM/PM < 0.5, ANOVA $p < 0.05$) and not-preferentially-partitioned proteins (DRM/PM < 2.0 or > 0.5, ANOVA $p > 0.05$) were classified into 13 functional categories, based on Bevan et al. (1998; Fig. 3-5). These

results clearly showed that specific protein groups were enriched in DRM fractions. In NA samples, the proportion of transporters in the DRM-enriched proteins was greater (by 7.3 times in oat and 6.7 times in rye) than in DRM-non-enriched proteins (Fig. 3-5A and 3-5C). Proteins classified in the category of energy, metabolism and protein synthesis were not so enriched in the DRM. I found that there are differences between oat and rye in the proportion of DRM-enriched disease/defense-related proteins. Oat contained a significantly higher proportion of DRM-enriched disease/defense proteins than rye did, based on Fisher's exact test ($p < 0.01$). In oat, the proportions of disease/defense proteins were less in DRM-non-enriched proteins than in DRM-enriched ones.

Considering CA conditions, the proportions of each category of DRM-enriched and non-enriched proteins such as energy, protein synthesis, disease/defense and transporters did not change after CA. Although cell structure-related proteins such as actins and tubulins are also known as DRM-enriched proteins and are CA-responsive (Kerr and Carter, 1990; Örvar et al., 2000; Ouellet et al., 2001; Abdrakhamanova et al., 2003; Kawamura and Uemura, 2003), proportional changes of these proteins during CA were not significant in either species. These results indicate that CA does not affect the DRM proteome qualitatively. Many not-preferentially-partitioned proteins, which were not affected by detergent treatment on ice, were also identified in oat and rye. While proteins related to protein synthesis and signal transductions tended not to be enriched in or were removed from DRM fractions, transporters were considerably underrepresented in non-preferentially-partitioned proteins than in DRM-enriched proteins after CA. These results indicate that transport proteins are susceptible to the effects of lateral segregation on the PM.

Next, I calculated the CA/NA ratio of proteins in the DRM and PM to reveal what proteins significantly increased and decreased or did not change after CA (Fig. 3-6). Changes in PM and DRM protein compositions during CA seemed to be similar in both oat and rye. For example, in all fractions examined, disease/defense- and signal transduction-related proteins increased in the DRM and PM after CA, and protein synthesis and transport-related proteins decreased after CA. When looking at the data in detail, the decrease of the proportion of protein synthesis proteins mostly represented decreases in ribosomal proteins in the fraction. For example, the CA/NA ratios of gi|3986695 in oat and rye PM were 0.27 and 0.45, respectively (Supplemental Table 3-3). Ribosomal proteins are related to protein translation and are located in the endoplasmic reticulum (ER; Barakat et al., 2001). In barley, CA resulted in an induction of the transcript level of ribosomal proteins (Svensson, 2006). Considering these results,

changes to the PM-ER interaction may occur during CA and result in decreased ribosomal proteins in the PM.

I also found that some transporters decreased after CA in the PM and DRM fractions, including many V-type ATPases and aquaporins. V-type ATPase is known to be located in various membranes, including the PM, in plant cells, in addition to tonoplast (Depta et al., 1991; Robinson et al., 1996; Kluge et al., 2004), and responds to salt stress (Batelli et al., 2007) and CA (Kawamura and Uemura, 2003). Thus, V-type ATPase may be involved in the CA mechanism through intracellular pH regulation. The number of CA-increased disease/defense-related proteins accounted for 13% in the PM and 24% in the DRM in oat, whereas they accounted for 11% in the PM and 7.6% in the DRM, in rye. The components of the proteins in this category were quite different between oat and rye. Oat had several CA-increased heat shock proteins, especially in DRM fractions. On the other hand, there were a variety of cold stress-related proteins such as dehydrins/LEA proteins and lipocalins in both the PM and DRM of rye. In particular, dehydrin is well known to have multiple functions to enhance cold tolerance, such as cryoprotective and antifreeze activities (Wisniewski et al., 1999). Dehydrin was observed to bind lipid vesicle and has important roles for protection and stabilization of lipids and proteins under freezing temperature (Hara et al., 2003; Koag et al., 2003). Thus, it may be reasonable to hypothesize that rye has a number of cold stress-related proteins that protect the microdomain and, hence, increase freezing tolerance during CA. Collectively, the differences in alterations in PM and DRM proteome described above suggest that cold responses in the PM are different, both inside of the DRM (e.g., microdomains) and outside of the DRM.

Abundance-based Analysis of DRM-enriched Proteins in Oat and Rye

I further calculated the normalized abundance of each of DRM-enriched protein using Progenesis software and the proportions of the proteins in each functional category (Fig. 3-7). In NA DRM samples, transporters accounted for 63% and 66% of proteins by abundance in oat and rye, respectively (Fig. 3-7A and 3-7B). Almost all the transporters enriched in the DRM were ATPases and aquaporins (Supplemental Table 3-3). ATPase has been demonstrated to accumulate in lipid rafts in yeast cells (Bagnat et al., 2001). In addition, sterols, which are enriched in microdomains, and the proportion and the class of which differs considerably in oat and rye DRM fractions (Takahashi et al., 2011), are able to regulate ATPase activity (Grandmougin-Ferjani et al., 1997). Taken together, these results suggest that microdomains are associated with a sterol-ATPase regulation mechanism as a scaffold, and that sterol compositions affect

intra- and extracellular pH and membrane potential, which would ultimately influence freezing tolerance of plants.

The second predominant category in NA DRM samples was disease/defense- and cell structure-related proteins in oat and rye, respectively (Fig. 3-7A and 3-7B). Cell structure-related proteins (such as actin) enriched in rye the DRM are considered to be closely associated with microdomains and restrict PM protein mobility cooperatively with microdomains in animal cells (Oliferenko et al., 1999; Holowka et al., 2000; Villalba, 2001; Lenne et al., 2006). Thus, the functional roles of microdomains purified as DRM fractions may be different between oat and rye. However, no substantial changes of any functional categories during CA were found in either species. This result suggests that the global functional balance of DRM and PM proteins in each functional category is not affected by CA treatment. Fig. 3-5 also shows the enrichment of each functional category of during CA.

Remarkable differences between oat and rye DRMs were observed in the proportions of disease/defense- and cell structure-related proteins (Fig. 3-7). Oat DRMs contained a considerable amount of hypersensitive-induced reaction proteins (HIR) classified into disease/defense proteins (e.g., the DRM/PM ratios of gi|23345042 were 5.1 and 3.2 in NA and CA, respectively). Some HIR proteins are proposed as PM-associated regulators of hypersensitive cell death and interact with leucine-rich repeat (LRR) proteins (Jung et al., 2007; Jung and Hwang, 2007; Zhou et al., 2009; Zhou et al., 2010). HIR proteins were also identified as DRM-related proteins (Fujiwara et al., 2009; Minami et al., 2009) and stress responsive proteins (Nadimpalli et al., 2000; Rostoks et al., 2003). However, the functions of these proteins in freezing tolerance or CA remain unknown. Information about the relationship between CA and the functions of HIR proteins is required.

In contrast, rye DRMs contained a large amount of cell structure-related proteins, such as tubulins. Tubulin, a cytoskeleton component, is dynamically reconstructed during the CA process in rye (Kerr and Carter, 1990), and a decline of tubulins is reported to be important for CA performance in wheat (Abdrakhamanova et al., 2003). Microdomains and tubulin and actin function cooperatively, and their cooperation has important roles in localization and movement of proteins in animal cells (Head et al., 2006). Interestingly, microtubule depolymerization enhances cold shock-induced calcium channels (Mazars et al., 1997). Similarly, reorganization of the actin cytoskeleton is induced by membrane rigidification and reacts to low-temperature signal transduction (Örvar et al., 2000). Thus, it is possible that tubulins and actins are associated with microdomain functions as an integral component of PM-cytoskeleton

interactions during CA and these regulatory mechanisms influence freezing tolerance in rye.

Abundance-based Analysis of CA-responsive DRM Fraction Proteins in Oat and Rye

I then determined quantitative changes of CA-responsive DRM proteins in oat and rye (the difference of normalized abundance between CA and NA samples). When the proteins were categorized based on their functions according to Bevan et al. (1998), there were significant differences between oat and rye in the functional categories into which CA-responsive DRM proteins (ANOVA $p < 0.05$; CA/NA ratio, > 2.0 or < 0.5) were classified. Among CA-decreased DRM fraction proteins, disease/defense-related proteins and transporters were abundant in oat (Fig. 3-8A), while almost all CA-responsive proteins were transporters (except for proteins in unclassified category) in rye (Fig. 3-8B). Meanwhile, 83% of CA-increased proteins were disease/defense related proteins in oat (Fig. 3-8C) and, in rye, 16, 34 and 14% of CA-increased proteins were disease/defense-, energy-related and transporter proteins, respectively (Fig. 3-8D).

In rye DRMs, 83% of CA-decreased proteins were transporters, most of which were aquaporins (Supplemental Table 3-3). It has been reported that overexpression of a *Rhododendron catawbiense* aquaporin, *RcPIP2*, led to a decrease of freezing tolerance of transgenic *Arabidopsis* plants (Peng et al., 2008). The authors considered that these results reflected a low level freeze-induced desiccation and faster rehydration during thawing. Improper water transport under CA conditions may result in severe dehydration caused by extracellular ice formation. Supplemental Table 3-3 shows that aquaporins were highly enriched in the DRM (e.g., DRM/PM of gi|162460423 was 3.2 in NA oat and gi|68533200 was 3.9 in NA rye) and a remarkable decline of aquaporin abundance was found, particularly in rye DRM, during CA (e.g., CA/NA of gi|115334277 was 0.3 in rye DRM). Thus, decline of aquaporins in rye DRM may be one mechanism for avoiding injury during thawing after freezing. Furthermore, the activities of some of PM aquaporins can be regulated by phosphorylation (Johansson et al., 1998) and are affected by heteromerization. Thus, segregation of aquaporins into microdomains may modulate water transport activity through regulation of aquaporin activity, and contribute to quantitative and functional changes of aquaporins during CA.

In oat DRMs, CA resulted in an increase in heat shock protein 70 (HSP70), which is classified into the disease/defense category (e.g., gi|356505100 identified in DRM, was 2.9 times higher in CA than in NA, see Supplemental Table 3-3). HSP70 plays important roles in protein folding and protein transport, and responds to low temperature (Miernyk, 1999; Sung et al., 2001). In fact, a positive correlation between

HSP70 accumulation and CA was found in soybean, spinach and poplar (Cabané et al., 1993; Anderson et al., 1994; Renaut et al., 2005). In our previous study, DRMs in oat were shown to comprise lipids with high melting temperatures that may cause liquid crystal-gel phase transition under freezing temperatures (Takahashi et al., 2011). These data may support the view that oat microdomains tend to denature proteins, and is one of vulnerable domains at freezing temperatures. In addition, lipid raft-HSP interactions in animal cells have been discussed in association with the signaling platform (Horváth et al., 2008). Therefore, it is possible that oat HSP70 facilitates protein refolding or other unknown processes in plant microdomains during CA and freeze/thawing. On the other hand, in rye DRMs, the noticeable CA-increased proteins were transporters, mostly represented by induction of P-type ATPase (Supplemental Table 3-3.). As described above, ATPases are predicted to be located in microdomains, and their activity is affected by surrounding microdomain-enriched sterol molecules. In addition to sterol changes in the DRM during CA, an increase in ATPases in rye DRMs may support the hypothesis that cooperative changes of ATPase and sterols in rye microdomains result in changes in the modulation of intra- and extracellular pH and membrane potential, ultimately contributing to enhanced freezing tolerance.

Changes in the Ratio of CA/NA and DRM/PM in Oat and Rye

To see whether there are changes in the partitioning of each protein into DRMs during CA and if there are any effects of CA on the distributions of specific protein groups in DRM, \log_2 values of the DRM/PM ratio of NA samples were plotted against \log_2 values of DRM/PM ratio of CA samples for each protein (Fig. 3-9A and 3-9B). In these panels, the proteins with lower DRM/PM values under NA and higher DRM/PM values under CA (proteins plotted in the upper-left quarter) indicate that enrichment of the protein into DRMs increased during CA. Conversely, the proteins with a combination of higher \log_2 DRM/PM values in NA and lower \log_2 DRM/PM values in CA (proteins plotted in the lower-right quarter) indicate that partitioning of the protein into DRM decreased during CA. In general, both in oat and rye, the DRM/PM ratio of each protein did not change during CA, and there were no significant differences in the enrichment in the DRM of proteins, regardless of functional categories to which the protein belongs. These data indicate that the distribution of each protein in the PM (i.e., inside and outside the DRM) is not significantly affected by CA treatment.

In both oat and rye, however, I observed that some proteins were found to behave differently to the majority of proteins. For example, in oat, focusing on proteins that increased their enrichment in the DRM during CA, a predicted protein

(gi|326519689) classified into unclassified proteins, was plotted on the point (-0.6, 1.9) (Fig. 3-9A). The DRM/PM ratios in NA and CA were 0.7 ($p>0.05$) and 3.8 ($p<0.0005$), respectively (Supplemental Table. 3-3). This means that the relative abundance of this protein in the DRM and/or partitioning of this protein into the DRM increased after CA. Putative leucine-rich repeat (LRR) domains were detected in the amino acid sequence of this protein, which is similar to the LRR sequence found in *Medicago truncatula* proteins (Blast score: 633). LRR receptor-like kinases were also detected and enriched in *Arabidopsis* DRMs (Shahollari et al., 2004). LRR is one of representative motifs of amino acid sequence structure that are included in a broad range of functional proteins, and is often important for protein-protein interaction (Jia et al., 2000). Changes of affinity of the LRR-containing proteins for DRM may suggest that LRR protein-microdomain interactions are regulated by CA treatment, and hence affect protein function through changes in protein-protein accessibilities.

In rye, there are proteins for which enrichment in the DRM increased during CA. Two sugar transporting proteins, gi|357115762 and gi|357158410, changed from non-DRM-enriched proteins in NA to DRM-enriched proteins in CA (Fig. 3-9B). The DRM/PM ratio increased for gi|357115762 from 1.1 ($p>0.05$) in NA to 16 ($p<0.005$) in CA. For gi|357158410, the DRM/PM ratio increased from 1.8 ($p>0.05$) in NA to 23 ($p<0.005$) in CA. These results clearly indicate that sugar transporters become enriched in the DRM after CA. Intracellular sugar concentration is one of the most important factors for acquiring freezing tolerance during CA. Intracellular ice formation is lethal for plant survival (Guy, 1990). Therefore, solute accumulation inside the cell is necessary to increase osmotic concentration, which results in lowering of the freezing point of the cell, thus decreasing the probability of the cell freezing. In addition, sugars can act as cryoprotective solutes to prevent macromolecules (e.g., proteins) denaturing during freeze-induced stresses. Actually, rye accumulates a variety of solutes, including glycinebetaine, proline, and soluble sugars, during CA (Koster and Lynch, 1992) and relocates fructans and simple sugars in the apical region and crown tissues during freezing at -3°C (Livingston et al., 2006). Thus, re-partitioning of sugar transporters to the DRM in the PM after CA may indicate that microdomain-dependent regulation of sugar transportation is involved in proper solute modulation at the cellular and/or tissue level.

The \log_2 values of the CA/NA ratio of PM samples were then plotted against \log_2 values of the CA/NA ratio of DRM samples for each of protein (Fig. 3-9C and 3-9D). In oat, I found interesting behavior of temperature-induced lipocalins in the PM and DRM during CA (Fig. 3-9C, Supplemental Table 3-3). Four distinct lipocalins were

identified in oat and, among them, two lipocalins (gi|18650668 and gi|77744845) statistically increased after CA in the PM (by 3.2 and 3.5-fold, respectively, $p < 0.001$). In the DRM during CA, however, there was no statistical change in gi|18650668, and only a slight decrease in gi|77744845 (CA/NA: 0.6; $p < 0.05$). Lipocalins are widely distributed in plant, animal and microbial species and are characterized by three highly conserved domains (Flower, 1996). *Arabidopsis temperature-induced lipocalin 1 (TIL1)* is responsive to heat stress and a *TIL1*-knock-out mutant (*til1-1*) is vulnerable to heat stress because TIL1 is essential for protecting lipids and proteins from oxidation induced by heat stress (Chi et al., 2009). In addition, NA protoplasts isolated from *Arabidopsis lipocalin*-overexpressing mutants showed enhanced freezing tolerance (Uemura et al., 2006). Therefore, lipocalins may help to acquire freezing tolerance during CA through an association with the PM. On the other hand, lipocalins may have different interaction behaviors between microdomain and non-microdomain areas during CA because of differences in the lipid environments between inside and outside the microdomain and/or changes in the lipid environment during CA, resulting in different patterns of change between the PM and DRM.

In Supplemental Table 3-4, the DRM-enriched proteins that were found in NA samples and that statistically changed, either increased or decreased, during CA are listed. Twenty-four and 37 DRM-enriched proteins were identified as CA-responsive proteins in oat and rye, respectively. Interestingly, many DRM-enriched proteins statistically decreased after CA. In both oat and rye, aquaporins were commonly identified as DRM-enriched and CA-decreased proteins. Additionally, there were other common proteins in oat and rye, such as cellulose synthase and V-type proton ATPase. Decreases of PM proteins are, at least in part, considered to be caused by endocytosis. In animal cells, raft-dependent endocytosis is observed, and there are various endocytic pathways mediated by raft-enriched caveolins and dynamins (Lajoie and Nabi, 2007). Some of the PM modifications during CA may be caused by microdomain-dependent endocytosis, and this process may result in removal of specific DRM-enriched proteins, such as aquaporins, from the PM bilayer.

Changes of Post-translationally Modified Proteins during CA in DRM Fractions

In animal cells, post-translational modifications of proteins are important for defining protein functions in microdomains (Lingwood and Simons, 2010). Among them, the addition of a glycosylphosphatidylinositol (GPI) anchor is associated with microdomains (Paulick and Bertozzi, 2008; Lingwood and Simons, 2010). GPI is embedded in the exoplasmic leaflet of the PM and is bound to protein (Kinoshita et al.,

2008). Some GPI-anchored proteins observed to be localized in a cholesterol-dependent microdomain-like structure with 70 nm diameter by fluorescence resonance energy transfer analysis (Varma and Mayor, 1998). When the Big-PI plant predictor predicted GPI-anchored proteins, I found more GPI-anchored proteins in the DRM of rye (n=21) than in oat (n=9) (Fig. 3-10A). CA-induced changes in the abundance of GPI-anchored proteins in the DRM were significant in rye (Fig. 3-10B). Interestingly, in rye, all the CA-responsive GPI-anchored proteins in the DRM increased during CA. Among them, two GPI-anchored proteins, gi|326502418 and gi|326494592, increased in rye DRM by 12- and 2.6-fold, respectively. These proteins are structurally similar to 1,3- β -glucosidase-like proteins (BLAST scores 606 and 764). In *Arabidopsis*, the β -glucosidase-like-protein encoded by the *SFR2* gene, which is located in chloroplast outer envelope, has an ability to protect chloroplasts against freezing (Fourrier et al., 2008). However, it remains unknown how the SFR2 protein protects the chloroplast membrane. Furthermore, other GPI-anchored proteins, such as fasciclin-like proteins (FLAs), were identified in the rye PM and increased after CA (e.g., gi|115349890 and gi|115349914; Supplemental Table 3-3). These proteins are cell adhesion molecules and are responsive to several environmental stresses. In *Arabidopsis* roots, FLA was suggested to be related to responsiveness to salt stress through cell adhesion (Shi et al., 2003). In wheat, some FLAs were induced by CA treatment (Faik et al., 2006). Taken together, the stress responsiveness of GPI-anchored proteins, including 1,3- β -glucosidase-like proteins and FLAs, may be important and significant during plant CA. Thus, further studies to reveal the functional involvement of these GPI-anchored proteins in CA are clearly warranted.

Another important post-translational modification of membrane proteins is myristoylation, which plays roles in localization of proteins to microdomains (Zacharias et al., 2002). Myristoylation consists of a C14 saturated fatty acid bound to a specific protein. When the Plant-Specific Myristoylation Predictor predicted myristoylated proteins (Fig. 3-10A and 3-10B), the number of putative myristoylated proteins identified was similar in oat (n=31) and rye (n=27) (Fig. 3-10C). In oat and rye DRMs, several myristoylated proteins increased after CA, including signal transduction-related proteins, such as calcium-dependent kinase (gi|84626055) and receptor-like kinase (gi|255537473; Fig. 3-10D, Supplemental Table 3-3). Signal transduction, which is a putative microdomain function, may support smooth reconstruction of CA cells in plants via myristoylated protein-microdomain interactions.

Supporting information

Supplemental Table 3-1. Identified PM and DRM fraction proteins in oat and rye.

Supplemental Table 3-2. Functional categorizations of identified PM and DRM fraction proteins in oat and rye.

Supplemental Table 3-3. Identified CA-responsive proteins and peptides in oat and rye as determined by Progenesis software.

Supplemental Table 3-4. DRM-enriched and CA-responsive proteins in oat and rye.

Supplemental Table 3-5~12. Identified peptides lists in each fractions and experiments.

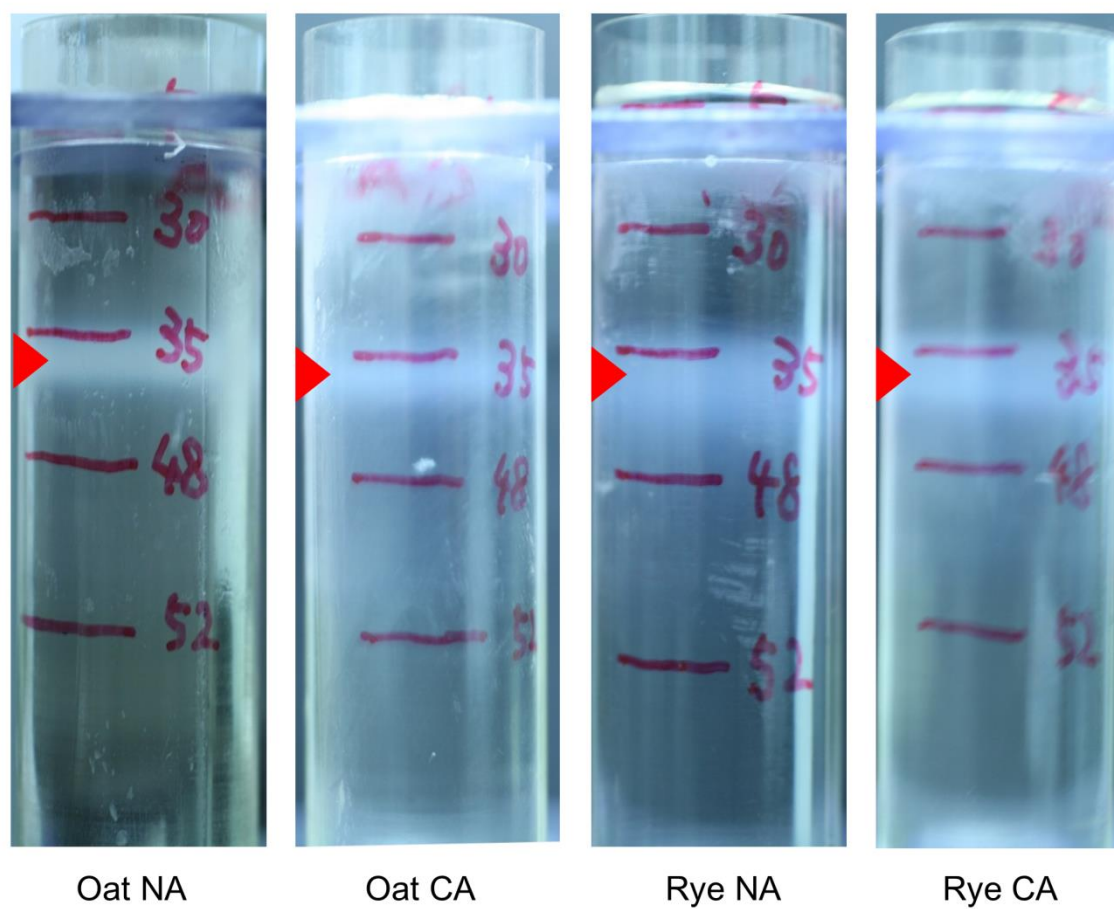


Fig. 3-1. Detergent-resistant membrane fractions after sucrose density gradient centrifugation. Red arrowheads at the interface of 30 and 35% sucrose layers indicate DRM fractions in both oat and rye. DRM layers were recovered and subjected to further experiments.

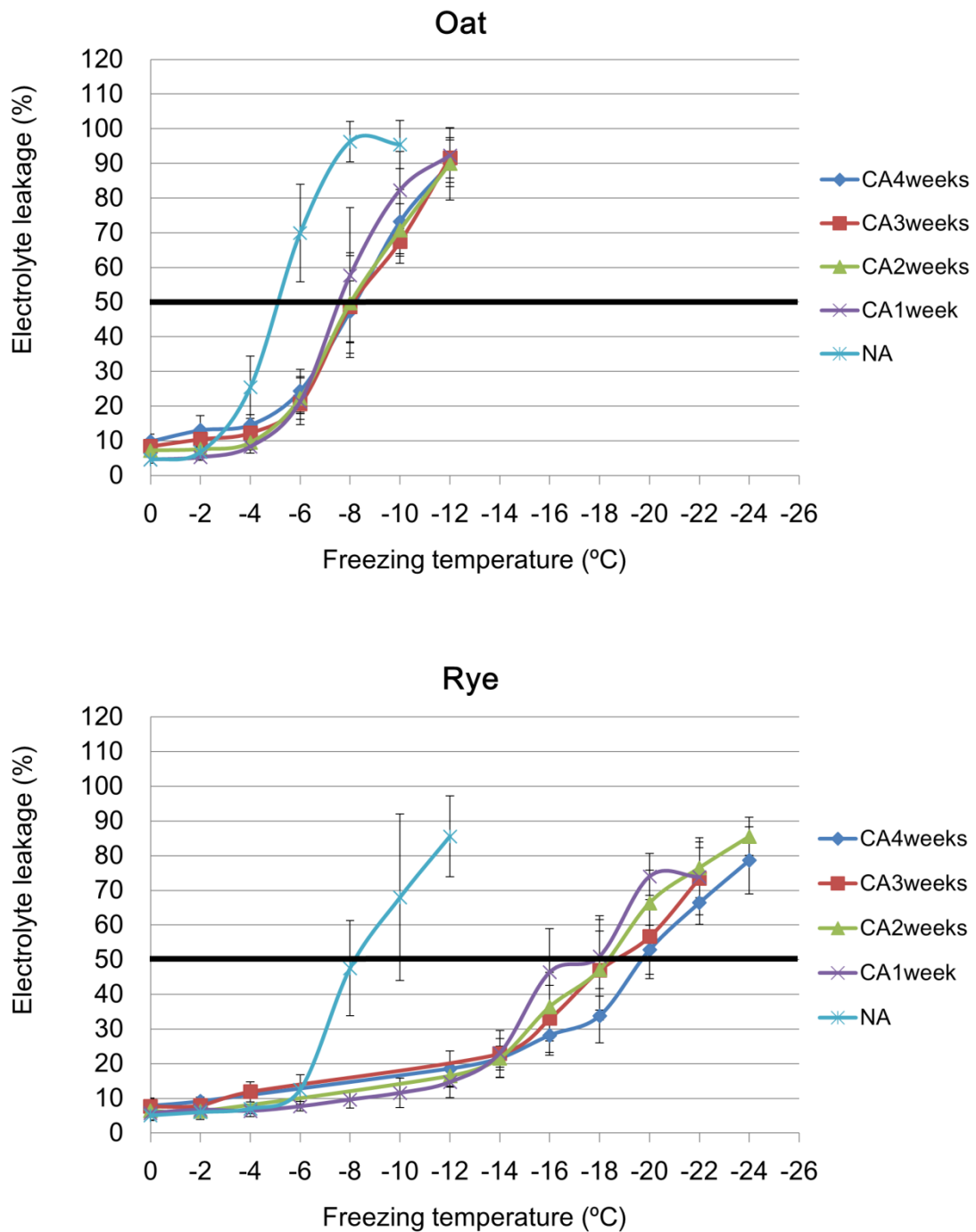


Fig. 3-2. Freezing tolerance of oat and rye leaves. Freezing tolerance is expressed as the percentage of electrolyte leakage, which reflects the extent of freezing injury of the PM. In this experiment, oat and rye were cold acclimated for 0, 1, 2, 3 and 4 weeks, and then the electric conductance was measured after subjecting to a freeze-thaw cycle (n=3-12).

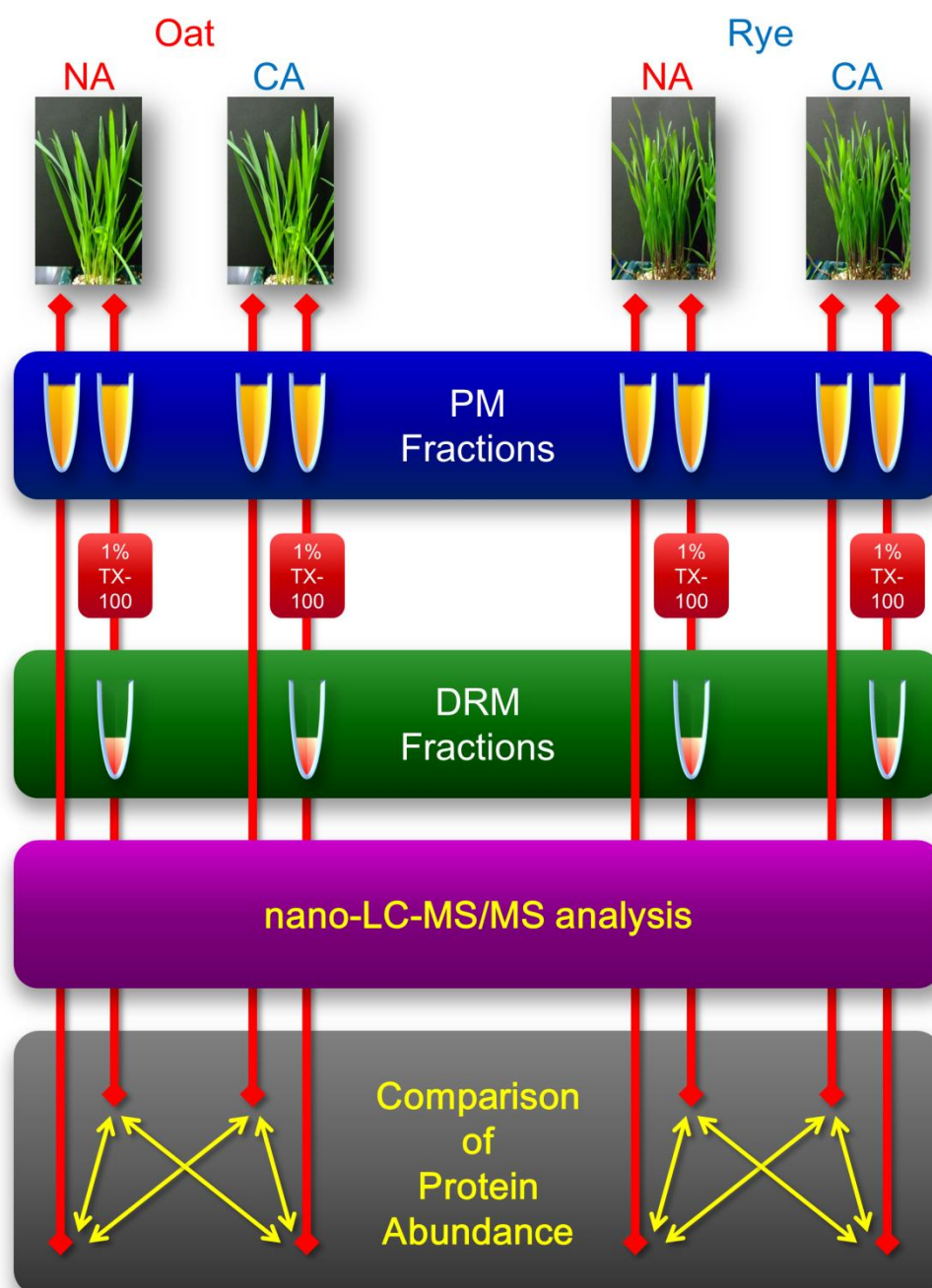


Fig. 3-3. Work flow of large-scale, quantitative proteomics of DRM fractions in oat and rye. PM fractions were purified from oat and rye before and after CA. Half of each PM sample was added into Triton X-100 solution and subjected to DRM purification procedure. All the PM and DRM fractions were subjected to peptide identification with nano-LC-MS/MS analysis. Signal intensities of each peptide were calculated by Progenesis software. The abundance of each protein was then determined and compared among samples. All experiments were repeated with four biologically independent samples.

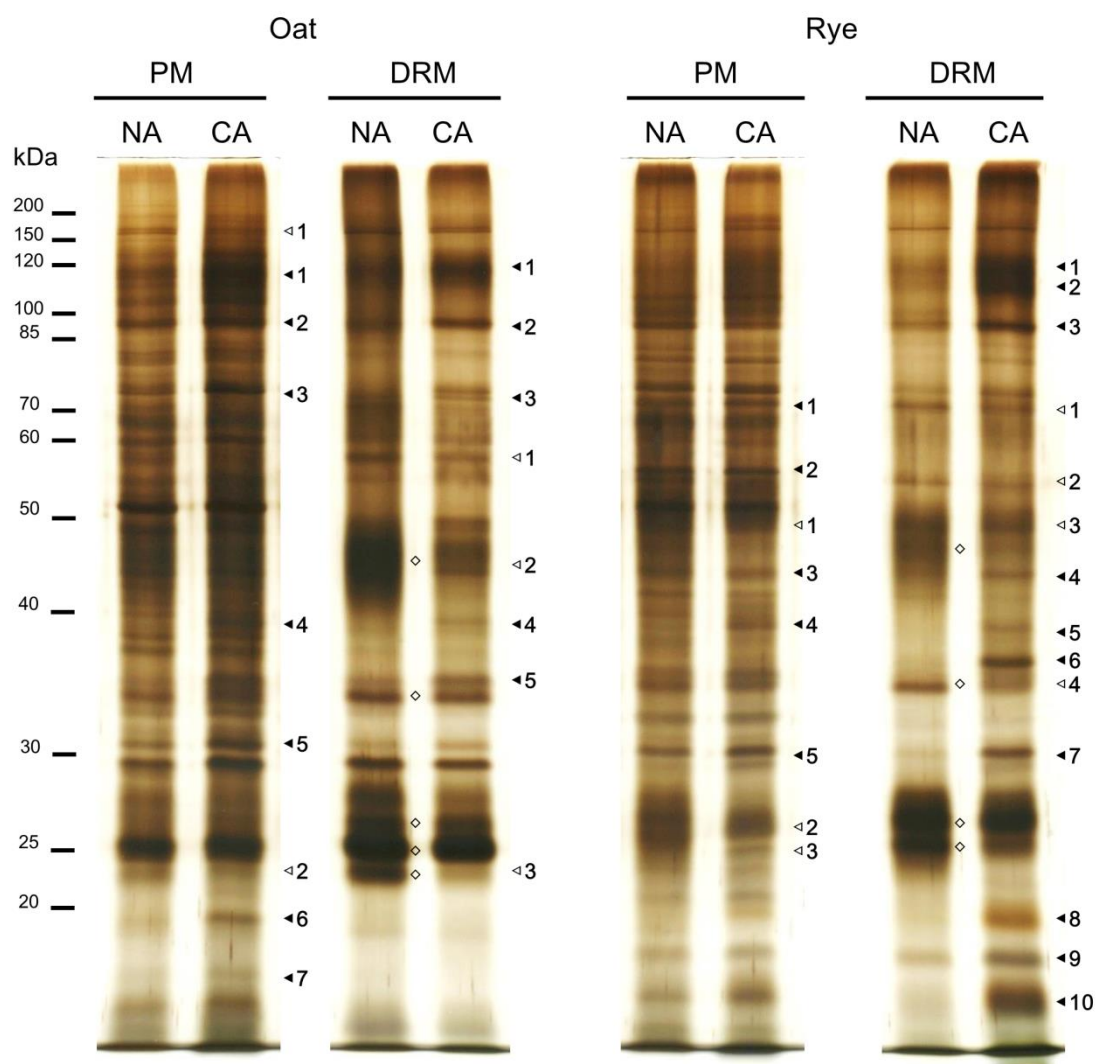


Fig. 3-4. One-dimensional SDS-PAGE profiles of PM and DRM proteins in oat and rye during CA. PM and DRM proteins prepared from NA and CA oat and rye (1 μ g protein equivalent) were separated using SDS-PAGE and visualized by silver-staining. Diamonds indicate highly accumulated DRM fraction proteins. Filled and open triangles indicate CA-increased and CA-decreased proteins, respectively.

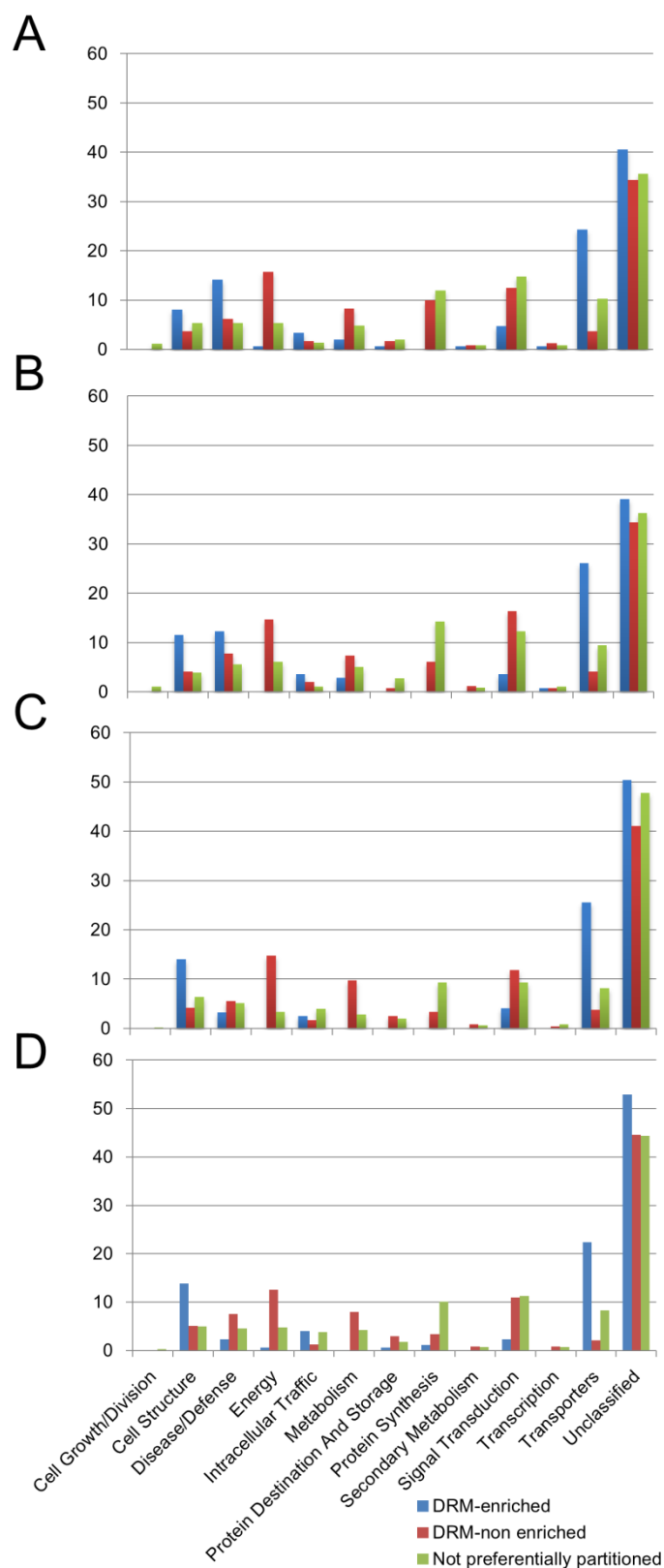


Fig. 3-5. Functional categorization of proteins that were differentially contained in the PM and DRM. Peptides were selected according to the following criteria using Progenesis LC-MS software: ANOVA $p < 0.05$; DRM/PM ratio, > 2.0 or < 0.5 ; expect value cut off, > 0.05 . Proteins were then identified using the Mascot server and classified into 13 functional categories based on Bevan et al. (1998). A, B, C and D show distribution of DRM-localized and non-localized proteins in the NA oat, CA oat, NA rye and CA rye, respectively.

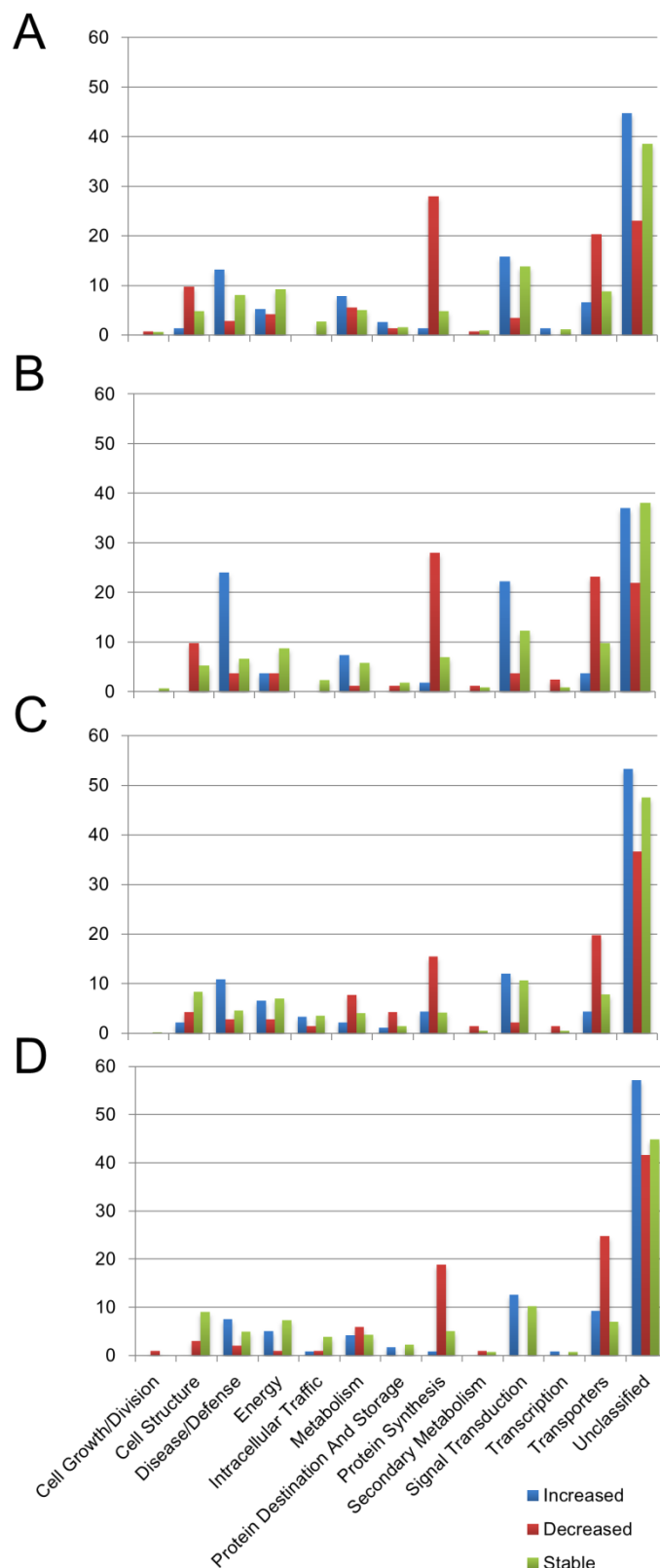


Fig. 3-6. Functional categorization of proteins that significantly changed during CA. Peptides were selected according to the following criteria using Progenesis LC-MS software: ANOVA $p < 0.05$; CA/NA ratio, > 2.0 or < 0.5 ; expect value cut off, > 0.05 . Proteins were then identified using the Mascot server and classified into 13 functional categories based on Bevan et al. (1998) as described in Fig. 3-5. A, B, C and D show distribution of CA-increased and CA-decreased proteins in the oat PM, oat DRM, rye PM and rye DRM, respectively.

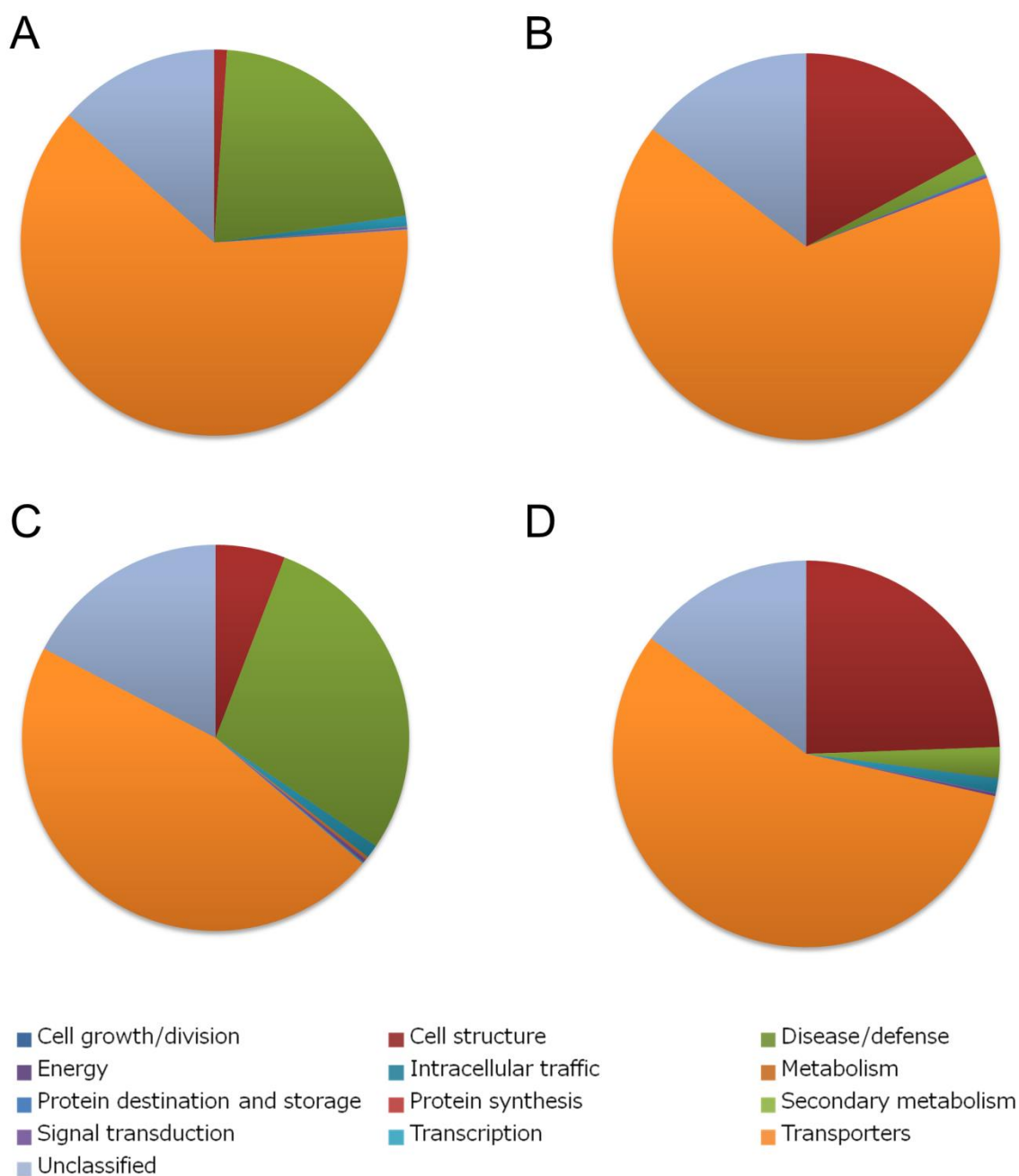


Fig. 3-7. Functional categorization of DRM-enriched proteins in NA and CA samples based on protein abundance. Peptides were selected according to the following criteria using Progenesis LC-MS software: ANOVA $p < 0.05$; DRM/PM ratio, > 2.0 ; expect value cut off, > 0.05 . Proteins were then identified using the Mascot server and classified into 13 functional categories based on Bevan et al. (1998) as described in Fig. 3-5. Percentage shown is based on normalized abundance of proteins classified in each category. A, B, C and D show abundance of DRM-enriched proteins in each functional category of the NA oat, NA rye, CA oat and CA rye, respectively.

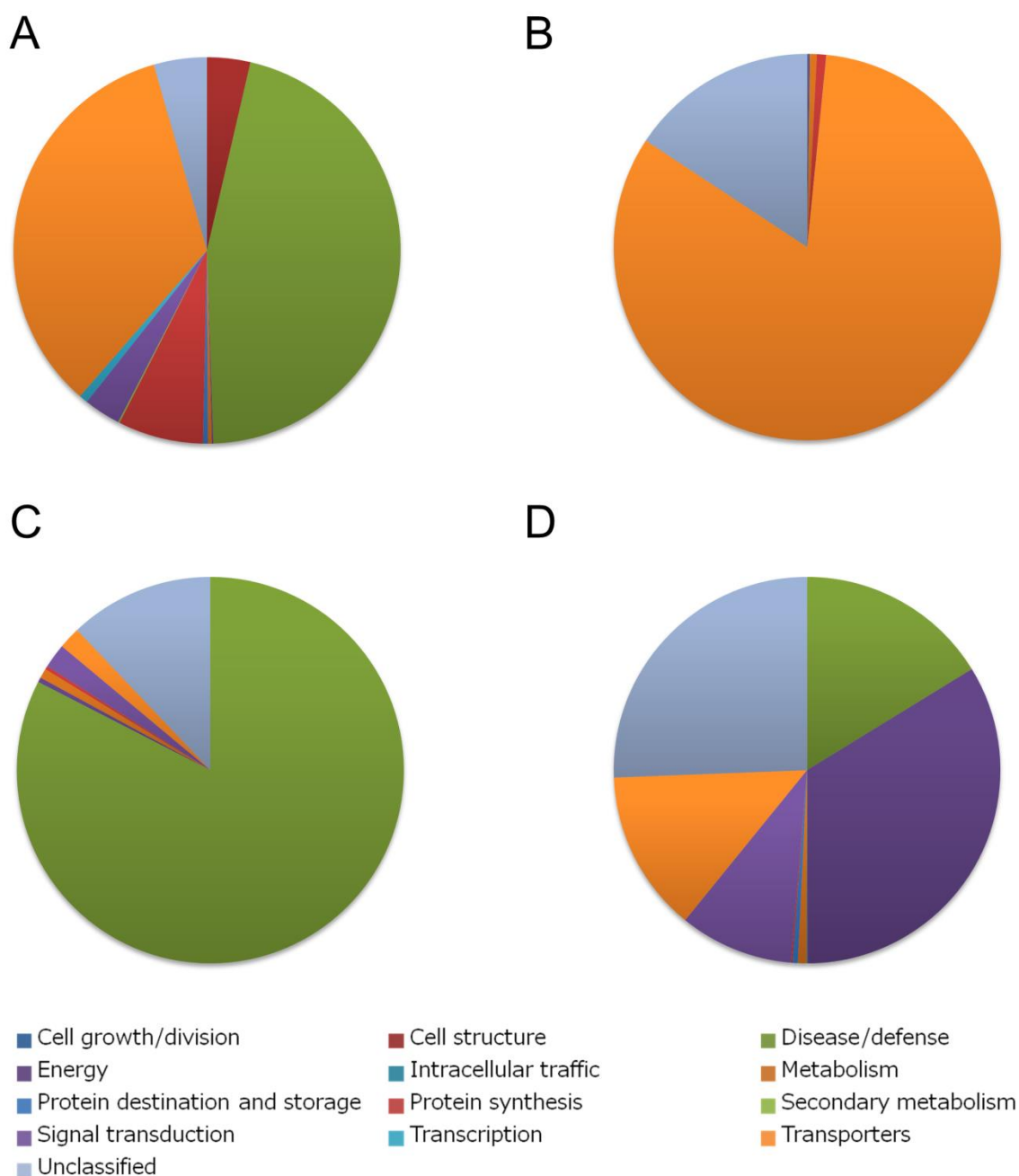


Fig. 3-8. Functional categorization of CA-responsive proteins based on protein abundance. Peptides were selected according to the following criteria using Progenesis LC-MS software: ANOVA $p < 0.05$; CA/NA ratio, > 2.0 or < 0.5 ; expect value cut off, > 0.05 . Proteins were then identified using the Mascot server and classified into 13 functional categories based on Bevan et al. (1998) as described in Fig. 3-5. Percentage shown is based on normalized abundance of proteins in each functional category. A, B, C and D show abundance of CA-decreased proteins in oat, CA-decreased proteins in rye, CA-increased proteins in oat and CA-increased proteins in rye, respectively.

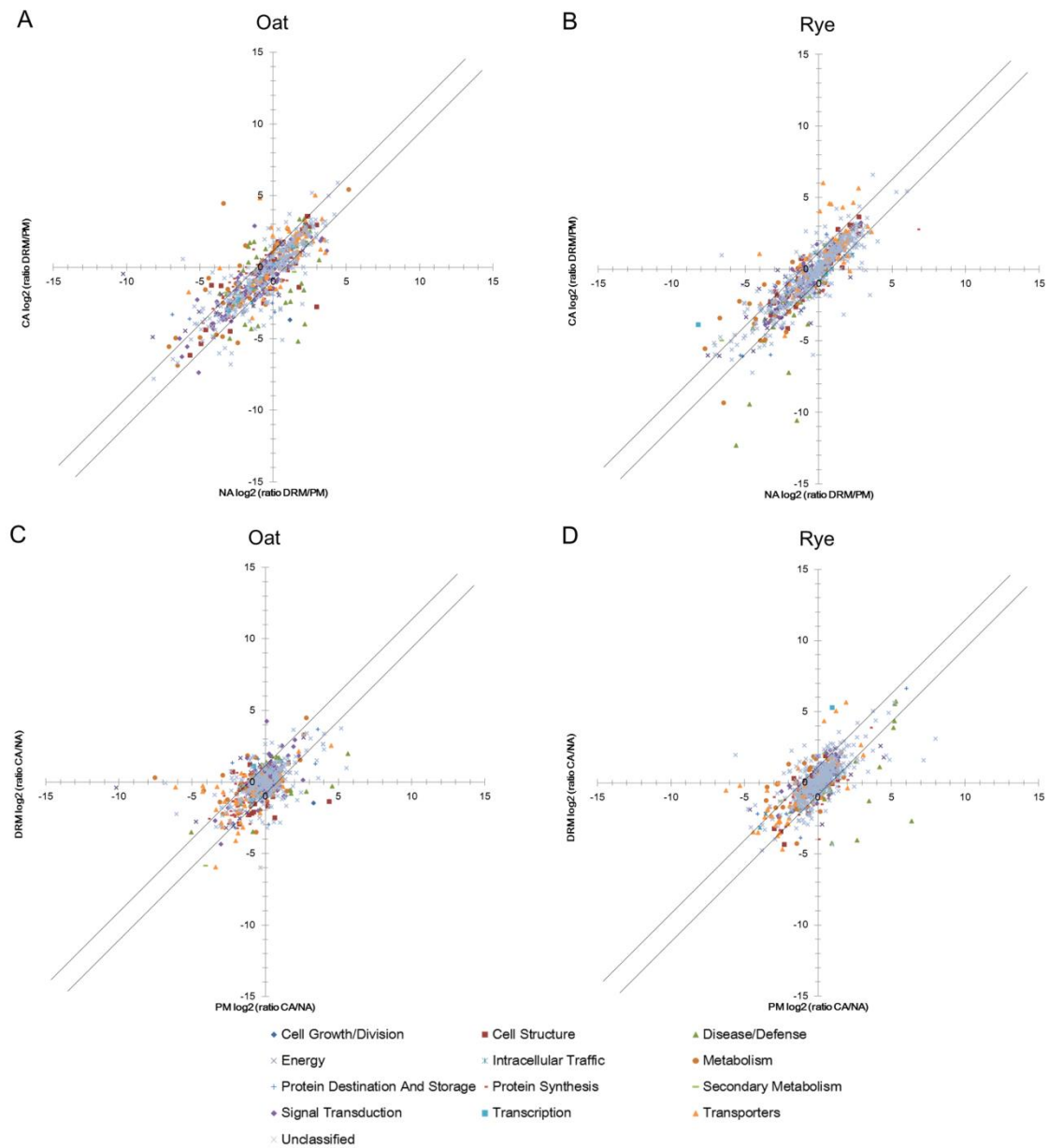


Fig. 3-9. Scatter plots of identified proteins in oat and rye. Normalized abundance of all identified proteins was calculated using Progenesis LC-MS software. The log₂ value of the signal abundance of each protein in two determinations (i.e., DRM vs. PM in NA and CA samples and CA vs. NA in PM and DRM samples) were calculated and plotted. A and B; log₂ values of DRM/PM in NA on the X-axis and DRM/PM in CA on the Y-axis in oat (A) and rye (B). C and D; log₂ values of CA/NA in PM on the X-axis and CA/NA in DRM on the Y-axis in oat (A) and rye (B).

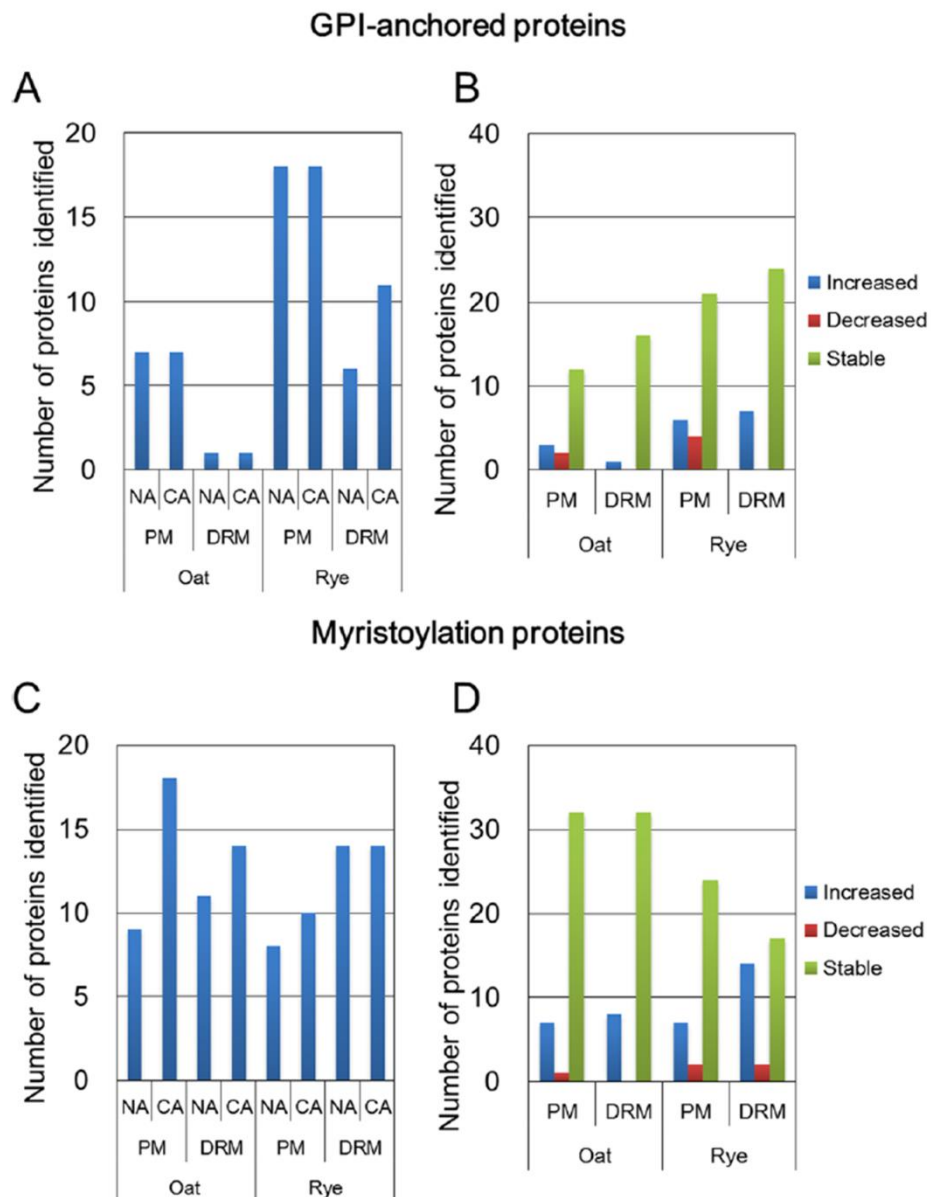


Fig. 3-10. Identification of the putative GPI-anchored (A, B) and N-terminal myristoylated proteins (C, D) in oat and rye. Putative GPI-anchored proteins and myristoylated proteins were predicted by Big-PI plant predictor and Plant-Specific Myristoylation Predictor, respectively. (A, C) Number of potential GPI-anchored proteins and myristoylated proteins in each experimental section, respectively. (B, D) Number of CA-increased (ANOVA $p < 0.05$; CA/NA ratio > 2.0), CA-decreased (ANOVA $p < 0.05$; CA/NA ratio < 0.5), and stable (unchanged) GPI-anchored proteins and myristoylated proteins, respectively.

Chapter 4

Lipid profiles of detergent resistant fractions of the plasma membrane in oat and rye associated with cold acclimation and freezing tolerance

Summary

Cold acclimation (CA) results in alteration of the plasma membrane (PM) lipid composition in plants, which plays a crucial role in the acquisition of freezing tolerance via membrane stabilization. Recent studies have indicated that the PM is represented by the fluid mosaic model but it is considered non-homologous and contains microdomains that are enriched in sterols, sphingolipids and specific proteins. In plant cells, however, the function of these microdomains in relation to CA and freezing tolerance is not yet fully understood. The present study aimed to investigate the lipid compositions of microdomains prepared from the leaves of low-freezing tolerant oat and high-freezing tolerant rye. The oat and rye microdomains contained higher proportions of sterols, sphingolipids and saturated phospholipids than the PM. In particular, a sterol class, acylated sterylglucoside, was the predominant sterol in oat microdomains while rye microdomains contained free sterol. The change patterns of microdomain lipids such as sterols and 2-hydroxy fatty acids of sphingolipids during CA were different between oat and rye. Taken together, these results indicate that CA-induced changes of lipid classes and molecular species in microdomains seem to be involved in the thermodynamic properties and physiological functions of microdomains during CA, and may influence plant freezing tolerance.

Introduction

Cold acclimation (CA) is one of the most important processes for adaptation to freezing temperatures in plants. During this process, the plasma membrane (PM) composition changes dynamically, which is crucial for acquisition of freezing tolerance. The PM is composed of a variety of proteins and lipids. PM-associated proteins and lipids are also important for determining the structure and function of microdomains, which are enriched in specific proteins and lipids, and can be extracted as detergent-resistant plasma membrane (DRM) fractions. In previous studies (Takahashi et al., 2012; Takahashi et al., 2013; Chapters 2 and 3 in this thesis), DRM-enriched proteins were identified and the responsiveness of these proteins to CA was determined in oat and rye. The results suggested that some microdomain proteins associated with CA in the two plant species contribute to their vastly different freezing tolerance.

In addition to proteins, many studies have suggested that lipids are necessary for microdomain functions. The microdomain concept was proposed by Simons and Ikonen based on the fluid mosaic model (Singer and Nicolson, 1972; Simons and Ikonen, 1997). They considered the lateral organization of raft-like lipid microdomains to be due to preferential packing of sphingolipids and cholesterol in specific small regions. Sphingolipids, in fact, form nanodomains in phosphatidylcholine (PC)-based lipid bilayers and cholesterol fills the intermolecular spaces of sphingolipids (Sankaram and Thompson, 1990; Silvius, 1992). Thus, microdomain formation and stabilization may be driven by lipid–lipid and lipid–protein interactions in addition to protein–protein interactions (Simons and Ikonen, 1997; Friedrichson and Kurzchalia, 1998; Lingwood and Simons, 2010; Simons and Sampaio, 2011). In plants, some studies have examined the significance of lipids in microdomains. Borner et al. (2005) and Mongrand et al. (2004) first conducted lipid quantifications from the perspectives of lipid classes and fatty acid compositions using DRM fractions as microdomain-enriched fractions. In the same way, the DRM lipid compositions of maize embryos and bean leaves have already been characterized (Carmona-Salazar et al., 2011; Carmona-Salazar et al., 2015). Furt et al. (2010) reported that phosphatidylinositol-4,5-bisphosphate forms a cluster-like structure that is not influenced by sterol depletion, and that phosphoinositide metabolism-related enzyme activities in DRMs are higher than in the PM.

Lipid changes in DRMs were reported in *Arabidopsis* leaves during CA (Minami et al., 2009). Although free sterol proportions changed in DRMs of the *Arabidopsis* PM during CA (Minami et al., 2009), the author performed only lipid composition measurements at the lipid class level, and did not examine the molecular species in each lipid class. In the present study, I took biochemical and lipidomic

approaches to determine the lipid compositions in oat and rye DRMs during CA. Considering a previous study that dealt with PM lipid compositions in oat and rye during CA (Uemura and Steponkus, 1994), I aimed to (a) compare lipid compositions between the PM and DRMs, (b) investigate compositional changes of PM and DRM lipids during CA and (c) compare lipid compositions and CA-induced changes between low freezing-tolerant oat and high freezing-tolerant rye. The physical properties of membrane lipids influence membrane stability and are important for the acquisition of plant freezing tolerance during CA (Steponkus, 1984; Gordon-Kamm and Steponkus, 1984b; Webb et al., 1995). Therefore, both the cryostability of the PM and microdomains and the biochemical functions of microdomains during CA will be discussed by comparing oat and rye.

Experimental procedures

Plant Materials and Isolation of DRM Fractions

Non-acclimated and cold-acclimated Oat (*Avena sativa* L. cv. New almighty) and rye (*Secale cereale* cv. Maskateer) were grown at the same condition with Takahashi et al. (2013; Chapter 3 in this thesis). PM and DRM isolation was performed in accordance with Takahashi et al. (2013; Chapter 3 in this thesis).

Total Lipid Extraction and Thin Layer Chromatography

Extraction of total lipids from PM and DRM fractions was carried out according to the method of Bligh and Dyer (1959). Isopropanol (2.5 ml) was added into 1 ml of PM and DRM suspensions. Subsequently, 1.25 ml of chloroform was added twice and samples in a test tube were mixed well. After adding 1.25 ml of 0.9% (w/v) NaCl, samples were incubated for more than 15 min at room temperature. Test tubes were then centrifuged at $196 \times g$ for 5 min and a resultant lower phase was collected in a new test tube. Chloroform (1.5 ml) was added in remaining upper phase to re-extract lipids, test tubes were centrifuged ($784 \times g$ for 10 min) and lower phase was corrected in the test tubes. After adding 2 ml of chloroform/isopropanol/0.9% (w/v) NaCl (3:47:48, v/v/v) in collected lower phase, samples were centrifuged at $196 \times g$ for 5 min and lower phase was collected in the new test tube. The resultant lower phase was dried with heating at 40°C and under the presence of blowing N₂ gas, and after completion of drying; an aliquot of chloroform was added and stored at -20°C under N₂ gas until use.

Thin layer chromatography (TLC) analysis of total lipids was conducted using silica gel plate (Silica gel 60, 0.25-mm thickness, Merck, Darmstadt, Germany) with a

developing solvent, chloroform/methanol/water (65:25:4, v/v/v). After developing samples, solvent on thin layer plate was vaporized completely and lipids were visualized by spraying 0.1% (w/v) primuline in acetone (Sigma-Aldrich, St Louis, MO, USA).

Quantification of Sterols, Glucocerebrosides and Phospholipids

Silica gel layers of spot corresponding to free sterol (FS), sterylglucoside (SG), acylated sterylglucoside (ASG), glucocerebrosides (GlcCer) and phospholipids (PLs) were collected and subjected to quantification of each lipid class.

For sterol quantification, 1.1 ml of acetic acid was added in sample tubes and sonicated. An aliquot (1 ml) of *o*-phthalaldehyde in acetic acid (0.1%, w/v) and 1 ml of concentrated sulfuric acid were added successively and mixed well. Sample tubes were cooled to room temperature for 15 min and centrifuged at $196 \times g$ for 10 min to precipitate silica powder. Absorbance of supernatants at 550 nm was measured. Standard curve was made by dilution series of 10 mM cholesterol in acetic acid.

For GlcCer, 1 ml of water was added in silica gels in sample tubes and silica gels were sonicated. Subsequently, 0.5 ml of 5% (w/v) phenol and 2.5 ml of concentrated sulfuric acid were successively added and mixed well. Sample tubes were cooled to room temperature for 15 min and centrifuged at $196 \times g$ for 10 min. Supernatants were collected and absorbance at 485 nm was measured. Standard curve was made by dilution series of 5 mM sucrose solution.

For PLs, 50 μ l of water and 0.5 ml of 70% perchloric acid were added in sample tubes containing silica gels and mixed well. Subsequently, tubes were heated at 200°C for 30 min. After cooling to room temperature, 3 ml of water and 0.5 ml of 2.5% (w/v) ammonium molybdate, 0.2 ml of Fiske-SubbaRow reagent (30 g of sodium hydrogen sulfite, 1 g of sodium sulfite and 1 g of 1-amino-2-naphthol-4-sulfonic acid in 200 ml of water) were added in sequence and mixed well. Tubes were boiled for 7 min, cooled to room temperature and centrifuged at $196 \times g$ for 10 min. Supernatants were collected and absorbance at 700 nm was measured. Standard curve was made by dilution series of 5 mM KH_2PO_4 .

Determination of Molecular Species of Sterols, Glucocerebrosides and Phospholipids

Total lipid fractions obtained from 50 μ g of PM proteins were separated into neutral lipid (e.g. FS), glycolipid (SG, ASG and GlcCer), and phospholipids using silica gel column chromatography according to the method of Lynch and Steponkus (1987). Each of separated fractions was dried out with blowing N_2 gas, dissolved in 1 ml

chloroform/acetic acid (100:1, v/v) and transferred to a Sep-Pak Silica Classic Cartridge (Waters, Milford, MA, USA) coupled to a glass syringe barrel. Neutral lipids were eluted by 10 ml chloroform/acetic acid (100:1, v/v). Glycolipids were then eluted by the sequential addition of 5 ml acetone and 5 ml acetone/acetic acid (100:1, v/v). Subsequently, phospholipids were eluted by addition of 7.5 ml methanol/chloroform/water (100:50:40, v/v/v). Water/chloroform (12:9, v/v) was added to phospholipid fractions and the fractions were then centrifuged at $1000 \times g$ for 5 min. Resultant lower phase was collected and dried out with blowing N_2 gas. Lipids fractioned were dried out with blowing N_2 gas, dissolved chloroform/acetic acid (100:1, v/v) again and stored at -20°C under N_2 gas until use.

For determination of molecular species of FS, neutral lipid fractions was dried again and dissolved in 100 μl chloroform and transferred into a vial insert (Shimadzu Scientific, Kyoto, Japan). After drying chloroform in the vial insert, lipids were dissolved again in 5 μl chloroform. Subsequently, the sample (0.5 μl) was injected to GC-18A gas chromatograph (Shimadzu Scientific) coupled with dimethyl polysiloxane coated TC-1 capillary column (0.25 mm \times 15 m; GL Science, Tokyo, Japan) and detected by hydrogen flame ionization detector (FID). Temperature of the column was increased at $3^\circ\text{C}/\text{min}$ from 180°C to 240°C . Injector and detector temperature was set at 250°C . Each sterol species was identified by the retention time of peaks corresponded to following standards: Cholesterol, campesterol, stigmasterol and sitosterol (Wako Chemicals, Tokyo, Japan).

For GlcCer molecular species analysis, total lipid extracts were treated with mild alkaline hydrolysis to remove glycerolipids by reference to Imai et al. (2000b). Briefly, total lipid extracts completely dried were dissolved in 133 μl of 0.4 M KOH in methanol at 37°C for 1 h and neutralized with 5 μl of HCl. Subsequently, 2666 μl of chloroform, 2533 μl of methanol and 1333 μl of water were sequentially added to samples and resultant lower phases were collected. Sample fractions containing GlcCer was transferred to a Sep-Pak Plus Silica Cartridge (Waters, Milford, MA, USA) coupled to a glass syringe barrel and solvent composed by chloroform/acetic acid (100:1, v/v) was passed through the column. The fractions containing GlcCer were then eluted with chloroform/methanol (2:1, v/v) and injected into LC-10AT pump (Shimadzu Scientific) coupled with ACQUITY TQD tandem quadrupole mass spectrometer (Waters) as described in Watanabe et al. (2011). Samples were separated by 3 μm TSKgel ODS-100Z column (Tosoh, Tokyo, Japan) with elution gradient from 80% solvent A (methanol/formic acid, 1000/1, v/v)/20% solvent B (water/formic acid, 1000/1, v/v) to 100% solvent A for 30 min and then solvent A for 70 min at a flow rate of 200 $\mu\text{l}/\text{min}$.

In detection part of LC-MS/MS, following conditions were used: capillary voltage, 3 kV; desolvation gas flow, 600 L/h; nebulizer gas flow, 50 L/h; source temp., 120°C; and collision gas flow, 0.3 ml/min (4-5 mbar). Identification of GlcCer was carried out based on 30 pairs of precursor ions $[M + H]^+$ and product ions of sphingoid base moieties as listed in Watanabe et al. (2011) in the positive ionization MRM mode.

Determination of molecular species of SG and ASG was carried out by direct-infusion electrospray ionization triple quadrupole mass spectrometry according to Schrick et al. (2012) with minor modifications. Aliquot amounts of each sample (0.2 ml) were combined with 0.15 nmol PG (di20:0 [phytanoyl]) as an internal standard in a total sample volume of 1 ml of chloroform/methanol/300 mM ammonium acetate in water (300/665/35, v/v/v). This sample was directly infused at 30 μ L per min. The analytical parameters and data processing were as described previously (Schrack et al., 2012).

Determination of phospholipid species was performed using direct-infusion electrospray ionization triple quadrupole mass spectrometry according to the method described in the supplemental data of Xiao et al. (2010) with minor modifications. The samples were dissolved in 1 ml chloroform. An aliquot of extract (200 μ l) in chloroform was used. Precise amounts of internal standards, obtained and quantified as previously described (Welti et al., 2002), were added in the following quantities (with some small variation in amounts in different batches of internal standards): 0.27 nmol PC (di12:0), 0.27 nmol PC (di24:1), 0.27 nmol Lyso PC (13:0), 0.27 nmol Lyso PC (19:0), 0.14 nmol PE (di12:0), 0.14 nmol PE (di23:0), 0.14 nmol Lyso PE (14:0), 0.14 nmol Lyso PE (18:0), 0.14 nmol PG (di14:0), 0.14 nmol PG (di20:0 [phytanoyl]), 0.14 nmol Lyso PG (14:0), 0.14 nmol Lyso PG (18:0), 0.10 nmol PI (16:0-18:0), 0.07 nmol PI (di18:0), 0.09 nmol PS (di14:0), 0.09 nmol PS (di20:0 [phytanoyl]), 0.14 nmol PA (di14:0), 0.14 nmol PA (di20:0 [phytanoyl]), 0.22 nmol DGDG (16:0-18:0), 0.32 nmol DGDG (di18:0), 0.90 nmol MGDG (16:0-18:0), and 0.18 nmol MGDG (di18:0). The sample and internal standard mixture were combined with solvents composed of chloroform/methanol/300 mM ammonium acetate in water (300/665/35, v/v/v) at the final volume 0.8 ml. This sample was directly infused at 30 μ L per min. The analytical parameters and data processing were as described previously (Xiao et al., 2010).

Results

Determination of Lipid Profiles in Oat and Rye during CA

Microdomains were extracted as DRM fractions by adding Triton X-100 to PM fractions as described in Peskan et al. (2000). A white layer was observed at the

interface of the 30% and 35% (w/w) sucrose layers. As previously described (Takahashi et al., 2013; Chapter 3 in this thesis), the recovery rates of DRMs from PM fractions (based on protein amount) were 10–20%, 8–12%, 6–12% and 8–12% in NA oat, NA rye, CA oat and CA rye, respectively.

In the present study, I extracted lipids from PM and DRM fractions corresponding to 100 µg proteins to conduct experiments under the same conditions to maintain reproducibility and lipid stability, and subsequently separated the extracted lipids with TLC. The patterns of PM and DRM lipids developed with commercial markers showed that the PM and DRM fractions contained FS, ASG, SG and PLs (PE, phosphatidylethanolamine; PG, phosphatidyl glycerol; PA, phosphatidic acid; PC, phosphatidylcholine; PS, phosphatidylserine; PI, phosphatidylinositol) as major lipid components (Fig. 4-1). The DRM lipids contained smaller amounts of PLs in comparison with PM lipids. For sterols, three sterol classes (FS, ASG and SG) were more brightly stained in DRMs than the PM. Specifically, ASG and FS were the major components in oat and rye DRMs, respectively. Because the fluorescence intensity of the primuline reagent does not allow us to compare amounts among different lipid groups, I quantified the absolute amounts of sterols, glycolipids and PLs by picking up each spot from the TLC plates and measuring sterol rings, sugar and phosphate moieties, respectively. PE, PG, PA, PC, PS and PI were mixed into one glass tube because the spots were close together and difficult to separate as distinct spots.

The quantification results of lipids in NA and CA oat are described in Table 4-1 and Fig. 4-2. Each value of lipids analyzed represents mol% of total lipids and nmol/100 µg protein. The proportions of sterols and PLs were quite different between the PM and DRMs in oat. For sterols, the mol% of sterols in the total lipids accounted for 42.6% and 73.6% in the PM and DRMs, respectively. The major sterol component in oat was ASG. Specifically, the relative amount of ASG in DRMs accounted for a substantial proportion (50.3%), which was 21.8% higher than in the PM. In contrast to sterols, the proportion of PLs in the PM was greater than in DRMs (41.9% in PM and 11.4% in DRMs). The GlcCer proportion in the PM was similar to that in DRMs (15.5% in PM vs 15.0% DRMs). These results indicate that oat DRMs are enriched in sterols and that PLs are excluded from oat DRMs.

In rye, DRMs contained much greater amounts of sterols and lower amounts of PLs than the PM, similar to oat DRMs (Table 4-2, Fig. 4-2). In rye, however, FS was the major sterol in both the PM and DRMs. Specifically, FS accounted for 50.5% of the total lipids in DRMs. The proportions of PLs were lower in DRMs than the PM (48.0% in PM vs 20.6% in DRMs). DRMs contained slightly higher proportions of GlcCer

(15.6% in DRMs vs 13.4% in PM). Therefore, rye DRMs had higher sterols and lower PLs than the PM, and had a different sterol composition from oat DRMs.

After CA treatment, the total amount of sterols in the oat PM decreased from 42.6% to 37.7% (Table 4-1). Similarly to the PM, sterols in oat DRMs also decreased from 73.6% to 66.0% (Table 4-1). However, there were no significant changes in the total sterol proportions in the rye PM and DRMs (Table 4-2). Looking at the detailed changes in sterol compositions during CA, the proportions of FS and ASG in the oat PM decreased from 10.2% to 7.4% and 28.5% to 24.8%, respectively, while no changes were observed in the rye PM (Tables 4-1 and 4-2, Fig. 4-2A). In oat DRMs, FS significantly decreased from 21.1% to 14.4% during CA. On the other hand, ASG in rye DRMs significantly decreased from 9.6% to 5.8% during CA (Tables 4-1 and 4-2, Fig. 4-2B). GlcCer decreased from 15.5% to 12.6% and 13.8% to 7.8% in the oat and rye PMs, respectively, during CA (Tables 4-1 and 4-2, Fig. 4-2A). However, there were no statistically significant changes of GlcCer in either oat or rye DRMs during CA (Tables 4-1 and 4-2, Fig. 4-2B). PLs increased during CA from 41.9% to 49.7% in the oat PM and from 48.0% to 52.1% in the rye PM (Tables 4-1 and 4-2, Fig. 4-2A). PLs in DRMs during CA increased 4.3% (11.4% to 15.7%) in oat and 0.6% (20.6% to 21.2%) in rye. Therefore, PL changes in DRMs were almost the same as those in the PM in both species.

Sterol Compositions of the PM and DRM in Oat and Rye during CA

Figure 4-3 shows the sterol compositions in the oat and rye PM and DRMs during CA. In both the PM and DRMs, the sterol composition in oat was quite different from that in rye. In oat, ASG was the major sterol in both the PM and DRMs while FS was abundant in the rye PM and DRMs. In the oat PM and DRMs, the proportions of FS increased but those of SG decreased during CA. In contrast, there were no significant changes in the proportions of FS and SG in the rye PM during CA. However, the proportion of ASG in rye DRMs decreased from 14.7% to 7.7% but the proportion of SG increased from 5.3% to 10.0%.

To obtain detailed FS compositional data, I performed gas chromatography analysis. I examined four major sterol species, sitosterol, stigmasterol, campesterol and cholesterol, and calculated the proportion of each sterol in the total FS (Fig. 4-4, Supplemental Table 4-1). Oat FSs were mainly composed of sitosterol, stigmasterol and cholesterol. The proportions of each sterol species in the PM were slightly different from those in DRMs. Among these abundant sterols, stigmasterol increased 1.19- and 1.33-fold while cholesterol decreased 0.68- and 0.40-fold in the oat PM and DRMs,

respectively, during CA. However, in the rye PM and DRMs, sitosterol and campesterol were the predominant sterol species. Although campesterol, stigmasterol and cholesterol were significantly enriched in rye NA DRMs compared with the rye NA PM (1.14-, 1.53- and 2.54-fold, respectively), the overall tendency was similar between the rye PM and DRMs. During CA, sitosterol and campesterol changed slightly in both the rye PM and DRMs (for rye, sitosterol, 1.07-fold in the PM and 1.10-fold in DRMs; for oat, campesterol, 0.79-fold in the PM and 0.82-fold in DRMs).

For SG and ASG, I used a newly developed quantification method with electrospray ionization tandem (triple quadrupole) mass spectrometry (ESI-MS/MS) as reported by Schrick et al. (2012) and calculated the proportions of four major sterol species in the total SG and ASG signals (Fig. 4-5, Supplemental Table 4-1). Although, I could not make a simple comparison between FS and SG/ASG compositions because of the different analysis methods, the proportions of stigmasterol in oat SG and ASG were 2.80 to 3.78 times less than those in FS. In the rye PM and DRMs during CA, ASG contained 3.90 to 10.1 times more cholesterol than FS. In both oat and rye, however, the predominant sterol species in SG and ASG was sitosterol as well as FS and most of the CA-induced changes were common among FS, SG and ASG (Figs. 4-5A and 4-5B).

In addition to sterol rings, I determined the compositions of the acyl chains bound to ASGs (Fig. 4-5C). The predominant acyl species in ASGs was 16:0 in both oat and rye. In oat and rye, DRMs contained significantly higher proportions of 16:0 than the PM. Specifically, rye DRMs had 1.33 and 1.26 times higher proportions of 16:0 than the PM. Although the proportions of unsaturated acyl chains such as 16:1, 18:1, 18:2, 18:3 and 20:1 were higher in the rye PM than the oat PM (32.0% in oat PM vs 43.1% in rye PM), no remarkable changes were observed during CA in either the oat or rye PM. During CA, unsaturated lipid species such as 18:3 and 18:1 slightly increased (1.27-fold) and the proportion of 16:0 decreased (0.89-fold) in rye DRMs.

GlcCer Compositions of the PM and DRMs in Oat and Rye during CA

GlcCer is composed of a C18 sphingoid base and a 2-hydroxy fatty acid. First, I measured the sphingoid base, which contains three major species (d18:1, 8-sphingadienine; d18:2, 4,8-sphingadienine; t18:1, 4-hydroxy-8-sphingenine) with *cis*-8 (*Z*) and *trans*-8 (*E*) isomers (Imai et al., 2012), and calculated the sphingoid base compositions against the total sphingoid base content in oat and rye during CA (Fig. 4-6, Supplemental Table 4-2). t18:1 (*Z*) was the predominant sphingoid base in the PM and DRMs isolated from both oat and rye during CA. Under NA conditions, the proportion of d18:1 (*E*) differed between the oat and rye PM (6.7% and 3.4%, respectively). In oat

NA DRMs, t18:1 (*E*) was 2.0 times higher than in the oat NA PM, while the DRM/PM ratio of t18:1 (*E*) in rye was 0.47. During CA, the proportion of d18:1 (*E*) in the oat PM decreased from 6.7% to 2.5%. Similarly, the proportion of t18:1 (*E*) in the rye PM decreased from 6.5% to 2.8%. In oat DRMs, there were no remarkable sphingoid base composition changes during CA. However, t18:1 (*E*) increased from 3.1% to 6.5% in rye DRMs.

For the 2-hydroxy fatty acid, the proportions of two major components, 24h:0 and 24h:1, were different between oat and rye (Fig. 4-7, Supplemental Table 4-2). In the NA PM, 24h:0 accounted for a relatively higher proportion in rye than in oat (25.1% and 15.0%, respectively). In comparison between the PM and DRMs, oat had a higher proportion of 24h:1 in DRMs than in the PM (65.8% and 47.6%, respectively). On the other hand, rye DRMs contained a higher proportion of 24h:0 than the PM (37.8% and 25.1%, respectively) and the proportion of 24h:1 was lower in DRMs than in the PM (29.0% and 38.3%, respectively). No obvious shifts of 2-hydroxy fatty acid composition were observed in the oat or rye PM during CA. Although the 2-hydroxy fatty acid compositions in oat DRMs were also unchanged during CA, the proportions of 24h:0 and 24h:1 in rye DRMs significantly decreased (37.8% to 29.9%) and increased (29.0% to 41.5%), respectively, during CA.

PL Compositions of the PM and DRMs in Oat and Rye during CA

I also determined the PL molecular species composition of PA, PS, PI, PE, PC, PG, LysoPE, LysoPC and LysoPG, and then calculated the proportions of each PL class (Fig. 4-8, Supplemental Table 4-3). In all of the samples I examined, PA and PC were the predominant PLs and accounted for more than 79.4%. In the PMs from NA plants, the proportion of PC was higher in rye than in oat (54.0% in oat PM vs 68.8% in rye PM). In NA DRMs, the proportion of PC in both oat and rye was lower than that in the PM (39.4% in oat DRMs and 59.1% in rye DRMs). Conversely, PE was enriched in DRMs and the DRM/PM ratios for PE were 5.1 and 3.8 in oat and rye, respectively. During CA, the proportion of PE in the oat PM increased 4.84-fold, while the rye PM did not exhibit major changes. After CA, the PC and PA proportions increased and decreased by 1.44- and 0.65-fold, respectively, in oat DRMs. Similarly to oat, the PA and PC proportions changed by 1.28- and 0.29-fold, respectively, in rye DRMs.

To examine the unsaturation levels of PLs in oat and rye, I computed the proportions of each PL with 0–6 double bonds in a single PL molecule (Fig. 4-9A). In NA oat and rye, the pair of fatty acids in a single PL molecule mainly contained 2, 3, 4, or 5 double bonds. For example, PC (34:2), PC (34:3) and PC (36:4) in NA oat and PC

(34:2), PC (36:4) and PC (36:5) in NA rye were the three most abundant PL species. After CA, the overall trends of unsaturation level did not change in either oat or rye. Conversely, in oat, less and higher unsaturated PLs decreased and increased, respectively, during CA. For example, PLs containing 2 double bonds significantly decreased by 15% from NA, while PLs containing 5 double bonds significantly increased by 24% during CA. In the same way, PLs containing 2 double bonds significantly decreased by 14%, and PLs containing 4 double bonds increased by 16% in rye during CA. NA DRMs contained more low-unsaturated PL species such as 2 double bond-containing PLs in both oat and rye (1.39- and 1.49-fold greater than the NA PM in oat and rye, respectively). The proportions of PLs containing 3 double bonds in NA were 1.33-fold greater than those in CA oat, while rye did not show any statistical changes in the proportions of each PL.

Based on the results in Fig. 4-9A, I calculated the mean unsaturation degree in each fraction and plant species during CA (Fig. 4-9B). When comparing the PM and DRMs under NA, mean unsaturation levels in the PM were greater than those in DRMs in both oat and rye (1.23- and 1.25-fold in oat and rye, respectively). In the PM, the unsaturation level increased in both oat and rye from 3.24 to 3.42 and from 3.37 to 3.46 during CA. In DRMs, however, there were no statistical changes in rye during CA even though oat DRMs showed an increased unsaturation level from 2.62 to 2.82.

Discussion

Previously, PM lipid compositions in oat (cv. Ogle) and rye (cv. Puma) were determined and discussed in relation to differences in the freezing tolerance of oat and rye (Uemura and Steponkus, 1994). Webb et al. (1994) reported that freeze-induced lesions of the PM occurred at different temperatures in oat and rye and extensively observed the behavior of the PM surface under freezing temperature in oat and rye. In the present study, the lipid compositions of microdomain-enriched DRM fractions and the PM were determined in oat and rye both before and after CA and are discussed from the viewpoint of the properties of each lipid species and the influence of these lipids on freezing tolerance with reference to previous studies.

Microdomain Compositions in Oat and Rye before CA

In the present study, DRM fractions were isolated as microdomain-enriched fractions by detergent treatment of the PM and subsequent sucrose-density gradient centrifugation. This procedure gave us a white band at the interface between the 30/35% (w/w) sucrose layers, which was collected. The procedure was very similar to many

previous reports carried out with plant samples such as *Arabidopsis*, tobacco, leek and potato (Peskan et al., 2000; Mongrand et al., 2004; Laloi et al., 2006; Krügel et al., 2008; Minami et al., 2009; Raffaele et al., 2009). PM and DRM lipid separation and subsequent primuline visualization revealed that PLs were depleted in the DRM fractions in both oat and rye and the fluorescence patterns of sterols were different between oat and rye before CA treatment (Fig. 4-1). When the lipids were quantified, sterols were accounted for 73.6% and 63.8% of the total NA DRM lipids in oat and rye, which was 1.73- and 1.63-fold greater than that of the NA PM in oat and rye, respectively (Tables 4-1 and 4-2, Fig. 4-2). Conversely, the proportions of PLs were much lower in DRMs (11.4% in oat and 20.6% in rye) than those in the PM (41.9% in oat and 48.0% in rye; Tables 4-1 and 4-2, Fig. 4-2). A sphingolipid, GlcCer, did not show statistical differences between the PM and DRMs in either oat or rye (Tables 4-1 and 4-2, Fig. 4-2). Because sphingolipids can be relatively tightly associated with each other and have a high melting point because of the long chain fatty acid in their molecular structure and high hydrophobicity, they form a lipid nanodomain with low fluidity that differs from the fluidic phase mainly composed of PLs and probably contribute to microdomain formation (Simons and Ikonen, 1997). On the other hand, sterols are also considered to be a major component of microdomains because they have an affinity to GlcCer and fill the intermolecular spaces of GlcCer (Simons and Ikonen, 1997). In previous studies on *Arabidopsis*, tobacco and leek, DRM fractions also showed lower proportions of PLs and higher proportions of sphingolipids and sterols than PM fractions (Mongrand et al., 2004; Borner et al., 2005; Laloi et al., 2006). Therefore, the results in the present study are consistent with previous reports that oat and rye microdomains before CA treatment mainly consist of sphingolipids and sterols, and that PLs are depleted in microdomains. However, sterols accounted for significantly higher proportions than GlcCer. Thus, these results indicate that sterols may be a particularly important constituent of microdomains to determine their functions and structure in oat and rye.

Alterations of PM and Microdomain Compositions in Oat and Rye during CA

The relationship between PM lipid compositions and freezing tolerance in oat (cv. Ogle) and rye (cv. Puma) has been investigated and discussed previously (Uemura and Steponkus, 1994; Webb et al., 1994). These studies demonstrated that freeze-induced dehydration results in ultrastructural changes associated with the PM, fracture-jump lesions and lamellar-to-hexagonal II (H_{II}) phase transitions, and that changes of PM lipid compositions decrease the occurrence of these

membrane-associated lesions. However, the PM lipid compositions obtained in the present study were somewhat different from previous reports. For example, the GlcCer and PLs compositions in oat determined by Uemura and Steponkus (1994) were 27.2% and 28.8%, respectively. Here, the proportions of GlcCer and PLs in oat were 15.5% and 41.9%, respectively. Differences in cultivars, growth conditions and experimental systems may affect PM lipid compositions. Although CA treatment resulted in many compositional changes in the PM, the patterns of PM lipid changes (e.g. an increase of PLs and a decrease of GlcCer in oat) were common in both the previous and present studies. In oat and rye, the proportions of PLs and GlcCer in the PM changed, which may influence lipid bilayer hydration because PLs and GlcCer are highly and poorly hydrated lipid classes, respectively. Hydration of the PM surface is important for preventing H_{II} phase transition, which is an inter-bilayer event that occurs when interaction between the PM and various closely-positioned endomembranes triggered by freeze-induced dehydration becomes stronger (Gordon-Kamm and Steponkus, 1984b; Webb et al., 1994). Therefore, greater hydration of the PM surface in both oat and rye achieved by increasing PLs and decreasing GlcCer during CA may contribute to increasing PM stability under freezing conditions. Additionally, because the PL/GlcCer ratio was higher in rye than in oat (6.68 and 3.94, respectively), the rye PM may have a lower incidence of H_{II} phase transition and a more stable membrane structure than the oat PM under freezing temperatures.

In oat DRMs during CA, the proportion of sterols significantly decreased (by 7.6%) and the proportion of PLs increased (by 4.3%) as with the PM, while the GlcCer proportion did not change (Table 4-1, Fig. 4-2). Conversely, rye DRMs did not show any statistical changes in the proportions of sterols, GlcCer or PLs. Because GlcCer is a main component of microdomains (Simons and Ikonen, 1997), the proportion of GlcCer in both oat and rye may not change in DRMs during CA (but decreases in the PM). This tendency has been confirmed in *Arabidopsis* DRMs (Minami et al., 2009). The proportions of sterols decreased in oat DRMs (73.6% to 66.0%) during CA but did not change in rye DRMs (63.8% to 64.5%). Plant sterols are considered to promote lipid domain formation (Xu et al., 2001) and also to be important for regulating the temperature sensitivity of raft-like membrane structures (Beck et al., 2007). Although the proportions of PLs increased by 4.3% during CA in oat DRMs (11.4% to 15.7%), rye DRMs did not show a change in PL proportion and maintained a higher proportion of PLs than oat DRMs after CA (20.6% in oat and 21.2% in rye after CA). As described above, PLs are important for maintaining PM stability under freezing conditions (Gordon-Kamm and Steponkus, 1984b; Webb et al., 1994). Thus, the high proportion of

PLs in rye DRMs suggests that high PL amounts contribute to microdomain stability during freezing.

Alterations of Sterol Compositions in Oat and Rye during CA

ASG and FS were the predominant sterols in the oat and rye PM, respectively, which was also observed in DRM samples (Fig. 4-3). In DRMs, the proportion of ASG increased in oat (68.2% to 71.7%) but decreased in rye (14.7% to 7.7%) during CA. Webb et al. (1995) revealed that ASG is more effective than FS for H_{II} phase formation in lipid mixtures of dioleoyl-PC (DOPC) and dioleoyl-PE (DOPE) under dehydration conditions. ASGs contain a sterol ring, sugar and acyl group and are more hydrophobic than other sterols (Webb et al., 1995). Therefore, the higher hydrophobicity of ASGs may help promote lamellar-to-H_{II} phase transitions under freeze-induced dehydration conditions and ultimately influence plant freezing tolerance. The biosynthesis of SG and ASG is catalyzed by UDP-glucose: sterol glucosyltransferases (UGTs, EC 2.4.1.173, 22, 23). Thus, the activity of UGTs possibly contributes to the different ASG proportions in oat and rye.

In addition to sterol lipid classes, the molecular species of sterols were determined before and after CA (Figs. 4-4 and 4-5). In oat and rye, sitosterol was commonly the predominant phytosterol among FSs, SGs and ASGs (Figs. 4-4, 4-5A and 4-5B). Oat FS contained more stigmasterol than rye FS in NA DRMs (38.7% in oat and 4.5% in rye) and DRMs prepared from NA rye had more sitosterol than NA oat DRMs (36.3% in oat and 70.7% in rye) although the SG and ASG sterol compositions were only slightly different between oat and rye. Although no studies have examined the effects of sitosterol on lipid mixtures under freeze-induced dehydration conditions in comparison with stigmasterol, the vast differences in sterol species may contribute to the difference in freezing tolerance between oat and rye.

The acyl chain lipid species of ASGs were also determined (Fig. 4-5C). The acyl chain compositions in ASGs also did not change considerably during CA in oat and rye. DRM ASGs contained more saturated fatty acids (16:0 and 18:0) than PM ASGs in NA oat (68.0% in PM and 75.8% in DRMs) and the same was true in NA rye (56.9% in PM and 73.6% in DRMs). Given that microdomains are considered to be enriched in hydrophobic and high-melting point lipids such as sphingolipids and sterols (Simons and Ikonen, 1997), saturated acyl chain ASGs may also tend to gather in microdomain areas in the PM.

Sterol is also important for the modulation of H⁺-ATPase activity (Grandmougin-Ferjani et al., 1997). H⁺-ATPase is known as a DRM-enriched protein

(Minami et al., 2009; Takahashi et al., 2012; Takahashi et al., 2013; Chapters 2 and 3 in this thesis) and was demonstrated to be enriched in microdomains of the yeast *Saccharomyces cerevisiae* (Bagnat et al., 2001). H⁺-ATPase activity is also up-regulated by cold temperatures and may be involved in the regulation of intracellular pH levels and membrane potential (Ishikawa and Yoshida, 1985). Thus, it is possible that sterol compositions and their changes in microdomains may affect the activities of microdomain-associated proteins, and sterol-enriched microdomains may have an important role for the modulation of protein structure and function as a functional scaffold during CA.

Alterations of GlcCer Compositions in Oat and Rye during CA

Among the two major parts of GlcCer, the C18 sphingoid base showed some significant changes during CA in both oat and rye (Fig. 4-6) and t18:1 was the predominant C18 sphingoid base in both species as reported in *Brassicaceae* (Imai et al., 2000a). However, the overall profiles of sphingoid base compositions were similar between oat and rye and the maximum amount of CA-induced changes was less than 4.2% (d18:1[E] in the oat PM; Fig. 4-6) even though Kawaguchi et al. (2000) revealed that higher proportions of t18:1 (Z) were positively correlated with freezing tolerance in grapevine leaves. On the other hand, the 2-hydroxy fatty acid composition was different in oat and rye during CA (Fig. 4-7). In both oat and rye, 24h:0 and 24h:1 were the major 2-hydroxy fatty acid species. When comparing the PM and DRMs under NA conditions, the 2-hydroxy fatty acid composition in oat DRMs mimicked that in the oat PM. In rye, DRMs contained more 24h:0 and less 24h:1 than the PM. Although the total GlcCer proportions in rye did not differ between the PM and DRMs (Fig. 4-2), rye microdomains may be enriched in 24h:0-containing GlcCer, which has a relatively higher melting point than 24h:1. During CA, there were no notable changes of 2-hydroxy fatty acid composition in the oat and rye PMs or oat DRMs. Only rye DRMs showed CA-induced changes in 2-hydroxy fatty acid composition (37.8% to 29.9% for 24h:0 and 29.0% to 41.5% for 24h:1). As with the acyl chain changes in ASGs, these changes in 2-hydroxy fatty acid composition during CA may increase the unsaturation degree of fatty acids and the stability of microdomains in the PM under freezing conditions. Therefore, the 2-hydroxy fatty acid composition of microdomains and its changes during CA may be important for the higher freezing tolerance in rye.

In addition, sphingolipids have numerous functions in plant cells. A sphingolipid metabolite, sphingosine-1-phosphate, is responsive to drought-induced signal transduction in guard cells (Ng et al., 2001; Worrall et al., 2003) and sphingolipid fatty

acid 2-hydroxylase (FAH) in *Arabidopsis* is required for oxidative stress responses (Nagano et al., 2012). The relationship between the 2-hydroxy fatty acid composition in microdomains and many signaling pathways derived from sphingolipids may be involved in the CA mechanism and the acquisition of freezing tolerance.

Alterations of PL Compositions in Oat and Rye during CA

Looking at the composition of PL species in Fig. 4-8, PC and PA were the two most abundant PL species. However, Uemura and Steponkus (1994) reported that PC and PE were the predominant PL species in oat and rye PMs (1994). This difference may have been caused by endogenous phospholipase D (PLD) activity during the PM preparation process. PLD has the ability to produce PA mainly from PC and PE and some PLDs such as PLD γ 1 and PLD δ prefer PE rather than PC (Li et al., 2009). These PLDs require micromolar levels of Ca²⁺ for PA-producing activity and are located in intracellular membranes and the PM (Li et al., 2009). Although I added EGTA to chelate Ca²⁺ and performed PM preparation on ice to repress PLD activity, PL analysis is a long process from PM preparation to PL extraction/quantification. During this process, PE may have been degraded and changed to PA by PLD activity. Nevertheless, it is likely that PC is still the predominant PL species in both the PM and DRMs (Fig. 4-8). A previous study of tobacco leaves and BY-2 cells revealed that PC is one of the major PL species in both the PM and DRMs (Furt et al., 2010). Therefore, PC is universal in monocotyledonous and dicotyledonous plants as the predominant PL in the PM and microdomains. In mammalian cells as represented by humans, extracellular leaflets of the PM are considered to be enriched in sphingomyelin and cytoplasmic leaflets are composed of PC, PE and PS as the major components of lipid rafts (Kiessling et al., 2009). In plants, PC also may play a role as a main component of inner leaflets in microdomains.

Focusing on the unsaturation degree of fatty acids in PLs, PLs containing double or triple unsaturated fatty acids were abundant in both the PM and DRMs. A previous study (Uemura and Steponkus, 1994) found that 16:0/18:2 and 16:0/18:3 fatty acid pairs were the major combinations in PC and PE. However, the present study revealed that PC (34:2) and PC (34:3) were abundant PLs in both oat and rye, accounting for 16.8% and 11.1% of the total PLs, respectively, in the PM fraction prepared from NA oat (Supplemental Table 4-3). Therefore, the fatty acid composition profile in our study is in agreement with the previous study. In the PM, PC (36:4) and PC (36:5) accounted for large proportions of the total PLs as major PL species in both NA oat and rye (e.g. 10.9% for PC [36:4] and 8.8% for PC [36:5] in the oat NA PM;

Supplemental Table 4-3). In DRM fractions, however, these two PLs were much less abundant (less than 5%) and CA treatment increased their proportions (e.g. 1.63-fold for PC [36:4] and 2.47-fold for PC [36:5] in oat; Supplemental Table 4-3). Phase transitions of membranes can be promoted by saturated fatty acids at low temperature (Wu and Browse, 1995; Iba, 2002) and microdomain-enriched DRMs contained relatively greater proportions of saturated fatty acids than the PM (Fig. 4-9B). Although saturated fatty acids tend to be associated with sterols and other microdomain components (Xu et al., 2001; Simons and Sampaio, 2011), plants may be able to change these interactions to increase the availability of unsaturated PLs such as PC (36:4) and PC (36:5) in microdomains more frequently during CA and avoid phase transitions in microdomains under low temperature. The overall unsaturation degree of PLs, in fact, increased in the oat and rye PM and oat DRMs during CA in agreement with the relationship between the physicochemical properties of unsaturated PLs and membrane stability at low temperature (Fig. 4-9B). In rye DRMs, however, the mean unsaturation degree of PLs did not change during CA. Rye DRMs were rich in FS, which is less effective for freeze-induced phase transitions in membranes than ASG (Webb et al., 1995), and even the acyl chain of ASGs in rye was relatively enriched in unsaturated species in comparison with oat (Figs. 4-3 and 4-5C). Considering these factors in oat and rye, sterol compositions favorable for stability at freezing temperatures in rye microdomains may be sufficient to maintain microdomain stability and, hence, freezing tolerance so that no statistical changes in the mean unsaturation degree of PLs are necessary during CA.

Supporting information

Supplemental Table 4-1. Sterol compositions in oat and rye during CA.

Supplemental Table 4-2. GlcCer compositions in oat and rye during CA.

Supplemental Table 4-3. PLs compositions in oat and rye during CA.

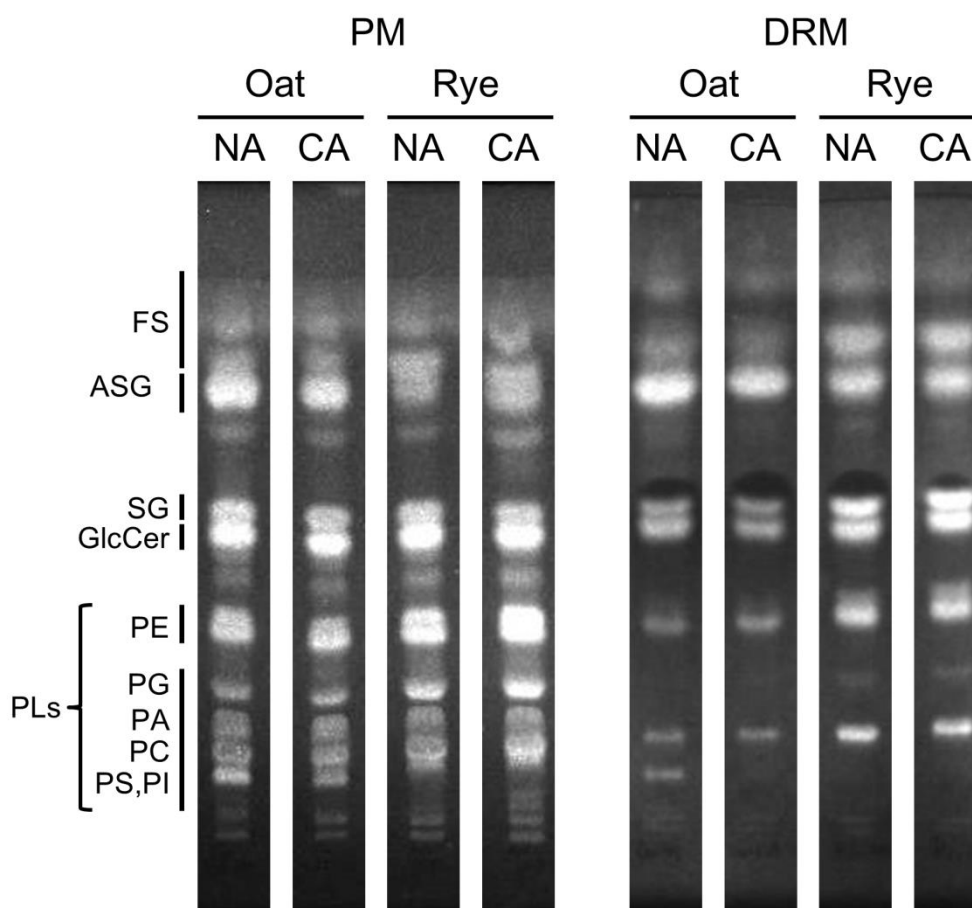


Fig. 4-1. TLC patterns of PM and DRM fractions in oat and rye. PM and DRM fractions isolated from oat and rye leaves were examined by TLC with developing solvent composed by chloroform/methanol/water (65:25:4, v/v/v). FS, free sterol; ASG, acylated sterylglucoside; SG, sterylglucoside; GlcCer, glucocerebroside; PE, phosphatidylethanolamine; PG, phosphatidylglycerol; PA, phosphatidic acid; PC, phosphatidylcholine; PS, phosphatidylserine; PI, phosphatidylinositol.

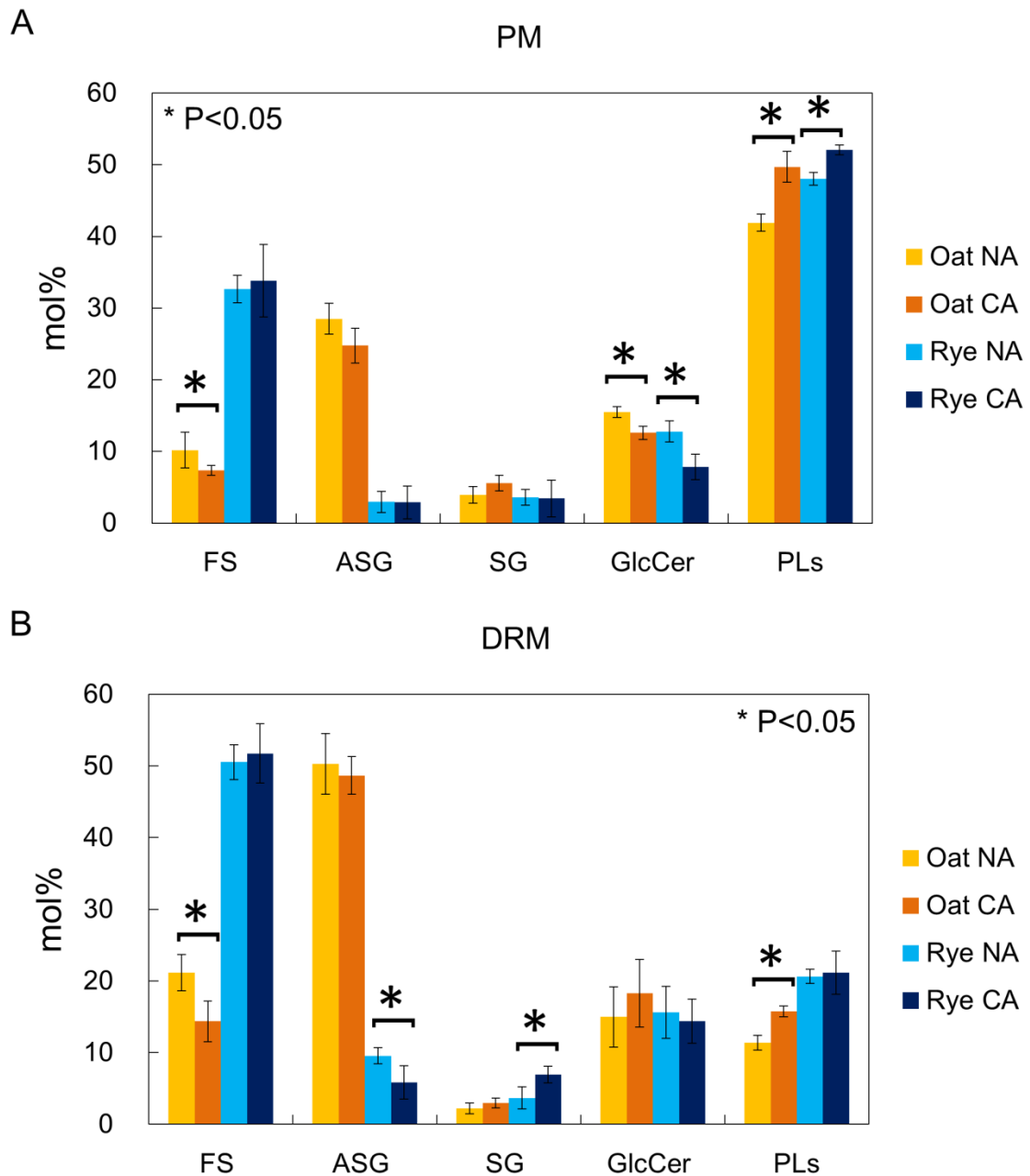


Fig. 4-2. Lipid compositions of PM and DRM fractions in oat and rye. Lipid compositions of PM (A) and DRM (B) were represented as bar graphs and Y-axis of the graph is mol% of each lipid class in total lipid contents. Error bars indicate standard deviations (n=3-5). FS, free sterol; ASG, acylated sterylglucoside; SG, sterylglucoside; GlcCer, glucocerebroside; PLs, phospholipids. * $p < 0.05$ by student's t -test.

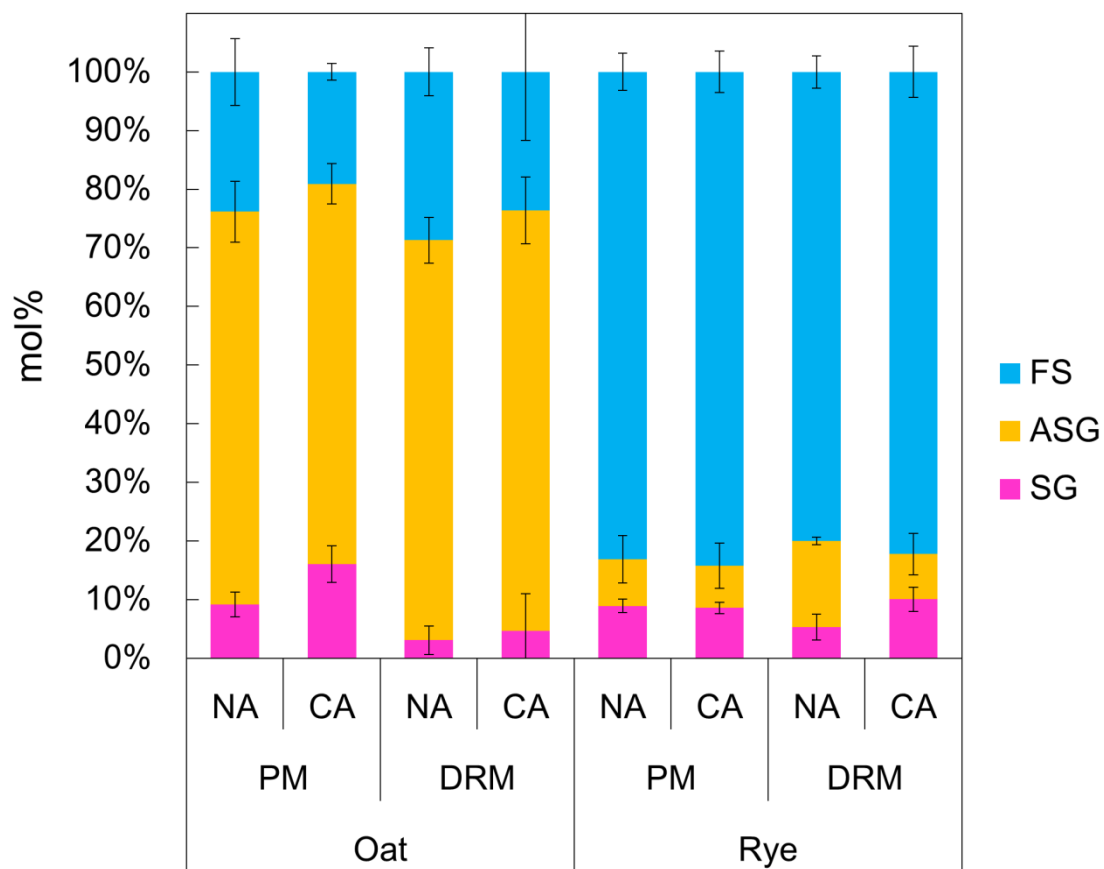


Fig. 4-3. Sterol compositions of PM and DRM fractions in oat and rye. Sterol compositions of PM and DRM were quantified and Y-axis of the graph is mol% of each sterol in total sterol contents. Error bars indicate standard deviations (n=3-5). FS, free sterol; ASG, acylated sterylglycoside; SG, sterylglycoside.

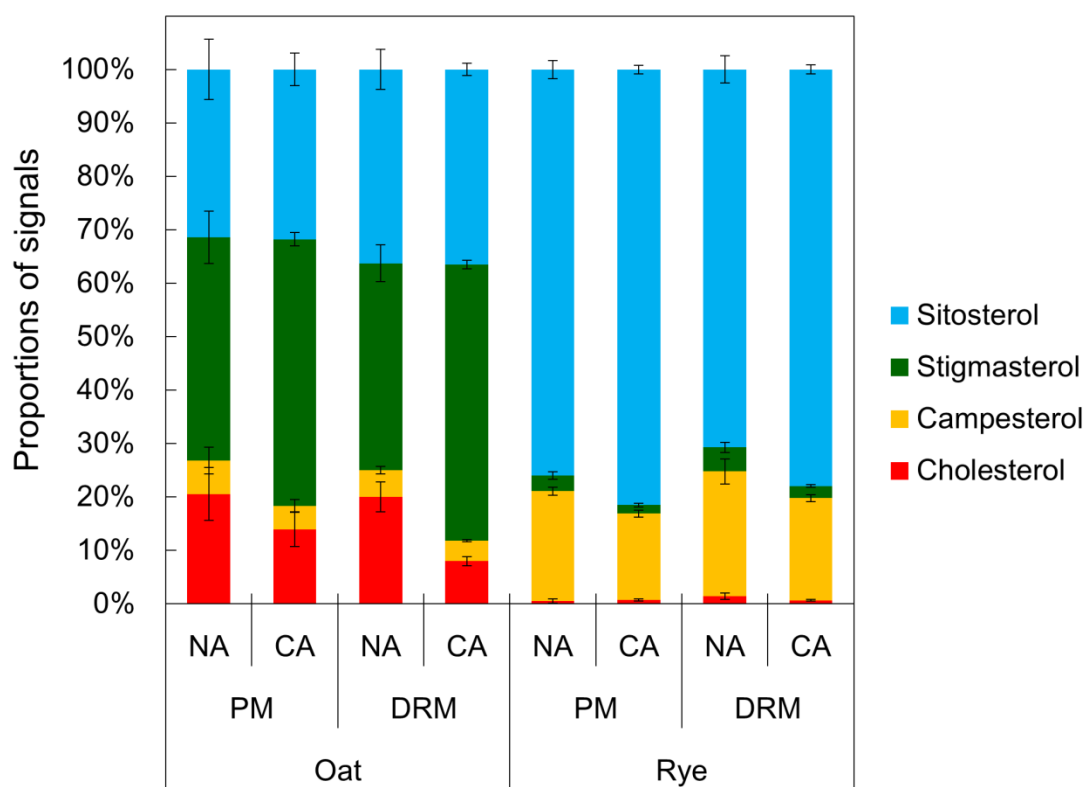


Fig. 4-4. Molecular species compositions of FS in PM and DRM fractions. Molecular species compositions of FS in PM and DRM were quantified by GC analysis. Y-axis of the graph is proportions of signals derived from each sterol species in total FS signals. Error bars indicate standard deviations (n=4-8).

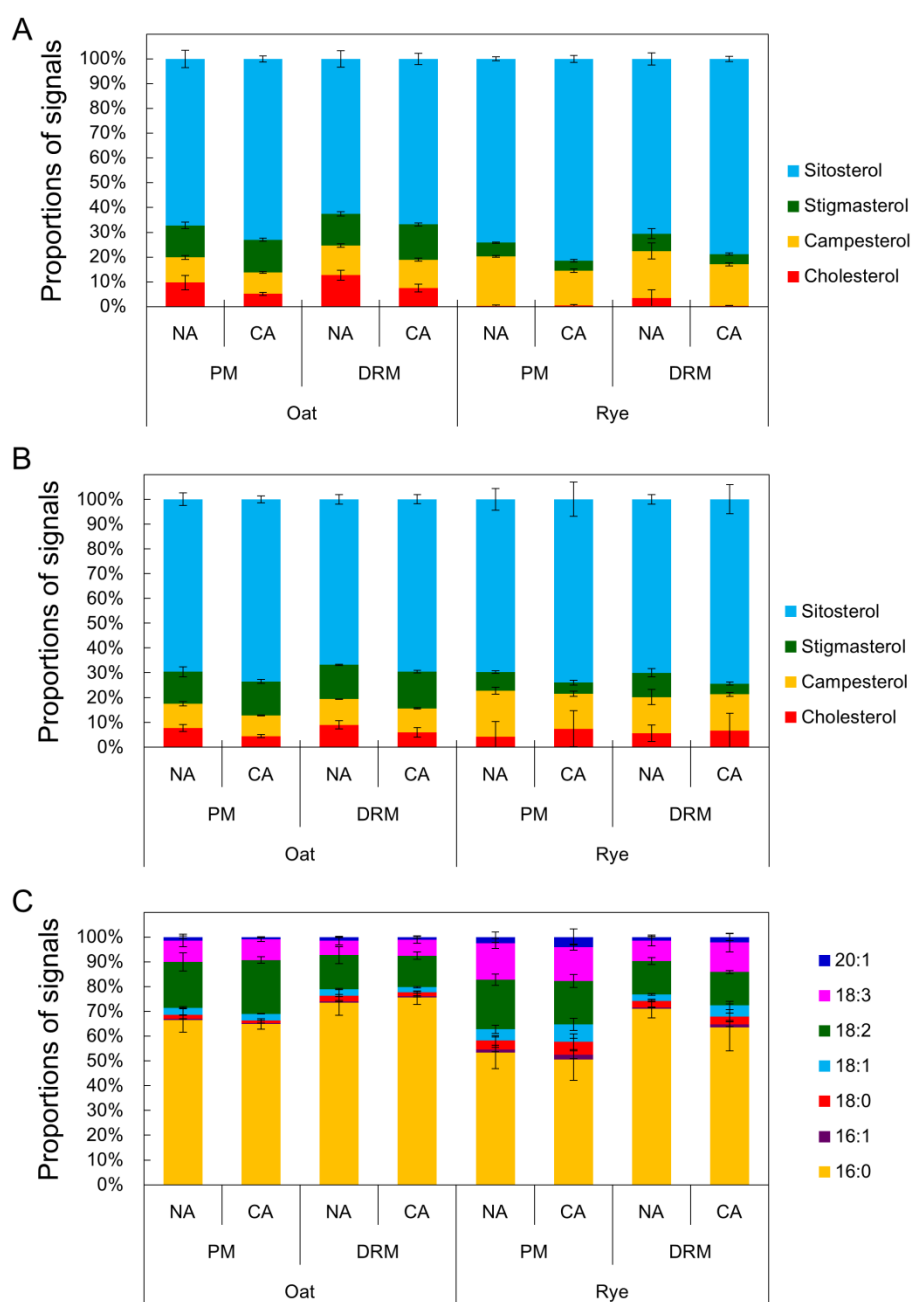


Fig. 4-5. Molecular species compositions of SG and ASG in PM and DRM fractions.

Molecular species compositions of SG and ASG in PM and DRM were quantified by direct infusion MS/MS analysis. The Y-axis of the graph represents the proportion of signals derived from each sterol or acyl species in total SG or ASG signals. Error bars indicate standard deviations (n=4). Molecular species compositions of the sterol part of SG and ASG are shown in A and B, respectively. C shows molecular species compositions of acyl chains of ASG.

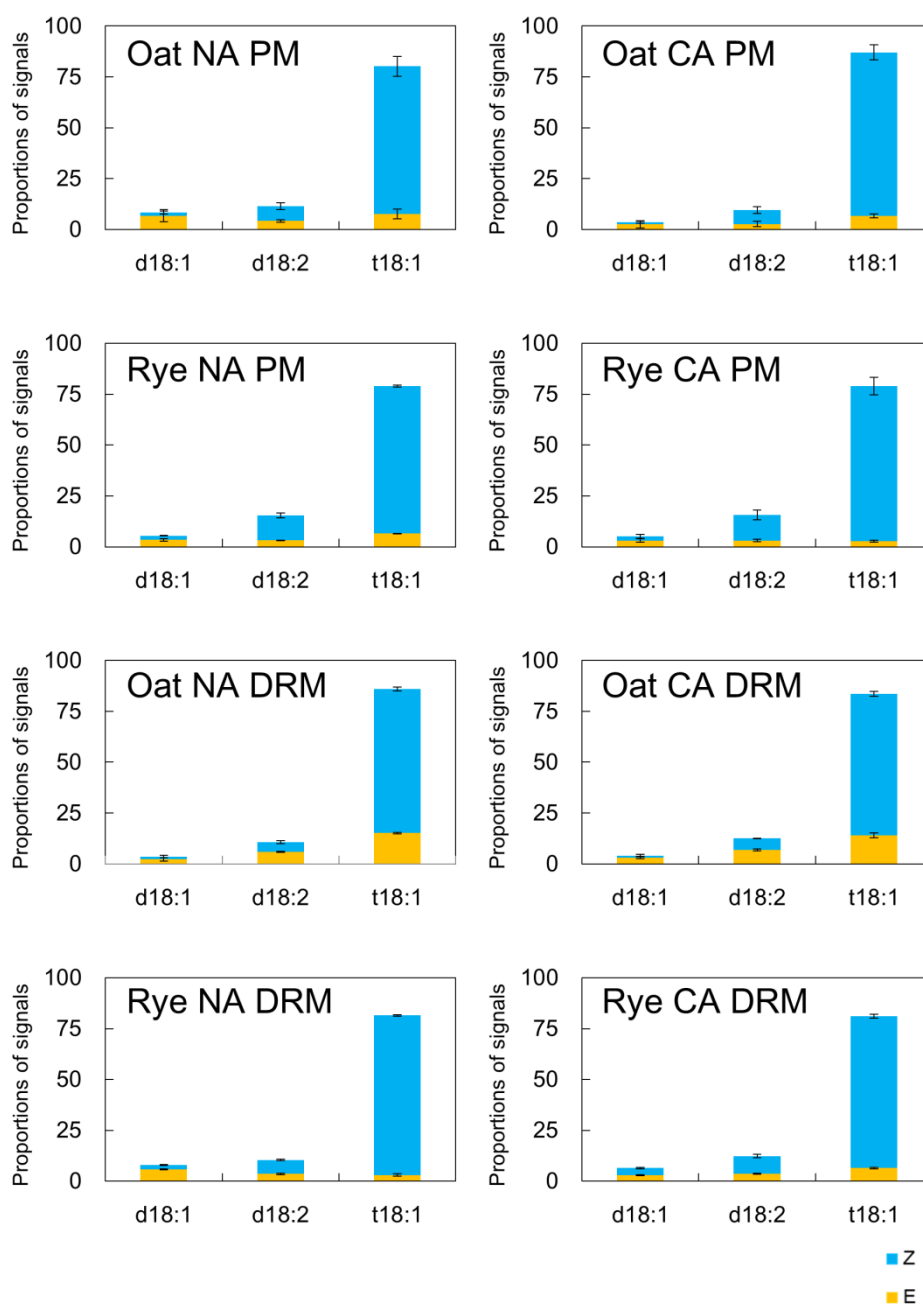


Fig. 4-6. Molecular species compositions of C18 sphingoid bases of GlcCer in PM and DRM fractions. Molecular species compositions of C18 sphingoid bases of GlcCer in PM and DRM were quantified by LC-MS/MS analysis. Y-axis of the graph indicates proportions of signals derived from each sphingoid base species in total GlcCer signals. Error bars indicate standard deviations (n=3). Z and E mean cis-8 and trans-8 isomers, respectively. d18:1, 8-sphingadienine; d18:2, 4,8-sphingadienine; t18:1, 4-hydroxy-8-sphingenine.

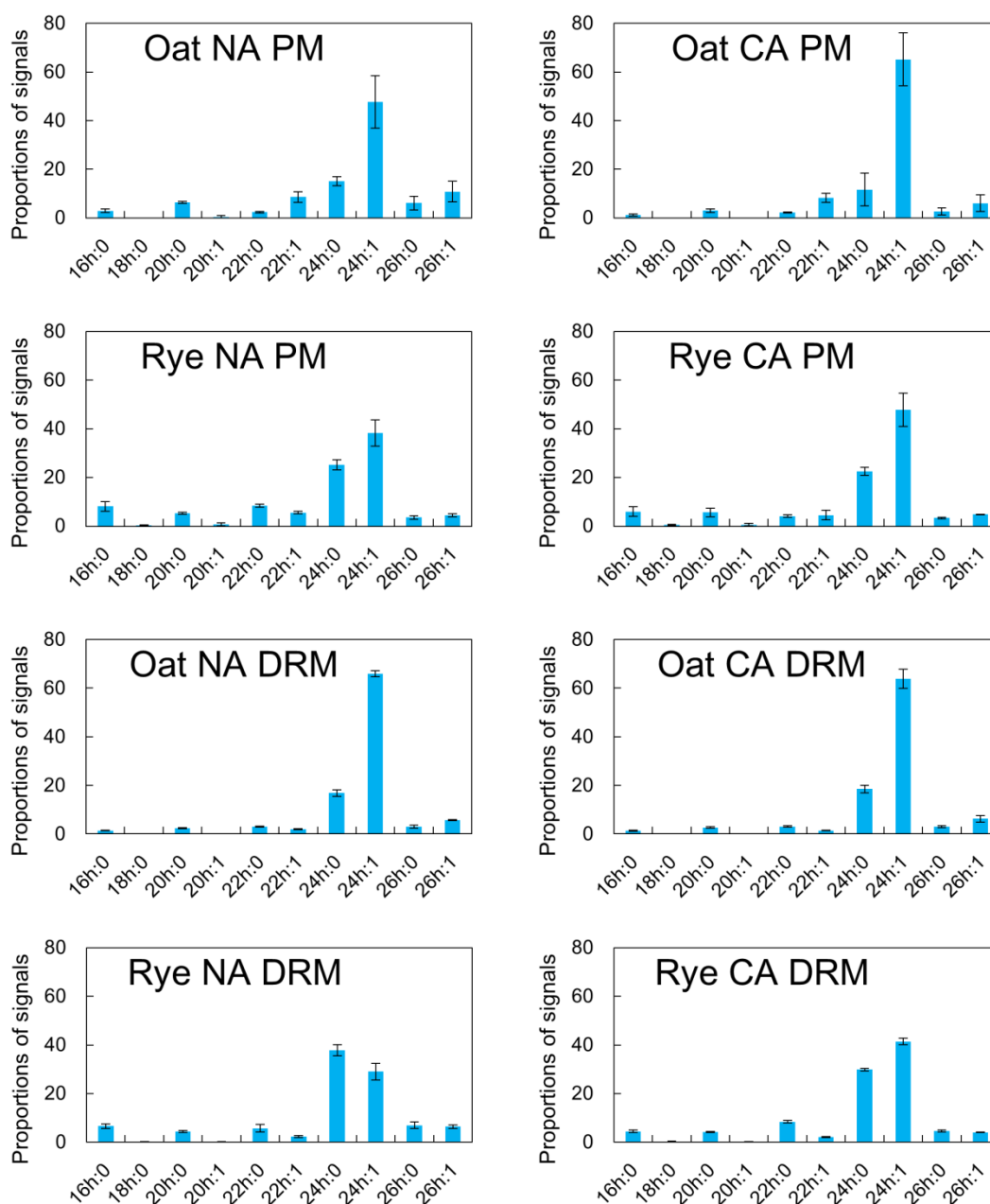


Fig. 4-7. Molecular species compositions of 2-hydroxy fatty acids of GlcCer in PM and DRM fractions. Molecular species compositions of 2-hydroxy fatty acids of GlcCer in PM and DRM were quantified by LC-MS/MS analysis. Y-axis of the graph indicates proportions of signals derived from each 2-hydroxy fatty acid in total GlcCer signals. Error bars indicate standard deviations (n=3).

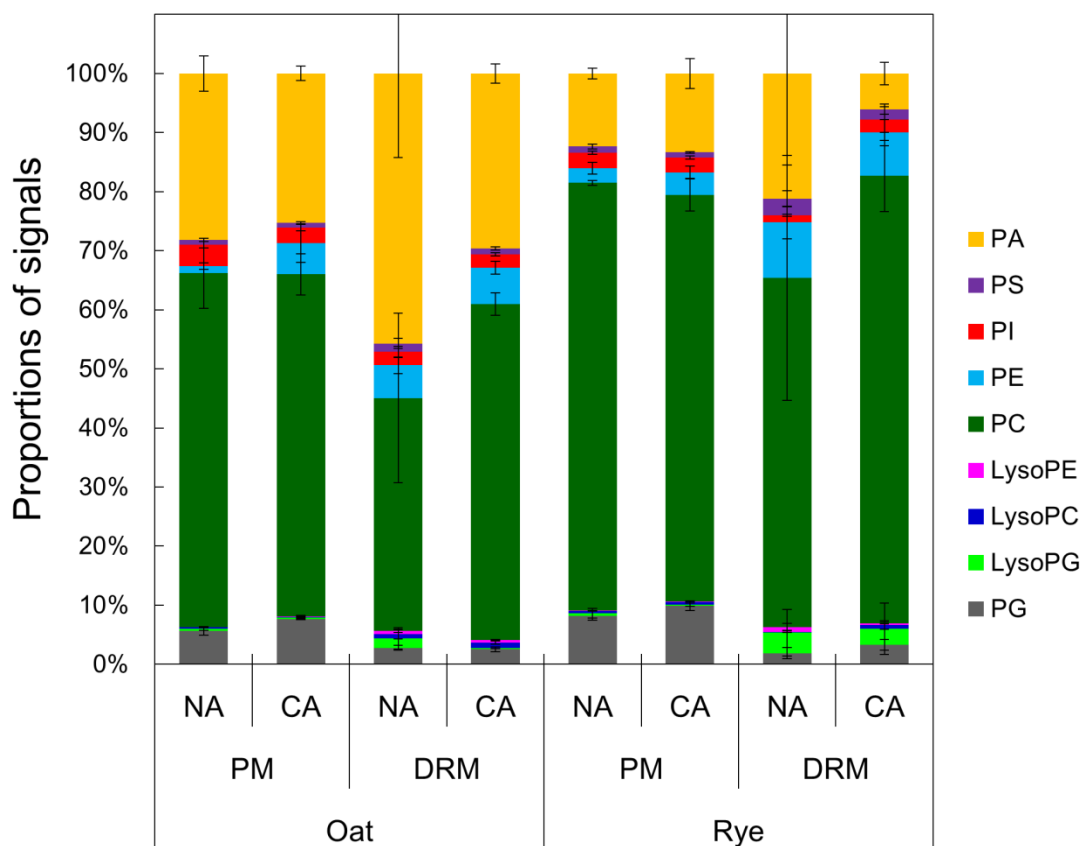


Fig. 4-8. PL compositions of PM and DRM fractions in oat and rye. PL compositions of PM and DRM were quantified and the Y-axis of the graph represents proportions of signals derived from each PL class in total PL signals. Error bars indicate standard deviations (n=4). PA, phosphatidic acid; PS, phosphatidylserine; PI, phosphatidylinositol; PE, phosphatidylethanolamine; PC, phosphatidylcholine; LysoPE, lysophosphatidylethanolamine; LysoPC, lysophosphatidylcholine; LysoPG, lysophosphatidylglycerol; PG, phosphatidylglycerol.

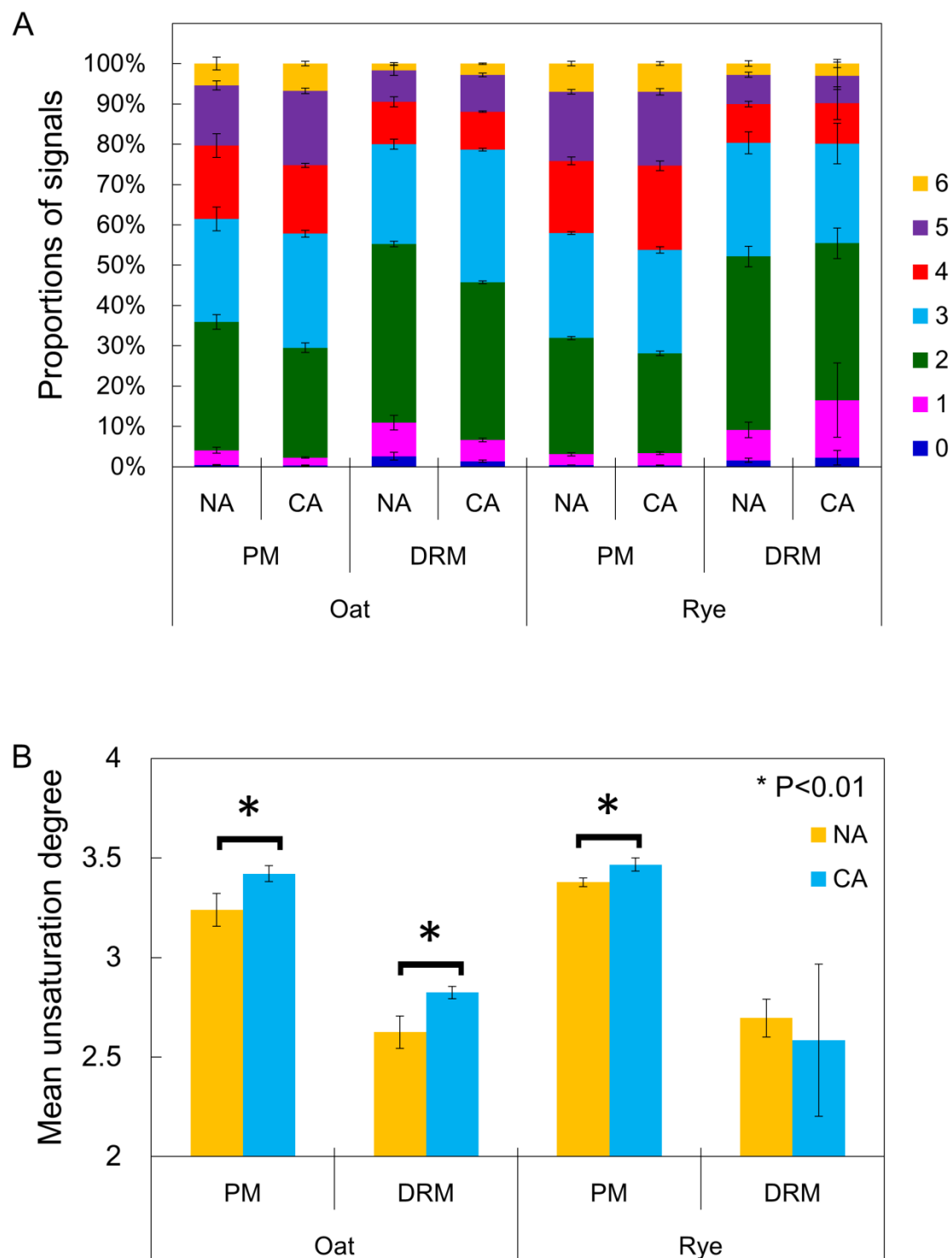


Fig. 4-9. Unsaturation levels of fatty acid in PLs in PM and DRM fractions. (A) PL molecules were categorized based on the sum of unsaturated bonds in two acyl chains. (B) The Mean unsaturation degree was calculated for PM and DRM fractions in oat and rye. Error bars indicate standard deviations (n=4). * $p < 0.01$ by student's t -test.

Table 4-1. Compositions of lipid class in oat PM and DRM. The values of results are the mean \pm SD (n=3-5) of mol% of total lipids and nmol of 100 μ g protein (as indicated in parentheses). * p <0.05 by student's t -test. FS, free sterol; ASG, acylated sterylglucoside; SG, sterylglucoside; GlcCer, glucocerebroside; PLs, phospholipids.

Lipid	PM		DRM	
	NA (n=3)	CA (n=4)	NA (n=3)	CA (n=5)
Sterols	42.6 \pm 3.1 (96 \pm 23)	37.7 \pm 2.5 (70 \pm 10)	73.6 \pm 3.8 (175 \pm 37)	66.0 \pm 3.7* (188 \pm 28)
FS	10.2 \pm 2.5 (22 \pm 4)	7.4 \pm 0.7 (14 \pm 1*)	21.1 \pm 2.5 (50 \pm 6)	14.4 \pm 2.8* (40 \pm 6)
ASG	28.5 \pm 2.2 (65 \pm 18)	24.8 \pm 2.4 (46 \pm 8)	50.3 \pm 4.2 (121 \pm 32)	48.7 \pm 2.6 (139 \pm 25)
SG	3.9 \pm 1.2 (9 \pm 4)	5.6 \pm 1.1 (10 \pm 2)	2.2 \pm 0.8 (5 \pm 1)	2.9 \pm 0.7 (8 \pm 3)
GlcCer	15.5 \pm 0.7 (35 \pm 8)	12.6 \pm 0.9* (24 \pm 6)	15.0 \pm 4.2 (35 \pm 10)	18.3 \pm 4.7 (53 \pm 22)
PLs	41.9 \pm 1.2 (94 \pm 22)	49.7 \pm 2.2* (94 \pm 19)	11.4 \pm 1.0 (28 \pm 11)	15.7 \pm 0.8* (46 \pm 12)
Total	100 (225 \pm 41)	100 (188 \pm 29)	100 (238 \pm 42)	100 (287 \pm 48)

Table 4-2. Compositions of lipid class in rye PM and DRM. The values of results are the mean \pm SD (n=3-5) of mol% of total lipids and nmol of 100 μ g protein (as indicated in parentheses). * p <0.05 by student's t -test. FS, free sterol; ASG, acylated sterylglucoside; SG, sterylglucoside; GlcCer, glucocerebroside; PLs, phospholipids.

Lipid	PM		DRM	
	NA (n=4)	CA (n=3)	NA (n=4)	CA (n=5)
Sterols	39.2 \pm 2.1 (105 \pm 16)	40.1 \pm 1.8 (122 \pm 42)	63.8 \pm 4.6 (156 \pm 64)	64.5 \pm 3.3 (190 \pm 37)
FS	32.9 \pm 1.9 (87 \pm 13)	33.8 \pm 5.0 (100 \pm 22)	50.5 \pm 2.4 (123 \pm 48)	51.7 \pm 4.1 (153 \pm 36)
ASG	2.9 \pm 1.5 (8 \pm 4)	2.9 \pm 2.3 (10 \pm 11)	9.6 \pm 1.1 (24 \pm 10)	5.8 \pm 2.3* (16 \pm 4)
SG	3.2 \pm 1.1 (10 \pm 4)	3.4 \pm 2.5 (12 \pm 12)	3.7 \pm 1.5 (9 \pm 6)	6.9 \pm 1.2* (20 \pm 6*)
GlcCer	13.4 \pm 1.5 (34 \pm 2)	7.8 \pm 1.8* (25 \pm 14)	15.6 \pm 3.7 (37 \pm 17)	14.4 \pm 3.1 (42 \pm 11)
PLs	48.0 \pm 0.9 (128 \pm 17)	52.1 \pm 0.7* (158 \pm 52)	20.6 \pm 1.0 (48 \pm 15)	21.2 \pm 3.0 (64 \pm 29)
Total	100 (267 \pm 28)	100 (305 \pm 87)	100 (241 \pm 79)	100 (296 \pm 61)

Chapter 5

Extensive proteomic approaches to identifying glycosylphosphatidylinositol-anchored proteins in *Arabidopsis* reveal diverse responses during cold acclimation

Summary

When plants are exposed to non-freezing low temperatures they can increase their freezing tolerance (cold acclimation, CA). CA induces compositional changes of the plasma membrane (PM) and sterol/sphingolipid-enriched microdomain proteins. Previous studies in animal cells have demonstrated that glycosylphosphatidylinositol-anchored proteins (GPI-APs), which are lipid-modified proteins, are associated with microdomains. However, the functional significance of GPI-APs is not yet fully understood and no studies have reported the relationship between GPI-APs and the CA mechanism. In this study, I aimed to investigate the responsiveness of GPI-APs to CA treatment in *Arabidopsis*. Because GPI-APs are thought to be localized in the PM, microdomains and apoplast, I isolated PM, microdomain, apoplast and GPI-AP enriched fractions and subjected these fractions to label-free quantitative shotgun proteomics. A number of GPI-APs (163) were identified and some of them significantly changed during CA in each fraction. Cell wall and lipid metabolism-related GPI-APs were predominantly up-regulated in PM and GPI-AP enriched fractions while the GPI-APs in microdomain and apoplast fractions changed differently during CA. Therefore, this study shows a variety of GPI-AP responses to CA and suggests possibilities for GPI-AP functions in the acquisition of freezing tolerance during CA.

Introduction

Plants are often exposed to severe external stresses, such as extreme temperatures, drought, flooding, high salinity, non-preferable nutrition, high or low light and high UV. Among these, freezing is one of the most severe stresses, because of the multiplicity of factors involved. Freezing stress consists of cold, mechanical, drought and osmotic stresses—all of which are caused by a combination of low temperature and extracellular ice formation (Steponkus, 1984).

To survive at freezing temperatures, plants have developed an adaptation strategy, which is referred to as cold acclimation (CA). When recognizing a decline in temperature and shortening of light period, plants can increase their freezing tolerance by changing their cellular metabolism in the CA process. An example of the representative changes during CA is the increase of cellular osmolality by accumulation of compatible solutes, such as sugars and amino acids (Koster and Lynch, 1992), and specific proteins (mostly with hydrophilic properties) to prevent membranes and proteins from freeze-induced disruption and/or denaturing (Koster and Lynch, 1992; Wanner and Junttila, 1999).

Another important change during CA is the alteration of plasma membrane (PM) properties. Changes of PM lipids and proteins in association with CA have been studied for the last 30 years. Uemura and Steponkus (1994) reported different lipid changes of the PM in oat and rye, which show a vast difference in freezing tolerance. The authors suggested that the rye PM maintains higher fluidity during CA than the oat PM through differences in lipid composition and the melting temperature of the lipid species present in the PM. Kawamura and Uemura (2003) first identified PM proteins that changed during CA by gel-based proteomic techniques with a relatively large scale. Minami et al. (2009) then reported compositional changes of microdomain-enriched detergent-resistant membrane (DRM) fractions during CA. The authors suggested that microdomains contain specific proteins and act as a functional scaffold in association with membrane transport, trafficking and signal transduction proteins that are important during the CA process.

I previously established methods for comprehensive shotgun proteomics of PM and DRM fractions in oat and rye (Takahashi et al., 2012; Takahashi et al., 2013; Chapters 2 and 3 in this thesis). In these studies, a number of proteins were found to be concentrated in the microdomain area in the PM and microdomain proteins changed considerably during CA treatment. Most of the significantly changed proteins that were highly enriched in the DRM fraction were transmembrane proteins and peripheral proteins. Among the proteins identified, several were predicted to be

glycosylphosphatidylinositol-anchored proteins (GPI-APs) by the big-PI plant predictor tool (Eisenhaber et al., 2003). GPI-APs are a group of lipid-modified proteins chemically bound between the carbohydrate chain of the protein and phosphatidylinositol of the PM, and are localized in the extracellular side of the PM surface or in the extracellular matrix when cleaved from the PM surface by the endogenous phosphatidylinositol-specific phospholipase C (PI-PLC). I previously found a larger number of GPI-APs in the PM of rye (31) than oat (17), and that GPI-APs changed considerably in cold-tolerant rye but not so much in the less cold-tolerant oat during CA (Takahashi et al., 2013; Chapter 3 in this thesis). These results suggested the possibility that GPI-APs are involved in the CA process and contribute to differences in freezing tolerance among plants.

However, the detection of GPI-APs with classical gel-based proteomics is quite difficult compared with other PM proteins because the amounts of GPI-APs in general are small in the PM and not all GPI-APs can be detected in the presence of other proteins in larger amounts. Previously, Borner et al. (2003) attempted to predict GPI-APs using a GPI-prediction algorithm that they developed, and identified 244 potential GPI-APs encoded in the *Arabidopsis* genome. They successfully isolated a GPI-AP fraction using 15 mg membrane proteins by cleaving them from the membrane surface with exogenous PI-PLC and subsequently partitioning them into a soluble fraction after temperature-induced phase partitioning with Triton X-114 detergent. However, they succeeded in experimental identification of only 30 GPI-APs. Elortza et al. (2006) also extracted GPI-APs from *Arabidopsis* PM fractions by phospholipase D treatment and identified only 35 proteins. Thus, the majority of GPI-APs in the plant PM have not been identified yet and a new protocol for comprehensive identification of GPI-APs is strongly desired. In addition, very few studies have examined GPI-AP responses to environmental stimuli. In particular, the relationship between GPI-APs and abiotic stress including cold and freezing stresses is not yet well characterized. Therefore, in the present study, I aimed to (a) develop a method to identify GPI-APs comprehensively with a shotgun proteomics technique and (b) investigate proteomic changes during CA of GPI-APs in PM, DRM, extracellular matrix and GPI-AP fractions isolated from the leaves of the model plant *Arabidopsis thaliana*.

Experimental procedures

Plant Materials

Seeds of *Arabidopsis thaliana* (ecotype Columbia) were sown in a vermiculite-perlite mixture supplemented with Hoagland solution at 23°C with a 24 h

photoperiod (50 $\mu\text{mol}/\text{m}^2/\text{s}$). After 25 to 30 days, leaves were harvested for experiments as NA plants. To obtain CA plants, NA *Arabidopsis* plants were further incubated at 2°C with a 12 h photoperiod (100 $\mu\text{mol}/\text{m}^2/\text{s}$) for 1 week.

Isolation of Plasma Membrane and Detergent-resistant Membrane Fractions

PM isolation was performed in accordance with Uemura et al. (1995). All procedures were conducted on ice or 4°C. Aerial part of plants were harvested and grinded in a medium composed of 0.5 M sorbitol, 50 mM Mops/KOH (pH 7.6), 5 mM EGTA, 5 mM EDTA, 1.5% (w/v) polyvinylpyrrolidone (MW: 40,000), 5% (w/v) BSA, 2 mM phenylmethanesulfonyl fluoride, 4 mM salicylhydroxamic acid and 2 mM dithiothreitol using a Polytron (Kinematica PT10-35, Brinkmann Instruments, Westbury, NY, USA). Resultant homogenates were centrifuged at $2,770 \times g$ for 10 min to remove debris and subsequently at $231,000 \times g$ for 35 min to obtain microsomal pellets. The pellets were suspended in a medium (0.3 M sucrose and 10 mM $\text{KH}_2\text{PO}_4/\text{K}_2\text{HPO}_4$ [pH 7.8]) and centrifuged again as above. Microsomal pellets were homogenized and resuspended in a two-phase partition medium composed of 5.6% (w/w) polyethylene glycol (MW: 3,350; Sigma-Aldrich, St Louis, MO, USA), 5.6% (w/w) dextran (Sigma-Aldrich), 0.3 M sucrose, 30 mM NaCl, and 10 mM $\text{KH}_2\text{PO}_4/\text{K}_2\text{HPO}_4$ (pH 7.8). Subsequently, the two-phase mixture was centrifuged at $2,770 \times g$ for 5 min to set two phases. The upper phase was collected and transferred into a newly-prepared lower phase. These steps were repeated three times to increase the purity of the PM fraction. At last, the upper phase was collected, diluted with 5 times volume of a PM suspension medium (0.3 M sucrose, 10 mM Mops/KOH [pH 7.3] and 2 mM EGTA) and centrifuged twice as described above. Resultant PM pellets were suspended in the PM suspension medium and stored at -80°C until use.

DRM fraction was prepared based on the protocol of Peskan et al. (2000). PM fractions were precipitated and resuspended in 2.7 ml of TED buffer (50 mM Tris-HCl [pH 7.4], 3 mM EDTA, and 1 mM dithiothreitol). Next, 10% (w/v) Triton X-100 in TED buffer (300 μl) was added and incubated for 30 min on ice. Subsequently, 65% (w/w) sucrose in TED buffer (12 ml) were added and mixed well immediately to obtain 52% (w/w) sucrose solution. Then, 35, 30, and 5% (w/w) sucrose-TED solutions (5 ml each) were successively overlaid and centrifuged at $141,000 \times g$ for 20 h at 4°C in a swing-type rotor P28S (Hitachi Koki, Tokyo, Japan). A white band at the interface of the 30/35% (w/w) sucrose layers was collected as DRM, mixed into the PM suspension medium and centrifuged at $231,000 \times g$ for 35 min. Resultant pellets were resuspended in aliquot of the PM suspension medium. Protein content of PM and DRM suspensions

were determined using Bradford assay (Bio-Rad, Munich, Germany) with BSA as a standard.

Isolation of Apoplastic Fluids

To obtain extracellular matrix proteins, apoplastic fluids were extracted based on Boudart et al. (2005) with modifications that mannitol was replaced with sorbitol and most steps were conducted on ice. Aerial parts of plants were carefully removed and washed with water. Plants (approximately 10 g FW) were placed into a 30 ml syringe and then the syringe was set onto a 50 ml conical centrifuge tube. A 0.3 M sorbitol solution was then added to the syringe with plants, placed into a desiccator and vacuum-infiltrated for 5 min. Subsequently, the 0.3 M sorbitol solution was discarded and the syringe with plants was transferred into a second 50 ml corning tube. The tube was centrifuged in a swinging bucket at $1000 \times g$ for 10 min and the sorbitol solution was discarded. These steps were repeated three times. Afterwards, plants were vacuum-infiltrated again with 0.2 M CaCl_2 , centrifuged at $1000 \times g$ for 10 min and apoplast fluids were collected. To reduce the volume of apoplast fluids, ultrafiltration was performed using an Amicon Ultra 0.5 centrifugal filter system (molecular weight cutoff = 3,000, Millipore, Bedford, MA). Protein concentration of the filtrate was measured by Bradford assay as described above. To evaluate the purity of apoplastic fluids, malate dehydrogenase activity as a marker enzyme of the cytoplasm (MDH, EC 1.1.1.37) was determined as described by Boudart et al. (2005). PBS buffer composed of 137 mM NaCl, 2.7 mM KCl, 10 mM Na_2HPO_4 and 1.76 mM KH_2PO_4 at pH 7.4 (940 μl), 5 μl apoplastic fluid or 5-fold diluted total protein extracts, 10 μl of 20 mM oxaloacetate in PBS were mixed and the reaction was initiated by adding 40 μl of 5 mM NADH in PBS. The reduction of absorbance of NADH was measured at 340 nm for 3 min at 25°C.

Extraction of GPI-anchored Protein (GPI-AP) Fractions

GPI-AP fraction was prepared by the method of Borner et al. (2003) with some modifications, To burst isolated PM vesicles to remove cytosolic proteins that might be entrapped in the vesicle, the PM fraction containing 2 mg proteins was diluted to at least 20 times in volume with the PM suspension medium without sucrose. After ultracentrifugation as described above, PM pellet was homogenized and resuspended in 0.1 M Na_2CO_3 to remove soluble and weakly-bound membrane proteins and retrieve only integral membrane protein (Marmagne et al., 2007). After ultracentrifugation, the resultant pellet was resuspended in 2% (v/v) Triton X-114 in TNE buffer (25 mM

Tris-HCl, 150 mM NaCl, and 5 mM EDTA [pH 7.5]) and incubated on ice for 5 min. To induce phase separation, membrane suspension was then incubated at 37°C for 20 min. The volume of the upper aqueous phase was estimated by pipetting and discarded. An aliquot (the same volume to the discarded aqueous phase) of Tris-buffered saline (10 mM Tris and 150 mM NaCl [pH 7.4 at 37°C]) was added, mixed and then induced phase separation again. Steps of discarding upper phase and adding Tris-buffered saline were repeated three times. PI-PLC (invitrogen) in Tris-buffered saline was then added into sample at a final concentration of 1.5 units ml⁻¹ and sample solution was mixed well. The membrane fraction with PI-PLC was incubated at 37°C for 3 h and then phase separated (GPI-AP/PI-PLC [+]). In half of the samples, same steps were carried out without PI-PLC addition as control (GPI-AP/PI-PLC [-]). Aqueous phase was recovered, added into Triton X-114 at a final concentration of 2% (v/v) and repartitioned. These washing steps were repeated twice. The final aqueous phase was then concentrated by ultrafiltration as described above and the volume was adjusted to 15 µl.

One-dimensional SDS-PAGE

Proteins (1 µg) were mixed with an equal volume of sodium dodecyl sulfate (SDS) sample buffer (2% [w/v] SDS, 50 mM Tris-HCl [pH 6.8], 6% [v/v] β-mercaptoethanol, 10% [w/v] glycerol and bromophenol blue) and subsequently transferred to an aluminum block bath heated at 95°C for 10 min for protein denaturing. Protein solutions were then loaded on 10% (w/v) polyacrylamide gel with a 4.5% (w/v) stacking gel, separated by electrophoresis and visualized by silver staining (Kawamura and Uemura, 2003).

Sample Preparation and Data Acquisition for Nano-LC-MS/MS Analysis

Protein samples were subjected to in-gel tryptic digestion for nano-LC-MS/MS analysis according to the protocol of Li et al. (2012). Membrane fractions were dissolved in an equal volume of SDS buffer (2% [w/v] SDS, 50 mM Tris-HCl [pH 6.8], 6% [v/v] β-mercaptoethanol, 10% [w/v] glycerol and bromophenol blue) and boiled at 95°C for 10 min. After one dimensional electrophoresis to embed proteins in 7.5% polyacrylamide gel (E-R7.5L, ATTO), gel with a protein band was cut into four pieces and put into a new 1.5 ml microtube. The gel was fixed with fixer (40% [v/v] ethanol and 10% [v/v] acetic acid) and washed with deionized water. Then, the gel was dehydrated with acetonitrile and rehydrated with 100 mM NH₄HCO₃. After drying out with a centrifugal concentrator, the gel was rehydrated again with 10 mM dithiothreitol and 55 mM iodoacetamide. The gel was dehydrated and rehydrated with acetonitrile and

100 mM NH_4HCO_3 . The gel was then dried out again, the digestion buffer containing 50 mM NH_4HCO_3 , 5 mM CaCl_2 and 12.5 ng ml^{-1} of trypsin (sequencing grade, Promega) was added, and samples were incubated for 45 min on ice. After discarding the supernatant, the gel was added into 100 mM NH_4HCO_3 and incubated at 37°C for 20 h. The resultant peptides dissolved in the solution were retrieved by adding an equal volume of acetonitrile and transferred into a new tube. The gels were added into 5% (v/v) trifluoroacetic acid in 50% (v/v) acetonitrile, and mixed well to retrieve peptides. The solution containing peptides was dried down and the resultant peptides were dissolved in 0.1% (v/v) trifluoroacetic acid. The peptide samples were desalted with SPE C-TIP (AMR, Tokyo, Japan) and the volume was adjusted to 15 μl with 0.1% (v/v) trifluoroacetic acid. Peptide solutions were subjected to nano-LC-MS/MS analysis (Takahashi et al., 2013; Chapter 3 in this thesis). Digested peptide solution was concentrated with a trap column (L-column Micro 0.3 \times 5 mm; CERI, Japan) using an ADVANCE UHPLC system (MICHROM Bioresources, Auburn, CA) and eluted with 0.1% (v/v) formic acid in acetonitrile. Subsequently, peptides were separated with a Magic C18 AQ nano column (0.1 \times 150 mm; MICHROM Bioresources) using a linear gradient of acetonitrile (from 5% [v/v] to 45% [v/v]) at a flow rate of 500 nL/min. Separated peptides were ionized by an ADVANCE spray source (MICHROM Bioresources) with a spray voltage of 2.0 kV for identification of GPI-APs and the other fractions, respectively. Mass analysis was performed using an LTQ Orbitrap XL mass spectrometer (Thermo Fisher Scientific, Waltham, MA) equipped with Xcalibur software (version 2.0.7, Thermo Fisher Scientific). Full scan mass spectra were obtained in the range of 400 to 1800 m/z with a resolution of 30000. Collision-induced fragmentation was applied to the ten most intense ions for identification of GPI-APs and the other fractions, respectively at a threshold above 500.

Analysis of Nano-LC-MS/MS Data Using Progenesis LC-MS Software

Obtained MS/MS spectra were subjected to Progenesis LC-MS software (version 4.0, Nonlinear Dynamics, New Castle, UK). Quantification processes of Progenesis consists of 7 steps: 1) import raw files into Progenesis software, 2) reference run set up, 3) align retention time of each sample, 4) peak detection, 5) experimental design set up, 6) peptide identification with MASCOT server (version 2.3.02, Matrix Science, London, UK), 7) calculation of each protein abundance based on peptide signal intensities (<http://www.nonlinear.com/products/progenesis/lc-ms/tutorial/v4.0>). Because gaps of retention time among samples are automatically corrected with high accuracy during

step 3, it is difficult to compare between two samples exhibiting vastly-different elution patterns (e.g. PM fractions and apoplast fractions). In addition, the quantification process in step 4 is based on MS spectra intensities and do not rely on existence or non-existence of MS/MS spectra, and Progenesis software treat multiple samples as one 'aggregated sample' during MASCOT identification. Therefore, the more samples that have elution pattern roughly similar to each other that I applied into software, the more proteins Progenesis can detect and quantify. In present study, peptide spectra and elution patterns obtained from GPI-AP/PI-PLC (+) and PM fractions were quite similar to those from GPI-AP/PI-PLC (-) and DRM fractions, respectively. Thus, in step 1, raw files of GPI-AP/PI-PLC (+) and PM fractions were combined with those of GPI-AP/PI-PLC (-) and DRM fractions, respectively in Progenesis software and information in each experimental design was integrated each other during identification and quantification processes.

In step 2 and 3, a reference run sample in each experimental design was selected for quantification and identification and the experimental errors of peptide peak times in each run were aligned. As a normalization process, the quantitative abundance ratio of the reference run and each sample run was adjusted. After peak picking and experimental design set up in steps 4 and 5, peptide information was exported from the Progenesis software as mgf format and subjected into MASCOT search engine for searching against the TAIR 10 *Arabidopsis* protein database (version 20101214) according to the following parameters: number of missed cleavage, 1; fixed modifications, carbamidomethylation (C); variable modifications, oxidation (M); peptide mass tolerance, 5 ppm; MS/MS tolerance, 0.6 Da; and Peptide charges, +1, +2 and +3. The false discovery rate (FDR), which is based on a search of the MASCOT decoy database, was less than 5%. Definitions of identified proteins were based on the following criteria: including at least one unique top-ranking peptide and ion score cut off ≤ 0.05 . If a peptide was assigned to multiple proteins, the highest-scoring protein was selected in the list. Protein information was integrated with Progenesis software and exported as csv format. Finally, significantly changed proteins were defined with ANOVA ($p < 0.05$) and fold change (> 2.0).

According to GPI-AP/PI-PLC (\pm) fractions, GPI-AP/PI-PLC (+) fractions were anticipated to contain greater amounts of GPI-APs and few amounts of PI-PLC-unresponsive GPI-APs and non-GPI-APs. Although GPI-AP/PI-PLC (-) fractions notionally did not contain any PM-derived proteins, it was also considered to be contaminated by GPI-AP, PI-PLC-unresponsive GPI-APs and non-GPI-APs during sample extraction processes. When an aliquot of proteins in GPI-AP/PI-PLC (\pm)

fractions was injected in nano-LC-MS/MS and quantified their relative abundances, apparent amounts of PI-PLC-unresponsive GPI-APs in GPI-AP/PI-PLC (-) fractions might be higher than those in GPI-AP/PI-PLC (\pm) fractions. Therefore, quantitative values of GPI-APs in GPI-AP/PI-PLC (-) fractions in comparison with GPI-AP/PI-PLC (+) fractions were considered not to be reflected actual situation. Thus, proteomic results of GPI-AP/PI-PLC (-) fractions were not used for figures dealing with normalized abundances of each GPI-AP.

Topology and Post-translational Modification Prediction

Acquired proteins were used for prediction of sites of glycosylphosphatidylinositol (GPI) modification using the following online tools: Big-PI Plant Predictor (http://mendel.imp.ac.at/gpi/plant_server.html), GPI-SOM (<http://gpi.unibe.ch/>), PredGPI (<http://gpcr.biocomp.unibo.it/predgpi/pred.htm>) FragAnchor (<http://navet.ics.hawaii.edu/~fraganchor/NNHMM/NNHMM.html>), and the potential GPI-AP protein list in *Arabidopsis* described in Borner et al. (2003). Prediction of subcellular localization was carried out by SUBA3 program (<http://suba3.plantenergy.uwa.edu.au/>). To clarify functional distributions of each fraction, all proteins identified were classified first into 35 functional categories with Mapman bins (<http://mapman.gabipd.org/>) and then re-classified into simpler 11 functional categories based on Bevan et al. (1998).

Results

Isolation of GPI-APs from the PM and Identification of GPI-APs

A workflow of sample preparation is shown in Fig. 5-1. *Arabidopsis* plants were harvested and vacuum-infiltrated to isolate apoplastic fluids according to the method of Boudart et al. (2005). MDH activity, which is an indicator of symplastic contamination, was less than 0.1% of the total activity in both NA and CA samples (Table 5-1). *Arabidopsis* leaves were also used to isolate highly-purified PM fractions using a two-phase partitioning technique according to Uemura et al. (1995). The PM fractions obtained were used for isolation of microdomain-enriched DRM and GPI-AP fractions. GPI-AP fractions after or before the PI-PLC treatment were subjected to 1-D SDS-PAGE to check the efficiency of PI-PLC treatment for the enrichment of GPI-APs. The band intensities of proteins were much higher in the sample with the PI-PLC treatment (GPI-AP/PI-PLC [+]) than without the PI-PLC treatment (GPI-AP/PI-PLC [-]; e.g., band Nos. 1, 2, 4 and 5 in Fig. 5-2.). These results indicated that GPI-APs associated with the PM were effectively cleaved by PI-PLC at the phosphodiester bond

in phosphatidylinositol of the GPI moiety, released from the PM surface and then concentrated in a soluble fraction. This fraction was designated GPI-AP/PI-PLC (+).

When comparing GPI-AP/PI-PLC (+) fractions between NA and CA, the intensities of many protein bands increased after CA (e.g., Nos. 1, 3, 4, 6 and 7). In contrast, the intensities of some proteins did not change during CA (e.g., No. 5). These results suggested that some proteins in the GPI-AP/PI-PLC (+) fraction responded to CA treatment and their amount in the PM was increased.

Identification and Computational Prediction of GPI-APs

GPI-AP/PI-PLC (+), GPI-AP/PI-PLC (-), PM, DRM and apoplast fractions were subjected to nano-LC-MS/MS analysis and the data obtained were analyzed by database searching with the MASCOT and Progenesis LC-MS software. During the Progenesis analysis to obtain semi-quantitative data for the proteins identified, peptide spectra obtained from GPI-AP/PI-PLC (+) and GPI-AP/PI-PLC (-) fractions were combined as in the case of the PM and DRM fractions as stated in the Materials and Methods. From the Progenesis analysis, I identified many proteins in the three samples (728, 1051 and 563 proteins in the GPI-AP/PI-PLC (\pm), PM+DRM and apoplast fractions, respectively). To predict GPI-APs based on the amino acid sequences of the proteins identified, I used five different programs that are frequently used in plant proteomics studies: GPI-AP lists predicted by Borner et al. (2003), big-PI Plant Predictor (Eisenhaber et al., 2003), PredGPI (Pierleoni et al., 2008), GPI-SOM (Fankhauser and Maser, 2005) and fragAnchor (Poisson et al., 2007). These programs predict N- and/or C-terminal signal sequences including the ER-export signal peptide and the C-terminal GPI signal. The C-terminal GPI signal can be divided into four parts (Eisenhaber et al., 1999): 1, linker region; 2, GPI attachment and cleavage site; 3, spacer region; 4, hydrophobic tail. Although the C-terminal GPI signal is an essential factor for GPI-AP identification, there are many exceptions and it is difficult to apply this single criterion to the identification of many kinds of GPI-APs (Poisson et al., 2007). In addition, the N-terminal signal is sometimes absent or not clearly identifiable in experimentally-verified GPI-APs (Poisson et al., 2007). With the additional specific algorithms that each GPI-AP prediction program employs, 79, 63, 112, 127 and 93 potential GPI-APs were predicted by Borner's potential GPI-APs list, big-PI Plant Predictor, PredGPI, GPI-SOM and fragAnchor, respectively. Among them, 44 proteins were predicted as GPI-APs by all the algorithms, while a number of proteins were only identified as GPI-APs by a single program. For example, 33 proteins were predicted as

potential GPI-APs by GPI-SOM only (Fig. 5-3A). Each GPI-AP prediction program seems to have different algorithms for the prediction of GPI-APs.

Using the five GPI-AP prediction programs described above, 114, 71 and 59 GPI-APs were predicted in the GPI-AP/PI-PLC (\pm), PM+DRM and apoplast fractions, respectively. Among them, 25 were identified in all three fractions (Fig. 5-3B). However, 59, 17 and 31 GPI-APs were specifically identified in the GPI-AP/PI-PLC (\pm), PM+DRM and apoplast fractions, respectively. Fig. 5-3C shows how the five GPI-AP prediction programs predicted proteins in the three sample fractions as GPI-APs. In the GPI-AP/PI-PLC (\pm) fraction, 44 proteins were predicted as GPI-APs by all five prediction programs while 20 GPI-APs were predicted with a single program. On the other hand, in the PM+DRM and apoplast fractions, only 20 and 13 proteins were judged as GPI-APs by all five prediction programs and 26 and 29 proteins were predicted by a single prediction program. The GPI-AP/PI-PLC (\pm) fraction seemed to contain GPI-APs that were predicted by multiple prediction programs, but the PM+DRM and apoplast fractions showed the opposite trend.

Prediction of Subcellular Localization and Functional Categorization of GPI-APs in GPI-AP, PM+DRM and Apoplast Fractions

The subcellular localization of each potential GPI-AP was predicted by the SUBA3 program (Fig. 5-4). Most of the GPI-APs identified were classified as extracellular or PM targeting proteins. The PM+DRM fraction contained a higher proportion of PM-targeted GPI-APs (37 GPI-APs, 52%) than the other two fractions (16 GPI-APs, 27%, in the apoplast fraction and 49 GPI-APs, 43%, in the GPI-AP/PI-PLC (\pm) fraction). For GPI-APs potentially targeted to the extracellular matrix, the proportion was higher in the apoplast fraction (38 GPI-APs, 64%) than the GPI-AP/PI-PLC (\pm) fraction (45 GPI-APs, 39%) and PM+DRM fraction (20 GPI-APs, 28%). Originally, all proteins identified in the GPI-AP/PI-PLC (\pm) and PM+DRM fractions were derived not from the extracellular or cytosolic space but the PM or DRM surface. However, the apoplast fraction isolated the extracellular matrix and notionally contains endogenously-released GPI-APs. Therefore, the localizations of the GPI-APs identified seemed to reflect the isolation and identification process of each fraction.

Next, with the abundance of each protein, I determined the functional categories that the proteins and GPI-APs were classified into in the GPI-AP/PI-PLC (\pm), PM+DRM and apoplast samples. The proteins and GPI-APs were classified into 11 functional categories based on Bevan et al. (1998; Fig. 5-5).

Among the total proteins, the GPI-AP/PI-PLC (+) fraction mainly contained cell structure- and metabolism-related proteins (20.0% and 39.1%, respectively). Among the total PM and DRM proteins, transporter proteins were the most abundant (31.4% for both PM and DRM proteins). The apoplast fraction contained proteins related with a variety of functions such as cell structure, disease/defense, metabolism and transcription. For GPI-APs, the functional distribution in the GPI-AP/PI-PLC (+) fraction was similar to that of the total protein fraction, which was consistent with the expectation that the GPI-AP/PI-PLC (+) fraction was enriched in GPI-APs. In the PM and DRM fractions, the functional distribution of potential GPI-APs was similar with cell structure- and metabolism-related functions comprising the dominant categories. Furthermore, the characteristics of the functional distribution of PM and DRM GPI-APs were somewhat similar to those of the GPI-AP/PI-PLC (+) fraction, probably because the GPI-AP/PI-PLC (+) and DRM fractions were originally prepared from PM fractions. The apoplast fraction showed a different functional distribution from the PM-derived fractions. In the apoplast fraction, disease/defense-related GPI-APs accounted for a high proportion (34.3%), which was not observed in other fractions. These results suggest the possibility that specific GPI-APs associated with disease/defense could be released from the PM surface by endogenous phospholipase when necessary and transferred to the apoplastic space.

Responsiveness of GPI-APs to CA Treatment

To determine the responsiveness of GPI-APs to CA treatment, I first quantified the protein content in GPI-AP/PI-PLC (+) fractions (Fig. 5-6A). In the NA sample, the amount of proteins in the GPI-AP/PI-PLC (+) fraction was 10.24 μ g when starting from 2000 μ g PM proteins while the amount in GPI-AP/PI-PLC (-) was only 4.85 μ g. Thus, the proteins released by PI-PLC treatment, which were predominantly predicted as GPI-APs, increased 2.64 times after CA treatment.

Next, based on the protein abundance obtained by proteome analysis, I calculated the proportions of GPI-APs in the GPI-AP/PI-PLC (+), PM, DRM and apoplast fractions (Fig. 5-6B). As expected, the proportion of GPI-APs was quite large in the GPI-AP/PI-PLC (+) fraction under NA conditions (85%). After CA treatment, the proportion increased to 94%. In the PM fraction, the proportion of GPI-APs increased from 6.0% to 10.8% (1.81-fold) during CA. Conversely, in the DRM fraction, the proportion of GPI-APs was only 2.6% of the total proteins in the NA sample and did not change after CA. The apoplast fraction had a relatively higher proportion of GPI-APs (9.1%) before CA and did not change significantly during CA. These results indicated

that GPI-APs associated with the PM surface considerably increased during CA, while those in microdomain area and apoplastic space did not respond to CA.

For the GPI-AP/PI-PLC (+) fraction, I calculated the normalized abundance and logarithmically transformed fold changes of GPI-APs (Supplemental Table 5-3) and identified GPI-APs with statistically significant abundance changes during CA (Table 5-2). In total, I found 20 increased and 11 decreased GPI-APs during CA (Supplemental Table 5-3). The mean normalized abundance of CA-responsive GPI-APs ranged from 137.6 (At5g53870.1) to 9905082.7 (At4g27520.1) in NA and from 0 (At4g32150.1) to 23925864.4 (At4g27520.1) in CA. During CA, the CA-response magnitude varied from 0.50-fold (At2g34510.1) to infinity (At4g32150.1) and from 2.07-fold (At1g08500.1) to 48.2-fold (At1g32860.1). In addition to the numerical diversity of GPI-APs, CA-responsive GPI-APs had a variety of functions. For example, the CA-decreased GPI-APs included two COBRA-like proteins (At4g16120.1 and At3g16860.1) and two syntaxin proteins (At1g16240.1 and At5g16830.1). On the other hand, the CA-increased GPI-APs contained three early nodulin-like proteins (At1g08500.1, At4g27520.1 and At5g53870.1), two glycosyl hydase family proteins (At1g32860.1 and At3g04010.1) and other receptor, lipid-transfer and cell wall-related proteins.

Next, to understand the functional changes of GPI-APs in the GPI-AP/PI-PLC (+), PM, DRM and apoplast fractions, I calculated the difference in abundance of GPI-APs belonging to each of 11 functional categories between NA and CA samples (Fig. 5-7). In both GPI-AP/PI-PLC (+) and PM fractions, changes in cell structure-related, metabolism-related and unknown GPI-AP abundance were commonly observed during CA. In the DRM fraction, cell structure-related proteins increased as with unknown GPI-APs during CA but metabolism-related proteins did not change. Interestingly, the changes of GPI-APs in the apoplast fraction were quite different from those of the other fractions. Cell structure-, metabolism- and disease/defense-related GPI-APs decreased during CA (Fig. 5-7).

To see more detailed changes in each sample fraction during CA at the level of individual GPI-APs, I created a histogram based on the log₂ values of fold changes during CA in each sample fraction (Fig. 5-8A). In the GPI-AP/PI-PLC (+) fraction, a number of GPI-APs (48) increased more than 1.41-fold (equivalent to 0.5 in log₂ transformed value) during CA. Similarly, many GPI-APs in the PM fractions (44) were up-regulated more than 1.41-fold during CA. In contrast, many GPI-APs were stable in DRM during CA. Apoplastic GPI-APs were mostly down-regulated during CA.

Next, I selected GPI-APs commonly identified in the GPI-AP/PI-PLC (+), PM, DRM and apoplast fractions and calculated log₂ values of fold changes during CA in

each sample fraction (Fig. 5-8B to D). The relationship between the fold change during CA in the GPI-AP and total PM fractions (Fig. 5-8B) seemed strong judging by a high correlation coefficient ($R=0.681$). The correlation coefficient of values between the GPI-AP/PI-PLC (+) and DRM fractions was not so strong ($R=0.391$; Fig. 5-8C) and the correlation coefficient between the GPI-AP/PI-PLC (+) and apoplast fractions (Fig. 5-8D) was very low ($R=0.0837$). In this comparison, most GPI-APs that were commonly identified in the GPI-AP/PI-PLC (+) and apoplast fractions decreased in the apoplast and increased or showed little change in the GPI-AP/PI-PLC (+) fraction during CA. These data suggested that GPI-APs had different responsiveness to CA in each cellular fraction.

Discussion

In this study, I performed comprehensive and extensive proteome analyses of GPI-APs during CA in *Arabidopsis*. This is, to my knowledge, the first report on the responsiveness of GPI-APs to abiotic stress such as CA in three potential GPI-AP-localizing sites—the PM surface, microdomain and apoplastic space. CA processes comprise many different cellular responses including temperature perception, gene expression, and proteome and metabolome responses. The PM is considered to play one of the most important roles in CA processes because it is the primary site of freezing injury and CA must increase the tolerance of the PM against freeze-induced stresses (Steponkus, 1984; Murray et al., 1989). In fact, the *Arabidopsis* PM shows lipidomic and proteomic changes in response to cold temperature (Uemura et al., 1995; Kawamura and Uemura, 2003). In addition to these reports, the present study provides an important foundation to understand the functional involvement of the PM in the CA process through the detection of CA-regulated changes of GPI-APs.

Preparations of Potential GPI-AP-Localizing Fractions

GPI-APs in plants have been studied for the last 20 years. The existence of a GPI-anchored nitrate reductase was reported by Stöhr et al. (1995) using *Chlorella saccharophila*. Subsequently, Morita et al. (1996) reported another GPI-AP with alkaline phosphatase activity in the aquatic plant *Spirodela oligorrhiza*. In higher plants, Takos et al. (1997) confirmed that six and seven GPI-APs were released by PI-PLC treatment from the outer surface of *Nicotiana tabacum* cultured cells and leaf protoplasts, respectively. In *Arabidopsis*, Sherrier et al. (1999) identified GPI-APs isolated from suspension cultured cells with PI-PLC and a subsequent Triton X-114 phase separation system. These studies aimed to characterize individual GPI-APs in

relation to specific physiological functions but not to identify the “GPI-anchored proteome” in plant systems.

The first proteomic study focused on GPI-APs was conducted by Borner et al. (2003). In their study, a large amount of total endomembranes (10–15 mg proteins) were treated with PI-PLC and then the released GPI-AP enriched fraction was separated using a Triton X-114 phase separation system. As a result, the authors successfully identified 30 GPI-APs. Although this was a pioneering work on GPI-anchored proteomics in plants, the amount of membrane sample they employed has sometimes been too large for successful characterization of GPI-APs in subsequent studies. In the present study, however, I succeeded in identifying a GPI-anchored proteome by isolating highly purified PM fractions based on the method of Uemura et al. (1995) and applying only 2 mg PM proteins to GPI-AP enrichment steps such as (1) bursting PM vesicles to remove entrapped proteins and (2) washing the PM vesicles with Na_2CO_3 to remove externally associated soluble proteins. Visualization of the proteins in 1 μl of the isolated GPI-AP fraction showed that the protein bands were much stronger with the PI-PLC treatment than without treatment (Fig. 5-2). The enrichment of GPI-APs with PI-PLC treatment was consistent with previous reports describing PI-PLC applications for GPI-AP enrichment (Borner et al., 2003; Elortza et al., 2003; Elortza et al., 2006). The proportions of GPI-APs computationally predicted in the total protein fractions were much higher in the GPI-AP/PI-PLC (+) fraction than the total PM fractions (14.3-fold in NA and 8.69-fold in CA). The proportion of GPI-APs in the NA PM was 6.0%, which was consistent with the proportion (6.0%) reported in a previous study with the *Arabidopsis* PM (Marmagne et al., 2007). Thus, the enrichment process for GPI-APs employed in the present study was considered to have worked properly and the samples obtained could be used for further experiments.

Composition of GPI-APs in the PM, DRM, Apoplast and GPI-AP Fractions

I successfully identified 163 GPI-APs in total from the PM, DRM, apoplast and GPI-AP/PI-PLC (\pm) fractions. In most organisms, GPI-APs are synthesized in the luminal side of the endoplasmic reticulum (ER) and transported to the extracellular leaflet of the PM via the vesicular transport system (Udenfriend and Kodukula, 1995; Eisenhaber et al., 1999; Ferguson, 1999). Additionally, because the GPI moiety of some GPI-APs is a substrate of specific phospholipases, these GPI-APs can be released from the PM surface by endogenous phospholipase activity and localized as extracellular soluble and/or PM-anchored proteins (Griffith and Ryan, 1999). SUBA3 prediction (Tanz et al., 2013) revealed that more than 80% of the primary amino acid sequences of

GPI-APs contained sequence features to localize to the ER, PM or extracellular region (Fig. 5-4). In the PM+DRM and GPI-AP/PI-PLC (\pm) fractions, PM-targeted GPI-APs accounted for relatively higher proportions than ER- and extracellular space-targeted GPI-APs, but in the apoplastic fraction, extracellular space-targeted GPI-APs accounted for more than 60% (Fig. 5-4). These results indicate that secretion of GPI-APs into the apoplastic space by endogenous phospholipase activity varies considerably with the molecular species of GPI-APs. In a study of the PER1 enzyme, which is involved in lipid remodeling of the GPI anchor in yeast (Fujita et al., 2006), *per1* Δ mutants synthesized GPI-APs with different lipids from the WT and showed enhanced abnormal targeting of Gas1p, a GPI-AP, to PM microdomains, which resulted in excessive release of Gas1p into the culture medium. In addition, there are multiple processes for the extracellular release of some GPI-APs such as metalloprotease gp63 in the parasite *Leishmania* (McGwire et al., 2002). Extracellular gp63 is produced via autoproteolytic cleavage of the N-terminal region of the protein or alternatively, direct secretion via vesicular trafficking. Therefore, it is expected that there are a number of regulation systems for GPI-AP targeting in plants such as lipid remodeling in the ER lumen, various secretion processes for GPI-APs including direct secretion, and autoproteolytic and phospholipase cleavage. Ultimately, these systems for GPI-AP release into the extracellular space may depend on the physical and biochemical properties of each GPI-AP.

The functions of GPI-APs in the PM and DRM fractions were quite similar (Fig. 5-5). These two fractions contained many transporters and signaling-related proteins (e.g. aquaporins and leucine-rich repeat protein kinases). This is consistent with previous PM and DRM proteome studies in *Arabidopsis* (Kawamura and Uemura, 2003; Alexandersson et al., 2004; Marmagne et al., 2004; Borner et al., 2005; Morel et al., 2006; Marmagne et al., 2007; Minami et al., 2009). Thus, my results clearly show the appropriateness of the PM and DRM purification process in the present study. However, the GPI-APs were dominated by cell structure- and metabolism-related proteins as represented by fasciclin-like arabinogalactan protein (FLA) and glycerophosphoryldiester phosphodiesterase-like protein, which are well-known GPI-APs reported earlier (Eisenhaber et al., 1999; Borner et al., 2003; Elortza et al., 2006). These proteins are considered to be important for primary cell wall organization and cell adhesion in the developmental process (Johnson et al., 2003; Hayashi et al., 2008), which occurs at the interface of the PM and cell wall. These results suggest that GPI modification is important for proper targeting to the extracellular leaflet of the PM

and gives GPI-APs greater flexibility than membrane-embedded integral proteins for promoting enzymatic reactions on the PM surface (Chevalier et al., 2006).

Compared with the PM fraction, the DRM fraction contained a relatively high proportion of unclassified GPI-APs and a low proportion of metabolism-related GPI-APs (Fig. 5-5). These results indicate that the microdomain structure may contain specific GPI-APs and eventually forms a functional platform for specific physiological events. Muñiz and Riezman (2000) suggested that saturated acyl chains in the GPI moiety might result in compartmentalization of GPI-APs into lipid nanodomains. Oxley and Bacic (1999) characterized the structure of the GPI anchor attached to the arabinogalactan protein in *Pyrus communis*. They showed that although the backbone of the GPI anchor is common to animals, protozoa and yeast, the lipid part contains phytosphingosine, which is the most abundant long chain base of plant sphingolipids. Therefore, plant GPI-APs may have a unique distribution pattern in lipid nanodomains. However, more detailed analysis of the structural organization of the GPI moiety with various GPI-APs must be conducted for discussion of the relationship between GPI anchor structure (including lipid and carbohydrate) and microdomain compartmentalization.

The apoplast fraction had a unique GPI-AP composition such as a higher proportion of disease/defense-related proteins than the other sample fractions (Fig. 5-5). Germin-like protein 1 (At1g72610.1) was identified as a GPI-AP and was abundant in the disease/defense-related category (Supplemental Table 5-3). This protein has been demonstrated to localize to the extracellular matrix and is considered to be involved in many physiological responses including environmental stress (Membré et al., 2000). Localization of the Germin-like protein to the apoplast is probably regulated by the GPI-anchor moiety.

CA-Induced Changes of the GPI-Anchored Proteome

The amount of proteins in the GPI-AP/PI-PLC (+) fraction in the NA sample was 2.12 times higher than that in the GPI-AP/PI-PLC (-) fraction. This result is consistent with the electrophoresis profiles shown in Fig. 5-2 as well as the results of a previous work (Elortza et al., 2003). Thus, it is clear that there are many PI-PLC-responsive proteins, which are likely to be GPI-APs, on the surface of PM vesicles.

However, not all GPI-APs were cleaved from the PM surface by the PI-PLC treatment. For example, At1g32860.1 was identified as a GPI-AP by all GPI-AP predictors employed, but proteomic experiments showed that the mean abundance of

At1g32860.1 in an aliquot of the GPI-AP fraction was lower with the PI-PLC treatment (1716.5) than without the PI-PLC treatment (6498.4). Roberts et al. (1988) and Rosenberry (1991) reported that inositol modification of the human GPI moiety results in resistance to PI-PLC cleavage. The structure of the GPI anchor in plants is slightly different from that in animals and yeast (Oxley and Bacic, 1999). Thus, it is possible that differences in GPI-anchor structure have an unexpected influence on PI-PLC cleavage in the GPI-AP enrichment process.

Interestingly, the protein amounts in the GPI-AP/PI-PLC (+) fraction significantly increased (2.64 times) during CA (Fig. 5-6A). Figure 5-6B shows the proportions of GPI-AP abundance to total protein abundance determined by proteomics. Given that the GPI-AP/PI-PLC (+) fraction was considered to be enriched in GPI-APs, it was expected that the proportion of GPI-APs in the GPI-AP/PI-PLC (+) fraction, accounting for more than 85% in the NA sample, would be unchanged by CA treatment. On the other hand, the GPI-AP abundance in the PM fraction in the CA sample was 1.81 times higher than that in the NA sample. This is consistent with the results shown in Fig. 5-6A. Therefore, it is estimated that the total amount of GPI-AP on the surface of the PM almost doubles after CA. However, it is unlikely that the GPI-AP biosynthesis pathway in general is enhanced during CA because there were many unchanged GPI-APs in the GPI-AP/PI-PLC (+) and PM fractions after CA. Collectively, the biosynthetic pathways of specific GPI-APs are stimulated by cold, which results in increases of specific GPI-APs on the PM surface during CA. As evidence, in the PM fraction, 26 GPI-APs increased but two GPI-APs eventually decreased during CA.

The change patterns in the functional distribution of GPI-APs (shown in Fig. 5-7) were quite similar in the GPI-AP/PI-PLC (+) and PM fractions and this correlation was also observed when looking at individual GPI-APs (Fig. 5-8). Figure 5-7 shows a dominant increase of cell structure-related, metabolism-related and unknown GPI-APs during CA in the GPI-AP/PI-PLC (+) and PM fractions. Given that the GPI-AP and PM fractions were enriched in cell structure-related, metabolism-related and unknown GPI-APs (Fig. 5-5), the dominant increase in these functional categories during CA in the GPI-AP and PM fractions may be reflected by their compositions. Among the cell structure-related GPI-APs, ten and six fasciclin-like arabinogalactan proteins (FLA) were abundant in the GPI-AP/PI-PLC (+) and PM fractions, respectively, and all increased during CA. Although the functions and physiological significance of these proteins during the CA process are not yet characterized, wheat FLAs have been reported to respond to various environmental stresses (Faik et al., 2006). Interestingly, none of the TaFLAs examined responded to heat, ABA, salt or dehydration treatment

and only CA treatment resulted in enhanced mRNA expression of some TaFLAs. Thus, GPI-anchored FLA may contribute to the CA process but further investigation is required to show the detailed mechanism.

Among the metabolism-related GPI-APs, PLC-like phosphodiesterase family protein (SHV3, At4g26690.1) and SHV3-like proteins (SVL1, At5g55480.1 and SVL2, At1g66970.1) were abundant and increased during CA in the GPI-AP/PI-PLC (+) and PM fractions. Characterization of SHV3 and SVL1 deficient mutants (*shv3* and *svl1*) revealed that the *shv3svl1* double mutant has abnormal cellulose deposition and pectin network formation (Hayashi et al., 2008). The authors proposed the involvement of these proteins in cell wall rigidity. In winter oilseed rape, CA treatment increased the cell wall and pectin content (Kubacka-Zębalska and Kacperska, 1999) and cell wall thickness (Stefanowska et al., 1999). These responses are thought to contribute to tolerance against freeze-induced dehydration and mechanical stress. Therefore, the functions of SHV3 and SVL1 may be connected with CA-induced responses of the cell wall in plant cells. The metabolism-related GPI-APs including SHV3 and SVL1 were unchanged in the DRM fraction and eventually decreased in the apoplast fraction. Thus, further investigation of the functions of SHV3 and SVL1 in relation to microdomain function and the apoplastic space is needed to show their functional involvement in the CA process.

The changes of individual GPI-APs during CA in the GPI-AP/PI-PLC (+) fraction were highly correlated with those in the PM fraction ($R=0.68$; Fig. 5-8B). However, changes in the DRM fraction were not well correlated with those in the GPI-AP/PI-PLC (+) fraction ($R=0.3905$; Fig. 5-8C) and the correlation factor between changes in the GPI-AP/PI-PLC (+) and apoplastic fractions was considerably lower ($R=0.0837$; Fig. 5-8D). Although many PM-associated GPI-APs increased during CA (Figs. 5-6B, 5-7 and 5-8A), a large number of apoplastic GPI-APs tended to be down-regulated (Figs. 5-7 and 5-8A). To show these different responses of GPI-APs to CA, GPI-specific PLC (GPI-PLC) activity should be examined. GPI-PLC is considered to play a role in the cleavage of GPI-APs from the PM and the release of the protein moiety from the PM surface to the apoplastic space. Thus, differences in the change patterns of GPI-APs in the PM and apoplast fractions may be partly mediated by endogenous GPI-PLC activity. GPI-PLC has been reported in animals and microorganisms (Roberts, 1996). In plants, Bütikofer and Brodbeck (1993) succeeded in purifying GPI-PLC from peanut seeds. The hydrolyzing activity of peanut GPI-PLC was confirmed by detection of solubilized GPI, but the enzyme could not hydrolyze a membrane-bound GPI-anchored substrate. Although many PLCs are encoded by the

Arabidopsis genome, a PLC that hydrolyzes PM-bound GPI-APs has not yet been identified. Investigation of the molecular mechanisms of the GPI-AP release process from the PM surface to the apoplastic space by endogenous phospholipase activity may help to understand the diversified changes of GPI-APs in the PM and apoplast during CA.

Supporting information

Supplemental Table 5-1. Peptide list of identified GPI-anchored proteins.

Supplemental Table 5-2. Lists of identified and quantified total proteins.

Supplemental Table 5-3. Lists of identified and quantified GPI-APs.

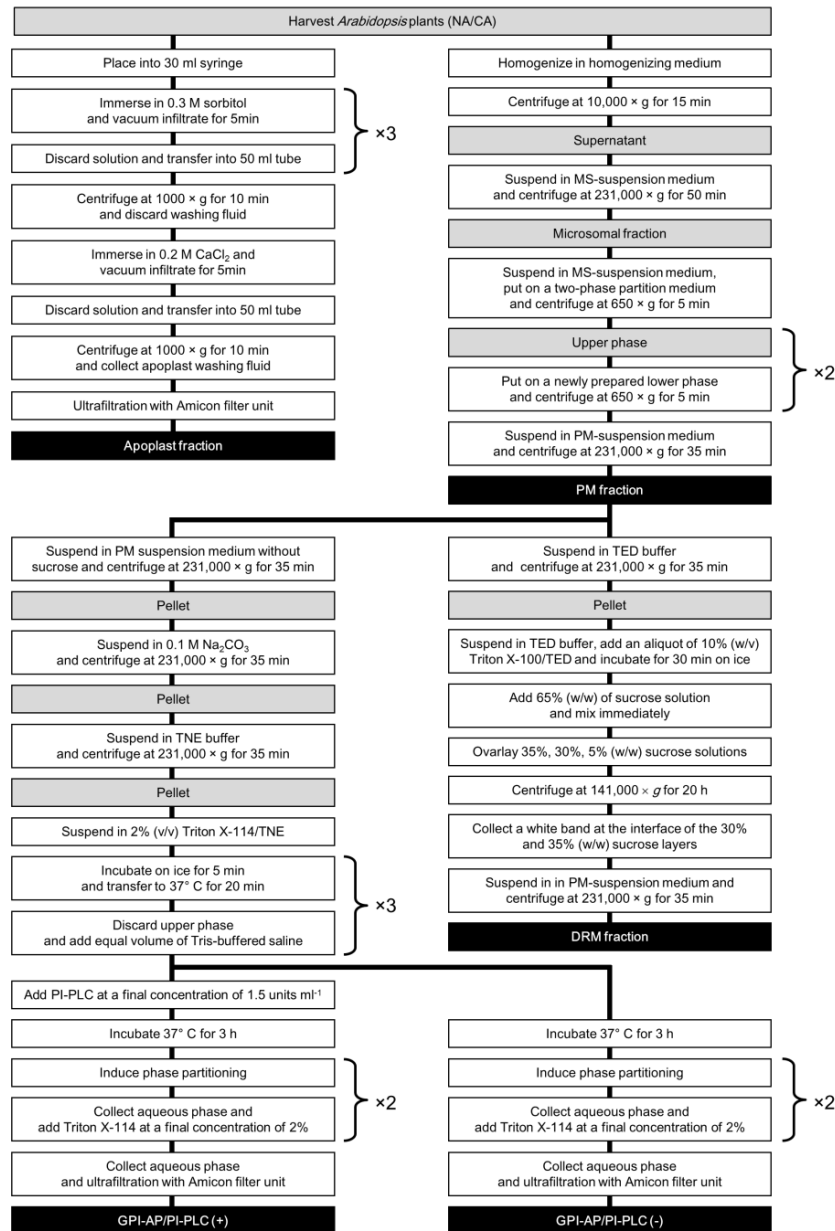


Fig. 5-1. Work flow of comprehensive proteomic approach for GPI-APs during CA in *Arabidopsis*. Highly purified PM and apoplast fractions were extracted from NA and CA *Arabidopsis* leaves. A part of PM fraction was used for preparations of DRM fraction and GPI-AP enriched fractions. DRM extraction was carried out based on Peskan et al. (2000). Protocol of GPI-AP fraction isolation was adapted from Borner et al. (2003). In this process, PM vesicles were treated with or without PI-PLC. These fractions were designated “GPI-AP/PI-PLC (+)” and “GPI-AP/PI-PLC (-)”, respectively. All fractions were subjected into nano-LC-MS/MS analysis equipped with Progenesis software. All experiments were repeated at least three times with biologically independent plants.

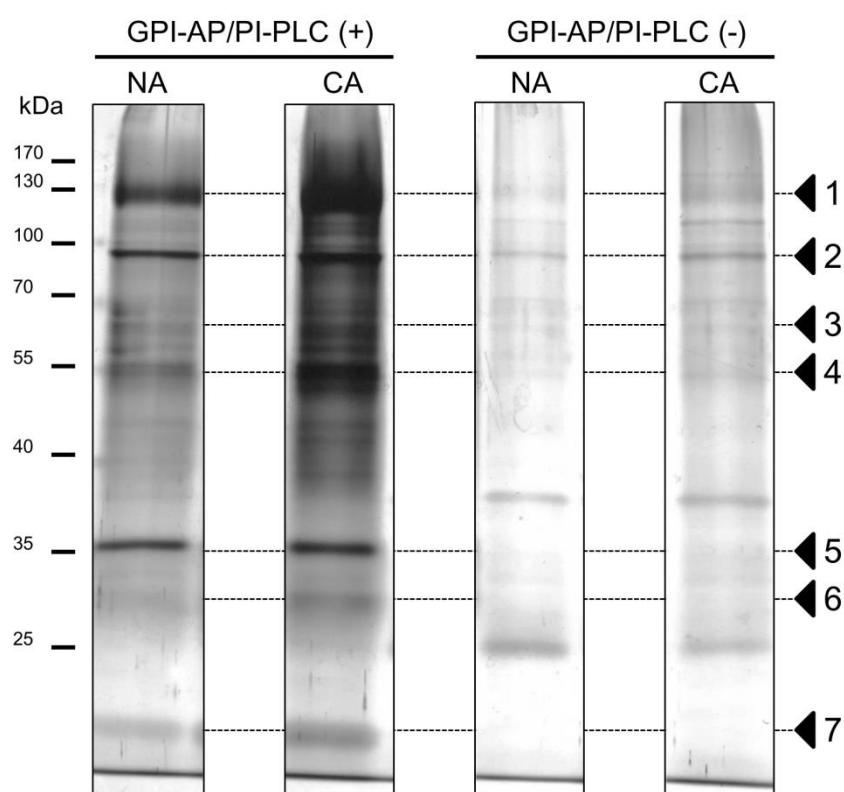


Fig. 5-2. One-dimensional SDS-PAGE profiles of GPI-AP fractions with or without PI-PLC treatment. Each GPI-AP fraction (1 μ g protein equivalent) was loaded on polyacrylamide gel, separated and visualized by silver staining (Kawamura and Uemura, 2003). Filled triangles indicate major protein bands visualized in the presence or absence of exogenous PI-PLC during preparation process, respectively. NA and CA samples were used.

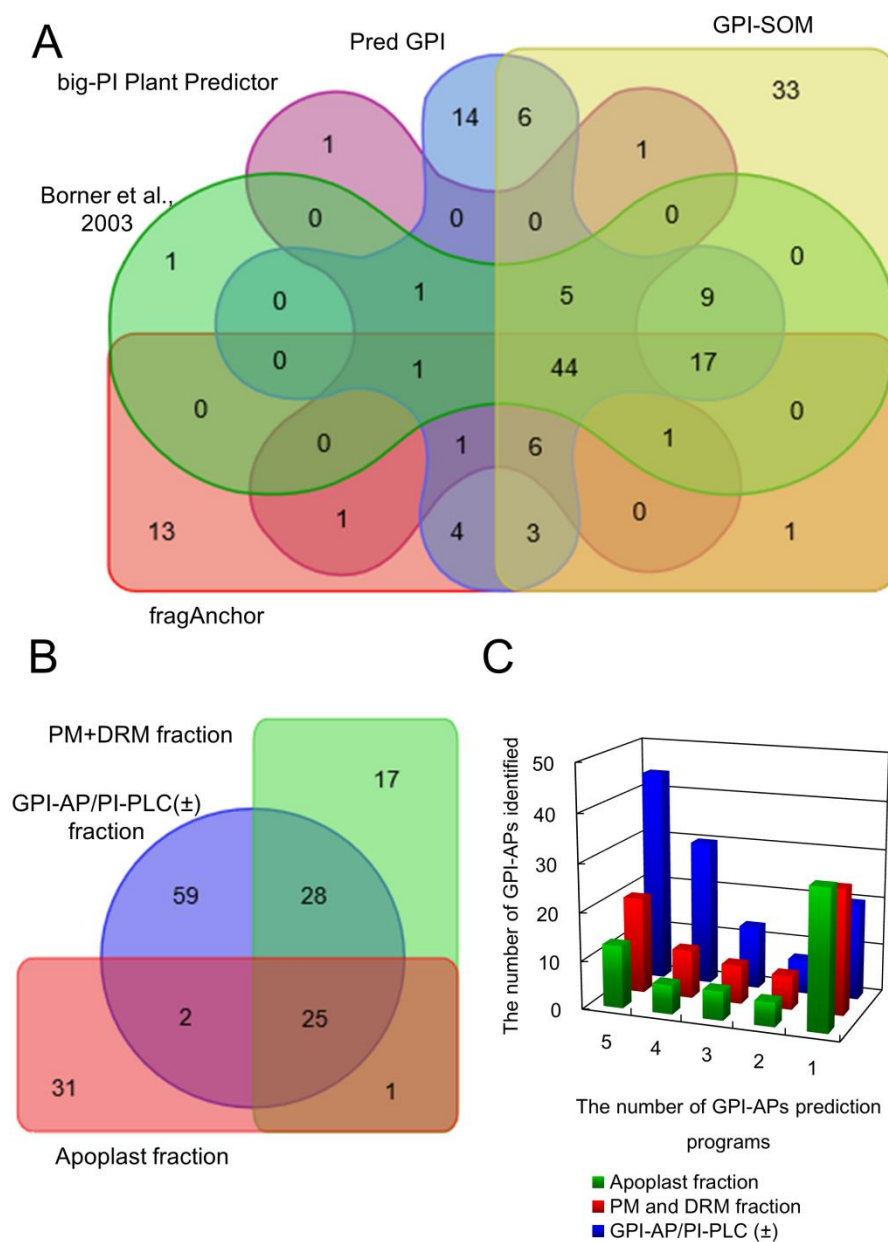


Fig. 5-3. Venn diagrams and bar graph of GPI-APs identified in each GPI-AP predictor and sample fraction. (A) The relationship among five different GPI-AP prediction programs in GPI-AP lists identified in the present study. (B) Similarities and dissimilarities of GPI-APs identified among each fraction. Venn diagrams were generated based on AGI code using online Venn diagram drawing program (<http://bioinformatics.psb.ugent.be/webtools/Venn/>). (C) The number of GPI-APs identified in each sample fraction in following five different GPI-APs prediction programs: Borner et al. (2003), big-PI Plant Predictor (Eisenhaber et al., 2003), PredGPI (Pierleoni et al., 2008), GPI-SOM (Fankhauser and Maser, 2005), fragAnchor (Poisson et al., 2007).

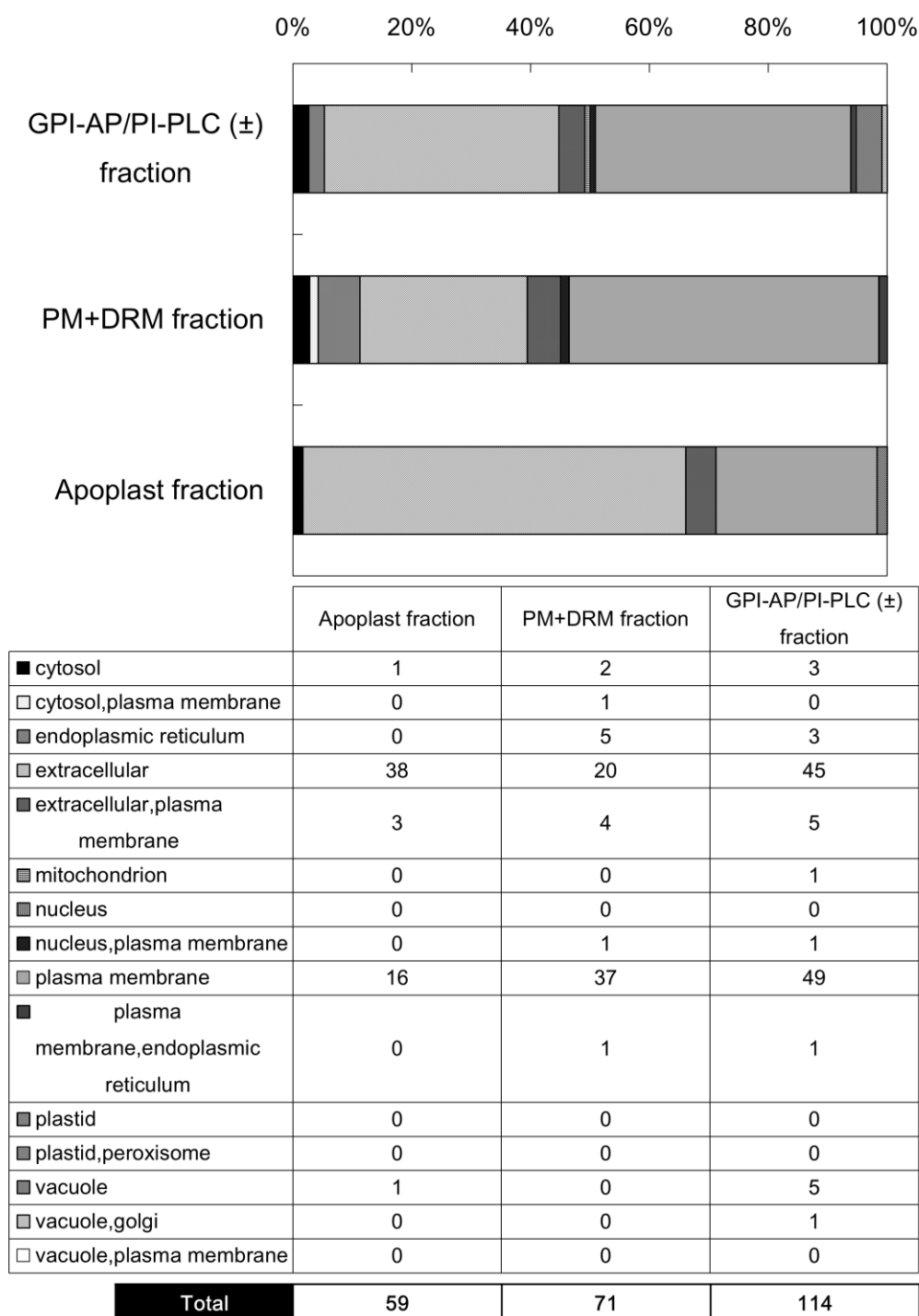


Fig. 5-4. Predictions of subcellular localization of GPI-APs identified in each sample fraction. Subcellular localization of GPI-APs was predicted by SUBA3 program (<http://suba3.plantenergy.uwa.edu.au/>) for GPI-AP/PI-PLC (\pm), PM, DRM and apoplast fractions. Proportions of GPI-APs in each location are based on the number of the protein.

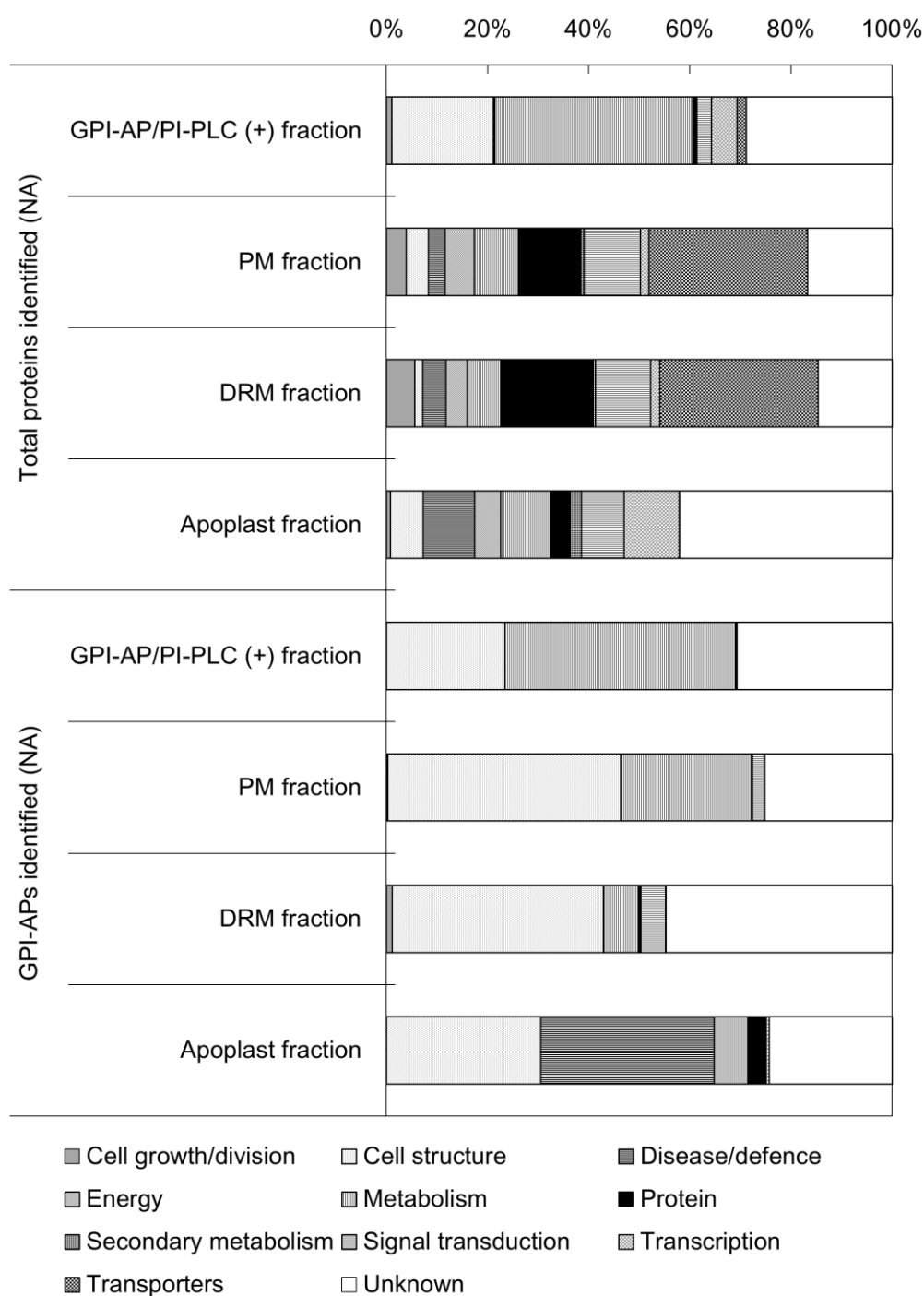


Fig. 5-5. Functional categorization of total proteins and GPI-APs identified in NA samples. All GPI-APs identified were classified into 11 functional categories based on definition proposed by Bevan et al. (1998). Proportions of each functional category in bar charts were calculated by the proportions of each functional categories based on normalized abundance of each GPI-AP identified. Upper and lower part of graph indicates functional distribution of total proteins and only GPI-APs identified in NA.

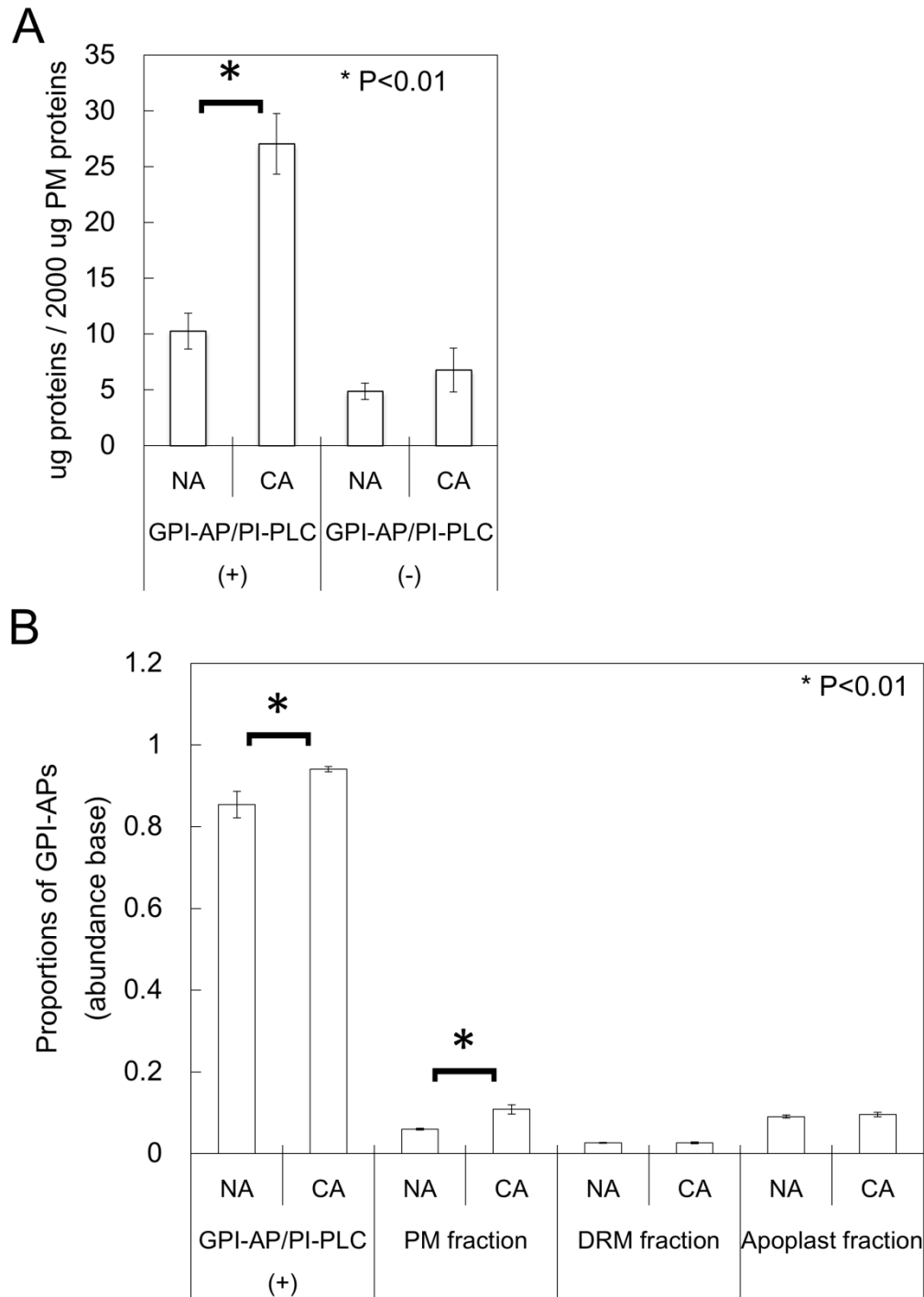


Fig. 5-6. Cold-responsiveness of GPI-APs. PM samples (equivalent of 2 mg protein) were incubated with or without PI-PLC. After the treatment, protein content of each fraction was determined by Bradford assay (n=4, A). Alternatively, the proportions of identified GPI-APs in the total proteins in each sample were calculated based on the abundance of each protein obtained from quantitative proteomic approach (n=3-7, B).

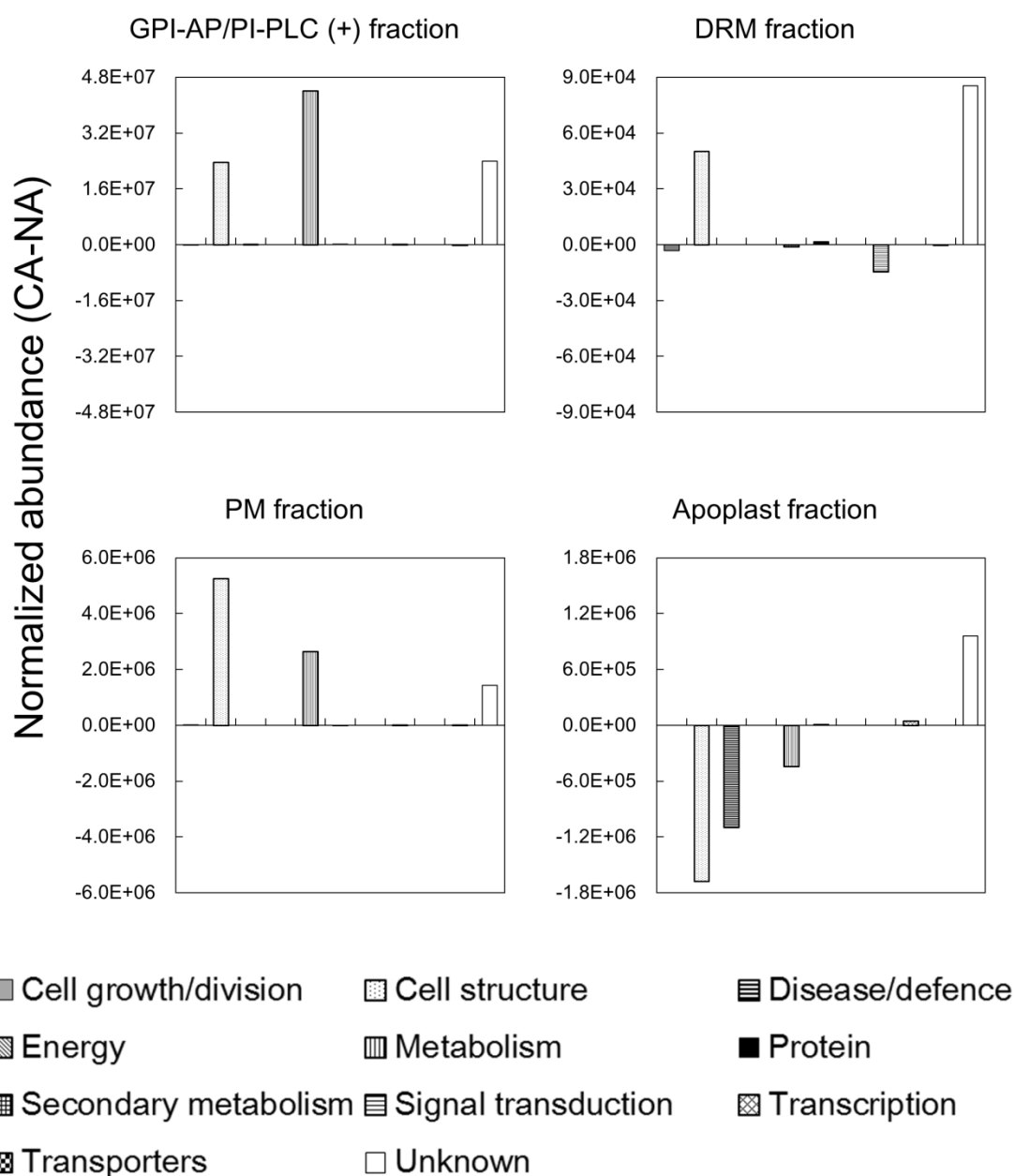


Fig. 5-7. Global proteomic changes of GPI-APs in each functional category during CA. GPI-APs identified in the four sample fractions were categorized into 11 functions as described in Fig. 5-5. Mean normalized abundance of GPI-APs in each functional category was summed and differences in this value between CA and NA were calculated.

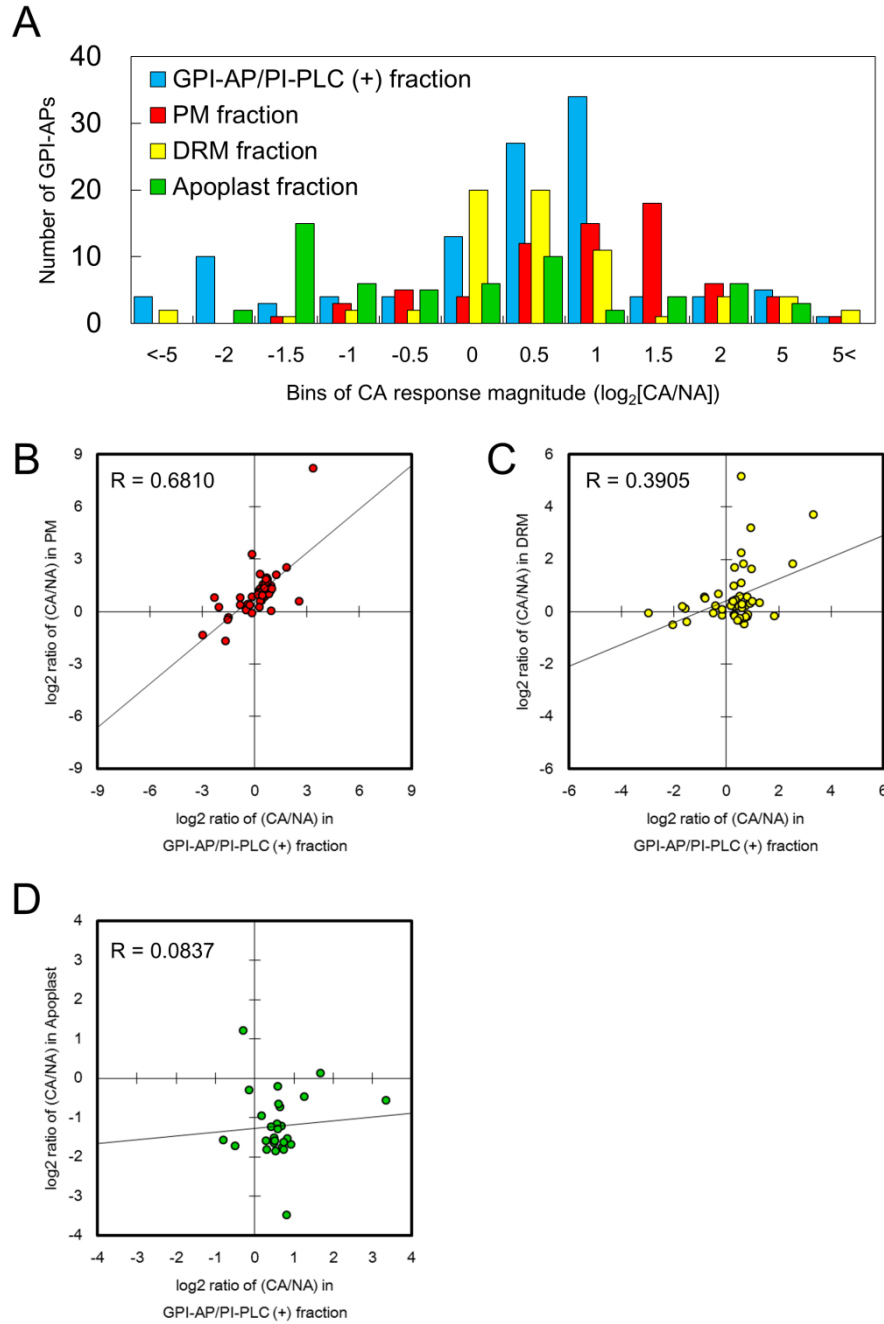


Fig. 5-8. Differences in CA-induced changes of GPI-APs in each sample fraction. Changes in abundance of each GPI-AP during CA were transformed to the \log_2 values. (A) Distribution of CA changes of GPI-APs from GPI-AP/PI-PLC (+), PM, DRM and Apoplast fractions. (B-D) GPI-APs were plotted on scatter graph with the \log_2 values of CA/NA in GPI-AP/PI-PLC (+) fraction on the X-axis and CA/NA in PM (B), DRM (C) or apoplast (D) fractions on the Y-axis. Correlation factors in each scatter plot were also calculated.

Table. 5-1. Purity of apoplastic fluids. The values of results are the mean (\pm SD) of MDH activity (nkat/g⁻¹ FW, n=4).

Treatment	MDH activity (nkat g ⁻¹ FW)		
	Whole leaf extract	Apoplastic fluid	Contamination (%)
NA	335.0 (\pm 86.2)	0.045 (\pm 0.006)	0.013
CA	279.9 (\pm 34.6)	0.215 (\pm 0.078)	0.077

Table 5-2. List of significantly changed GPI-APs in GPI-AP fraction. Statistically decreased or increased GPI-APs during CA based on following criteria were listed: ANOVA $p < 0.05$, fold change > 2.0 . Normalized abundance was transformed to logarithmic value ($n=7$). a, Accession number (AGI code) in *Arabidopsis* TAIR10 database; b, total number of peptide sequences identified in GPI-AP/PI-PLC (+) fraction; c, mean normalized abundance of 7 biological replicates in NA and CA samples; d, simplified functional category based on Bevan et al. (1998).

Accession ^a	Description	Confidence score	Peptide count ^b	Mean normalized abundance ^c		Fold change [log ₂ (CA/NA)]	Anova (p)	Functional category ^d
				NA	CA			
AT4G27520.1	Early nodulin-like protein 2 (ENODL2)	1,359.81	14	9.91E+06	2.39E+07	1.27	1.37E-08	Unknown
AT2G32240.1	Unknown function protein	988.85	22	1.99E+04	6.31E+03	-1.66	4.57E-04	Unknown
AT1G21880.2	LysM domain GPI-anchored protein 1 precursor (LYM1)	631.85	9	7.65E+04	2.42E+05	1.66	1.52E-06	Unknown
AT1G77630.1	Peptidoglycan-binding LysM domain-containing protein	603.83	10	2.55E+04	8.49E+04	1.74	1.58E-08	Unknown
AT4G16120.1	COBRA-like protein-7 precursor (COBL7, SEB1)	518.20	8	8.56E+04	8.66E+03	-3.31	6.52E-10	Transporters
AT3G60900.1	FASCICLIN-like arabinogalactan-protein 10 (FLA10)	451.38	7	1.08E+04	5.00E+04	2.21	1.05E-03	Cell structure
AT5G11150.1	Vesicle-associated membrane protein 713 (VAMP713)	440.85	11	5.40E+04	1.49E+03	-5.18	1.01E-08	Cell growth/division
AT3G04010.1	O-Glycosyl hydrolases family 17 protein	402.39	7	2.75E+04	9.79E+04	1.83	1.23E-08	Unknown
AT2G34510.1	Protein of unknown function (DUF642)	298.06	5	2.56E+04	1.28E+04	-1.00	2.91E-07	Unknown
AT1G32860.1	Glycosyl hydrolase superfamily protein	237.55	4	1.72E+03	8.28E+04	5.59	1.53E-09	Unknown
AT4G29520.1	Unknown function protein	232.61	5	3.78E+04	7.79E+03	-2.28	8.76E-07	Unknown
AT5G64080.1	Bifunctional inhibitor (Lipid-transfer protein, Seed storage 2S albumin superfamily protein)	214.09	3	3.19E+04	1.02E+05	1.68	1.06E-05	Unknown
AT2G42800.1	Receptor like protein 29 (RLP29)	198.48	5	3.89E+03	2.27E+04	2.54	1.77E-07	Unknown
AT5G62210.1	Embryo-specific protein 3 (ATS3)	181.77	2	3.14E+03	1.48E+04	2.23	3.60E-03	Cell growth/division
AT1G08500.1	Early nodulin-like protein 18 (ENODL18)	154.55	2	7.32E+03	1.52E+04	1.05	8.68E-04	Unknown
AT4G15630.1	Uncharacterised protein family (UPF0497)	153.49	5	9.16E+03	3.13E+03	-1.55	1.69E-04	Unknown
AT4G34480.1	O-Glycosyl hydrolases family 17 protein	133.18	3	9.43E+03	1.74E+03	-2.44	3.78E-11	Unknown
AT5G22780.1	Adaptor protein complex AP-2 alpha subunit	130.60	3	4.89E+03	2.24E+03	-1.12	2.31E-03	Cell growth/division
AT5G62200.1	Embryo-specific protein (ATS3)	112.13	2	4.69E+04	9.66E+03	-2.28	3.35E-09	Cell growth/division
AT5G14030.1	Translocon-associated protein beta (TRAPB) family protein	108.27	1	7.30E+03	5.98E+02	-3.61	1.25E-04	Unknown
AT3G16860.1	COBRA-like protein 8 precursor (COBL8)	97.50	3	1.02E+04	3.73E+03	-1.46	2.19E-06	Transporters
AT2G45140.1	Plant VAP homolog 12 (PVA12)	92.50	3	5.00E+03	1.22E+03	-2.03	4.53E-07	Unknown
AT4G27500.1	Proton pump interactor 1 (PPI1)	88.52	3	6.48E+03	2.29E+03	-1.50	1.85E-03	Unknown
AT1G64640.1	Early nodulin-like protein 8 (ENODL8)	77.50	1	2.23E+04	1.08E+04	-1.05	8.89E-05	Unknown
AT5G16830.1	Syntaxin of plants 21 (SYP21, PEP12)	74.96	2	8.41E+02	2.41E+01	-5.13	4.64E-05	Cell growth/division
AT1G06530.1	Tropomyosin-related protein	59.74	2	3.08E+03	4.39E+02	-2.81	3.05E-07	Cell growth/division
AT5G46860.1	Syntaxin/t-SNARE family protein (VAM3, SYP22, SGR3)	59.51	2	1.50E+04	2.95E+02	-5.67	2.11E-04	Cell growth/division
AT1G16240.1	Syntaxin of plants 51 (SYP51)	54.51	2	1.48E+03	7.87E+01	-4.23	7.75E-04	Cell growth/division
AT5G53870.1	Early nodulin-like protein 1 (ENODL1)	47.41	1	1.38E+02	1.40E+03	3.34	4.76E-03	Unknown
AT4G32150.1	Vesicle-associated membrane protein 711 (VAMP711)	20.61	1	2.28E+02	0.00E+00	Infinity	2.42E-03	Cell growth/division
AT3G27570.1	Sucrase/ferredoxin-like family protein	19.57	1	2.18E+03	2.35E+02	-3.22	1.98E-03	Unknown

Chapter 6

A GPI-anchored glycosyl hydrolase 17 family protein is involved in the enhancement of freezing tolerance during cold acclimation

Summary

When the temperature drops to a non-freezing low temperature, cold acclimation (CA) occurs in many temperate plants to adapt to coming severe freezing temperatures. Changes of plasma membrane (PM) components are important for the CA process. In Chapter 5, I described proteomic changes of lipid-modified PM proteins, glycosylphosphatidylinositol-anchored proteins (GPI-APs), during CA. Here, I selected one of the CA-induced GPI-APs, At3g04010, and characterized its functions during CA. At3g04010 encodes a putative plasmodesmal callose-degrading β -1,3-glucanase. Analysis of its temporal and tissue-specific expression revealed that the *At3g04010* gene was transiently up-regulated more than 100 times by 12 h CA treatment and was locally expressed in substance transport-related tissues such as the vascular bundles of petioles and hypocotyls. Knock-down of the *At3g04010* gene resulted in impaired freezing tolerance, retarded regrowth and enhanced callose deposition in phloem tissue during CA. These results suggest that At3g04010 plays an important role in the regulation of plasmodesmal opening and phloem transport during CA, and ultimately influences the acquisition of freezing tolerance.

Introduction

Plant performance is often affected by external stimuli such as drought, flooding, high salinity, light conditions and ambient temperature. Low temperature is one of the most influential factors for plants and is sometimes accompanied by freezing events. Freezing stress in plants, often induced by extracellular freezing, is very complex and consists of multiple stresses including cold, mechanical, dehydration and osmotic stresses (Steponkus, 1984). However, plants can survive freezing temperatures by induction of cold acclimation (CA), which occurs when plants are exposed to non-freezing low temperatures for a certain period (Thomashow, 1999). In the CA process, the accumulation of compatible solutes (Koster and Lynch, 1992) and specific proteins (Koster and Lynch, 1992; Wanner and Junttila, 1999) occurs to increase osmolality to reduce osmotic dehydration during freezing and to maintain membrane and protein structure and function.

One of the most important CA-induced changes is the alteration of plasma membrane (PM) lipid and protein composition. Lipid changes in the PM during CA have been studied for the last 30 years and are important for maintaining membrane fluidity to prevent the PM from phase transition and dysfunction in the freeze/thaw period (Steponkus, 1984; Gordon-Kamm and Steponkus, 1984b; Steponkus et al., 1988; Webb et al., 1993; Webb and Steponkus, 1993; Uemura and Steponkus, 1994; Webb et al., 1994). Kawamura and Uemura (2003) first reported dynamic changes of PM proteins during CA on a large scale. Additionally, Minami et al. (2009) reported the proteomics of the PM microdomain, which is a unique area accumulating specific PM components and is extracted as detergent-resistant membrane (DRM) fractions, and revealed specific protein enrichment in the microdomain and changes of microdomain proteins during CA. Based on these studies, I conducted proteome analysis of microdomain-enriched DRM fractions in oat and rye, which show different freezing tolerance after CA (Takahashi et al., 2012; Takahashi et al., 2013; Chapters 2 and 3 in this thesis). In these studies, a number of proteins were identified as CA-responsive microdomain proteins. Among them, I focused on glycosylphosphatidylinositol-anchored proteins (GPI-APs), which showed considerable changes in the cold-tolerant rye PM. The extent of these changes was much larger than in the less cold-tolerant oat (Takahashi et al., 2013; Chapter 3 in this thesis).

GPI-APs are representative of lipid-modified peripheral PM proteins. GPI-APs are attached to PM lipids via the GPI moiety and anchored to the extracellular leaflet of the PM (Sherrier et al., 1999; Borner et al., 2002). GPI-APs can be cleaved by an endogenous phosphatidylinositol-specific phospholipase C (PI-PLC) and released to the

apoplastic space (Bütikofer and Brodbeck, 1993). To investigate the behavior of GPI-APs more extensively during CA, I prepared GPI-AP-enriched fractions in addition to PM, DRM and apoplast fractions from *Arabidopsis* leaves and subjected these fractions to nano-LC-MS/MS based proteomics (Chapter 5). As a result, I successfully identified 163 GPI-APs in total, which showed characteristic responses to CA treatment in each fraction.

Based on these results, I selected some CA-increased GPI-APs and ordered T-DNA inserted GPI-AP mutant lines from the Arabidopsis Biological Resource Center (ABRC) to investigate the functional involvement of these GPI-APs in CA and freezing tolerance. These GPI-AP-deficient mutants were subjected to pre-screening with an imaging pulse amplitude modulation (PAM) fluorometer to evaluate their freezing tolerance (Ehlert and Hinch, 2008). Subsequently, I highlighted At3g04010 as a putative CA-associated GPI-AP. A pre-screening test showed that At3g04010 deficiency in plants resulted in impaired freezing tolerance after CA. As shown in Chapter 5, At3g04010 was predicted as a GPI-AP by Borner's GPI-AP list (Borner et al., 2003), big-PI Plant Predictor (Eisenhaber et al., 2003), GPI-SOM (Fankhauser and Maser, 2005) and fragAnchor (Poisson et al., 2007), and was identified with a high confidence score (402.4 in the GPI-AP enriched fraction). The proportion of At3g04010 in the whole PM proteome increased 5.78 times after CA. Similarly, *Arabidopsis* microarray datasets in the botany array resource (Toufighi et al., 2005) showed increased mRNA expression of At3g04010 after 1 d cold treatment. Considering the factors mentioned above, I hypothesized that the GPI-AP At3g04010 plays a crucial role for obtaining freezing tolerance in the CA process and is involved in PM surface functions during CA. In the present study, I aimed to investigate the local expression of At3g04010 at the tissue and cellular level during CA and the effect of At3g04010 deficiency on the freezing tolerance of each tissue, and finally propose a model for its function in freezing tolerance acquisition.

Experimental procedures

Plant Materials and Isolation of Plasma Membrane and Detergent-resistant Membrane Fractions

Seeds of *Arabidopsis thaliana* (ecotype Columbia) were successively surface-sterilized with 70% (v/v) ethanol and 20% (v/v) commercial bleach and sown onto Hoagland agar plates containing 1% (w/v) sucrose and 1% (w/v) agar. After incubation for 1 d at 4°C under a dark condition, the plates were transferred to and kept in a growth chamber (23°C with 16 h photoperiod at 90 $\mu\text{mol}/\text{m}^2/\text{s}$) for 14 d to obtain

NA plants. To obtain CA plants, plates with NA plants were transferred to and kept in a low temperature chamber (2°C with 12 h photoperiod at 90 $\mu\text{mol}/\text{m}^2/\text{s}$) for specified period.

Establishment of T-DNA Knock-down Lines

T-DNA tagged *At3g04010* locus (SALK_112132C) was obtained from ABRC. Genotypes of these plants were confirmed by genomic PCR using several sets of primers (P1, P2 and P3; Table 6-1). SALK_112132C obtained were backcrossed twice with WT plants. Resultant heterozygous lines were self-fertilized and homozygous lines were subsequently selected.

Quantitative Real-Time PCR

Total RNA was extracted from aerial parts of plants after CA for specified periods with RNeasy Plant Mini Kit (Qiagen, Tokyo, Japan). cDNA was synthesized from 1000 ng total RNA using ReverTra Ace® qPCR RT Master Mix (TOYOBO, Osaka, Japan) with random primers (Table 6-1). SYBR® Premix Ex Taq™ II (Takara Bio Inc., Otsu, Japan) and Thermal Cycler Dice® Real Time System II (Takara) were used for quantitative RT-PCR analysis and *At3g04010* gene in 25 time diluted cDNA samples were quantified with Primer P4 and P5. *GTP binding Elongation factor Tu family protein (EF1a, At5g60390)* was used as a reference gene (Primer sets: P6 and P7). All samples were biologically repeated three times.

GUS-reporter Assay

At3g04010pro::GUS vectors were constructed by the amplification of *At3g04010* promoter region and cloned into the binary vector pGWB3 using Gateway technology. Upstream (983 bp) from initiation codon in *At3g04010* gene was amplified by primer set (P8 and P9; Table 6-1). PCR product was digested by HindIII and XbaI, purified with Wizard® SV Gel and PCR Clean-Up System (Promega, Madison, WI, USA) and cloned into pENTR®/D-TOPO (Invitrogen Life Technologies, Gaithersburg, MD, USA) with Ligation high Ver.2 kit (Takara Bio Inc.). These plasmid vectors were introduced into *E. coli* with electroporation and applied on LB medium supplemented with kanamycin for selection of colonies which had plasmid vectors. Plasmid was purified from cultivated *E. coli* with AxyPrep Plasmid Prep Kit (Axygen Scientific, Union City, CA, USA) and applied for LR reaction with pGWB3 vector using LR clonase enzyme mix (Invitrogen Life Technologies). Resultant pGWB3 vector was introduced into *E. coli* again in the presence of kanamycin and hygromycin and the

vector purified was introduced into *A. tumefaciens* (GV3101) by a freeze-thawing method. Transformed *A. tumefaciens* was screened on LB medium containing kanamycin, hygromycin and rifampicin. *Arabidopsis* plants were then transformed using the flower dip method as described by Clough and Bent (1998). Seeds of T1 plants were sown on Hoagland plates supplemented with hygromycin and carbenicillin. Transformation of plants was checked by genomic PCR with M13 primer.

To observe GUS activity distribution, X-Gluc solution (150 μ l 38.3 mM X-Gluc in N,N-dimethylformamide, 120 μ l of 12.5 mM $K_3Fe(CN)_6$, 120 μ l of 12.5 mM $K_4Fe(CN)_6$, 9 μ l of Triton X-100 and 601 μ l of water) was prepared. After three-fold dilution, plants were soaked in X-Gluc solution and incubated for 6 h or longer at 37°C. Plants were then transferred to 0.24 N HCl in 20% (v/v) methanol and incubated at 57°C for 15 min. Solutions were replaced with 7% (w/v) NaOH in 60% (w/v) ethanol for 15 min at room temperature. Subsequently, plants were rehydrated in a series of ethanol (40%, 20% and 10% [v/v], successively) for 5 min each. Finally, plants were infiltrated in a solution of 5% (v/v) ethanol and 25% (v/v) glycerol for 30 min and then mounted in 50% (v/v) glycerol.

Evaluation of Freezing Tolerance

Freezing tolerance was evaluated by fresh weight measurement, imaging PAM analysis, 2,3,5-triphenyl tetrazolium chloride (TTC) and electrolyte leakage assay after freezing. All of the plants were sown on agar plate. NA plants were designated as plants grown at 23°C for 10 d for weight measurement and imaging PAM analysis and for 14 d for TTC and electrolyte leakage assay. CA plants were obtained by further incubation of NA plants at 2°C for specified period. NA and CA plants were transferred into a freezing chamber that was set at specified freezing temperature and incubated for 20 min. Subsequently, four corners of the plates were frozen by a touch of liquid nitrogen and the plates were incubated further for 2 h. Subsequently, plants were transferred to a growth chamber (23°C) for thawing process.

For fresh weight measurement, plants after a freeze-thawing were grown at 23°C for 7 d. Greenish parts of each plant were cut out and weighed.

For imaging PAM analysis, plants after a post-thaw treatment for specified periods or non-frozen control plants were adapted to dark for 20 min in a cardboard box. Subsequently, plants were transferred into imaging PAM fluorometer equipped with FluoroCam 7.0 software (Closed FluoroCam FC 800-C, Photon Systems Instruments, Brno, Czech Republic) and images of maximal PSII quantum yield (F_v/F_m) were taken. Images were given false color based on F_v/F_m value.

TTC assay was conducted as described in Livingston et al. (2013) with a slight modification. Frozen plants were transferred to a growth chamber (23°C) for specified periods listed in figure. Then, plants were soaked in a solution composed of 0.5% (w/v) TTC and 50 mM HEPES (pH 7.3), infiltrated with vacuum pump for 1 h and incubated at room temperature for 6 h under vacuum condition in dark. Pictures were taken with a digital single-lens reflex camera.

Electrolyte leakage assay was conducted as Takahashi et al. (2013; Chapter 3 in this thesis) with slight modifications. *Arabidopsis* leaves were harvested, washed with precooled water and put into glass tubes with aliquots of water (100 µL). Glass tube was cooled in alcohol bath (NCB-3400, EYELA, Tokyo, Japan) at specified temperature for 15 min and frozen with addition of ice crystals. Samples were cooled for further 2 h at the same temperature. After incubation overnight at 4°C, 500 µL of water was added and samples were shaken for 30 min. Electrolytes were leaked from plant tissues during freeze-thawing and measured with a conductance meter (Twin Cond, HORIBA, Kyoto, Japan). After boiling samples for 20 min, fully leaked electrolyte was measured again. Using the two measured values, the ratio of electrolyte leakage caused by freeze-thawing was calculated (leakage at the measurement before boiling/leakage at the measurement after boiling).

Determination of Osmolar Concentration

Plant leaves, petioles, roots and hypocotyls were collected and ground in 1.5 ml microtubes and obtained homogenate solutions were subjected to osmometer (Vapro Osmometer 5520, Wescor Inc., Logan, UT, USA).

Construction of At3g04010- mCherry Fusion Proteins

At3g04010pro::mCherry-At3g04010 construct was established by overlap PCR methods. This construct was composed of *At3g04010pro/secretory signal*, *mCherry* and *At3g04010* coding sequence (CDS). *At3g04010pro/secretory signal* was amplified from genomic DNA using primers P10 and P11 (Supplemental Table 1). *mCherry* CDS were amplified from pFCG-G-rb vector using primers P12 and P13 (Supplemental Table 1). cDNA clone of *At3g04010* (DKLAT3G04010) purchased from ABRC and amplified using primers P14 and P15 (Supplemental Table 1). Fragments of *At3g04010pro/secretory signal*, *mCherry* and *At3g04010* CDS were terminally-processed with BamHI/EcoRI, EcoRI/XhoI and XhoI/PstI, respectively and conducted gel extraction with Wizard® SV Gel and PCR Clean-Up System (Promega). pCAMBIA1300 vector was also treated with BamHI/PstI and purified as described

above. The three fragments and pCAMBIA1300 was mixed and ligated with Ligation high Ver.2 kit (Takara Bio Inc.). These plasmid vectors were introduced into *E. coli* with electroporation and applied on LB medium in the presence of kanamycin and X-gal for selection of colonies that had plasmid vectors with insertion of above three fragments. After purification from cultivated *E. coli* with AxyPrep Plasmid Prep Kit (Axygen), the plasmid was introduced into *A. tumefaciens* (GV3101) by a freeze-thawing method. Transformed *A. tumefaciens* was screened on LB medium containing kanamycin, hygromycin and rifampicin. *At3g04010* knock-down mutants were then transformed and seeds of T1 plants were screened as described above. Transformation of plants was checked by genomic PCR with primers P12 and P13 (Supplemental Table 1).

Microscopic Analysis

For callose staining, fresh plants were dipped into ECA buffer (60% ethanol, 30% chloroform, 10% acetic acid) immediately and fixed for at least 2 h to prevent from wounding-induced callose deposition (Xie et al., 2011). Subsequently, samples were treated with 2 N NaOH for 30 min and washed with 0.1 M K₂HPO₄, pH 8.5 for at least 2 h. Callose was stained by treatment of 0.05% aniline blue solution for 30 min. I used a Nikon C2 laser scanning confocal microscope (Nikon, Tokyo, Japan) with an excitation filter of 408 nm and emission filter of 455–505 nm. Images were subjected to quantification analysis with NIS elements AR ver. 4.30. First, non-callose stained phloem parts were selected as background and mean intensities of these parts were subtracted from overall image. Callose-stained phloem parts were selected as region of interest and mean intensity of these parts were measured. For each time point in WT and *at3g04010*, 63 to 118 images were collected. Because *F*-test denoted unequal variance between WT and *at3g04010* in each time point, statistical analysis was performed using a Mann-Whitney *U*-test.

For visualization of At3g04010, mCherry fluorescent protein was excited by 561 nm laser and fluorescence at 575-615 nm was detected. To quantify fluorescence intensity of mCherry-At3g04010, confocal images taken from petioles of 29 biologically independent samples in each time point were subjected to intensity analysis as described above. Phloem parts were selected as the region of interest and mean intensity of these parts were measured.

Results

Proteomics Data Series Identified At3g04010 as a CA-responsive GPI-AP

Global proteomic changes of GPI-APs during CA are described in Chapter 5. In these experiments, the total amount of GPI-APs on the PM was estimated to increase 2.64 and 1.81 times after a 7 d CA period as determined by Bradford assay and shotgun proteomics, respectively. The compositions of GPI-AP enriched fractions treated with or without PI-PLC (GPI-AP/PI-PLC [\pm] fraction) and PM, DRM and apoplast fractions were also affected by CA treatment. Among the four fractions analyzed, I focused on changes of GPI-APs in the GPI-AP/PI-PLC (+) fraction, which had high reliability for the GPI-AP identification process. From the GPI-AP lists, I selected GPI-APs that exhibited quantitative increases during CA with statistical significance (fold change > 2.0, $p < 0.05$) and high confidence scores. I conducted simple screening by imaging PAM analysis of various mutant lines obtained from the ABRC after freeze/recovery treatment (freezing at -12°C and recovery at 23°C for 7 d). Then, I selected the SALK_112132C mutant with a T-DNA insertion in the *At3g04010* gene as an experimental plant. In a suite of proteomic results, the amount of At3g04010 increased 3.56 and 5.78 times in the GPI-AP/PI-PLC (+) and PM fractions, respectively, during CA but did not change significantly in DRMs (1.12 times) and could not be detected in the apoplast fraction (Fig. 6-1).

Establishment of an at3g04010 Knock-down Mutant

T-DNA inserted homozygous mutants were obtained from the ABRC. T-DNA insertion was checked by genomic PCR. From the PCR product patterns, I confirmed that T-DNA was inserted in the promoter region of the *at3g04010* mutant (Fig. 6-2A and 6-2B). To reduce the possibility of multiple T-DNA insertions in the *Arabidopsis* genome, back crossing with the WT (Col-0) was conducted twice and homozygous mutants were obtained by self-fertilization of the resultant heterozygous plants. During the life cycle including the vegetative and reproductive stages, there were no phenotypic differences between the WT and *at3g04010* (Fig. 6-2C).

Temporal and Histological Expression of At3g04010 during CA

Next, I performed temporal analysis of *At3g04010* gene expression during CA (Fig. 6-3). In the WT, relative *At3g04010* gene expression was transiently up-regulated 112 times after 12 h CA and rapidly decreased over a prolonged CA period. *At3g04010* gene expression in the *at3g04010* mutant was repressed by 22% in comparison with the WT after a 12 h CA period.

To clarify the tissue-specific expression of the *At3g04010* gene, a GUS-fused promoter assay was conducted. As described in Fig. 6-3, strong transient expression of

the *At3g04010* gene was observed throughout the plant at 1 d CA that gradually decreased as the CA period progressed (Fig. 6-4A). Looking at specific plant parts at 1 d CA, hypocotyls, petioles, roots and veins were strongly stained (Fig. 6-4B–E, respectively). A transverse section of the petiole showed that *At3g04010* gene expression was concentrated in the central parts of the tissue indicating the vascular bundle (Fig. 6-4F). These parts included xylem vessels and phloem (Fig. 6-4G).

Impaired Freezing Tolerance of the at3g04010 Knock-down Mutant

To measure the influence of *At3g04010* gene knock-down on plant freezing tolerance, I compared freezing tolerance between the WT and *at3g04010* by measuring the fresh weight of living plant parts after freezing for 2 h and subsequent recovery for 7 d. In NA plants, the fresh weight of each plant after the freezing/recovery process was not statistically different between the WT and *at3g04010* (Fig. 6-5A). No morphological differences were observed during the freezing/recovery process (Fig. 6-5B). On the other hand, the fresh weight of cold-acclimated *at3g04010* was statistically reduced in comparison with the WT after -10°C or -12°C freezing treatment (Fig. 6-5C). After -12°C freezing treatment, the WT kept a greenish color and the central part of the plant still grew while *at3g04010* plants were completely bleached.

Next, I measured chlorophyll fluorescence as an indicator of freezing tolerance (Ehlert and Hinch, 2008) and visualized it based on Fv/Fm values (Fig. 6-6). In NA plants, the Fv/Fm intensity of *at3g04010* was almost the same as the WT. A similar tendency was observed for CA plants in the absence or presence of freezing/recovery treatment. However, CA *Arabidopsis* plants treated with -8°C freezing exhibited slightly decreased Fv/Fm values in their leaves compared with the WT. At -10°C , the Fv/Fm intensity was severely decreased in *at3g04010* while the WT exhibited higher Fv/Fm values in a larger area. After -12°C freezing, Fv/Fm signals were barely visible in the central part of *at3g04010* plants and signals in the leaves and petioles of *at3g04010* completely disappeared. Meanwhile, the WT kept a higher Fv/Fm intensity in the regrowing part during the recovery process.

To investigate freezing tolerance at the tissue level, I conducted a TTC assay. Unfrozen CA plants turned red because the plant tissues could actively reduce tetrazolium salts, indicating little injury by freezing (Fig. 6-7A). Plants soaked in TTC buffer immediately after freezing, however, were damaged and did not have TTC reduction activity even though the plants were still green. Among plants frozen at -10°C , the leaves, veins and petioles of *at3g04010* were more severely injured than those of the WT and I noted the same tendency in the plants after a post-thaw period of

1 d and 3 d (Fig. 6-7). After -12°C freezing, the leaves completely lost TTC reduction activity. At the same time, the WT could reduce tetrazolium salts in the petiole and hypocotyl while the hypocotyls of *at3g04010* plants barely survived after freeze/thawing. Although the WT and *at3g04010* plants frozen at -8°C and -10°C grew well and developed inflorescence stems after a 7 d post-thaw period, the number of healthy leaves and the length of the inflorescence stem were lower in *at3g04010* plants than in the WT. In plants frozen at -12°C , two to four leaves regrew from the WT hypocotyl, whereas the growth of *at3g04010* plants was completely arrested or occurred very slowly (Fig. 6-7). Interestingly, the roots did not exhibit any differences in the extent of injury between WT and *at3g04010* plants.

Electrolyte leakage assay is one of the most common methods for determining freezing injury to the PM (Murray et al., 1989; Maier et al., 1994). The temperatures at which 50% electrolyte leakage occurred in leaves (LT50) were -2.3°C in both the WT and *at3g04010* before CA, and -4.7°C and -4.8°C in the WT and *at3g04010*, respectively, after CA. Thus, freeze-induced damage to the PM was similar between the WT and *at3g04010* after CA. Osmolality is considered to be one of the determinants of freezing tolerance. A previous study reported increased osmolality during CA (Levitt, 1980). In the present study, I therefore measured osmolality in four major plant parts expressing the *At3g04010* gene during CA (Fig. 6-9). The osmolality increased in WT leaves (from 234.5 mosmol to 358.3 mosmol), petioles (from 256.4 mosmol to 530.0 mosmol) and hypocotyls (from 232.8 mosmol to 416.7 mosmol) after 7 d CA. When comparing the WT and *at3g04010*, however, no statistical differences were observed in any plant part during CA.

Callose Deposition in the at3g04010 Mutant and Cellular Localization of At3g04010

A computational approach using the NCBI Blast search engine to understand the functions of *At3g04010* revealed that *At3g04010* contains two conserved domains; a glycosyl hydrolase 17 (GH17) and a X8 domain. The GH17 domain is thought to be important for hydrolyzing glycosidic bonds in β -1,3-glucan as represented by callose (Henrissat and Davies, 2000; Forslund et al., 2008). The X8 domain is considered to be involved in carbohydrate binding and other callose binding proteins also contain the X8 domain (Forslund et al., 2008; Simpson et al., 2009). Because *At3g04010* is thought to be a callose-degrading β -1,3-glucanase in vivo, I used a microscopic approach to examine callose deposition in the WT and *at3g04010* during CA. As shown in Fig. 6-10A, aniline blue-stained callose foci were observed that were located right by the xylem, which indicates callose deposition in sieve elements and/or plasmodesmata in

the phloem. After 1 d CA, both the WT and *at3g04010* showed increased callose deposition compared with NA (Fig. 6-10). Callose deposition in the WT decreased over a prolonged CA period, but *at3g04010* maintained a higher level than the WT throughout the CA period (Fig. 6-10).

To investigate cellular localization of At3g04010, I established transgenic lines expressing mCherry-conjugated At3g04010 protein. Microscopic observation of mCherry fluorescence revealed that At3g04010 was highly expressed in phloem (Fig. 6-11) which is consistent with the results shown in Fig. 6-4. Mean fluorescence intensity in phloem gradually increased up to 2.70-fold by 7 d CA treatment (Fig. 6-12A and 6-12B). Furthermore, distribution of fluorescence of mCherry-conjugated At3g04010 proteins after CA treatment for 7 d was patch-like structure located on the cell surface of phloem or intercellular border of mesophyll cells (Fig. 6-12C and 6-12D).

Discussion

Identification of the At3g04010 Gene and Its Response to CA in Arabidopsis

In Chapter 5, I identified 163 GPI-APs in total from the GPI-AP/PI-PLC (\pm), total PM, DRM and apoplast fractions. Among them, many GPI-APs responded to CA treatment in each sample fraction. At3g04010 was one of the CA-inducible GPI-APs found in the GPI-AP/PI-PLC (+) and PM fractions as described in Fig. 6-1. The normalized abundance of At3g04010 increased 3.56 and 5.78 times in the GPI-AP/PI-PLC (+) and PM fractions, respectively. Interestingly, the accumulation level of At3g04010 in the DRM and apoplast fractions was not as high as in the GPI-AP/PI-PLC (+) fractions and did not change during CA, indicating that At3g04010 is not a microdomain-enriched and/or apoplast-targeted protein and maintains a steady level in microdomains. The lipid raft concept was originally proposed by Simons and Ikonen (1997) and some GPI-APs are considered to be enriched in microdomains (Sargiacomo et al., 1993; Danielsen and van Deurs, 1995; Simons and Ikonen, 1997). This concept has also been accepted in many research papers on plant cells (Peskan et al., 2000; Borner et al., 2005; Bessueille et al., 2009). However, not all GPI-APs can be partitioned preferentially into the microdomain area in the PM and At3g04010 may be one of these non-microdomain-enriched GPI-APs.

To confirm the responsiveness of At3g04010 to CA treatment, temporal gene expression analysis was performed during CA by both qRT-PCR and GUS-promoter assay (Figs. 6-3 and 6-4A). The mRNA expression of *At3g04010* transiently and drastically increased during CA (Fig. 6-3). The same expression pattern was observed in

the GUS-promoter assay (Fig. 6-4A). In the proteomic results, I detected an increased amount of At3g04010 during a 7 d CA period (Fig. 6-1). After the 7 d CA period, the mRNA level of *At3g04010* returned to the level detected in NA (Fig. 6-3) and GUS expression was only slightly detectable in petioles, hypocotyls and roots (Fig. 6-4A). Turnover of the *At3g04010* mRNA may be fast, but the balance between biosynthesis and degradation may differ at the mRNA and protein levels. Thus, the At3g04010 protein may still remain on the PM surface after a 7 d CA period. mCherry-At3g04010 expression continued to increase throughout CA period (Fig. 6-11A and 6-11B) and these results may reflect actual expression of At3g04010 protein. Therefore, the timing of *At3g04010* expression at mRNA level during CA may not necessarily correspond to the one at the protein level. In fact, some proteins including two putative GPI anchored glycosyl hydrolase family proteins (At2g01630 and At5g04885) show different change patterns at the protein and transcript levels (Li et al., 2012).

Impaired Freezing Tolerance of at3g04010 Mutants after CA

Although the regrowth of plants after a freeze/thawing treatment was not different between the WT and *at3g04010* under NA (Fig. 6-5A and 6-5B), the regrowth of CA *at3g04010* plants was obviously much weaker than that of CA WT plants (Fig. 6-5C and 6-5D). Thus, knock-down of *At3g04010* expression resulted in decreased freezing tolerance after CA and *At3g04010* may play crucial roles for the acquisition of freezing tolerance during CA. Chlorophyll fluorescence imaging (PAM assay) showed that *At3g04010* deficiency resulted in greater leaf injury after CA, slower post-thaw recovery processes and a slower regrowth rate than in WT plants (Fig. 6-6). Therefore, the presence of At3g04010 in CA plants seems to influence post-thaw recovery. The results of the electrolyte leakage test and TTC assay, which measured the degree of cellular damage immediately after freeze/thawing without post-thaw recovery, indicate that At3g04010 is not important for reducing the extent of freezing injury to leaves right after freezing (Figs. 6-7 and 6-8).

At an early stage of the CA process (1 d CA treatment), *At3g04010* gene expression reached a peak (Figs. 6-3 and 6-4A). At this point, the *At3g04010* gene was highly expressed in the vascular bundles of hypocotyls, petioles, roots and veins (Fig. 6-4B-G). Histological determination of freezing tolerance by TTC assay revealed that TTC reduction activity in the petiole was reduced right after freezing and the regrowth process in the hypocotyl was severely retarded in *at3g04010* mutants (Fig. 6-7). Thus, the tissue-specific expression patterns of *At3g04010* were consistent with tissues having

decreased freezing tolerance and regrowth activity but At3g04010 may not be involved in freezing tolerance and the post-thaw regrowth process in roots.

Possible Role of At3g04010 in Phloem Transport Regulation during CA

Given that At3g04010 was predicted to be a β -1,3-glucanase based on its amino acid sequence characteristics, I considered a relationship between At3g04010 and callose degradation during CA. Callose deposition was measured using aniline blue staining in the petiole, and the data were processed by image analysis. As expected, *At3g04010* gene loss resulted in increased callose deposition but the WT showed a decreased callose accumulation level in the phloem during CA (Fig. 6-10). This difference was observed after a 1 d CA period. Transient expression of *At3g04010* (Figs. 6-3 and 6-4A) may be involved in promoting callose degradation in the phloem and the expressed At3g04010 protein may continue to degrade callose throughout the CA period. At3g04010 expression at the protein level was up-regulated after 1 d CA period and increased throughout CA period (Fig. 6-11A and 6-11B). These results are consistent with the results of proteomics (Fig. 6-1), qRT-PCR (Fig. 6-3), GUS-promoter assay (Fig. 6-4A) and callose deposition staining (Fig. 6-10). Therefore, the expression level of At3g04010 protein seems to correlate highly with callose deposition level. In addition to the expression patterns of At3g04010 protein during CA, cellular localization of At3g04010 was quite similar to callose localization (Fig. 6-11C and 6-11D). At3g04010 was mainly expressed in phloem and many fluorescent foci were observed on phloem surface and mesophyll cells in petiole. Thus, At3g04010 function and callose deposition level may be closely related during CA. The principal function of β -1,3-glucanase in the vegetative stage is to degrade plasmodesmal neck callose and regulate cell-to-cell communication in cooperation with callose synthase activity (Levy et al., 2007a; Levy et al., 2007b). Virus movement is also regulated by β -1,3-glucanase via enhanced callose deposition (Iglesias and Meins, 2000). Furthermore, callose deposition inhibits phloem transport by closing the sieve plate (Barratt et al., 2011; Xie et al., 2011) and conversely β -1,3-glucanase may be involved in sieve plate opening and promoting phloem transport. Therefore, in *at3g04010* plants, phloem transport could be inhibited by callose deposition at least once in the early stage of CA, which may be induced by an imbalance between callose synthase and reduced β -1,3-glucanase activities at cold temperatures. In the WT, increased expression of *At3g04010* after a 1 d CA period may well maintain the balance of callose turnover in the phloem and the phloem transport necessary for freezing tolerance acquisition. Phloem transport is thought to be important for translocation of CA-inducible osmolytes and compatible

solutes such as raffinose (Bachmann et al., 1994). If this is correct, different phenotypes should be observed between the WT and *at3g04010* mutants such as osmolyte levels during CA and the extent of freezing injury right after freezing. However, enhanced callose deposition in the phloem did not result in impaired osmolyte accumulation in all parts of *at3g04010* plants (Fig. 6-9). Additionally, the survival of *at3g04010* immediately after freezing was almost the same as that of the WT with the exception of the petiole (Figs. 6-7 and 6-8). Instead, *at3g04010* mutants showed clearly impaired freezing tolerance during the post-thaw recovery process (Figs. 6-5, 6-6 and 6-7). Increased expression of *At3g04010* in the early stage of CA and the opening of plasmodesmata and/or sieve plates in the phloem may have a significant role in rapid metabolite relocation and transport after freeze/thawing, which would strongly promote recovery from freeze-induced damage and keep survival rates high after damage. Interestingly, in poplar, β -1,3-glucanase is important for dormancy release (Rinne et al., 2001; Rinne et al., 2011). In the endodormancy process, cell-to-cell communications are interrupted, which is induced by phytochrome signaling under short-day conditions (offline state). In the eco-dormancy state, chilling induces digestion of plasmodesmal neck callose by β -1,3-glucanase activity but cell-to-cell communication is not yet activated (standby state). Along with an increase in temperature and water availability, cell-to-cell connections become active to exchange signals (online state). As described in Fig. 6-12, in *Arabidopsis* plants, cell-to-cell connections may be closed once by callose deposition during the early stage of CA (offline) state and then β -1,3-glucanases such as *At3g04010* may trigger opening of plasmodesmata and sieve plates (standby) state during the 3–7 d CA period. After freeze/thawing and during post-thaw recovery, the online state may be induced and necessary for nutrient and signal exchange and de novo development of leaves from the shoot apical meristem.

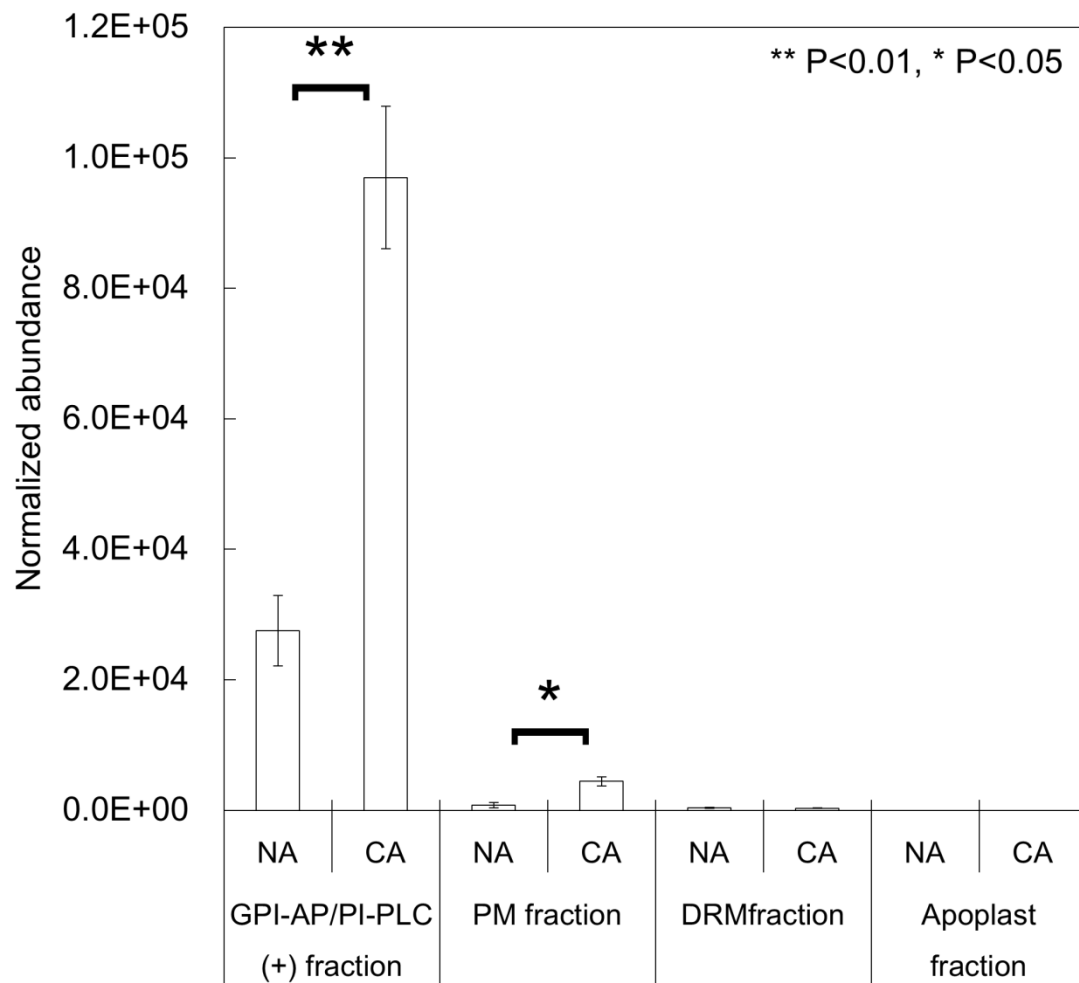


Fig. 6-1. Response of At3g04010 to CA treatment in proteomic datasets. Normalized abundances of At3g04010 were extracted from proteomic data sets in Chapter 5. Error bars indicate standard deviations (n=3-7). * p <0.05 and ** p <0.01 by student's t-test.

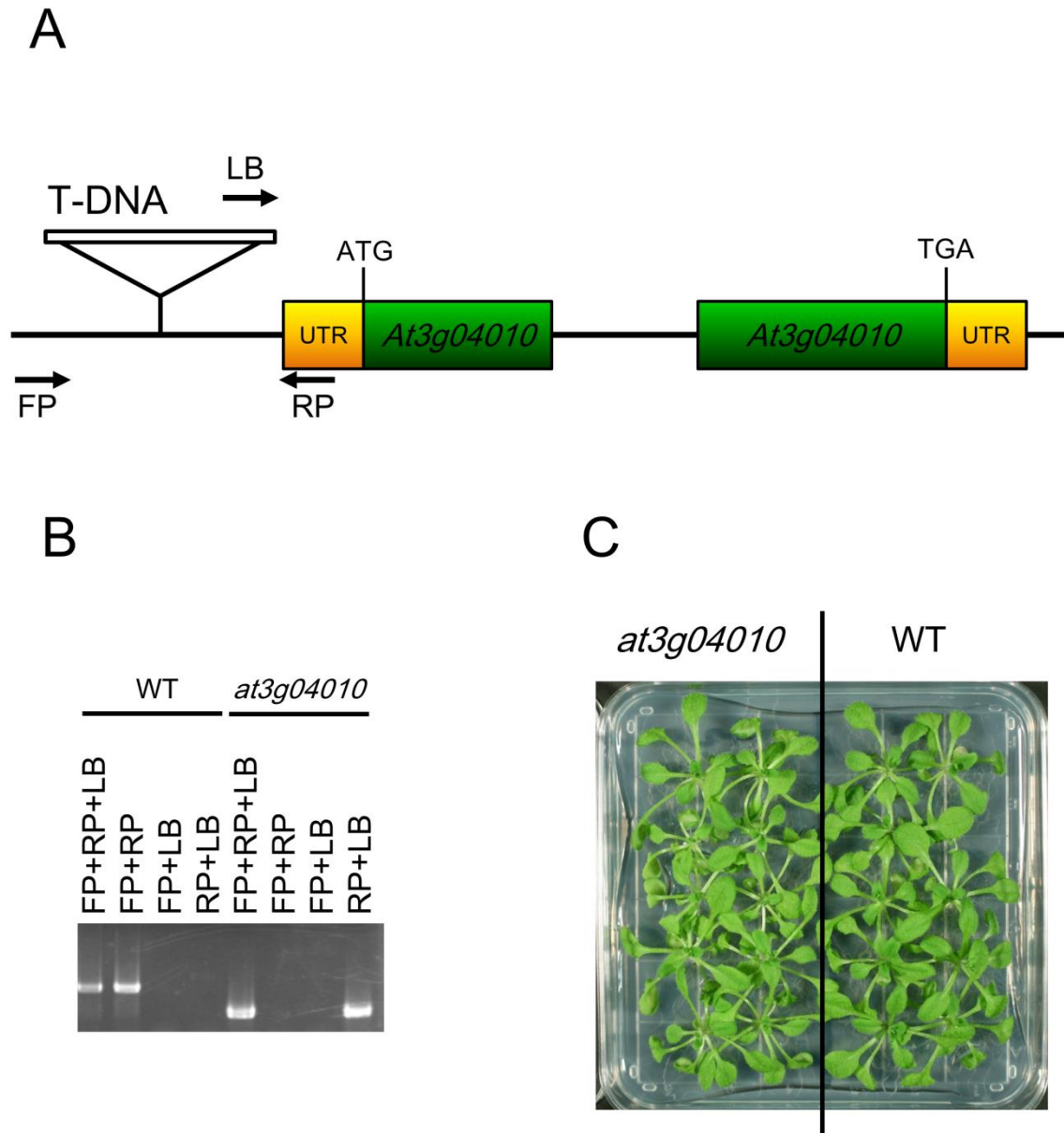


Fig. 6-2. Establishment of *At3g04010* knock-down mutant. (A) Structural organization of *At3g04010* gene and the position of T-DNA insertion within the promoter region of *At3g04010* gene in *at3g04010* mutant. Yellow and green box indicate UTR region and exon, respectively. Primers of LB, FP and RP (P1-3 in Table 6-1) were used for checking T-DNA insertion. (B) PCR analysis of genotype of WT and *at3g04010* mutant using four primer sets. (C) Plants were grown on Hoagland medium containing 1% sucrose under normal condition for 14 d.

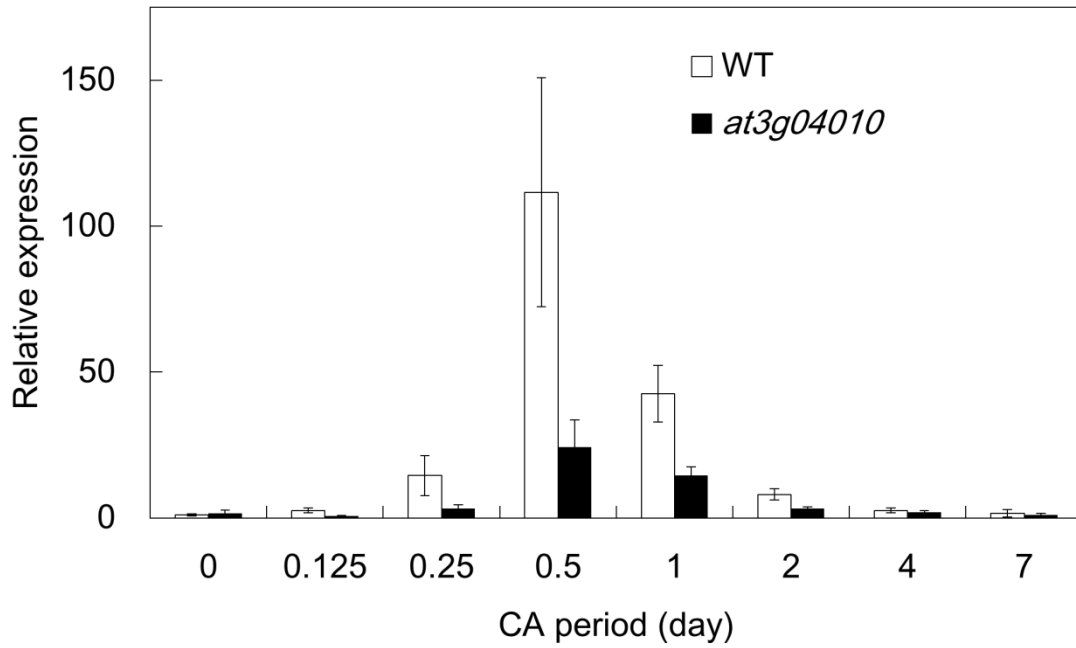


Fig. 6-3. Analysis of temporal *At3g04010* expression during CA by qRT-PCR. qRT-PCR analysis of *At3g04010* expression in WT and *at3g04010* mutant during CA. Plants were transferred to 2°C condition for each period and RNA was extracted. *EF1a* (*At5g60390*) was amplified as an internal control.

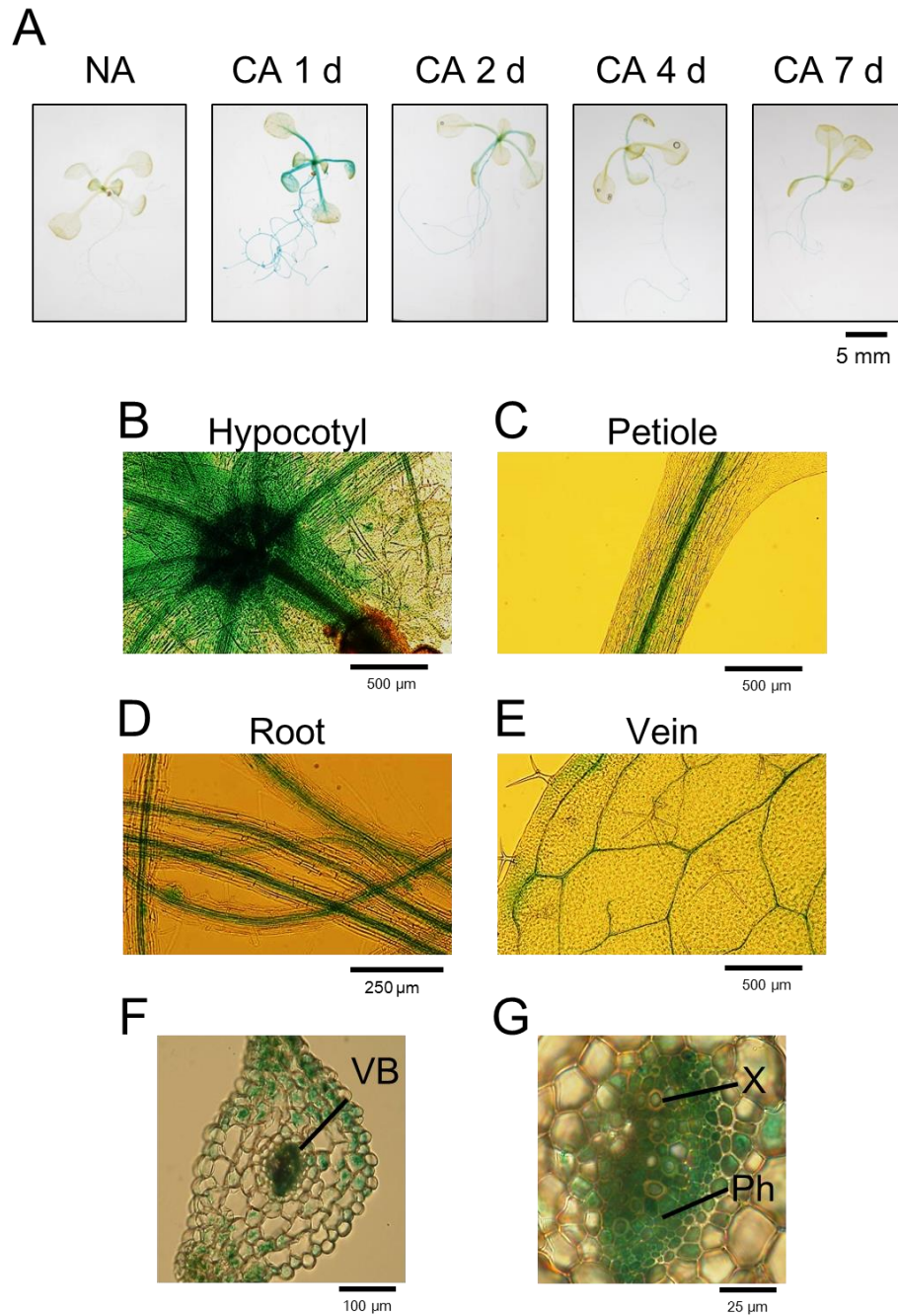


Fig. 6-4. Analysis of temporal and histological expression of *At3g04010* during CA by GUS-promoter assay. (A) Temporal expression of *At3g04010pro:GUS* during CA. Plants were grown on Hoagland medium containing 1% sucrose under normal condition for 10 d and transferred to CA chamber. Bar indicates 5 mm. (B-E) Magnified images of *At3g04010pro:GUS* mutants in 1 d CA period. Bars indicate 500 μ m in B, C and E and 250 μ m in D. (F-G) Magnified images of transverse sections of petioles in *At3g04010pro:GUS* mutants after 1 d CA period. Bars indicate 100 μ m in F and 25 μ m in G.

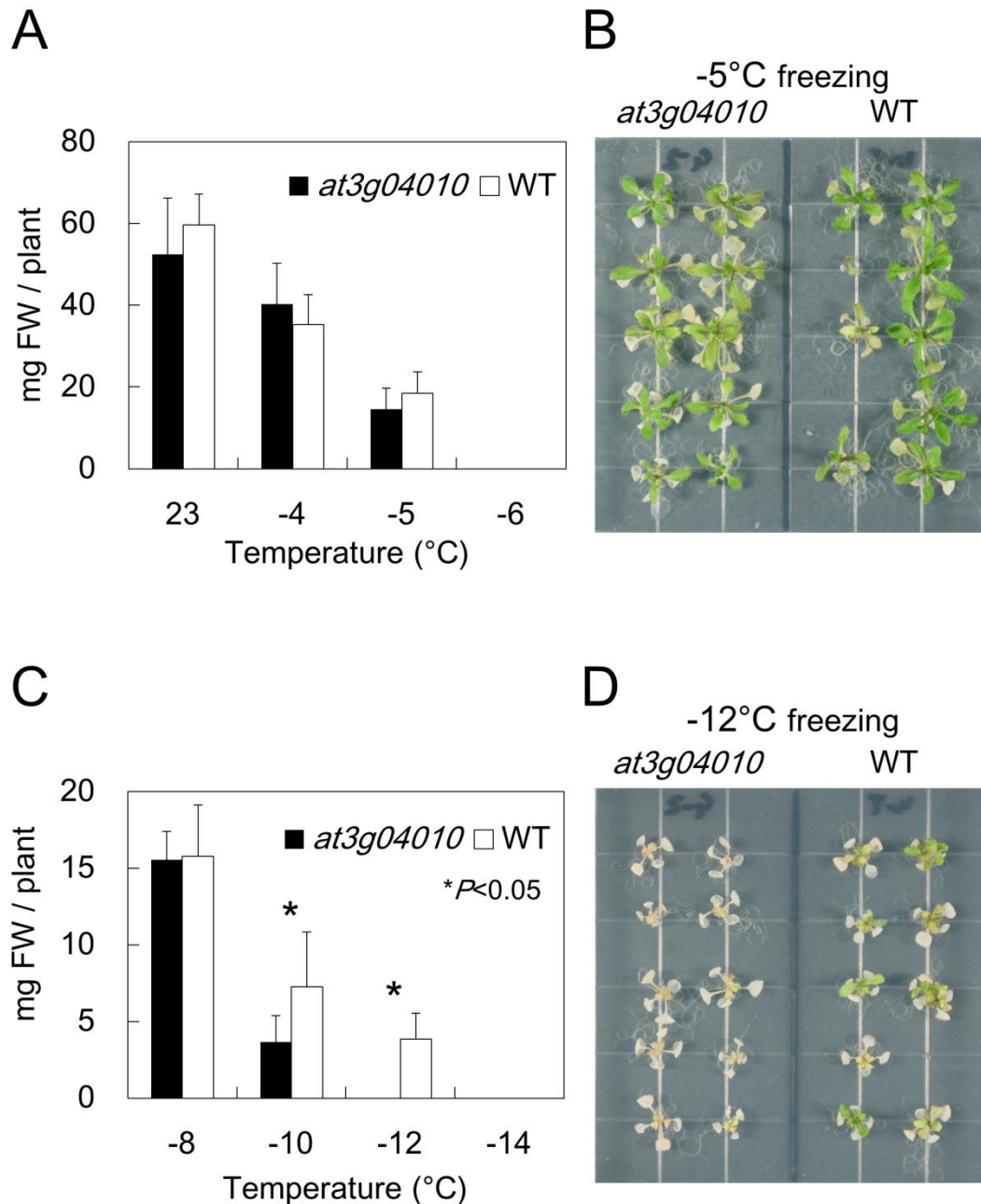


Fig. 6-5. Evaluation of freezing tolerance before and after CA by measurement of plant fresh weights. Freezing tolerance of 10 d old WT and *at3g04010* mutant in NA (A and B) and CA (C and D). Plants were grown on Hoagland medium containing 1% sucrose under normal condition for 10 d with or without subsequent CA treatment for 7 d and exposure to designated freezing temperature. Fresh weights of living part of plants were measured after freezing and post/thaw recovering treatment. Error bars indicate standard deviations (n=7-10). * $p < 0.05$ by student's t-test.

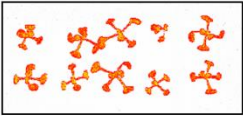
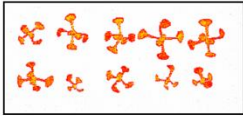


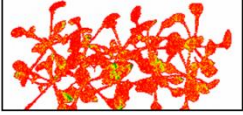
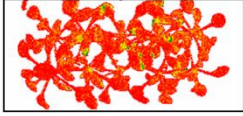


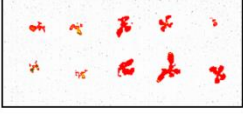
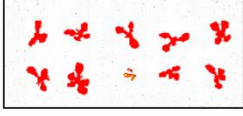
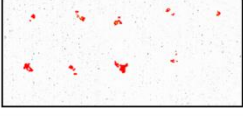
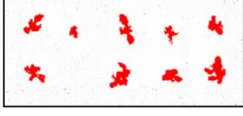
Growth Period	CA Period	Freezing Temp.	Recovering Period	Visualized Fv/Fm	
				<i>at3g04010</i>	WT
10 d	0 d	-	0 d		
10 d	7 d	-	0 d		
10 d	7 d	-	7 d		
10 d	7 d	-8°C	7 d		
10 d	7 d	-10°C	7 d		
10 d	7 d	-12°C	7 d		

Fig. 6-6. Evaluation of freezing tolerance in leaves during CA and freeze/thaw period by chlorophyll fluorescence. Plants were grown on Hoagland medium containing 1% sucrose under normal condition for 10 d with or without subsequent CA treatment for 7 d and exposure to designated freezing temperature. Chlorophyll fluorescence images were taken before CA, after CA or after CA and subsequent freezing and post/thaw recovering treatment.

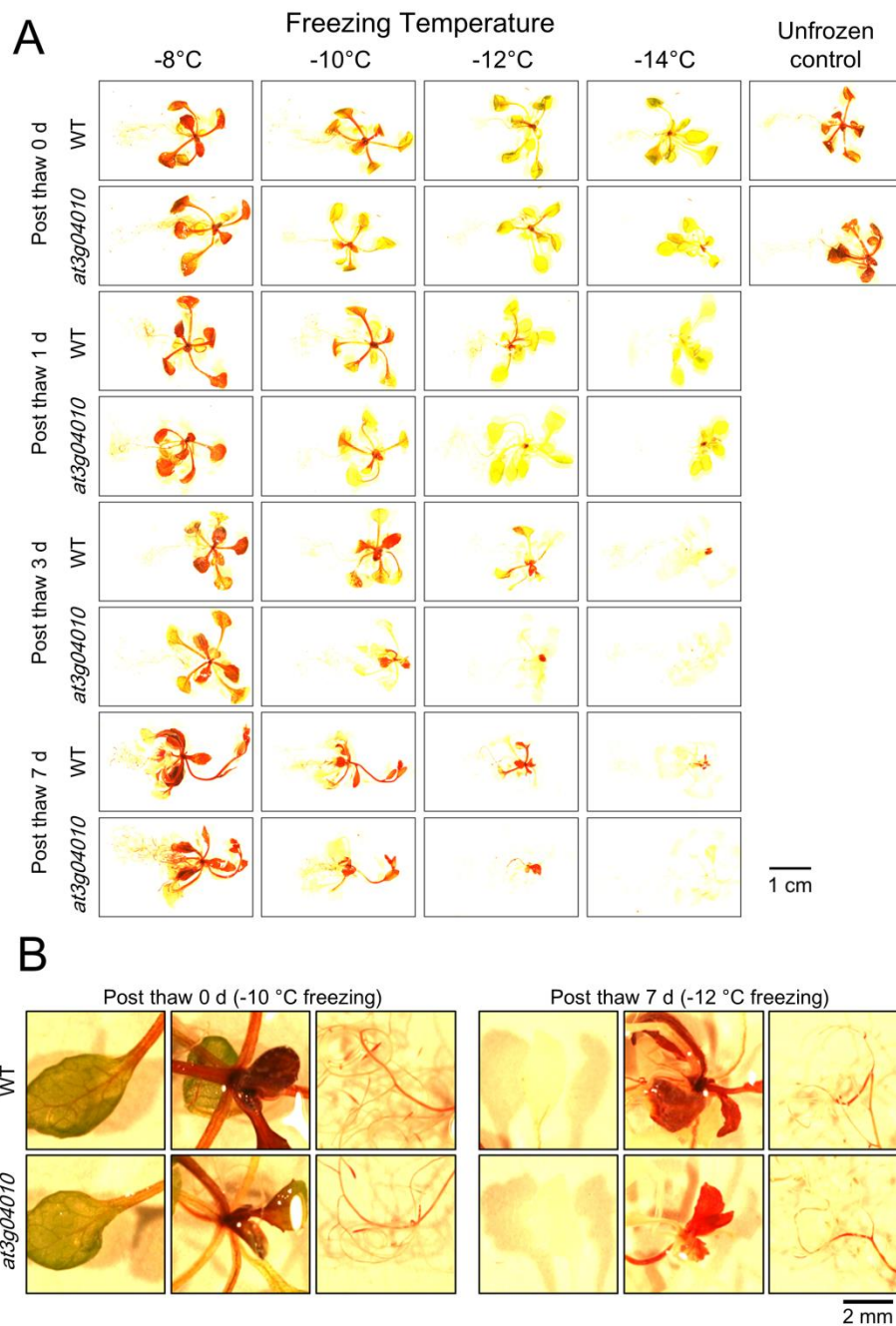


Fig. 6-7. Evaluation of freezing tolerance during CA and freeze/thaw period by TTC assay. (A) Plants were grown on Hoagland medium containing 1% sucrose under normal condition for 14 d with or without subsequent CA treatment for 7 d and exposure to designated freezing temperature. Plants were soaked in TTC solution. Images were taken before CA (unfrozen control) or after CA and subsequent freezing and post/thaw recovering treatment. (B) Magnified images of TTC-stained plants right after freeze/thaw treatment and post/thaw recovering for 7 d. Bars indicate 1 cm in A and 2 mm in B.

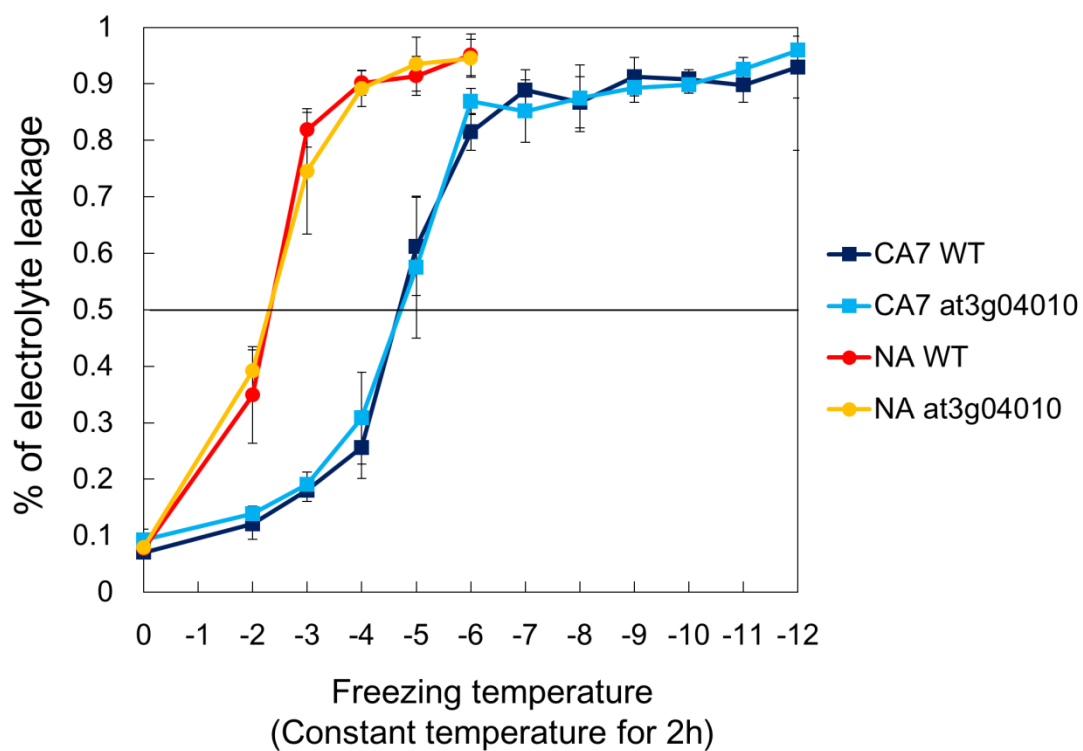


Fig. 6-8. Evaluation of freezing tolerance during CA by electrolyte leakage assay. Plants were grown on Hoagland medium containing 1% sucrose under normal condition for 14 d with or without subsequent CA treatment for 7 d. Leaves were collected and exposed to designated freezing temperature for 2 h. Y-axis is shown by the % of electrolyte leakage. Error bars indicate standard deviations (n=5).

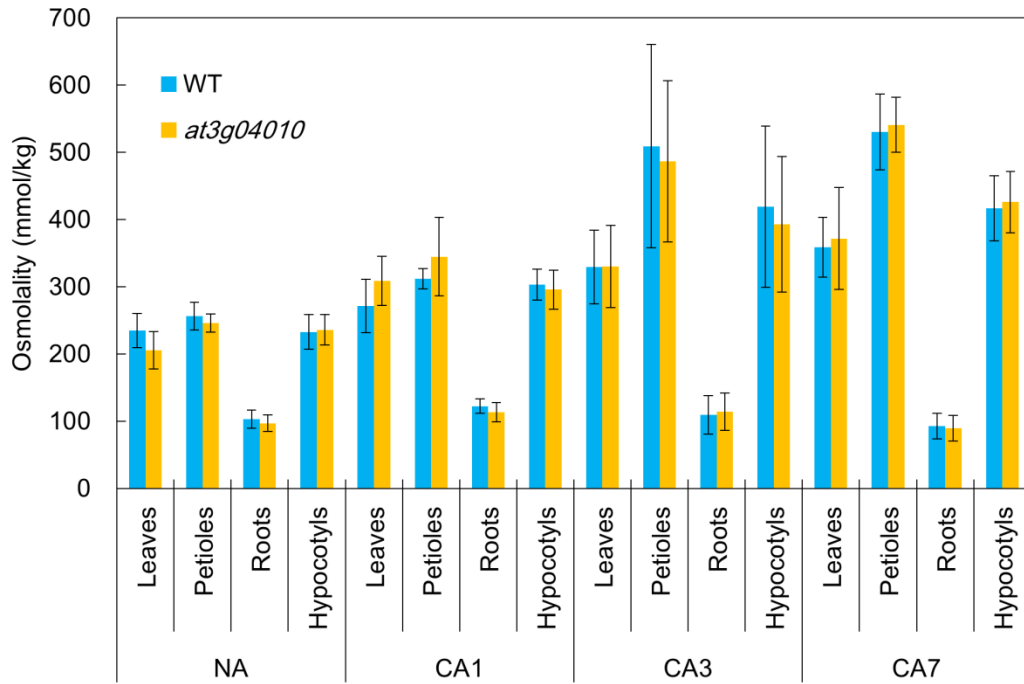


Fig. 6-9. Osmolyte concentration of leaves, petioles, roots and hypocotyls in WT and *at3g04010* mutants. Plants were grown on Hoagland medium containing 1% sucrose under normal condition for 14 d with or without subsequent CA treatment for 1, 3 and 7 d. Plants were separated into four parts (leaves, petioles, roots and hypocotyls) and ground immediately. Osmolality of each part of plants was measured with 5-fold diluted sample homogenates Y-axis is shown by osmolality (mmol/kg). Error bars indicate standard deviations (n=4-8).

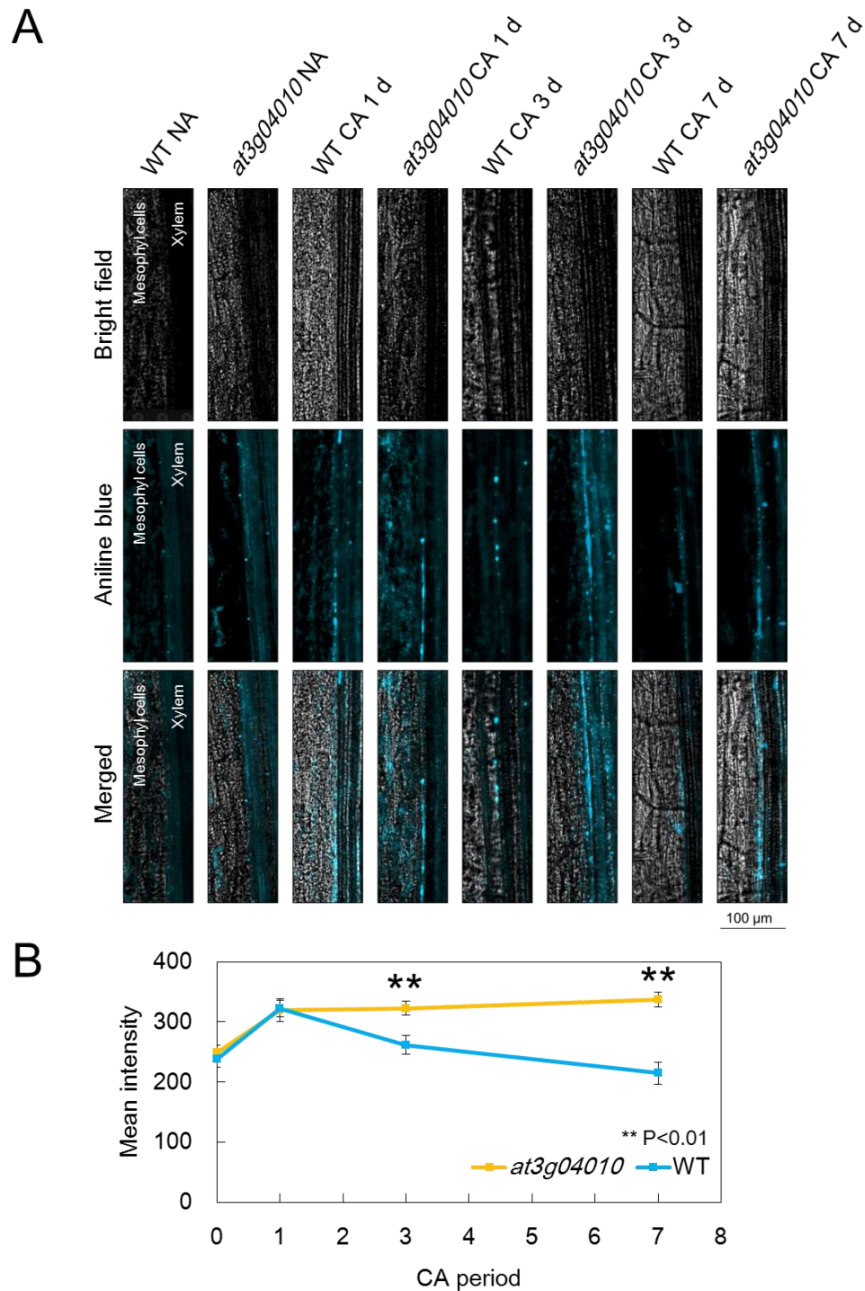


Fig. 6-10. Callose deposition in phloem during CA period. Plants were grown on Hoagland medium containing 1% sucrose under normal condition for 14 d (NA) and subsequently subjected to CA treatment for 1, 3 and 7 d. Plants were fixed with ECM solution and stained with 0.05% aniline blue solution. (A) Bright field and fluorescence images of petioles were taken and one representative image is shown. Bar indicates 100 μ m. (B) Areas and sum of intensities of callose stained phloem were quantified with background-subtracted images on NIS elements AR software. Y-axis is mean fluorescence intensity. Error bars indicate standard errors (n=63-118). ** p <0.01 by Mann-Whitney U test.

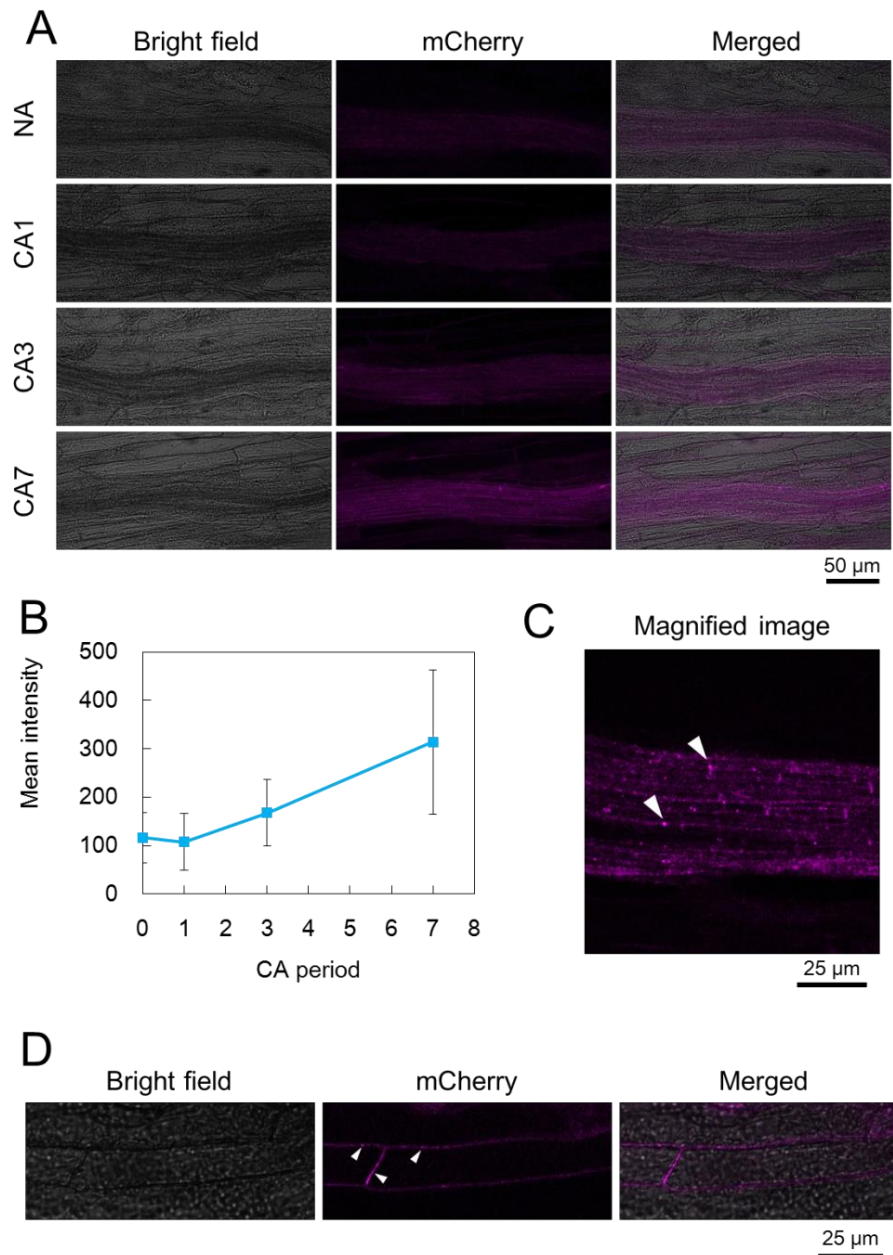


Fig. 6-11. Cellular Localization of At3g04010 during CA. Plants were grown on Hoagland medium containing 1% sucrose under normal condition for 14 d (NA) and subsequently subjected to CA treatment for 1, 3 and 7 d. (A) Transgenic expression of *At3g04010*pro::mCherry-*At3g04010* during CA in *Arabidopsis*. Fluorescence of *At3g04010*pro::mCherry-*At3g04010* was observed in petioles. (B) Areas and sum of intensities of callose stained phloem were quantified on NIS elements AR software. Y-axis is mean fluorescence intensity (n=29). (C) Magnified images of phloem in petioles taken after CA treatment for 7 d. Arrowheads indicate fluorescent foci of mCherry-*At3g04010*. (D) Magnified images of mesophyll cells in petioles taken after CA treatment for 7 d. Arrowheads indicate fluorescent foci of mCherry-*At3g04010*.

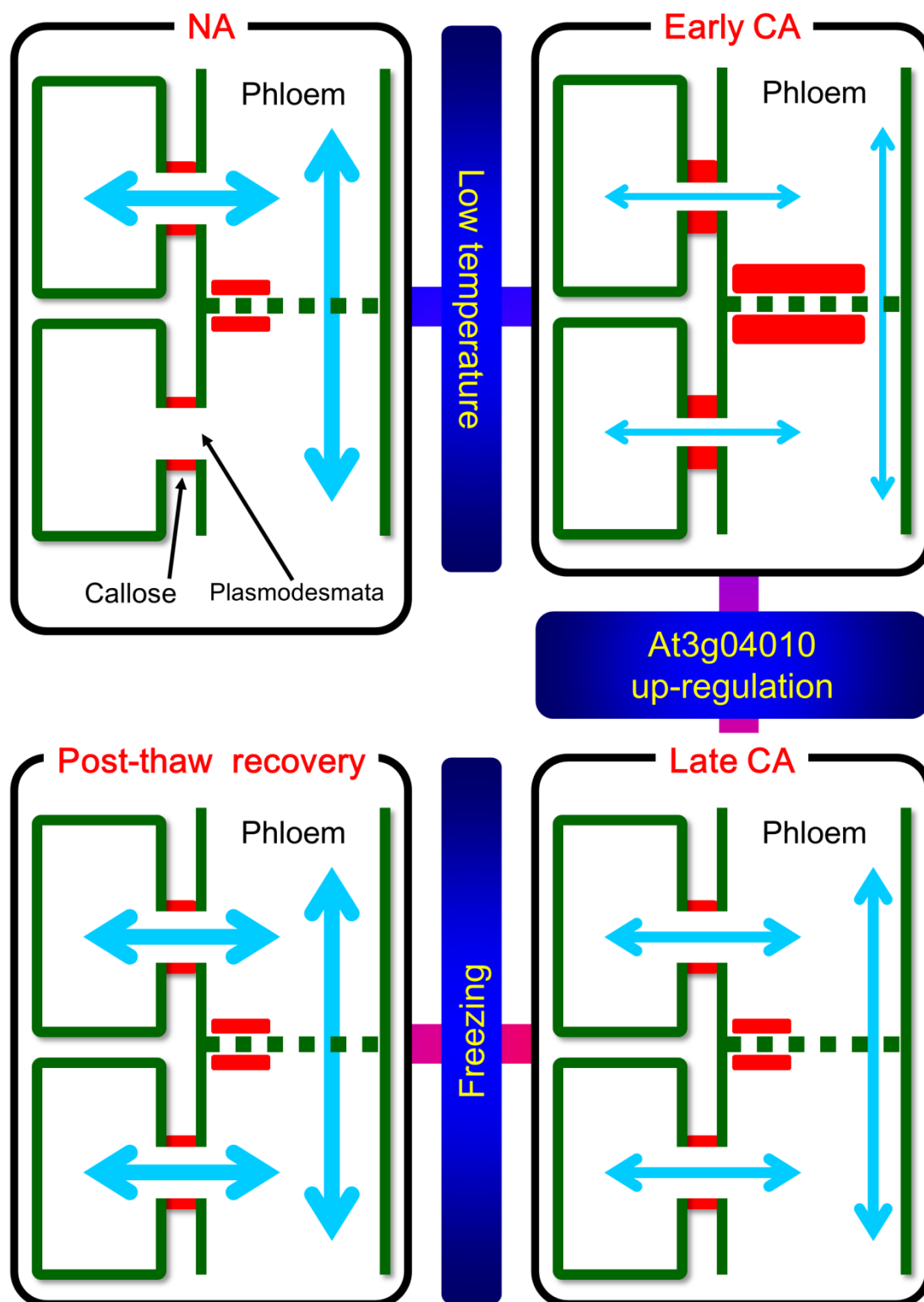


Fig. 6-12. Schematic representation of At3g04010 function during CA, freezing and post-thaw period.

Table 6-1. Primer sets used in this study

No.	AGI code	Gene		Sequence	notification
P1	(pROK2)	T-DNA	LBb1.3	ATTTTGCCGATTTTCGGAAC	Checking T-DNA insertion
P2	AT3G04010	O-glycosyl hydrolase family 17 protein	FW	AGGGATAGCCACCATCACTTC	
P3			RV	ATATCGAAACGATCGACCAAC	
P4	AT3G04010	O-glycosyl hydrolase family 17 protein	FW	AGCGATGGGAAACTATCAAA	Quantitative RT-PCR
P5			RV	CGTTGTACGCTGTCAAGAAC	
P6	At5g60390	GTP binding Elongation factor Tu family protein	FW	TGAGCACGCTCTTCTTGCTTTCA	Quantitative RT-PCR (control)
P7			RV	GGTGGTGGCATCCATCTTGTTACA	
P8	AT3G04010	O-glycosyl hydrolase family 17 protein	FW	CACCAAGCTTTTTCATGTCGACTCCCTAAT	Cloning promoter region using for GUS-promoter assay
P9			RV	TCTAGATTTTCCTTTGTTTTCCTCTG	
P10	AT3G04010	O-glycosyl hydrolase family 17 protein	FW	GCGGGATCCTTTCATGTCGACTCC	Cloning promoter and signal peptide sequence of <i>At3g04010</i> using for construction of mCherry-fused protein Primer contains BamHI restriction site
P11			RV	CGCGAATTCCAAACCAGAGACACC	Cloning promoter and signal peptide sequence of <i>At3g04010</i> using for construction of mCherry-fused protein Primer contains EcoRI restriction site
P12	(pFCG-G-rb)	mCherry	FW	GCGGAATTCATGGTGAGCAAGGGCGAG	Cloning mCherry sequence using for construction of mCherry-fused protein Primer contains EcoRI restriction site
P13			RV	CGCCTCGAGCTTGTACAGCTCGTCCATGC	Cloning mCherry sequence using for construction of mCherry-fused protein Primer contains XhoI restriction site
P14	AT3G04010	O-glycosyl hydrolase family 17 protein	FW	GCGCTCGAGGGAGTAAACTGGGGAACAATG	Cloning CDS region of <i>At3g04012</i> using for construction of mCherry-fused protein Primer contains XhoI restriction site
P15			RV	GCCTGCAGCTATATGAGAAGAAAGACCAAGCCACT	Cloning CDS region of <i>At3g04013</i> using for construction of mCherry-fused protein Primer contains PstI restriction site

Chapter 7

General discussion

Cold acclimation and plasma membrane microdomain

Cold acclimation (CA) is a crucial mechanism to adapt freezing tolerance. Since modern cryobiology in plants was founded in 1930's (Levitt and Scarth, 1936a; Levitt and Scarth, 1936b; Siminovitch and Scarth, 1938), general theory of freezing injury and frost hardening, such as intra- and extracellular freezing and freeze-induced dehydration for freezing injury and enhancement of osmotic pressure and change of cellular permeability during frost hardening has been discussed. In 1980's, the plasma membrane (PM) was recognized as the primary site of freezing injury and PM lipid changes have been thought to be important cellular event for acquisition of freezing tolerance (Gordon-Kamm and Steponkus, 1984a; Steponkus, 1984; Gordon-Kamm and Steponkus, 1984b; Lynch and Steponkus, 1987; Steponkus et al., 1988; Uemura and Steponkus, 1989; Webb and Steponkus, 1993; Uemura and Steponkus, 1994; Webb et al., 1994). Although changes of PM proteins during CA have been studied in 1980's (Uemura and Yoshida, 1984; Yoshida and Uemura, 1984), mass spectrometric approach broke new ground for analysis of CA-induced proteins comprehensively (Kawamura and Uemura, 2003).

Lipid bilayer structure of the PM and lateral diffusion of PM components were defined as fluid mosaic model (Singer and Nicolson, 1972). In 1997, Simons and Ikonen proposed microdomain model as a new perspective to fluid mosaic model (Simons and Ikonen, 1997). In this model, specific PM lipids and proteins are gathering in a small area and form raft-like structure in the sea of PM lipids. Peskan et al. (2000) first isolated plant microdomain as detergent resistant plasma membrane (DRM) fraction and many subsequent studies revealed that specific proteins are accumulated in DRM by proteomic approach (Mongrand et al., 2004; Borner et al., 2005; Morel et al., 2006; Lefebvre et al., 2007; Fujiwara et al., 2009). Minami et al. (2009) revealed compositional changes of DRM components during CA and discussed potential roles of microdomain as CA-associated structure in *Arabidopsis*. However, protein identification has been carried out with 2-dimensional electrophoresis (2-DE) based

proteomic approach, which has poor resolution and requires a large amount of samples (>50 µg proteins). Nano-liquid chromatography-tandem mass spectrometry (nano-LC-MS/MS) based approach is newly developed as peptide identification method and consists of ultrahigh performance liquid chromatography (UHPLC) system, electrospray ionization (ESI) device and high speed scanning, high accuracy and high sensitivity mass spectrometer. Iwasaki et al. (2010) accomplished detection of *Escherichia coli* proteome at microarray scale with advanced nano-LC-MS/MS approach. In the present study, I applied shotgun approach coupled with label-free peptide quantification software to DRM protein identification with small amount of proteins (<10 µg). As a result, 219 and 213 proteins were detected in DRM prepared from non-acclimated (NA) oat and rye, respectively (Takahashi et al., 2012; Fig. 2-2). In oat and rye, DRM was enriched in transporters, signal transducing and cytoskeleton-related proteins such as P-type ATPases, aquaporins, clathrins hypersensitive-induced reaction proteins and tubulins (Supplemental Table 2-1). These proteins were common in large part to previous studies using tobacco and *Arabidopsis* (Mongrand et al., 2004; Borner et al., 2005; Morel et al., 2006; Minami et al., 2009), meaning that microdomain function is highly conserved in both monocotyledonous and dicotyledonous plants. At the same time, these results are demonstrating that shotgun proteomic approach has high validity. In addition, CA-induced DRM changes (e.g. increase of P-type ATPases, decrease of aquaporins and tubulins, Supplemental Table 3-3) in both oat and rye was quite similar to previous study in *Arabidopsis* (Minami et al., 2009). These results ensure the validity of quantitative shotgun proteome approach used in the present study and clarify the generality of proteomic responses of microdomain to CA treatment among herbaceous plants.

Protein-protein, lipid-protein, lipid-lipid interactions are thought to be important for principal microdomain function or drive formations of lipid and/or protein nanodomain in the PM (Simons and Ikonen, 1997; Friedrichson and Kurzchalia, 1998; Lingwood and Simons, 2010; Simons and Sampaio, 2011). For protein-protein interaction, some members of intracellular trafficking machinery, dynamins, actins, tubulins and clathrins were identified as DRM-enriched proteins in both oat and rye (Supplemental Table 3-3). Endocytic trafficking is known to be mediated by lipid raft and caveolae-like structure in animal cells (Nabi and Le, 2003; Kirkham and Parton, 2005; Le Roy and Wrana, 2005; Lajoie and Nabi, 2007; Rollason et al., 2007). Microdomain may work as platform of endocytic machinery in plant. A major microdomain component, sterols were accounted for 73.6% and 63.8% of total DRM lipids in oat and rye, respectively (Tables 4-1 and 4-2, Fig. 4-2B), and sterol endocytic

pathway is accompanied by actin mediated trafficking (Grebe et al., 2003). Therefore, actin-dependent trafficking may be involved in maintenance of sterol-rich microdomain.

During CA, some proteins changed their partitioning characteristics to DRM fraction. For example, leucine-rich repeat (LRR) domain containing proteins were detected and enriched in DRM only after CA in oat (gi|326519689, DRM/PM ratio: 0.7 and 3.8 in NA and CA, respectively, Supplemental Table 3-3). During CA, this LRR domain containing protein may change its protein-protein or protein-lipid interactions in microdomain. Interestingly, LRR kinase is found in DRM fraction in NA *Arabidopsis* (Shahollari et al., 2004). Therefore, microdomain proteome is partly common in plants but some proteins are characteristically distributed in microdomain.

In rye, several sucrose transporters changed their partitioning properties to DRM fractions during CA. For example, the DRM/PM ratio of gi|357115762 increased from 1.1 in NA to 16 in CA. Interaction between sucrose transporter and membrane lipids are not yet fully characterized (Williams et al., 2000). Particularly, sterol environment is considered to be important for regulation of sucrose transport activity (Williams et al., 2000). During CA, sterol composition changed in our lipidomic studies (Figs. 4-3, 4-4 and 4-5). Therefore, microdomain sterol changes and preferential distribution of sucrose transporter to sterol-rich microdomain may influence on sucrose transporter-lipid interactions and be a part of mechanisms for modulation of sucrose transporting during CA. Since solute accumulation including sugars is important for preventing plant cells from intracellular ice formation (Guy, 1990), sucrose transporter activity is crucial for plant freezing tolerance. Therefore, the changes of sucrose transporter and sterol lipid modification may contribute to enhance freezing tolerance in rye after CA.

In addition, lipid modified proteins, myristoylated proteins, were identified in oat and rye by simple MASCOT search (31 in oat and 27 in rye) and Progenesis quantification (40 in oat and 33 in rye). Although, some myristoylated proteins were identified as CA-responsive protein in DRM (8 in oat and 16 in rye, Fig. 3-10), their changes were quite similar to the changes in the PM (correlation factor: 0.84 in oat and 0.88 in rye). Myristoyl modification can promote to form microdomain-like cluster (Zacharias et al., 2002). Particularly, proteins linked to saturated acyl chain tends to be partitioned into liquid-ordered phase domains (Melkonian et al., 1999). Acyl chain compositions in acylated steryl glycoside (ASG) and unsaturation degree of phospholipids (PLs) changed during CA. Aside from quantitative changes of myristoylated proteins during CA, saturation levels of microdomain lipids may affect function of microdomain-located myristoylated protein as a part of CA response.

Role of glycosylphosphatidylinositol-anchored protein in CA

Among many microdomain components, I focused on glycosylphosphatidylinositol-anchored proteins (GPI-APs) which showed considerable changes only in rye PM during CA (Fig. 3-10B). GPI anchor is one of the representative post-translational lipid modifications of PM protein. Many studies in animal cells mentioned that GPI-AP is segregated into microdomain compartment (Sargiacomo et al., 1993; Danielsen and van Deurs, 1995; Simons and Ikonen, 1997). In *Arabidopsis*, GPI-APs accounted for 6.0% of total PM proteins, but only 2.6% of total DRM proteins identified (Fig. 5-6B). In addition, only four GPI-APs (At3g29360.1, At4g15620.1, At4g15630.1 and At5g43600.1) were identified as DRM-enriched GPI-APs during CA. Therefore, in plant, GPI-APs may not be compartmentalized into microdomains in most cases. As Oxley and Bacic described (Oxley and Bacic, 1999), the structure of GPI moiety in an arabinogalactan protein (AGP) from *Pyrus communis* has phytosphingosine and different from the one in animal. They also suggested that phytosphingosine contains unsaturated sphingoid base (4-hydroxy-8-sphingenine: t18:1) and saturated fatty acid. t18:1 was also detected as major C18 sphingoid base in GlcCer prepared from oat and rye DRM. When comparing C18 sphingoid base compositions between the PM and DRM, t18:1 was not considerably enriched in DRM in both oat and rye during CA (Fig. 4-6). Thus, it is unlikely in the view of GlcCer compositions of DRM that GPI-APs containing t18:1 sphingoid base in lipid part is compartmentalized into microdomain by interaction between lipid part of GPI moiety and microdomain-enriched lipid.

When comparing \log_2 values of CA/NA ratio between PM and DRM fractions, PM and DRM was weakly correlated before and after CA ($R=0.49$; Supplemental Table 5-2). This result means that CA-induced changes of GPI-APs in DRM were partly affected by global PM proteome changes. In addition, \log_2 values of DRM/PM ratio was highly correlated between NA and CA ($R=0.87$; Supplemental Table 5-2). Therefore, it is considered that partitioning properties of each GPI-AP to DRM fraction do not change during CA, meaning that GPI-AP changes in DRM are linked to PM proteome changes. DRM fractions prepared from animal cells are enriched in sphingolipids, cholesterol and raft proteins including many kinds of GPI-APs (Lingwood and Simons, 2007). Particularly, sterol compositions in animal were quite different from those in plants because plant DRM sterols predominantly contained not cholesterol but phytosterols such as sitosterol, stigmasterol and campesterol in both free sterol and sterol glycosides. The presence of steryl glycoside and its acylated form in animal cell has not yet fully studied and gene encoding sterol glycosyltransferase is not isolated

from animals (Grille et al., 2010) while these sterols are found ubiquitously in oat and rye PM (Fig. 4-3). Thus, considerable difference of sterols between plant and animal may influence on behavior of GPI-APs on the PM surface and microdomain area.

In the present study, At3g04010 has been studied as putative CA-inducible and freezing tolerance-associated GPI-APs. At3g04010 is also a putative β -1,3-glucanase based on the characteristics of conserved domains and thought to be involved in plasmodesmal neck callose turnover as a callose-degrading enzyme for regulatory system of plasmodesmata communication (Fig. 6-10). Previously, only one plasmodesmata-targeted β -1,3-glucanase (At5g42100) has been identified in *Arabidopsis* and it has GPI anchor (Levy et al., 2007a). Therefore, At3g04010 may be a novel factor regulating callose turnover in plasmodesmata and GPI anchor of At3g04010 may be one of targeting factor to plasmodesmata. At5g42100 was also found in GPI-proteome analysis in Chapter 5. During CA, At5g42100 showed slight increase (1.59-fold) in GPI-AP fractions treated with PI-PLC (GPI-AP/PI-PLC [+]) while At3g04010 increased 3.56-fold and its normalized abundance after CA was quite higher than At5g42100 (685070 in At3g04010 and 406093 in At5g42100). Thus, it is possible that At3g04010 is a cold treatment-specific β -1,3-glucanase and maintain callose turnover during CA instead of existing β -1,3-glucanase expressing under NA condition.

Kierszniowska et al. (2009) revealed that 22 GPI-APs are responsive to sterol depletion by methyl- β -cyclodextrin (m β CD) treatment in DRM and these results indicate that GPI-APs are enriched in sterol-enriched microdomains. Furthermore, Raffaele et al. (2009) indicated that a putative microdomain component, Remorin is enriched in DRM fraction, shows patch-like distribution on the PM and localizes both in the PM and at plasmodesmata. The authors discussed about lipid raft as one of the plasmodesmata components. In addition, some studies demonstrated that detergent resistant microdomain is involved in callose biosynthesis in plant (Bessueille et al., 2009; Srivastava et al., 2013). Therefore, plasmodesmal neck callose accumulation may occur on microdomain making up plasmodesmata and callose-associated proteins including β -1,3-glucanase should be enriched in DRM fraction. However, a putative β -1,3-glucanase, At3g04010, was not identified as DRM-enriched GPI-APs (DRM/PM=0.49 in NA and DRM/PM=0.08 in CA). Although GPI-APs are thought to be tightly associated with sterols in DRM as described by Kierszniowska et al. (Kierszniowska et al., 2009), DRM does not really mirror functional raft in plant (Tanner et al., 2011). In fact, comparative proteomics of the PM and DRM is carried out only in poplar suspension cultured cells with an exception of the present study

(Srivastava et al., 2013). In this study, 80 proteins were enriched in DRM fractions but only two GPI-APs were identified as DRM-enriched proteins and this tendency is in agreement with the present study (Chapters 2, 3 and 5). Therefore, it is thought that microdomain has not simple but various patterns, composition and structure. Thus, distribution pattern of GPI-APs as represented by At3g04010 may be localized not only in detergent resistant membrane raft but also other type of sterol-rich microdomain compartments and coexistent with various microdomain in plasmodesmata during CA. Elucidation of the relationship between At3g04010 and various microdomain during CA is necessary for understanding functional At3g04010 activity on plasmodesmal callose turnover and its influence on freezing tolerance in plants.

Chapter 8

Concluding remarks and perspective

In present study, I aimed to investigate plasma membrane (PM) components including specific protein and lipid-enriched microdomains and glycosylphosphatidylinositol-anchored proteins (GPI-APs) during cold acclimation (CA), and mined many significant responses of these components to CA. First, I isolated microdomains as detergent resistant membrane (DRM) fractions and subjected these fractions to nano-LC-MS/MS. Shotgun proteomics of DRM identified putative microdomain-enriched proteins in low freezing-tolerant oat and highly freezing-tolerant rye, respectively. Among the proteins identified, the abundances of various proteins including transporters and signal transducing proteins were influenced by CA treatment. Some CA-responsive DRM proteins (e.g. heat shock protein 70) were differently regulated in oat and rye. Lipid compositions in DRM such as sterols were different between oat and rye. Therefore, present study suggests the possible functions of microdomain on acquisition of freezing tolerance. At the same time, GPI-APs which are one of major lipid modified PM proteins and putative microdomain-associated components considerably responded to CA treatment in *Arabidopsis* PM, DRM and apoplast and were predicted as novel freezing tolerance-related factors. Physiological approaches characterized that a CA-responsive GPI-AP, At3g04010 were associated with plant freezing tolerance via regulation of callose-dependent phloem transport during CA. These results provide new insight into the role of compositional changes of microdomains and GPI-APs for the mechanism to obtain freezing tolerance during CA. Other GPI-APs, for example At2g25060 responded to CA treatment in PM, DRM and apoplast fractions. Although At2g25060 increased in both PM and DRM and decreased in apoplast, DRM showed a drastic increase in At2g25060 amount during CA (35.3-fold). Therefore, At2g25060 is a possible to be associated with microdomain during CA and it may be necessary for functions of At2g25060. Understanding the role of microdomains and GPI-APs by further physiological analyses may provide information about novel CA mechanisms in PM and their significance for plant freezing tolerance. Knowledge about the cryobiology of model plants and crops such as oat and

rye will be important foundation for establishment of crops having multistress tolerance and efficient agricultural management and biomass production.

Acknowledgements

First of all, I would like to thank my supervisor, Professor Matsuo Uemura (Cryobiofrontier Research Center, Faculty of Agriculture, Iwate University) and Ms. Yasuko Uemura. They provided me with many valuable advices, encouragement and directions. Professor Matsuo Uemura also gave me many opportunities to take part in international conferences and interact with many domestic and foreign researchers.

I wish to thank my co-supervisors Professor Yukio Kawamura (Cryobiofrontier Research Center, Faculty of Agriculture, Iwate University) and Professor Kiyoaki Kato (Department of Crop Science, Obihiro University of Agricultural and Veterinary Medicine) for their important advice, critical inputs and encouragements.

I also thank to Professor Maki Kawai-Yamada (Graduate School of Science and Engineering, Saitama University) and Professor Michiko Sasabe (Faculty of Agriculture and Life Science, Hirosaki University) for reviewing my thesis at the final stage.

Special thanks to Professors Tetsuro Yamashita (Department of Biochemistry, Faculty of Agriculture, Iwate University), Masaharu Kamo (Division of Cellular Biosignal Sciences, Department of Biochemistry, Iwate Medical University) and Setsuko Komatsu (Institute of Crop Science, NARO, Tsukuba) for giving me technical advices on proteome analysis. I also thank to Professor Hiroyuki Imai (Graduate School of Natural Science, Konan University), Professor Ruth Welti (Kansas Lipidomics Research Center, Division of Biology, Kansas State University) and Dr. Mary Roth (Kansas Lipidomics Research Center, Division of Biology, Kansas State University) for helping lipidomic analysis. Determinations of steryl glycoside, acylated steryl glycoside and phospholipid lipid species described in this work were performed at the Kansas Lipidomics Research Center Analytical Laboratory, where instrument acquisition and lipidomics method development was supported by National Science Foundation, Kansas Technology Enterprise Corporation, K-IDeA Networks of Biomedical Research Excellence (INBRE) of National Institute of Health (P20GM103418), and Kansas State University.

I must express thanks to Professors Karen Tanino (Department of Plant Science, University of Saskatchewan, Canada), Javier Abadía (Estación Experimental de Aula Dei, Consejo Superior de Investigaciones Científicas, Spain), Ana-Flor López-Millán (Estación Experimental de Aula Dei, Consejo Superior de Investigaciones Científicas, Spain), Bin Li (College of Plant Science, Jilin University, China), Karen Sanguinet (College of Agricultural, Human and Natural Resource Science, Washington State University, United States of America) and Dirk Hinch (Max Planck Institute of Molecular Plant Physiology, Germany) for critical advice on my study and improvement of my English skills.

I am grateful to Professors Abidur Rahman (Cryobiofrontier Research Center, Faculty of Agriculture, Iwate University), Masumi Okada (Department of Agro-bioscience, Faculty of Agriculture, Iwate University) and Jun Kasuga (Department of Crop Science, Obihiro University of Agricultural and Veterinary Medicine) for critical advice, input and guidance on my study.

I am also grateful to Dr. Yoko Tominaga (Cryobiofrontier Research Center, Faculty of Agriculture, Iwate University) for technical assistance of genetic experiments and Dr. Andre Laroche (Agriculture and Agri-Food Canada) for providing rye seeds.

I really appreciate Mr. Elain Gutierrez-Carbonell (Estación Experimental de Aula Dei, Consejo Superior de Investigaciones Científicas, Spain), Ms. Laura Ceballos Laita (Estación Experimental de Aula Dei, Consejo Superior de Investigaciones Científicas, Spain), Dr. Mónica Calvo Polanco (Estación Experimental del Zaidín, Consejo Superior de Investigaciones Científicas, Spain), Mr. Jose Jorge Señorans Argibay, Ms. Reneeliza Jean Alejandro Melgar (International Rice Research Institute, Philippines), Mr. Ian Willick (Department of Plant Science, University of Saskatchewan, Canada) and Dr. Tirupaati Swaroopa Rani (Department of Plant Sciences, School of Life Sciences, University of Hyderabad) for giving chance to build international network and improve my English communication via their collaborative projects.

I also wish to thank Dr. Anzu Minami (Bioscience and Biotechnology Center, Nagoya University), Dr. Naoki Takata (Forestry and Forest Products Research Institute), Dr. Keita Endoh (Forestry and Forest Products Research Institute), Dr. Daisuke Tanaka (Interuniversity Bio-Backup Project, National Institute for Basic Biology), Mr. Yamato Hida (Department of Biochemistry, Graduate School of Medicine/Faculty of Medicine,

University of Yamanashi) and Mr. Junya Nakamura (Graduate School of Bioresource and Bioenvironmental Sciences, Kyushu University) for valuable advices on my career path and encouragements.

I appreciate to all current and previous members of the group including Dr. Arifa Ahmed, Dr. Yuji Tanaka, Mr. Hidehiro Hayashi, Mr. Satoshi Kaneko, Ms. Mariko Kondo, Ms. Juri Yakuwa, Mr. Takato Nakayama, Mr. Shion Kobayashi, Mr. Hiroyuki Imai, Mr. Yushi Miki, Mr. Hayato Hiraki, Ms. Maki Kanaya, Ms. Nao Yoshida, Ms. Ayumi Shimoda, Ms. Rina Suzuki, and Ms. Chiharu Kanaya.

Finally, I would like to thank the member of my family and Yuka Ito, my girlfriend, for understanding and generous support.

This study was in part supported by Grants-in-Aid for Scientific Research from the Japan Society for the Promotion of Science (#247373 to DT, #25292205 to YK and #22120003 and #24370018 to MU).

References

- Abdrakhamanova A, Wang QY, Khokhlova L, Nick P** (2003) Is microtubule disassembly a trigger for cold acclimation? *Plant Cell Physiol* **44**: 676–686
- Ahmed SN, Brown DA, London E** (1997) On the origin of sphingolipid/cholesterol-rich detergent-insoluble cell membranes: physiological concentrations of cholesterol and sphingolipid induce formation of a detergent-insoluble, liquid-ordered lipid phase in model membranes. *Biochemistry* **36**: 10944–10953
- Alexandersson E, Saalbach G, Larsson C, Kjellbom P** (2004) *Arabidopsis* plasma membrane proteomics identifies components of transport, signal transduction and membrane trafficking. *Plant Cell Physiol* **45**: 1543–1556
- Anderson JV, Li Q-B, Haskell DW, Guy CL** (1994) Structural organization of the spinach endoplasmic reticulum-luminal 70-kilodalton heat-shock cognate gene and expression of 70-kilodalton heat-shock genes during cold acclimation. *Plant Physiol* **104**: 1359–1370
- Bachmann M, Matile P, Keller F** (1994) Metabolism of the raffinose family oligosaccharides in leaves of *Ajuga reptans* L. *Plant Physiol* **105**: 1335–1345
- Bagnat M, Chang A, Simons K** (2001) Plasma membrane proton ATPase Pma1p requires raft association for surface delivery in yeast. *Mol Biol Cell* **12**: 4129–4138
- Bagnat M, Keränen S, Shevchenko A, Shevchenko A, Simons K** (2000) Lipid rafts function in biosynthetic delivery of proteins to the cell surface in yeast. *Proc Natl Acad Sci U S A* **97**: 3254–3259
- Barakat A, Szick-Miranda K, Chang I-F, Guyot R, Blanc G, Cooke R, Delseny M, Bailey-Serres J** (2001) The organization of cytoplasmic ribosomal protein genes in the *Arabidopsis* genome. *Plant Physiol* **127**: 398–415

- Barratt DHP, Kolling K, Graf A, Pike M, Calder G, Findlay K, Zeeman SC, Smith AM** (2011) Callose synthase *GSL7* is necessary for normal phloem transport and inflorescence growth in *Arabidopsis*. *Plant Physiol* **155**: 328–341
- Batelli G, Verslues PE, Agius F, Qiu Q, Fujii H, Pan S, Schumaker KS, Grillo S, Zhu J-K** (2007) *SOS2* promotes salt tolerance in part by interacting with the vacuolar H^+ -ATPase and pre-regulating its transport activity. *Mol Cell Biol* **27**: 7781–7790
- Baunsgaard L, Fuglsang AT, Jahn T, Korthout HA, de Boer AH, Palmgren MG** (1998) The 14-3-3 proteins associate with the plant plasma membrane H^+ -ATPase to generate a fusicoccin binding complex and a fusicoccin responsive system. *Plant J* **13**: 661–671
- Beck JG, Mathieu D, Loudet C, Buchoux S, Dufourc EJ** (2007) Plant sterols in “rafts”: a better way to regulate membrane thermal shocks. *FASEB J* **21**: 1714–1723
- Bessueille L, Sindt N, Guichardant M, Djerbi S, Teeri TT, Bulone V** (2009) Plasma membrane microdomains from hybrid aspen cells are involved in cell wall polysaccharide biosynthesis. *Biochem J* **420**: 93–103
- Bevan M, Bancroft I, Bent E, Love K, Goodman H, Dean C, Bergkamp R, Dirkse W, Van Staveren M, Stiekema W, Drost L, Ridley P, Hudson S-A, Patel K, Murphy G, Piffanelli P, Wedler H, Wedler E, Wambutt R, Weitzenegger T, Pohl T M, Terry N, Gielen J, Villarroel R, De Clerck R, Van Montagu M, Lecharny A, Auborg S, Gy I, Kreis M, Lao N, Kavanagh T, Hempel S, Kotter P, Entian K-D, Rieger M, Schaeffer M, Funk B, Mueller-Auer S, Silvey M, James R, Montfort A, Pons A, Puigdomenech P, Douka A, Vouklatou E, Milioni D, Hatzopoulos P, Piravandi E, Obermaier B, Hilbert H, Dusterhoft A, Moores T, Jones JDG, Eneva T, Palme K, Benes V, Rechman S, Ansorge W, Cooke R, Berger C, Delseny M, Voet M, Volckaert G, Mewes H-W, Klosterman S, Schueller C, Chalwatzis N** (1998) Analysis of 1.9 Mb of contiguous sequence from chromosome 4 of *Arabidopsis thaliana*. *Nature* **391**: 485–488
- Bhat RA, Miklis M, Schmelzer E, Schulze-Lefert P, Panstruga R** (2005) Recruitment and interaction dynamics of plant penetration resistance

- components in a plasma membrane microdomain. *Proc Natl Acad Sci U S A* **102**: 3135–3140
- Bligh EG, Dyer WJ** (1959) A rapid method of total lipid extraction and purification. *Can J Biochem Physiol* **37**: 911–917
- Borner GHH, Lilley KS, Stevens TJ, Dupree P** (2003) Identification of glycosylphosphatidylinositol-anchored proteins in *Arabidopsis*: a proteomic and genomic analysis. *Plant Physiol* **132**: 568–577
- Borner GHH, Sherrier DJ, Stevens TJ, Arkin IT, Dupree P** (2002) Prediction of glycosylphosphatidylinositol-anchored proteins in *Arabidopsis*: a genomic analysis. *Plant Physiol* **129**: 486–499
- Borner GHH, Sherrier DJ, Weimar T, Mchaelson LV, Hawkins ND, MacAskill A, Napier JA, Beale MH, Lilley KS, Dupree P** (2005) Analysis of detergent-resistant membranes in *Arabidopsis*: evidence for plasma membrane lipid rafts. *Plant Physiol* **137**: 104–116
- Boudart G, Jamet E, Rossignol M, Lafitte C, Borderies G, Jauneau A, Esquerré-Tugayé M-T, Pont-Lezica R** (2005) Cell wall proteins in apoplastic fluids of *Arabidopsis thaliana* rosettes: identification by mass spectrometry and bioinformatics. *Proteomics* **5**: 212–221
- Boylan MT, Quail PH** (1989) Oat phytochrome is biologically active in transgenic tomatoes. *Plant Cell* **1**: 765–773
- Briolay A, Bouzenzana J, Guichardant M, Deshayes C, Sindt N, Bessueille L, Bulone V** (2009) Cell wall polysaccharide synthases are located in detergent-resistant membrane microdomains in oomycetes. *Appl Environ Microbiol* **75**: 1938–1949
- Brown DA, London E** (1998) Functions of lipid rafts in biological membranes. *Annu Rev Cell Dev Biol* **14**: 111–136
- Brown DA, London E** (2000) Structure and function of sphingolipid- and cholesterol-rich membrane rafts. *J Biol Chem* **275**: 17221–17224

- Bütikofer P, Brodbeck U** (1993) Partial purification and characterization of a (glycosyl) inositol phospholipid-specific phospholipase C from peanut. *J Biol Chem* **268**: 17794–17802
- Cabané M, Calvet P, Vincens P, Boudet AM** (1993) Characterization of chilling-acclimation-related proteins in soybean and identification of one as a member of the heat shock protein (HSP 70) family. *Planta* **190**: 346–353
- Carmona-Salazar L, El Hafidi M, Enríquez-Arredondo C, Vázquez-Vázquez C, González de la Vara LE, Gavilanes-Ruíz M** (2011) Isolation of detergent-resistant membranes from plant photosynthetic and non-photosynthetic tissues. *Anal Biochem* **417**: 220–227
- Carmona-Salazar L, El Hafidi M, Gutiérrez-Nájera N, Noyola-Martínez L, González-Solís A, Gavilanes-Ruíz M** (2015) Fatty acid profiles from the plasma membrane and detergent resistant membranes of two plant species. *Phytochemistry* **109**: 25–35
- Chevalier F, Lopez-Prados J, Groves P, Perez S, Martín-Lomas M, Nieto PM** (2006) Structure and dynamics of the conserved protein GPI anchor core inserted into detergent micelles. *Glycobiology* **16**: 969–980
- Chi W-T, Fung RWM, Liu H-C, Hsu C-C, Charng Y-Y** (2009) Temperature-induced lipocalin is required for basal and acquired thermotolerance in *Arabidopsis*. *Plant Cell Environ* **32**: 917–927
- Clough SJ, Bent AF** (1998) Floral dip: a simplified method for *Agrobacterium*-mediated transformation of *Arabidopsis thaliana*. *Plant J* **16**: 735–743
- Danielsen EM, van Deurs B** (1995) A transferrin-like GPI-linked iron-binding protein in detergent-insoluble noncaveolar microdomains at the apical surface of fetal intestinal epithelial cells. *J Cell Biol* **131**: 939–950
- Danyluk J, Perron A, Houde M, Limin A, Fowler B, Benhamou N, Sarhan F** (1998) Accumulation of an acidic dehydrin in the vicinity of the plasma membrane during cold acclimation of wheat. *Plant Cell* **10**: 623–638

- DeBono A, Yeats TH, Rose JKC, Bird D, Jetter R, Kunst L, Samuels L** (2009) *Arabidopsis* LTPG is a glycosylphosphatidylinositol-anchored lipid transfer protein required for export of lipids to the plant surface. *Plant Cell* **21**: 1230–1238
- Depta H, Holstein SE, Robinson DG, Lützelshwab M, Michalke W** (1991) Membranes markers in highly purified clathrin-coated vesicles from *Cucurbita* hypocotyls. *Planta* **183**: 434–442
- Edstam MM, Laurila M, Höglund A, Raman A, Dahlström KM, Salminen TA, Edqvist J, Blomqvist K** (2014) Characterization of the GPI-anchored lipid transfer proteins in the moss *Physcomitrella patens*. *Plant Physiol Biochem* **75**: 55–69
- Ehlert B, Hinch DK** (2008) Chlorophyll fluorescence imaging accurately quantifies freezing damage and cold acclimation responses in *Arabidopsis* leaves. *Plant Methods* **4**: 12
- Eisenhaber B, Bork P, Eisenhaber F** (1999) Prediction of potential GPI-modification sites in proprotein sequences. *J Mol Biol* **292**: 741–758
- Eisenhaber B, Wildpaner M, Schultz CJ, Borner GHH, Dupree P, Eisenhaber F** (2003) Glycosylphosphatidylinositol lipid anchoring of plant proteins: sensitive prediction from sequence- and genome-wide studies for *Arabidopsis* and rice. *Plant Physiol* **133**: 1691–1701
- Elortza F, Mohammed S, Bunkenborg J, Foster LJ, Nühse TS, Brodbeck U, Peck SC, Jensen ON** (2006) Modification-specific proteomics of plasma membrane proteins: identification and characterization of glycosylphosphatidylinositol-anchored proteins released upon phospholipase D treatment. *J Proteome Res* **5**: 935–943
- Elortza F, Nühse TS, Foster LJ, Stensballe A, Peck SC, Jensen ON** (2003) Proteomic analysis of glycosylphosphatidylinositol-anchored membrane proteins. *Mol Cell Proteomics* **2**: 1261–1270
- Faik A, Abouzouhair J, Sarhan F** (2006) Putative fasciclin-like arabinogalactan-proteins (FLA) in wheat (*Triticum aestivum*) and rice (*Oryza*

sativa): identification and bioinformatic analyses. *Mol Genet Genomics* **276**: 478–494

Fankhauser N, Maser P (2005) Identification of GPI anchor attachment signals by a Kohonen self-organizing map. *Bioinformatics* **21**: 1846–1852

Ferguson MA (1999) The structure, biosynthesis and functions of glycosylphosphatidylinositol anchors, and the contributions of trypanosome research. *J Cell Sci* **112**: 2799–2809

Flower D (1996) The lipocalin protein family: structure and function. *Biochem J* **318**: 1–14

Forslund K, Henricson A, Hollich V, Sonnhammer ELL (2008) Domain tree-based analysis of protein architecture evolution. *Mol Biol Evol* **25**: 254–264

Fourrier N, Bédard J, Lopez-Juez E, Barbrook A, Bowyer J, Jarvis P, Warren G, Thorlby G (2008) A role for *SENSITIVE TO FREEZING2* in protecting chloroplasts against freeze-induced damage in *Arabidopsis*. *Plant J* **55**: 734–745

Friedrichson T, Kurzchalia TV (1998) Microdomains of GPI-anchored proteins in living cells revealed by crosslinking. *Nature* **394**: 802–805

Fujita M, Umemura M, Yoko-o T, Jigami Y (2006) *PER1* is required for GPI-phospholipase A₂ activity and involved in lipid remodeling of GPI-anchored proteins. *Mol Biol Cell* **17**: 5253–5264

Fujiwara M, Hamada S, Hiratsuka M, Fukao Y, Kawasaki T, Shimamoto K (2009) Proteome analysis of detergent-resistant membranes (DRMs) associated with OsRac1-mediated innate immunity in rice. *Plant Cell Physiol* **50**: 1191–1200

Furt F, König S, Bessoule JJ, Sargueil F, Zallot R, Stanislas T, Noirot E, Lherminier J, Simon-Plas F, Heilmann I, Mongrand S (2010) Polyphosphoinositides are enriched in plant membrane rafts and form microdomains in the plasma membrane. *Plant Physiol* **152**: 2173–2187

Gordon-Kamm WJ, Steponkus PL (1984a) The behavior of the plasma membrane following osmotic contraction of isolated protoplasts: implications in freezing injury. *Protoplasma* **123**: 83–94

- Gordon-Kamm WJ, Steponkus PL** (1984b) Lamellar-to-hexagonal_H phase transitions in the plasma membrane of isolated protoplasts after freeze-induced dehydration. *Proc Natl Acad Sci U S A* **81**: 6373–6377
- Grandmougin-Ferjani A, Schuler-Muller I, Hartmann M-A** (1997) Sterol modulation of the plasma membrane H⁺-ATPase activity from corn roots reconstituted into soybean lipids. *Plant Physiol* **113**: 163–174
- Grebe M, Xu J, Möbius W, Ueda T, Nakano A, Geuze HJ, Rook MB, Scheres B** (2003) *Arabidopsis* sterol endocytosis involves actin-mediated trafficking via ARA6-positive early endosomes. *Curr Biol* **13**: 1378–1387
- Griffith OH, Ryan M** (1999) Bacterial phosphatidylinositol-specific phospholipase C: structure, function, and interaction with lipids. *Biochim Biophys Acta* **1441**: 237–254
- Grille S, Zaslawski A, Thiele S, Plat J, Warnecke D** (2010) The functions of sterol glycosides come to those who wait: recent advances in plants, fungi, bacteria and animals. *Prog Lipid Res* **49**: 262–288
- Guy CL** (1990) Cold acclimation and freezing stress tolerance: role of protein metabolism. *Annu Rev Plant Physiol Plant Mol Biol* **41**: 187–223
- Hara M, Terashima S, Fukaya T, Kuboi T** (2003) Enhancement of cold tolerance and inhibition of lipid peroxidation by citrus dehydrin in transgenic tobacco. *Planta* **217**: 290–298
- Hardham AR, Jones DA, Takemoto D** (2007) Cytoskeleton and cell wall function in penetration resistance. *Curr Opin Plant Biol* **10**: 342–348
- Hayashi S, Ishii T, Matsunaga T, Tominaga R, Kuromori T, Wada T, Shinozaki K, Hirayama T** (2008) The glycerophosphoryl diester phosphodiesterase-like proteins SHV3 and its homologs play important roles in cell wall organization. *Plant Cell Physiol* **49**: 1522–1535
- Head BP, Patel HH, Roth DM, Murray F, Swaney JS, Niesman IR, Farquhar MG, Insel PA** (2006) Microtubules and actin microfilaments regulate lipid raft/caveolae localization of adenylyl cyclase signaling components. *J Biol Chem* **281**: 26391–26399

- Henrissat B, Davies GJ** (2000) Glycoside hydrolases and glycosyltransferases: families, modules, and implications for genomics. *Plant Physiol* **124**: 1515–1519
- Holowka D, Sheets ED, Baird B** (2000) Interactions between FcεRI and lipid raft components are regulated by the actin cytoskeleton. *J Cell Sci* **113**: 1009–1019
- Hon WC, Griffith M, Chong P, Yang DSC** (1994) Extraction and isolation of antifreeze proteins from winter rye (*Secale cereale* L.) leaves. *Plant Physiol* **104**: 971–980
- Horváth I, Multhoff G, Sonnleitner A, Vigh L** (2008) Membrane-associated stress proteins: more than simply chaperones. *Biochim Biophys Acta* **1778**: 1653–1664
- Hurry V, Keerberg O, Parnik T, Gardestrom P, Oquist G** (1995) Cold-hardening results in increased activity of enzymes involved in carbon metabolism in leaves of winter rye (*Secale cereale* L.). *Planta* **195**: 554–562
- Iba K** (2002) Acclimative response to temperature stress in higher plants: approaches of gene engineering for temperature tolerance. *Annu Rev Plant Biol* **53**: 225–245
- Iglesias VA, Meins F** (2000) Movement of plant viruses is delayed in a β-1,3-glucanase-deficient mutant showing a reduced plasmodesmatal size exclusion limit and enhanced callose deposition. *Plant J* **21**: 157–166
- Imai H, Hattori H, Watanabe M** (2012) An improved method for analysis of glucosylceramide species having cis-8 and trans-8 isomers of sphingoid bases by LC–MS/MS. *Lipids* **47**: 1221–1229
- Imai H, Morimoto Y, Tamura K** (2000a) Sphingoid base composition of monoglucosylceramide in *Brassicaceae*. *J Plant Physiol* **157**: 453–456
- Imai H, Yamamoto K, Shibahara A, Miyatani S, Nakayama T** (2000b) Determining double-bond positions in monoenoic 2-hydroxy fatty acids of glucosylceramides by gas chromatography-mass spectrometry. *Lipids* **35**: 233–236
- Ishikawa M, Yoshida S** (1985) Seasonal changes in plasma membranes and mitochondria isolated from Jerusalem artichoke tubers: possible relationship to cold hardiness. *Plant Cell Physiol* **26**: 1331–1344

- Iwasaki M, Miwa S, Ikegami T, Tomita M, Tanaka N, Ishihama Y** (2010) One-dimensional capillary liquid chromatographic separation coupled with tandem mass spectrometry unveils the *Escherichia coli* proteome on a microarray scale. *Anal Chem* **82**: 2616–2620
- Jia Y, McAdams SA, Bryan GT, Hershey HP, Valent B** (2000) Direct interaction of resistance gene and avirulence gene products confers rice blast resistance. *EMBO J* **19**: 4004–4014
- Johansson I, Karlsson M, Shukla VK, Chrispeels MJ, Larsson C, Kjellbom P** (1998) Water transport activity of the plasma membrane aquaporin PM28A is regulated by phosphorylation. *Plant Cell* **10**: 451–459
- Johnson KL, Jones BJ, Bacic A, Schultz CJ** (2003) The fasciclin-like arabinogalactan proteins of *Arabidopsis*: a multigene family of putative cell adhesion molecules. *Plant Physiol* **133**: 1911–1925
- Jung HW, Hwang BK** (2007) The leucine-rich repeat (LRR) protein, CaLRR1, interacts with the hypersensitive induced reaction (HIR) protein, CaHIR1, and suppresses cell death induced by the CaHIR1 protein. *Mol Plant Pathol* **8**: 503–514
- Jung HW, Lim CW, Lee SC, Choi HW, Hwang CH, Hwang BK** (2007) Distinct roles of the pepper hypersensitive induced reaction protein gene *CaHIR1* in disease and osmotic stress, as determined by comparative transcriptome and proteome analyses. *Planta* **227**: 409–425
- Kawaguchi M, Imai H, Naoe M, Yasui Y, Ohnishi M** (2000) Cerebrosides in grapevine leaves: distinct composition of sphingoid bases among the grapevine species having different tolerances to freezing temperature. *Biosci Biotechnol Biochem* **64**: 1271–1273
- Kawamura Y, Uemura M** (2003) Mass spectrometric approach for identifying putative plasma membrane proteins of *Arabidopsis* leaves associated with cold acclimation. *Plant J* **36**: 141–154
- Keinath NF, Kierszniowska S, Lorek J, Bourdais G, Kessler SA, Shimosato-Asano H, Grossniklaus U, Schulze WX, Robatzek S, Panstruga R** (2010) PAMP (pathogen-associated molecular pattern)-induced changes in plasma membrane

- compartmentalization reveal novel components of plant immunity. *J Biol Chem* **285**: 39140–39149
- Kerr GP, Carter JV** (1990) Relationship between freezing tolerance of root-tip cells and cold stability of microtubules in rye (*Secale cereale* L. cv Puma). *Plant Physiol* **93**: 77–82
- Khan MSH, Tawaraya K, Sekimoto H, Koyama H, Kobayashi Y, Murayama T, Chuba M, Kambayashi M, Shiono Y, Uemura M, Ishikawa S, Wagatsuma T** (2009) Relative abundance of Delta(5)-sterols in plasma membrane lipids of root-tip cells correlates with aluminum tolerance of rice. *Physiol Plant* **135**: 73–83
- Kierszniowska S, Seiwert B, Schulze WX** (2009) Definition of *Arabidopsis* sterol-rich membrane microdomains by differential treatment with methyl- β -cyclodextrin and quantitative proteomics. *Mol Cell Proteomics* **8**: 612–623
- Kiessling V, Wan C, Tamm LK** (2009) Domain coupling in asymmetric lipid bilayers. *Biochim Biophys Acta-Biomembr* **1788**: 64–71
- Kinoshita T, Fujita M, Maeda Y** (2008) Biosynthesis, remodelling and functions of mammalian GPI-anchored proteins: recent progress. *J Biochem (Tokyo)* **144**: 287–294
- Kirkham M, Parton RG** (2005) Clathrin-independent endocytosis: new insights into caveolae and non-caveolar lipid raft carriers. *Biochim Biophys Acta* **1745**: 273–286
- Kluge C, Seidel T, Bolte S, Sharma SS, Hanitzsch M, Satiat-Jeunemaitre B, Roß J, Sauer M, Gollack D, Dietz K-J** (2004) Subcellular distribution of the V-ATPase complex in plant cells, and *in vivo* localisation of the 100 kDa subunit VHA-a within the complex. *BMC Cell Biol* **5**: 29
- Koag M-C, Fenton RD, Wilkens S, Close TJ** (2003) The binding of maize DHN1 to lipid vesicles: gain of structure and lipid specificity. *Plant Physiol* **131**: 309–316
- Konopka CA, Backues SK, Bednarek SY** (2008) Dynamics of *Arabidopsis* dynamin-related protein 1C and a clathrin light chain at the plasma membrane. *Plant Cell* **20**: 1363–1380

- Kosová K, Holková L, Prášil IT, Prášilová P, Bradáčová M, Vítámvás P, Čapková V** (2008) Expression of dehydrin 5 during the development of frost tolerance in barley (*Hordeum vulgare*). *J Plant Physiol* **165**: 1142–1151
- Koster KL, Lynch DV** (1992) Solute accumulation and compartmentation during the cold acclimation of Puma rye. *Plant Physiol* **98**: 108–113
- Krügel U, Veenhoff LM, Langbein J, Wiederhold E, Liesche J, Friedrich T, Grimm B, Martinoia E, Poolman B, Kühn C** (2008) Transport and sorting of the *solanum tuberosum* sucrose transporter SUT1 is affected by posttranslational modification. *Plant Cell* **20**: 2497–2513
- Kubacka-Zębalska M, Kacperska A** (1999) Low temperature-induced modifications of cell wall content and polysaccharide composition in leaves of winter oilseed rape (*Brassica napus* L. var. *oleifera* L.). *Plant Sci* **148**: 59–67
- Kusumi A, Nakada C, Ritchie K, Murase K, Suzuki K, Murakoshi H, Kasai RS, Kondo J, Fujiwara T** (2005) Paradigm shift of the plasma membrane concept from the two-dimensional continuum fluid to the partitioned fluid: high-speed single-molecule tracking of membrane molecules. *Annu Rev Biophys Biomol Struct* **34**: 351–378
- Lajoie P, Nabi IR** (2007) Regulation of raft-dependent endocytosis. *J Cell Mol Med* **11**: 644–653
- Laloi M, Perret A-M, Chatre L, Melser S, Cantrel C, Vaultier M-N, Zachowski A, Bathany K, Schmitter J-M, Vallet M, Lessire R, Hartmann, M-A, Moreau P** (2006) Insights into the role of specific lipids in the formation and delivery of lipid microdomains to the plasma membrane of plant cells. *Plant Physiol* **143**: 461–472
- Lefebvre B, Furt F, Hartmann M-A, Michaelson LV, Carde J-P, Sargueil-Boiron F, Rossignol M, Napier JA, Cullimore J, Bessoule J-J, Mongrand S** (2007) Characterization of lipid rafts from *medicago truncatula* root plasma membranes: a proteomic study reveals the presence of a raft-associated redox system. *Plant Physiol* **144**: 402–418
- Lenne P-F, Wawrezynieck L, Conchonaud F, Wurtz O, Boned A, Guo X-J, Rigneault H, He H-T, Marguet D** (2006) Dynamic molecular confinement in

- the plasma membrane by microdomains and the cytoskeleton meshwork. *EMBO J* **25**: 3245–3256
- Levitt J** (1980) Responses of plants to environmental stresses, Ed 2. Academic Press, New York
- Levitt J, Scarth GW** (1936a) Frost-hardening studies with living cells: I. osmotic and bound water changes in relation to frost resistance and the seasonal cycle. *Can J Res* **14c**: 267–284
- Levitt J, Scarth GW** (1936b) Frost-hardening studies with living cells: II. permeability in relation to frost resistance and the seasonal cycle. *Can J Res* **14c**: 285–305
- Levy A, Erlanger M, Rosenthal M, Epel BL** (2007a) A plasmodesmata-associated β -1,3-glucanase in *Arabidopsis*: a plasmodesmal β -1,3-glucanase. *Plant J* **49**: 669–682
- Levy A, Guenoune-Gelbart D, Epel BL** (2007b) β -1,3-glucanases: plasmodesmal gate keepers for intercellular communication. *Plant Signal Behav* **2**: 404–407
- Li B, Takahashi D, Kawamura Y, Uemura M** (2012) Comparison of plasma membrane proteomic changes of *Arabidopsis* suspension-cultured cells (T87 line) after cold and ABA treatment in association with freezing tolerance development. *Plant Cell Physiol* **53**: 543–554
- Lillemeier BF, Pfeiffer JR, Surviladze Z, Wilson BS, Davis MM** (2006) Plasma membrane-associated proteins are clustered into islands attached to the cytoskeleton. *Proc Natl Acad Sci U S A* **103**: 18992–18997
- Li M, Hong Y, Wang X** (2009) Phospholipase D- and phosphatidic acid-mediated signaling in plants. *Biochim Biophys Acta* **1791**: 927–935
- Lingwood D, Simons K** (2007) Detergent resistance as a tool in membrane research. *Nat Protoc* **2**: 2159–2165
- Lingwood D, Simons K** (2010) Lipid rafts as a membrane-organizing principle. *Science* **327**: 46–50
- Liu P, Li R-L, Zhang L, Wang Q-L, Niehaus K, Baluška F, Šamaj J, Lin J-X** (2009) Lipid microdomain polarization is required for NADPH

- oxidase-dependent ROS signaling in *Picea meyeri* pollen tube tip growth. *Plant J* **60**: 303–313
- Livingston DP** (1998) Apoplastic sugars, fructans, fructan exohydrolase, and invertase in winter oat: responses to second-phase cold hardening. *Plant Physiol* **116**: 403–408
- Livingston DP, Henson CA, Tuong TD, Wise ML, Tallury SP, Duke SH** (2013) Histological analysis and 3D reconstruction of winter cereal crowns recovering from freezing: a unique response in oat (*Avena sativa* L.). *PLoS ONE* **8**: e53468
- Livingston DP, Premakumar R, Tallury SP** (2006) Carbohydrate partitioning between upper and lower regions of the crown in oat and rye during cold acclimation and freezing. *Cryobiology* **52**: 200–208
- Li Y, Qian Q, Zhou Y, Yan M, Sun L, Zhang M, Fu Z, Wang Y, Han B, Pang X, Chen M, Li J** (2003) *BRITTLE CULM1*, which encodes a COBRA-like protein, affects the mechanical properties of rice plants. *Plant Cell* **15**: 2020–2031
- London E, Brown DA** (2000) Insolubility of lipids in triton X-100: physical origin and relationship to sphingolipid/cholesterol membrane domains (rafts). *Biochim Biophys Acta* **1508**: 182–195
- Lynch DV, Steponkus PL** (1987) Plasma membrane lipid alterations associated with cold acclimation of winter rye seedlings (*Secale cereale* L. cv Puma). *Plant Physiol* **83**: 761–767
- MacMillan CP, Mansfield SD, Stachurski ZH, Evans R, Southerton SG** (2010) Fasciclin-like arabinogalactan proteins: specialization for stem biomechanics and cell wall architecture in *Arabidopsis* and *Eucalyptus*: FLAs specialized for stem biomechanics and cell walls. *Plant J* **62**: 689–703
- Maier FP, Lang NS, Fry JD** (1994) Evaluation of an electrolyte leakage technique to predict St. Augustinegrass freezing tolerance. *HortScience* **29**: 316–318
- Marmagne A, Ferro M, Meinnel T, Bruley C, Kuhn L, Garin J, Barbier-Brygoo H, Ephritikhine G** (2007) A high content in lipid-modified peripheral proteins and integral receptor kinases features in the *Arabidopsis* plasma membrane proteome. *Mol Cell Proteomics* **6**: 1980–1996

- Marmagne A, Rouet M-A, Ferro M, Rolland N, Alcon C, Joyard J, Garin J, Barbier-Brygoo H, Ephritikhine G** (2004) Identification of new intrinsic proteins in *Arabidopsis* plasma membrane proteome. *Mol Cell Proteomics* **3**: 675–691
- Masuda T, Tomita M, Ishihama Y** (2008) Phase transfer surfactant-aided trypsin digestion for membrane proteome analysis. *J Proteome Res* **7**: 731–740
- Matros A, Kaspar S, Witzel K, Mock H-P** (2011) Recent progress in liquid chromatography-based separation and label-free quantitative plant proteomics. *Phytochemistry* **72**: 963–974
- Mazars C, Thion L, Thuleau P, Graziana A, Knight MR, Moreau M, Ranjeva R** (1997) Organization of cytoskeleton controls the changes in cytosolic calcium of cold-shocked *Nicotiana plumbaginifolia* protoplasts. *Cell Calcium* **22**: 413–420
- McGwire BS, O’Connell WA, Chang K-P, Engman DM** (2002) Extracellular release of the glycosylphosphatidylinositol (GPI)-linked *Leishmania* surface metalloprotease, gp63, is independent of GPI phospholipolysis: implications for parasite virulence. *J Biol Chem* **277**: 8802–8809
- Melkonian KA, Ostermeyer AG, Chen JZ, Roth MG, Brown DA** (1999) Role of lipid modifications in targeting proteins to detergent-resistant membrane rafts: many raft proteins are acylated, while few are prenylated. *J Biol Chem* **274**: 3910–3917
- Membré N, Bernier F, Staiger D, Berna A** (2000) *Arabidopsis thaliana* germin-like proteins: common and specific features point to a variety of functions. *Planta* **211**: 345–354
- Miernyk JA** (1999) Protein folding in the plant cell. *Plant Physiol* **121**: 695–703
- Minami A, Fujiwara M, Furuto A, Fukao Y, Yamashita T, Kamo M, Kawamura Y, Uemura M** (2009) Alterations in detergent-resistant plasma membrane microdomains in *Arabidopsis thaliana* during cold acclimation. *Plant Cell Physiol* **50**: 341–359

- Minami A, Furuto A, Uemura M** (2010) Dynamic compositional changes of detergent-resistant plasma membrane microdomains during plant cold acclimation. *Plant Signal Behav* **5**: 1115–1118
- Mongrand S, Morel J, Laroche J, Claverol S, Carde J-P, Hartmann M-A, Bonneau M, Simon-Plas F, Lessire R, Bessoule J-J** (2004) Lipid rafts in higher plant cells: purification and characterization of Triton X-100-insoluble microdomains from tobacco plasma membrane. *J Biol Chem* **279**: 36277–36286
- Morel J, Claverol S, Mongrand S, Furt F, Fromentin J, Bessoule J-J, Blein J-P, Simon-Plas F** (2006) Proteomics of plant detergent-resistant membranes. *Mol Cell Proteomics* **5**: 1396–1411
- Morita N, Nakazato H, Okuyama H, Kim Y, Thompson GA** (1996) Evidence for a glycosylinositolphospholipid-anchored alkaline phosphatase in the aquatic plant *Spirodela oligorrhiza*. *Biochim Biophys Acta* **1290**: 53–62
- Muniz M, Riezman H** (2000) Intracellular transport of GPI-anchored proteins. *EMBO J* **19**: 10–15
- Murata N, Los DA** (1997) Membrane fluidity and temperature perception. *Plant Physiol* **115**: 875
- Murray MB, Cape JN, Fowler D** (1989) Quantification of frost damage in plant tissues by rates of electrolyte leakage. *New Phytol* **113**: 307–311
- Nabi IR, Le PU** (2003) Caveolae/raft-dependent endocytosis. *J Cell Biol* **161**: 673–677
- Nadimpalli R, Yalpani N, Johal GS, Simmons CR** (2000) Prohibitins, stomatins, and plant disease response genes compose a protein superfamily that controls cell proliferation, ion channel regulation, and death. *J Biol Chem* **275**: 29579–29586
- Nagano M, Takahara K, Fujimoto M, Tsutsumi N, Uchimiya H, Kawai-Yamada M** (2012) *Arabidopsis* sphingolipid fatty acid 2-hydroxylases (AtFAH1 and AtFAH2) are functionally differentiated in fatty acid 2-hydroxylation and stress responses. *Plant Physiol* **159**: 1138–1148
- Neilson KA, Mariani M, Haynes PA** (2011) Quantitative proteomic analysis of cold-responsive proteins in rice. *Proteomics* **11**: 1696–1706

- Ng CK, Carr K, McAinsh MR, Powell B, Hetherington AM** (2001) Drought-induced guard cell signal transduction involves sphingosine-1-phosphate. *Nature* **410**: 596–599
- Oliferenko S, Paiha K, Harder T, Gerke V, Schwärzler C, Schwarz H, Beug H, Günthert U, Huber LA** (1999) Analysis of CD44-containing lipid rafts recruitment of annexin II and stabilization by the actin cytoskeleton. *J Cell Biol* **146**: 843–854
- Oquist G, Hurry VM, Huner NP** (1993) Low-temperature effects on photosynthesis and correlation with freezing tolerance in spring and winter cultivars of wheat and rye. *Plant Physiol* **101**: 245–250
- Örvar BL, Sangwan V, Omann F, Dhindsa RS** (2000) Early steps in cold sensing by plant cells: the role of actin cytoskeleton and membrane fluidity. *Plant J* **23**: 785–794
- Ouellet F, Carpentier É, Cope MJT, Monroy AF, Sarhan F** (2001) Regulation of a wheat actin-depolymerizing factor during cold acclimation. *Plant Physiol* **125**: 360–368
- Oxley D, Bacic A** (1999) Structure of the glycosylphosphatidylinositol anchor of an arabinogalactan protein from *Pyrus communis* suspension-cultured cells. *Proc Natl Acad Sci U S A* **96**: 14246–14251
- Palta JP, Whitaker BD, Weiss LS** (1993) Plasma membrane lipids associated with genetic variability in freezing tolerance and cold acclimation of *Solanum* species. *Plant Physiol* **103**: 793–803
- Paulick MG, Bertozzi CR** (2008) The glycosylphosphatidylinositol anchor: a complex membrane-anchoring structure for proteins. *Biochemistry* **47**: 6991–7000
- Pelkmans L, Püntener D, Helenius A** (2002) Local actin polymerization and dynamin recruitment in SV40-induced internalization of caveolae. *Science* **296**: 535–539
- Peng Y, Arora R, Li G, Wang X, Fessehaie A** (2008) *Rhododendron catawbiense* plasma membrane intrinsic proteins are aquaporins, and their over-expression compromises constitutive freezing tolerance and cold acclimation ability of transgenic *Arabidopsis* plants. *Plant Cell Environ* **31**: 1275–1289

- Peskan T, Westermann M, Oelmüller R** (2000) Identification of low-density Triton X-100-insoluble plasma membrane microdomains in higher plants. *Eur J Biochem* **267**: 6989–6995
- Pierleoni A, Martelli P, Casadio R** (2008) PredGPI: a GPI-anchor predictor. *BMC Bioinformatics* **9**: 392
- Pike LJ** (2009) The challenge of lipid rafts. *J Lipid Res* **50 Suppl**: S323–328
- Plieth C** (1999) Temperature sensing by plants: calcium-permeable channels as primary sensors—a model. *J Membr Biol* **172**: 121–127
- Poisson G, Chauve C, Chen X, Bergeron A** (2007) FragAnchor: a large-scale predictor of glycosylphosphatidylinositol anchors in eukaryote protein sequences by qualitative scoring. *Genomics Proteomics Bioinformatics* **5**: 121–130
- Raffaele S, Bayer E, Lafarge D, Cluzet S, German Retana S, Boubekur T, Leborgne-Castel N, Carde J-P, Lherminier J, Noirot E, Satiat-Jeunemaitre B, Laroche-Traineau J, Moreau P, Ott T, Maule AJ, Reymond P, Simon-Plas F, Farmer EE, Bessoule J-J, Mongrand S** (2009) Remorin, a *Solanaceae* protein resident in membrane rafts and plasmodesmata, impairs potato virus X movement. *Plant Cell* **21**: 1541–1555
- Renaut J, Hoffmann L, Hausman J-F** (2005) Biochemical and physiological mechanisms related to cold acclimation and enhanced freezing tolerance in poplar plantlets. *Physiol Plant* **125**: 82–94
- Rinne PLH, Kaikuranta PM, Van Der Schoot C** (2001) The shoot apical meristem restores its symplasmic organization during chilling-induced release from dormancy: chilled AM restores its symplasmic network. *Plant J* **26**: 249–264
- Rinne PLH, Welling A, Vahala J, Ripel L, Ruonala R, Kangasjärvi J, van der Schoot C** (2011) Chilling of dormant buds hyperinduces FLOWERING LOCUS T and recruits GA-inducible 1,3- β -glucanases to reopen signal conduits and release dormancy in *Populus*. *Plant Cell* **23**: 130–146
- Roberts MF** (1996) Phospholipases: structural and functional motifs for working at an interface. *FASEB J* **10**: 1159–1172

- Roberts WL, Myher JJ, Kuksis A, Low MG, Rosenberry TL** (1988) Lipid analysis of the glycoinositol phospholipid membrane anchor of human erythrocyte acetylcholinesterase. Palmitoylation of inositol results in resistance to phosphatidylinositol-specific phospholipase C. *J Biol Chem* **263**: 18766–18775
- Robinson DG, Haschke H-P, Hinz G, Hoh B, Maeshima M, Marty F** (1996) Immunological detection of tonoplast polypeptides in the plasma membrane of pea cotyledons. *Planta* **198**: 95–103
- Rollason R, Korolchuk V, Hamilton C, Schu P, Banting G** (2007) Clathrin-mediated endocytosis of a lipid-raft-associated protein is mediated through a dual tyrosine motif. *J Cell Sci* **120**: 3850–3858
- Rosenberry TL** (1991) A chemical modification that makes glycoinositol phospholipids resistant to phospholipase C cleavage: fatty acid acylation of inositol. *Cell Biol Int Rep* **15**: 1133–1150
- Rostoks N, Schmierer D, Kudrna D, Kleinhofs A** (2003) Barley putative hypersensitive induced reaction genes: genetic mapping, sequence analyses and differential expression in disease lesion mimic mutants. *Theor Appl Genet* **107**: 1094–1101
- Roudier F, Fernandez AG, Fujita M, Himmelsbach R, Borner GHH, Schindelman G, Song S, Baskin TI, Dupree P, Wasteneys GO, Benfey PN** (2005) COBRA, an *Arabidopsis* extracellular glycosyl-phosphatidyl inositol-anchored protein, specifically controls highly anisotropic expansion through its involvement in cellulose microfibril orientation. *Plant Cell* **17**: 1749–1763
- Roudier F, Schindelman G, DeSalle R, Benfey PN** (2002) The COBRA family of putative GPI-anchored proteins in *Arabidopsis*. A new fellowship in expansion. *Plant Physiol* **130**: 538–548
- Le Roy C, Wrana JL** (2005) Clathrin- and non-clathrin-mediated endocytic regulation of cell signalling. *Nat Rev Mol Cell Biol* **6**: 112–126
- Sankaram MB, Thompson TE** (1990) Interaction of cholesterol with various glycerophospholipids and sphingomyelin. *Biochemistry (Mosc)* **29**: 10670–10675

- Sargiacomo M, Sudol M, Tang Z, Lisanti MP** (1993) Signal transducing molecules and glycosyl-phosphatidylinositol-linked proteins form a caveolin-rich insoluble complex in MDCK cells. *J Cell Biol* **122**: 789–807
- Schindelman G** (2001) COBRA encodes a putative GPI-anchored protein, which is polarly localized and necessary for oriented cell expansion in *Arabidopsis*. *Genes Dev* **15**: 1115–1127
- Schley PD, Brindley DN, Field CJ** (2007) (n-3) PUFA alter raft lipid composition and decrease epidermal growth factor receptor levels in lipid rafts of human breast cancer cells. *J Nutr* **137**: 548–553
- Schrack K, Fujioka S, Takatsuto S, Stierhof Y-D, Stransky H, Yoshida S, Jürgens G** (2004) A link between sterol biosynthesis, the cell wall, and cellulose in *Arabidopsis*. *Plant J* **38**: 227–243
- Schrack K, Shiva S, Arpin JC, Delimont N, Isaac G, Tamura P, Welti R** (2012) Steryl glucoside and acyl steryl glucoside analysis of *Arabidopsis* seeds by electrospray ionization tandem mass spectrometry. *Lipids* **47**: 185–193
- Schroeder RJ, Ahmed SN, Zhu Y, London E, Brown DA** (1998) Cholesterol and sphingolipid enhance the Triton X-100 insolubility of glycosylphosphatidylinositol-anchored proteins by promoting the formation of detergent-insoluble ordered membrane domains. *J Biol Chem* **273**: 1150–1157
- Schroeder R, London E, Brown D** (1994) Interactions between saturated acyl chains confer detergent resistance on lipids and glycosylphosphatidylinositol (GPI)-anchored proteins: GPI-anchored proteins in liposomes and cells show similar behavior. *Proc Natl Acad Sci U S A* **91**: 12130–12134
- Schuck S, Honsho M, Ekroos K, Shevchenko A, Simons K** (2003) Resistance of cell membranes to different detergents. *Proc Natl Acad Sci U S A* **100**: 5795–5800
- Shahollari B, Peskan-Berghofer T, Oelmüller R** (2004) Receptor kinases with leucine-rich repeats are enriched in Triton X-100 insoluble plasma membrane microdomains from plants. *Physiol Plant* **122**: 397–403

- Sharma P, Varma R, Sarasij RC, Ira null, Gousset K, Krishnamoorthy G, Rao M, Mayor S** (2004) Nanoscale organization of multiple GPI-anchored proteins in living cell membranes. *Cell* **116**: 577–589
- Sherrier DJ, Prime TA, Dupree P** (1999) Glycosylphosphatidylinositol-anchored cell-surface proteins from *Arabidopsis*. *Electrophoresis* **20**: 2027–2035
- Shi H, Kim Y, Guo Y, Stevenson B, Zhu J-K** (2003) The *Arabidopsis* *SOS5* locus encodes a putative cell surface adhesion protein and is required for normal cell expansion. *Plant Cell* **15**: 19–32
- Shogomori H, Brown DA** (2003) Use of detergents to study membrane rafts: the good, the bad, and the ugly. *Biol Chem* **384**: 1259–1263
- Silvius JR** (1992) Cholesterol modulation of lipid intermixing in phospholipid and glycosphingolipid mixtures. Evaluation using fluorescent lipid probes and brominated lipid quenchers. *Biochemistry (Mosc)* **31**: 3398–3408
- Siminovitch D, Scarth GW** (1938) A study of the mechanism of frost injury to plants. *Can J Res* **16c**: 467–481
- Simons K, Ikonen E** (1997) Functional rafts in cell membranes. *Nature* **387**: 569–572
- Simons K, Sampaio JL** (2011) Membrane organization and lipid rafts. *Cold Spring Harb Perspect Biol* **3**: a004697–a004697
- Simpson C, Thomas C, Findlay K, Bayer E, Maule AJ** (2009) An *Arabidopsis* GPI-anchor plasmodesmal neck protein with callose binding activity and potential to regulate cell-to-cell trafficking. *Plant Cell* **21**: 581–594
- Singer SJ, Nicolson GL** (1972) The fluid mosaic model of the structure of cell membranes. *Science* **175**: 720–731
- Srivastava V, Malm E, Sundqvist G, Bulone V** (2013) Quantitative proteomics reveals that plasma membrane microdomains from poplar cell suspension cultures are enriched in markers of signal transduction, molecular transport, and callose biosynthesis. *Mol Cell Proteomics* **12**: 3874–3885
- Staehelin LA** (1997) The plant ER: a dynamic organelle composed of a large number of discrete functional domains. *Plant J* **11**: 1151–1165

- Stanislas T, Bouyssie D, Rossignol M, Vesa S, Fromentin J, Morel J, Pichereaux C, Monsarrat B, Simon-Plas F** (2009) Quantitative proteomics reveals a dynamic association of proteins to detergent-resistant membranes upon elicitor signaling in tobacco. *Mol Cell Proteomics* **8**: 2186–2198
- Stefanowska M, Kuraś M, Kubacka-Zębalska M, Kacperska A** (1999) Low temperature affects pattern of leaf growth and structure of cell walls in winter oilseed rape (*Brassica napus* L., var. *oleifera* L.). *Ann Bot* **84**: 313–319
- Steponkus PL** (1984) Role of the plasma membrane in freezing injury and cold acclimation. *Annu Rev Plant Physiol* **35**: 543–584
- Steponkus PL, Uemura M, Balsamo RA, Arvinte T, Lynch DV** (1988) Transformation of the cryobehavior of rye protoplasts by modification of the plasma membrane lipid composition. *Proc Natl Acad Sci U S A* **85**: 9026–9030
- Stöhr C, Schuler F, Tischner R** (1995) Glycosyl-phosphatidylinositol-anchored proteins exist in the plasma membrane of *Chlorella saccharophila* (Krüger) Nadson: plasma-membrane-bound nitrate reductase as an example. *Planta* **196**: 284–287
- Sung DY, Vierling E, Guy CL** (2001) Comprehensive expression profile analysis of the *Arabidopsis Hsp70* gene family. *Plant Physiol* **126**: 789–800
- Svensson JT** (2006) Transcriptome analysis of cold acclimation in barley *Albina* and *Xantha* mutants. *Plant Physiol* **141**: 257–270
- Takahashi D, Furuto A, Minami A, Kamo, M, Yamashita T, Uemura M** (2011) Relationship between composition of plasma membrane microdomain and freezing tolerance in oat and rye. *Cryobiol Cryotechnol* **57**: 95–99
- Takahashi D, Kawamura Y, Uemura M** (2013) Changes of detergent-resistant plasma membrane proteins in oat and rye during cold acclimation: association with differential freezing tolerance. *J Proteome Res* **12**: 4998–5011
- Takahashi D, Kawamura Y, Yamashita T, Uemura M** (2012) Detergent-resistant plasma membrane proteome in oat and rye: similarities and dissimilarities between two monocotyledonous plants. *J Proteome Res* **11**: 1654–1665

- Takos AM, Dry IB, Soole KL** (1997) Detection of glycosyl-phosphatidylinositol-anchored proteins on the surface of *Nicotiana tabacum* protoplasts. *FEBS Lett* **405**: 1–4
- Tanner W, Malinsky J, Opekarová M** (2011) In plant and animal cells, detergent-resistant membranes do not define functional membrane rafts. *Plant Cell* **23**: 1191–1193
- Tanz SK, Castleden I, Hooper CM, Vacher M, Small I, Millar HA** (2013) SUBA3: a database for integrating experimentation and prediction to define the SUBcellular location of proteins in *Arabidopsis*. *Nucleic Acids Res* **41**: D1185–D1191
- Thomashow MF** (1998) Role of cold-responsive genes in plant freezing tolerance. *Plant Physiol* **118**: 1–8
- Thomashow MF** (1999) Plant cold acclimation: freezing tolerance genes and regulatory mechanisms. *Annu Rev Plant Biol* **50**: 571–599
- Toufighi K, Brady SM, Austin R, Ly E, Provart NJ** (2005) The botany array resource: e-northern, expression angling, and promoter analyses. *Plant J* **43**: 153–163
- Towler DA, Gordon JI, Adams SP, Glaser L** (1988) The biology and enzymology of eukaryotic protein acylation. *Annu Rev Biochem* **57**: 69–99
- Udenfriend S, Kodukula K** (1995) How glycosylphosphatidylinositol-anchored membrane proteins are made. *Annu Rev Biochem* **64**: 563–591
- Uemura M, Joseph RA, Steponkus PL** (1995) Cold acclimation of *Arabidopsis thaliana* (effect on plasma membrane lipid composition and freeze-induced lesions). *Plant Physiol* **109**: 15–30
- Uemura M, Steponkus PL** (1989) Effect of cold acclimation on the incidence of two forms of freezing injury in protoplasts isolated from rye leaves. *Plant Physiol* **91**: 1131–1137

- Uemura M, Steponkus PL** (1994) A contrast of the plasma membrane lipid composition of oat and rye leaves in relation to freezing tolerance. *Plant Physiol* **104**: 479–496
- Uemura M, Tominaga Y, Nakagawara C, Shigematsu S, Minami A, Kawamura Y** (2006) Responses of the plasma membrane to low temperatures. *Physiol Plant* **126**: 81–89
- Uemura M, Yoshida S** (1984) Involvement of plasma membrane alterations in cold acclimation of winter rye seedlings (*Secale cereale* L. cv Puma). *Plant Physiol* **75**: 818–826
- Uemura M, Yoshida S** (1983) Isolation and identification of plasma membrane from light-grown winter rye seedlings (*Secale cereale* L. cv Puma). *Plant Physiol* **73**: 586–597
- Varma R, Mayor S** (1998) GPI-anchored proteins are organized in submicron domains at the cell surface. *Nature* **394**: 798–801
- Veatch SL, Cicuta P, Sengupta P, Honerkamp-Smith A, Holowka D, Baird B** (2008) Critical fluctuations in plasma membrane vesicles. *ACS Chem Biol* **3**: 287–293
- Villalba M** (2001) Vav1/Rac-dependent actin cytoskeleton reorganization is required for lipid raft clustering in T cells. *J Cell Biol* **155**: 331–338
- Wanner LA, Junttila O** (1999) Cold-induced freezing tolerance in *Arabidopsis*. *Plant Physiol* **120**: 391–400
- Watanabe M, Miyagi A, Nagano M, Kawai-Yamada M, Imai H** (2011) Characterization of glucosylceramides in the *Polygonaceae*, *Rumex obtusifolius* L. injurious weed. *Biosci Biotechnol Biochem* **75**: 877–881
- Webb MS, Irving TC, Steponkus PL** (1995) Effects of plant sterols on the hydration and phase behavior of DOPE/DOPC mixtures. *Biochim Biophys Acta* **1239**: 226–238

- Webb MS, Sek Wen Hui, Steponkus PL** (1993) Dehydration-induced lamellar-to-hexagonal-II phase transitions in DOPE/DOPC mixtures. *Biochim Biophys Acta* **1145**: 93–104
- Webb MS, Steponkus PL** (1993) Freeze-induced membrane ultrastructural alterations in rye (*Secale cereale*) leaves. *Plant Physiol* **101**: 955–963
- Webb MS, Uemura M, Steponkus PL** (1994) A comparison of freezing injury in oat and rye: two cereals at the extremes of freezing tolerance. *Plant Physiol* **104**: 467–478
- Welin BV, Olson A, Nylander M, Palva ET** (1994) Characterization and differential expression of *dhn/lea/rab*-like genes during cold acclimation and drought stress in *Arabidopsis thaliana*. *Plant Mol Biol* **26**: 131–144
- Welti R, Li W, Li M, Sang Y, Biesiada H, Zhou H-E, Rajashekar CB, Williams TD, Wang X** (2002) Profiling membrane lipids in plant stress responses: role of phospholipase D α in freezing-induced lipid changes in *Arabidopsis*. *J Biol Chem* **277**: 31994–32002
- Williams LE, Lemoine R, Sauer N** (2000) Sugar transporters in higher plants—a diversity of roles and complex regulation. *Trends Plant Sci* **5**: 283–290
- Wisniewski M, Webb R, Balsamo R, Close TJ, Yu X-M, Griffith M** (1999) Purification, immunolocalization, cryoprotective, and antifreeze activity of PCA60: a dehydrin from peach (*Prunus persica*). *Physiol Plant* **105**: 600–608
- Worrall D, Ng CK-Y, Hetherington AM** (2003) Sphingolipids, new players in plant signaling. *Trends Plant Sci* **8**: 317–320
- Wu J, Browse J** (1995) Elevated levels of high-melting-point phosphatidylglycerols do not induce chilling sensitivity in an *Arabidopsis* mutant. *Plant Cell* **7**: 17–27
- Xia F, Gao X, Kwan E, Lam PPL, Chan L, Sy K, Sheu L, Wheeler MB, Gaisano HY, Tsushima RG** (2004) Disruption of pancreatic β -cell lipid rafts modifies K $_v$ 2.1 channel gating and insulin exocytosis. *J Biol Chem* **279**: 24685–24691
- Xiao S, Gao W, Chen Q-F, Chan S-W, Zheng S-X, Ma J, Wang M, Welti R, Chye M-L** (2010) Overexpression of *Arabidopsis* acyl-CoA binding protein ACBP3

- promotes starvation-induced and age-dependent leaf senescence. *Plant Cell* **22**: 1463–1482
- Xie B, Wang X, Zhu M, Zhang Z, Hong Z** (2011) *CalS7* encodes a callose synthase responsible for callose deposition in the phloem: a phloem-specific callose synthase. *Plant J* **65**: 1–14
- Xu X, Bittman R, Duportail G, Heissler D, Vilcheze C, London E** (2001) Effect of the structure of natural sterols and sphingolipids on the formation of ordered sphingolipid/sterol domains (rafts): comparison of cholesterol to plant, fungal, and disease-associated sterols and comparison of sphingomyelin, cerebroside, and ceramide. *J Biol Chem* **276**: 33540–33546
- Yoshida S, Uemura M** (1984) Protein and lipid compositions of isolated plasma membranes from orchard grass (*Dactylis glomerata* L.) and changes during cold acclimation. *Plant Physiol* **75**: 31–37
- Zacharias DA, Violin JD, Newton AC, Tsien RY** (2002) Partitioning of lipid-modified monomeric GFPs into membrane microdomains of live cells. *Science* **296**: 913–916
- Zheng X, Bollinger Bollag W** (2003) Aquaporin 3 colocalizes with phospholipase D2 in caveolin-rich membrane microdomains and is downregulated upon keratinocyte differentiation. *J Invest Dermatol* **121**: 1487–1495
- Zhou L, Cheung M-Y, Li M-W, Fu Y, Sun Z, Sun S-M, Lam H-M** (2010) Rice hypersensitive induced reaction protein 1 (OsHIR1) associates with plasma membrane and triggers hypersensitive cell death. *BMC Plant Biol* **10**: 290
- Zhou L, Cheung M-Y, Zhang Q, Lei C-L, Zhang S-H, Sun SS-M, Lam H-M** (2009) A novel simple extracellular leucine-rich repeat (eLRR) domain protein from rice (OsLRR1) enters the endosomal pathway and interacts with the hypersensitive-induced reaction protein 1 (OsHIR1). *Plant Cell Environ* **32**: 1804–1820